Universidad Autónoma de Madrid
Doctorado en Biociencias Moleculares

Mitochondrial DNA transfer through exosomes during immune synapsis primes antiviral innate immune response in dendritic cells

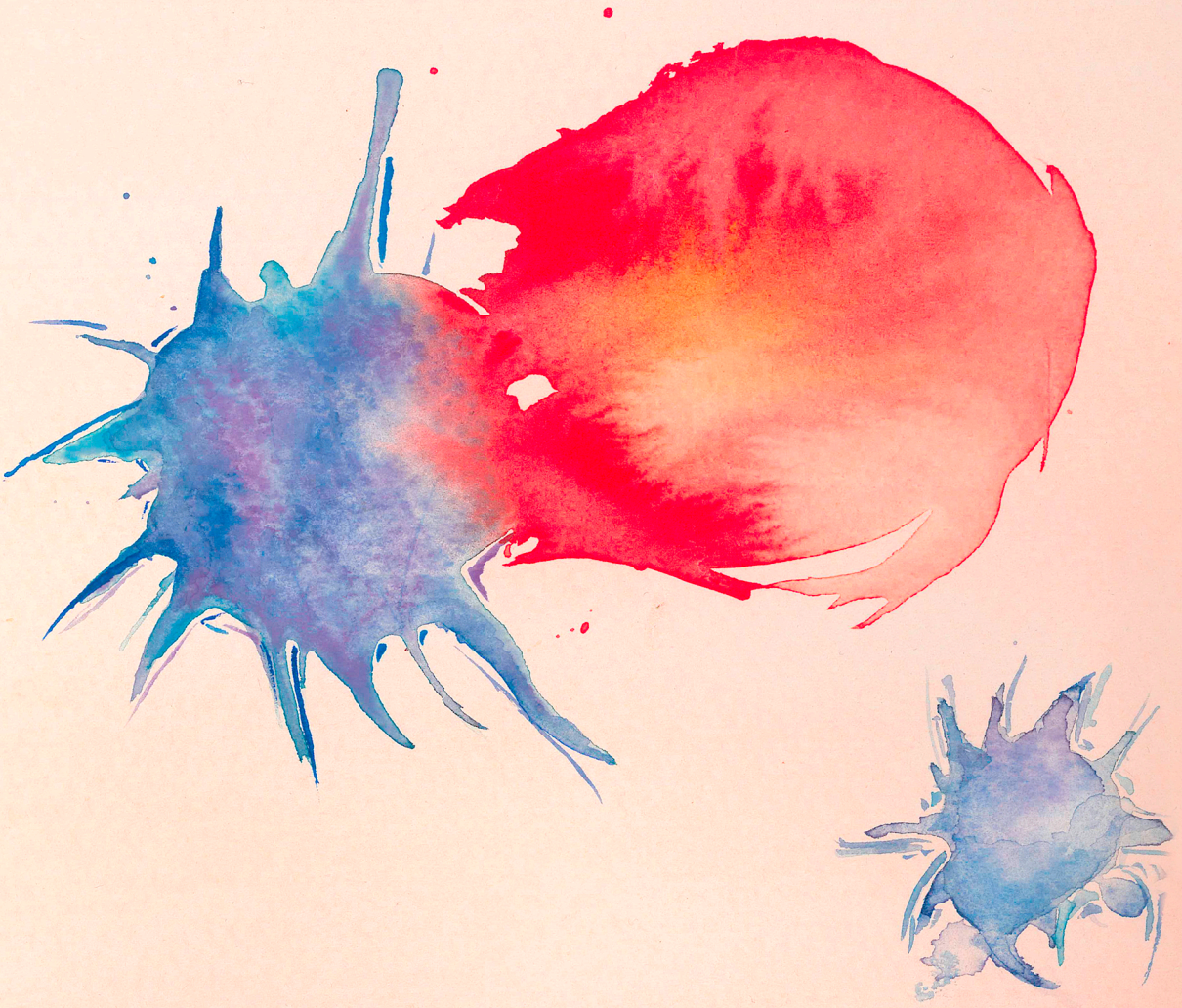

Daniel Torralba Grajales

Madrid, 2019

Universidad Autónoma de Madrid

Departamento de Bioquímica

Facultad de Medicina

Mitochondrial DNA transfer through exosomes during immune synapsis primes antiviral innate immune response in dendritic cells.

Doctoral Thesis

Daniel Torralba Grajales

Madrid, 2019

Universidad Autónoma de Madrid

Programa de Doctorado en Biociencias Moleculares

Facultad de Medicina

Departamento de Bioquímica

Mitochondrial DNA transfer through exosomes during immune synapsis primes antiviral innate immune response in dendritic cells.

Memoria presentada por el Licenciado en Bioquímica:

Daniel Torralba Grajales

Para optar al título de Doctor por la Universidad Autónoma de Madrid

Director de tesis: **Dr. Francisco Sánchez Madrid**, Doctor en Ciencias Biológicas y Catedrático de Inmunología de la Universidad Autónoma de Madrid

Este trabajo ha sido realizado en el Centro Nacional de Investigaciones Cardiovasculares (CNIC) y Servicio de Inmunología del Hospital Universitario de la Princesa

Madrid, 2019

A mis padres, a mi hermana

A mi mujer y mi hijo

*"**Un gran poder conlleva una gran responsabilidad**"*

Franklin D. Roosevelt/ Tío Ben

Agradecimientos

Agradecimientos

Dice el proverbio chino "*El leve aleteo de las alas de una mariposa se puede sentir al otro lado del mundo*". En un sistema dinámico complejo como es el de la vida, ligeras variaciones pueden amplificarse y desembocar en inmensos cambios. Es curioso cómo los pequeños actos de nuestra vida cotidiana tiene inmensas repercusiones completamente imprevisibles en nuestras vidas futuras. Creo que tener esto en mente puede ayudarnos a entender que tenemos un gran poder en todos nuestros actos diarios hacia los que nos rodean, pueden cambiar el destino de alguien por muy insignificantes que parezcan. Tenemos un gran poder y eso conlleva una gran responsabilidad.

Así que si hoy estoy aquí, concluyendo un gran hito académico, es gracias a muchas personas que a través de pequeños cambios me han hecho convertirme en quien soy hoy. Quizás no tenga otra oportunidad de agradecer formalmente a todos los que me rodean o me han rodeado en algún momento. Discúlpeme el lector por la extensión, la tesis comienza unas hojas más adelante. En primer lugar me gustaría darle las gracias al Dr. Sánchez-Madrid, conocido entre todos como Paco. Él fue mi profesor de Inmunología, probablemente la asignatura que más me fascinó durante la carrera. Esto definió mi destino en la investigación científica y en mi futuro profesional. Paco me aceptó en su laboratorio hace ya bastantes años para realizar mi proyecto de investigación de fin de carrera y finalmente la tesis doctoral. Gracias Paco por darme autonomía, espíritu crítico y perseverancia en los proyectos.

En segundo lugar gracias a todos los profesores que han formado parte de mi educación, su labor es fundamental, ellos crean a los ciudadanos del mañana y no podemos olvidar su labor. Me gustaría mencionar algunos en concreto. Gracias a José Miguel Serrano, mi profesor de Biología de secundaria, él pensó que éramos capaces de saber más de lo que se nos exigía y nos enseñó los misterios de la bioquímica y la biología celular. El encendió la llama que años más tarde terminaría haciendo que estudiara Bioquímica. Gracias al profesor Mateo, él despertó mi pasión por las ciencias formales y la lógica. Consiguió que pasara de odiar las matemáticas a amarlas, y lo hizo consiguiendo que las entendiera y no las memorizase. Este evento cambió mi perspectiva de la educación y mi desempeño a lo largo de toda la carrera y tesis.

He de hacer una mención a la ayuda de la Fundación La Caixa, su programa de becas me ha permitido centrarme en investigar y en estudiar sin preocuparme de la financiación. Sin duda esto es indispensable para poder desarrollarse a nivel profesional y personal. Gracias.

Para ser un buen científico creo que hay que desarrollar una buena imaginación. No me corresponde juzgar si soy un buen científico pero sin duda si alguien me ha ayudado a desarrollar esta habilidad han sido mis inseparables amigos Mario, Miguel, Ignacio y Jose. Pero esto no es el único regalo que he recibido de su parte, en ellos encuentro los mejores valores del ser humano y ellos han tenido una tremenda influencia en quien soy yo hoy. Gracias Mario por entrenarme en mi incansable empeño por discutir y traer sentido a todo lo que me rodea, quizás una de las razones por las que me dediqué a la ciencia. Gracias también por todos los buenos consejos que me has dado y por tu paciencia. Gracias Miguel por ser un ejemplo de voluntad y perseverancia luchando por un sueño, hay que ser muy valiente para dar un giro tan radical a tu vida. Gracias por estar siempre cerca y apoyarme en el camino. Gracias Ignacio por ser un ejemplo de lealtad, amistad y bondad. Una persona en la que se puede depositar una confianza absoluta porque nunca te fallará. Gracias Jose por tu buen sentido del humor y tu asertividad. Me habéis enseñado mucho. Gracias a los cuatro por estar a mi lado siempre.

En el colegio conocí a mucha gente y ese periodo definió en gran medida la personalidad que terminaría moldeando en los años venideros. Gracias a Juan Luis por tantos recreos de última hora, y por tan buenos ratos que vivimos y seguimos viviendo. También me gustaría agradecerle a Victoria por todas esas explicaciones y tanta ayuda que me dio, gracias por las confidencias y tu cariño. Gracias por último a David que ha sido un gran compañero y amigo desde el cole hasta hoy.

De mi etapa universitaria sin duda tengo que agradecer a mis amigos de Biología de la UAM, personas que permanecerán siempre cerca y que hicieron que mis años en la universidad pasaran como un suspiro y que guardé en mis recuerdos como una de las mejores etapas de mi vida. Dicen que un científico debe ser guiado por su curiosidad, y, ¿quién tiene más curiosidad que un niño? Sin duda alguna ellos me han hecho mantener a mi niño interior activo, de disfrutar de las pequeñas cosas y de valorar cada momento. Muchas gracias Barrio por la amistad y el apoyo a lo largo de estos años (a tu manera). Sin duda eres un ejemplo de lealtad y fidelidad hacia tus amigos. Él me enseñó que las cosas inolvidables son las que nunca se olvidan. Gracias por toda la morralla de YouTube que me ha hecho pasar tantas horas haciendo y diciendo tonterías. Si hablamos de niños grandes el premio se lo lleva Petrini, gracias por hacernos reír tanto y por todas las aventuras en las que nos has metido. Siempre apoyado por Cogollos que nunca defrauda para tener una nueva historia que contar. A veces la vida nos trae sorpresas, y cuál fue la mía cuando encontré a mi amigo de la infancia del colegio en mi clase de Biología, Miguel ese chico silencioso que siempre era nuevo en el colegio y que también fue nuevo en la Universidad logró ganarse nuestros corazones. Muchas gracias por

compartir conmigo tu humildad y buen corazón. Gracias a David, por retarme y hacerme querer llegar más lejos, un poco de competencia sana siempre puede alentarnos a ser mejores cada día, aunque probablemente el único que competía era yo… Gracias por ayudarme tan desinteresadamente y por resolver mis histéricas dudas de última hora antes del examen. Gracias a Hurtado por enseñarme como el esfuerzo y las ganas de conocer pueden llevarte a sitios maravillosos. Gracias a Didi, ella fue mi confidente durante los años de Universidad, gracias por tantos pequeños momentos y por darle alas a mi sentido del humor en la cafetería. Sobre todo muchas gracias por preocuparte tanto por mí y por todo el cariño que me has dado. Otro punto de inflexión en mi vida y mi carrera fue cuando Marina me invitó a hacerle una visita a su cabaña flotante en el Amazonas, mi forma de tomarme la vida dio un giro de 360 grados, muchas gracias por haberme dado esa oportunidad y por empujarme a ir a por la que a día de hoy es mi mujer. Por último gracias a Marta, Varela y Velilla por hacerme sentir en familia y porque gracias a vosotras cada día en la Uni era más divertido. En conjunto todos vosotros habéis tenido una tremenda influencia en quien soy hoy y a donde he llegado. No podré nunca agradecéroslo lo suficiente.

En mi época universitaria también entro en mi vida Alma, no lo sabía aun pero terminaría siendo parte de mi familia. Gracias por todo el cariño que nos has dado a mí y a Mery a lo largo de estos años. Gracias por estar siempre ahí sin importar que pasara y muchas gracias por aguantar mis chinches que tanto disfruto y que tanto te desesperan.

Victor y Fran, dos grandes amigos que me llevo de mi etapa predoctoral. Probablemente son de las personas con más capacidad que he conocido y de las que más admiro. Fran, creativo y trabajador donde los haya (aun siendo de Graná) y Victor, experto networker y proactivo a más no poder. Ambos con un excepcional sentido del humor. Gracias por tantas meriendas y por tantas discusiones científicas. Gracias por escuchar mis hipótesis por apoyarme en mis momentos de dudas. Sé que llegareis donde os propongáis

También me gustaría darle las gracias a Charlie, hablar con él es siempre un reto intelectual, gracias por esas reuniones para arreglar el mundo que ha permitido que mi imaginación volase. Una persona que sin duda sabe escuchar y siempre aporta sentido y lógica a la vida.

Tengo que hacer un agradecimiento especial a todos laboratorios que me han acogido antes de llegar al laboratorio de Paco. Muchas gracias Guada por darme la oportunidad de hacer el CICERONE contigo, fue una de las mejores experiencias que tengo de mis veranos en la Universidad, de allí me llevo a grandes personas: Lucho, Eli, Edgar y sobretodo Toñi.

Toñi me ha enseñado a “salir de la caja”, a pensar más allá de lo establecido y a que un científico tiene que ser flexible en el pensamiento puesto que debemos estar dispuestos a enfrentarnos a lo desconocido sin prejuicios. Que no debemos rechazar una idea por muy loca que sea. Probablemente al entrar en el laboratorio mi cabeza era lo contrario a esto, dogmático e inflexible, gracias a ella me he acercado un poco más a la ciencia de verdad. Gracias por ser mi mentora de esta etapa y por guiarme en este camino que a veces me ha resultado tan difícil.

Otro verano que recuerdo con especial cariño es el que pasé en el laboratorio de Mercedes Rincón en Vermont. Fue una experiencia que me ayudó a superar momentos complicados y que disfruté a más no poder. Gracias Mercedes por enseñarme lo que significa la verdadera vocación y a vivir la ciencia con pasión.

Durante estos años de laboratorio he tenido la oportunidad de conocer a mucha gente fuera del laboratorio. Muchas gracias a los “Sanchos”, en conjunto un ejemplo de dedicación y perseverancia. Gracias Salva por tan buenos consejos científicos y por las charlas informales en cualquier esquinita. Gracias Mary, Ruth, Sarai y Sofía por compartir esos ratitos de cultivos diciendo tonterías y amenizando esos largos ratos muertos.

En los 5 años de tesis en el laboratorio de Paco he podido compartir poyata con grandes personas. Gracias a los Jurásicos, grandes noches y momentos. Gracias Norman por enseñarme a encontrar la felicidad en pequeñas cosas. A Rafa por su sencillez y su capacidad de sacar un buen momento de cualquier situación. A Eu por su humor y por todas las conversaciones científicas y no tan científicas que hemos sacado. A Álvaro y Javi, gracias a vosotros y las conversaciones frikis me habéis hecho sentir siempre como en casa. Lo he pasado muy bien. Muchas gracias chicos.

Gracias a Noe tu simpatía y por montar planes tan divertidos fuera del laboratorio en los que he podido conocer a mis compañeros más a fondo. Gracias a Ana, con esa templanza que le caracteriza siempre ha conseguido que fuese capaz de verle el lado bueno a todas las cosas. Gracias por tus ánimos constantes. Gracias a Irene, que empezó como mi estudiante de CICERONE y ahora soy yo quien tiene que consultarle todo a ella. Una persona metódica y ordenada de la que tengo mucho que aprender. Gracias por crear tan buen ambiente en el laboratorio y por ayudarme cuando lo he necesitado. Gracias a Marta, la que podría ser nuestra hermana mayor del lab, ella nos guía y ayuda en todo, siempre tiene unas palabras para animarte. Gracias a Laurín, que siempre sacaba una sonrisa e intentaba animarte aunque el panorama estuviese negro. Eres una gran persona. Gracias también a Olga por haber

compartido tantos momentos y poyata, aunque mi desorden te pusiese nerviosilla. Gracias a Lola por estar siempre dispuesta a sacar una conversación interesante y por su contagiosa risa. Gracias a Raquel por ser un ejemplo de esfuerzo, me habéis enseñado mucho. Gracias a Nieves por su simpatía y buen rollo. Para que un laboratorio funcione hacen falta personas como vosotras. También es necesario que haya personas que hagan girar los engranajes del lab y ahí se encuentra La Secre María Ángeles. Muchas gracias por toda tu ayuda para resolver cualquier asuntillo. Gracias Jose María por tus chistes malos y por amenizarme tanto las horas de laboratorio. Gracias a Danay por ser un ejemplo de voluntad, vocación y focalización. Para mi eres una referencia del esfuerzo que debe hacer un científico para tener éxito. Gracias por todas las lecciones que me has enseñado. Gracias a Fran Baixauli, sin el cual claramente esta tesis sido tal y como es. Gracias por guiarme por el tortuoso camino de la tesis y por tu generosidad. Gracias a Noa, que sobre todo en esta última etapa me ha ayudado sobremanera, consiguió tirar para que el paper pudiera ser publicado. Gracias por tus consejos que me has dado. Gracias a Raúl y a Vicky, que me habéis tenido que soportar con diligencia en vuestros veranos, gracias por recordarme lo que es la pasión por aprender. También tengo que agradecer a todos los integrantes de las unidades de citometría y microscopía en las que he pasado tantas horas, gracias a todos los que habéis hecho que mi trabajo fuera un poco más sencillo.

Siempre guardaré en el corazón a todas las personas que he conocido en el laboratorio, ha sido una etapa dura y ellos han estado siempre ahí. Mi personalidad y mis objetivos en la vida han cambiado mucho desde el primer día que entré en el CNIC, ellos me han acompañado en este cambio y me han apoyado cuando me ha hecho falta. Gracias de vedad.

Hace unos años al casarme empecé una nueva familia y extendí la que ya tenía. Ellos me han acogido como si fuera un hijo y un hermano desde el principio. Gracias por darme tanto cariño y por dejarme formar parte de vuestras vidas. Sois una familia transparente y humilde y me encanta formar parte de ella. Gracias Juan padre por transmitirme tu sentido de la responsabilidad y por tu empeño y dedicación al trabajo. Gracias por valorarme y hacerme sentir parte de tu círculo. No puedo olvidar agradecerte que me invitaras aquel verano al barco, hoy no estaría aquí de no ser por eso. Muchas gracias Eleni, porque de verdad me he sentido como un hijo. Desprendes genialidad y felicidad, gracias por regalar tanta positividad y alegría, eres indispensable. Gracias a la Abuela por todo el cariño que me da y por toda la vitalidad y energía que trasmite cada día. Gracias a Juan hijo por hacerme sentir uno más, por

contar conmigo siempre, por valorarme y por hacérmelo pasar tan bien y conseguir sacarme una carcajada a la mínima de cambio.

Si alguien ha podido influir en mi sin duda alguna ha sido mi familia, ellos me han acompañado desde que tengo uso de razón y han forjado mi carácter. Gracias a mi tito Aure, posiblemente la persona más buena de corazón que conoceré, él lo daría todo por el resto, un ejemplo de amor y devoción por sus padres. Gracias a mi tío Jose, por confiar tanto en mí, él siempre dijo que yo sería un gran científico, espero que este logro académico le haga sentir que me acerqué un poco a sus predicciones. Gracias a mi abuelita María y a mi abuelo Antonio que tanto me han cuidado y querido, que me ha hecho querer ser alguien del que se pudieran sentir orgullosos. Siempre han sido pacientes conmigo y me han querido tal y como era. Gracias también a mi familia de Colombia, a mi Tia Upi por el amor que irradia al mundo, a mi tía Vicky por su carácter afable y cariñoso. Por supuesto a mi abuelo Hoover y a mi abuela Estrella, os he sentido muy cerca aunque tanto tiempo hayamos estado tan lejos. Si algo me ha enseñado mi abuelo, hombre de muchas virtudes, es el saber estar, la corrección y la elegancia. Gracias a mi abuela estrella por enseñarme a contar cuentos y el sentido de la actuación, hoy son de gran ayuda en mi vida profesional.

Dicen que el amor incondicional es el de una madre por su hijo, creo que puede extenderse al de unos abuelos por su nieto. Así lo he sentido de todos ellos, sé que a los que no pueden estar aquí hoy habrían sido felices viéndome delante del atril defendiendo mi tesis. A ellos se lo dedico.

Para acabar tengo que agradecer especialmente a mis padres y a mi hermana. Gracias a mi padre Antonio por ser un rol de vida, por ser un ejemplo de rectitud y bondad. Gracias por enseñarme a ser un hombre de bien y por darme los valores y principios morales que a día de hoy rigen mi vida. Gracias por enseñarme a llevar los problemas con estoicismo y valentía, siempre con una sonrisa y una buena actitud. También te agradezco profundamente haberme dado la oportunidad de elegir con total libertad lo que quería hacer en mi vida adulta. Sin duda esto es lo que me ha permitido estar hoy escribiendo una tesis doctoral.

Gracias a mi madre Cristina por enseñarme el valor de la ternura y el cuidado. Por escucharme incansablemente, por entenderme y por apoyarme sin condición en todos los proyectos que he tomado. Gracias por confiar en mí desde niño y por darme autonomía para tomar mis decisiones y equivocarme. Porque es desde el fallo desde donde se crea la experiencia y se crece. Gracias por enseñarme a no tener vergüenza y a hacer las cosas simplemente porque quiero sin preocuparme por los juicios de otras personas. Gracias por

inculcarme que para conseguir un objetivo hay que estar dispuesto a hacer sacrificios y que se requiere trabajo duro. Estas enseñanzas que todavía a día de hoy recibo me han ayudado a terminar este proyecto. Por último gracias por enseñarme junto a Papi la importancia de la familia. Ambos sois un ejemplo a seguir en todos los sentidos y siempre me he sentido muy orgulloso de vosotros. No me imagino una familia mejor en la que haber nacido.

Mencionaba en el inicio como pequeños cambios pueden transformar la vida de las personas, el día que mis padres decidieron tener a mi hermana Carol cambió mi mundo, ya nunca más iba a estar solo. No me imagino mi vida sin ella, ha estado siempre a mi lado y sé que estará hasta el último día, porque la familia es lo que siempre queda. Es difícil enumerar todas las razones por las que estoy agradecido, supongo que su mera existencia ya transformó para bien mi vida. En primer lugar gracias por ser mi mejor amiga, por todos los buenos momentos que hemos pasado juntos. Gracias por despertar mi vena sentimental y artística, gracias por enseñarme a no tener miedo a derramar lágrimas, pues más de una vez ha ocurrido durante esta tesis. Por supuesto un agradecimiento especial por haber diseñado la portada de la tesis donde como en el Renacimiento ciencia y arte han quedado integradas.

Como dice Paco, para ser un buen científico hay que ser primero una buena persona. Si hoy soy una buena persona es gracias a mis padres y mi hermana. Nunca podré agradecer suficiente todo lo que me habéis dado. Espero poder hacerlo tan bien con mis hijos como vosotros lo habéis hecho con nosotros.

En último lugar, no por casualidad, si no siguiendo el orden en las autorías de los trabajos científicos, está Mery, mi amiga, mi mujer y compañera de vida, mi mitad, mi aliento para seguir adelante y mi bastón cuando tropiezo. Ella es mi roca en medio de la tempestad, la única cosa que sé que no me fallará cuando todo el resto falle. Ella me ha levantado cada vez que me he caído con un simple: “Tu puedes, confío en ti”.

Si algo me ha enseñado Mery es que no podemos dejar de hacer cosas por lo que pueda ocurrir, a la gente le paraliza el miedo cuando tienen que tomar decisiones y arriesgar. Mery es un claro ejemplo de lo contrario. Ella me ha enseñado que solo cuando vamos más allá de nuestros límites del confort es cuando podemos desarrollarnos a nivel personal y crecer. Si nosotros no hubiéramos salido de esa zona de confort yo no sería el mismo y ella no estaría a mi lado. Como decía al principio son justo esas pequeñas acciones las que pueden cambiar por completo el transcurso de una o más vidas.

Mery me inspira a ser mejor en todos los ámbitos cada día, junto a ella aprendo cosas nuevas todos los días, quiero ayudar a los demás y ser mejor persona. Me contagia de felicidad y positividad. Me da energía y fuerzas para afrontar lo que sea, no importa que. Siento un profundo respeto y admiración por ti Mery. Sin ti no habría podido llegar al final gracias por regalarme tus fuerzas.

Por último ella me ha dado la oportunidad de crear una familia, uno de mis mayores deseos en la vida. Hace unos meses mi hijo Lucas, Luke para los amigos, llegó cual terremoto. Desde antes de nacer ha sido un gran motor de cambio y de crecimiento personal. El me inspira a querer ser mejor persona y padre cada día. Me conformaría con poder aportarle lo mismo que mi familia me ha dado a mí. Quizás en unos años lea esta tesis y espero que se sienta orgulloso de su padre. Muchas gracias hijo por adelantado por todo lo que me vas a dar.

Resumen

Las respuestas inmunitarias específicas frente a patógenos requieren de la interacción inicial de una célula T con una célula presentadora de antígeno (CPA), concretamente las células dendríticas (CD). El reconocimiento por parte de la célula T de un antígeno unido al complejo mayor de histocompatibilidad (CMH) conduce a la formación de una unión intercelular estable conocida como sinapsis inmune (SI). En las células T, la SI implica una importante redistribución del citoesqueleto y de los receptores asociados a membrana. También conlleva una polarización del tráfico intracelular y de los orgánulos secretores. La sinapsis inmune es una estructura adecuada para una comunicación intercelular eficiente. Durante este proceso las células T y las CD intercambian numerosas moléculas, incluyendo citoquinas, receptores de membrana aislados, moléculas de señalización y material genético. Las vesículas extracelulares (VE) son uno de los mecanismos que median la transferencia de información entre la célula T y las CD. Los cuerpos apoptóticos, los ectosomas y los exosomas son las principales vesículas extracelulares. Los exosomas se distinguen por su origen endocítico puesto que se forman por la invaginación de la membrana de los cuerpos multivesiculares (CMV) o endosomas tardíos. Cuando los CMV fusionan con la membrana liberan estas vesículas al medio. Los exosomas están particularmente enriquecidos en material genético; principalmente ARN, como los ARN pequeños y los ARN largos no codificantes, también se ha detectado presencia de ADN genómico. Esto los hace versátiles mediadores en la comunicación intercelular. No obstante, todavía queda mucho por explorar en los mecanismos de cómo el material genético contenido en los exosomas induce respuestas específicas en las células receptoras.

En este trabajo hemos demostrado que las células T secretan VE cargadas de proteínas y ADN mitocondrial (ADNmt) que pueden ser transferidas a las CD a través de la sinapsis inmune. Evidenciamos que algunas proteínas de origen mitocondrial y el ADNmt se encuentran en los cuerpos multivesiculares y que el bloqueo de la secreción de exosomas altera la función y morfología mitocondrial, lo que sugiere que la liberación de contenido mitocondrial mediado por los exosomas contribuye a la homeostasis mitocondrial. También demostramos que tanto las proteínas mitocondriales como el ADNmt se transfieren durante la SI de forma unidireccional desde la célula T a la CPA y que esta transferencia pre-activa a las células dendríticas protegiéndolas en infecciones virales posteriores. En conclusión, los datos resultantes ilustran un nuevo mecanismo por el cual las células T promueven un estado de alerta en las células dendríticas promovido por la transferencia exosomal de ADN. Estos hallazgos aportan información relevante sobre cómo la comunicación recíproca entre las células del sistema inmune innato y del sistema inmune adaptativo facilita respuestas más eficaces frente a patógenos.

Summary

The generation of a specific immune response against a pathogen requires the initial interaction of an antigen-specific T cell with antigen-presenting cells (APCs), specifically dendritic cells (DCs). T cell recognition of major histocompatibility complex (MHC) bound to antigens leads to the formation of a stable intercellular junction between the cells, the immune synapse (IS). In T cells the IS involves a redistribution of membrane-associated receptors, the cytoskeleton, and the polarization of intracellular trafficking and secretory organelles. The transfer of bioactive molecules from the T cell to the DC through the IS constitutes a main vehicle of intercellular communication. T cells and DCs exchange numerous molecules, including cytokines, membrane receptors, membrane patches, signaling molecules or genetic material (mainly functional microRNAs) during IS formation. Extracellular vesicles are one of the cellular mechanisms mediating information transfer between the T cell and the DCs. EVs comprise apoptotic bodies, ectosomes or microvesicles, and exosomes. Exosomes are distinguished by their unique endocytic origin. Exosomes form by invagination of the multivesicular body (MVB) membrane and are released to the extracellular medium upon the fusion of the MVB with the plasma membrane. Exosomes are particularly enriched in genetic material, mostly RNA species such as small RNAs and long non-coding RNAs, as well as DNA. This makes them attractive candidates to mediate cell-to-cell communication. However, the ability of the genetic material contained within exosomes to evoke immune signaling responses in recipient cells is largely unexplored.

Our data show that T cells secrete extracellular vesicles containing mitochondrial DNA (mtDNA) and mitochondrial proteins that can be transfer to the APC through cognate interactions. We provide evidence that mtDNA and related proteins segregate into MVB pathway. Blockage of exosome secretion alters mitochondrial function and morphology which suggests that release of mitochondrial content loaded into exosomes contributes to mitochondrial homeostasis. In addition, we demonstrate that both mitochondrial proteins and mtDNA are transferred during IS in a unidirectional way from the T cell to the APC.

Finally, our results show that T cells prime DCs through the transfer of exosomal DNA, supporting a specific role for antigen-dependent contacts in conferring protection to DCs against subsequent viral infections. In conclusion, our data illustrate a way by which T cells promote an alert state in DCs that protects them against posterior infection driven by the vesicular transfer of DNA. These findings shed new light on how the reciprocal communication between innate and adaptive immune cells allow efficacious responses to unknown threats.

Index

Index

List of Abbreviations

List of Abbreviations

8-OHdG	8-hydroxy-2' -deoxyguanosine
ADAP	adhesion and degranulation promoting adapter protein
APC	Antigen presenting cells
ATAD3	ATPase family AAA domain-containing protein 3
BCR	B Cell Receptor
BMDC	Bone marrow-derived dendritic cells
ChIP	Chromatin Immunoprecipitation
COX1	Human Complex IV subunit I
cSMAC	Central supramolecular activation cluster
CTVT	Transmissible canine venereal tumor
Cx43	Connexin 43
DAG	Diacylglycerol
DAMPs	Damage-associated molecular pattern
DC	Dendritic cells
EE	Early endosome
ER	Endoplasmic Reticulum
ESCRT	Endosomal sorting complex required for transport
EV	Extracellular Vesicles
FCCP	carbonilcyanide p-triflouromethoxyphenylhydrazone
GO	Gene Ontology
GTPase	guanosine triphosphate hydrolase
HGT	Horizontal gene transfer
Hrs	Hepatocyte growth factor-regulated tyrosine kinase substrate
ICAM-1	Intercellular Adhesion Molecule 1
IFNγ	Interferon gamma
ILV	Intraluminal vesicles
IP3	Inositol trisphosphate
IRF3	Interferon regulatory factor 3
IS	Immune Synapse
ISEV	International Society of Extracellular Vesicles
ISG	Interferon-stimulated gene
LBPA	Lysobisphosphatidic Acid
Lck	lymphocyte-specific protein tyrosine kinase
LE	Late endosome
LFA-1	Lymphocyte function-associated antigen 1
MDV	Mitochondrial derived vesicle
MERCs	Mitochondria and endoplasmic reticulum contact sites
MHC	Major histocompatibility complex
miRNA	micro RNA

MSC	Mesenchymal stem cells
mtDNA	mitochondrial DNA
mtExo	mitochondrial-containing extracellular vesicles
MTOC	Microtubule-organizing center
MVB	Multivesicular Bodies
NF-κB	nuclear factor κB
NFPs	N-formyl peptides
NMII	non-muscle myosin
nPKC	Protein kinase C isoforms
nSMase2	neutral sphingomyelinase 2
OXPHOS	oxidative phosphorylation
PA	Phosphatidic acid
PAMPs	Pathogen-associated molecular patterns
PC	Phosphatidylcholine
PCR	Polymerase chain reaction
PIP2	Phosphatidylinositol 4,5 bisphosphate
PKC- ε	Protein kinase C epsilon
PKC- η	Protein kinase C eta
PKC- θ	Protein kinase C theta
PLCγ1	Phospholipase C, gamma 1
PLD	Phospholipase D
PLP	Proteolipid
pMHC	peptide-bound MHC
pSMAC	Peripheral supramolecular activation cluster
RLC	Regulatory light chain
ROS	Reactive oxygen species
S1P	sphingosine 1-phosphate
SEE	Staphylococcal enterotoxin superantigen E
SMS2	Sphingomyelin Synthase 2
SphK2	sphingosine kinase 2
SSBP1	Single-stranded DNA-binding protein
StingGt/Gt	Sting deficient mice
TCR	T cell surface receptor
TEM	Tetraspanin-enriched domains
Tfam	Mitochondrial transcription Factor A
TIRF	Total internal reflection fluorescence
TLR	Toll-like receptor
TNTs	Tunneling nanotubes
Tsg101	tumor susceptibility gene
WB	Western Blot

Introduction

Introduction

The immune system is a highly specialized compartment that protects individuals against pathogens and external threats. Immune responses act through cell-based mechanisms to protect the organism against self and non-self menaces. When fighting against pathogens, two different branches of immune populations are involved: innate and adaptive. Innate and adaptive immunity components are independent and derive from different lineages. Innate subset is the first barrier of defense and it is specialized in responding against conserved types of molecules that are common to many pathogens, called pathogen-associated molecular patterns (PAMPs). The adaptive subset mounts a specific response to a particular antigen of a pathogen; by contrast with the innate response, the adaptive is slower and requires activation, clonal selection and expansion. Adaptive immunity is responsible for the generation of memory cells that will reactivate and respond faster upon reinfection. In order to trigger a strong and coordinated response against pathogens, the collaboration between both compartments is essential.

The adaptive compartment is formed mainly of B cells, mediators of the humoral immunity and T cells, mediators of the cellular immunity. Both cell types express cell surface receptors that allow them to recognize the antigens. B cells express the BCR (B Cell Receptor) and T cells express the TCR (T cell surface receptor). The TCR can recognize specific, processed peptides on the context of the major histocompatibility complex (pMHC) molecules. All nucleated cells express MHC class I (MHC-I) molecules bound to self-antigens on their surfaces and T cells are trained to tolerate them. In case of infection, cells present pathogenic antigens bound to MHC-I molecules and specialized cyototoxic CD8 T cells recognize with avidity the complex and terminate the presenting cell through cytolysis. On the other hand, professional antigen presenting cells (APC; such as dendritic cells) from the innate compartment express not only MHC-I but also MHC-II, which presents processed antigens from phagocyted proteins. CD4 T cells can recognize pathogenic peptides presented on the context of MHC-II and mount a specific response against them. Moreover, APCs are able to cross-present phagocyted antigens in MHC class I and activate CD8 responses [1].

In this context, the intercommunication between the adaptive and the innate compartments is evident. Adaptive T cells receive input from innate cells, e.g. dendritic cells, through well-delineated cell-cell contacts, appropriately known as Immune Synapses (IS).

1. The Immune Synapse

The cognate interaction between lymphocytes and APCs is performed through a highly specialized structure called the IS. The IS acts as a platform for intercellular communication; signals coming from this close interaction can modulate the final outcome of cells involved. Even though IS only covers around 20% of a T cell surface when stabilized, it involves an important rearrangement of proteins and organelles in both cell sides [2]. The formation of the IS requires the close contact of the T cell membrane and the APC membrane. Recognition of an antigenic peptide-bound MHC (pMHC) by the T cell receptor (TCR) induces IS stabilization. Other adhesive contacts contribute to the stabilization of the IS, e.g. integrin adhesion receptors and co-stimulatory receptors, such as CD2 or CD28 [3].

TCR receptors appear in the microvilli of resting T cells, enabling them to scan the surface of the APC in rapidly occurring cell contacts **(Figure I1 A)** [4,5]. Once the peptide is recognized, the area of contact is immediately enlarged, allowing firm adhesion through LFA-1 and ICAM-1 interaction. ICAM-1 rapidly accumulates at the interface between the T cell and the APC upon antigen recognition **(Figure I1 B)** [6]. This interaction and the conformation of LFA-1 is relevant to organize the actin cytoskeleton underneath the plasma membrane, which sustains cell-cell contacts[7,8].

The mechanisms that trigger TCR activation and accumulation at the IS include conformational changes in the αβTCR and associated CD3 complex (TCR/CD3); aggregation of receptors forming nano- and micro-clusters; and segregation by spatial constrictions through binding of partner receptors in cis and trans, cytoskeletal connections or by ectodomain-size spatial exclusion [9].

Receptors have been proposed to move through the T cell surface by passive lateral diffusion or directional actin dynamics once the TCR recognizes the pMHC. The ability of the actin cytoskeleton to cluster different receptors enables T cell activation upon engagement of low affinity TCRs by a few MHC complexes [10]. However, the possibility of TCR signaling without IS rearrangement makes clear that TCR signaling precedes the formation of the IS [11] **(Figure I1 B)**.

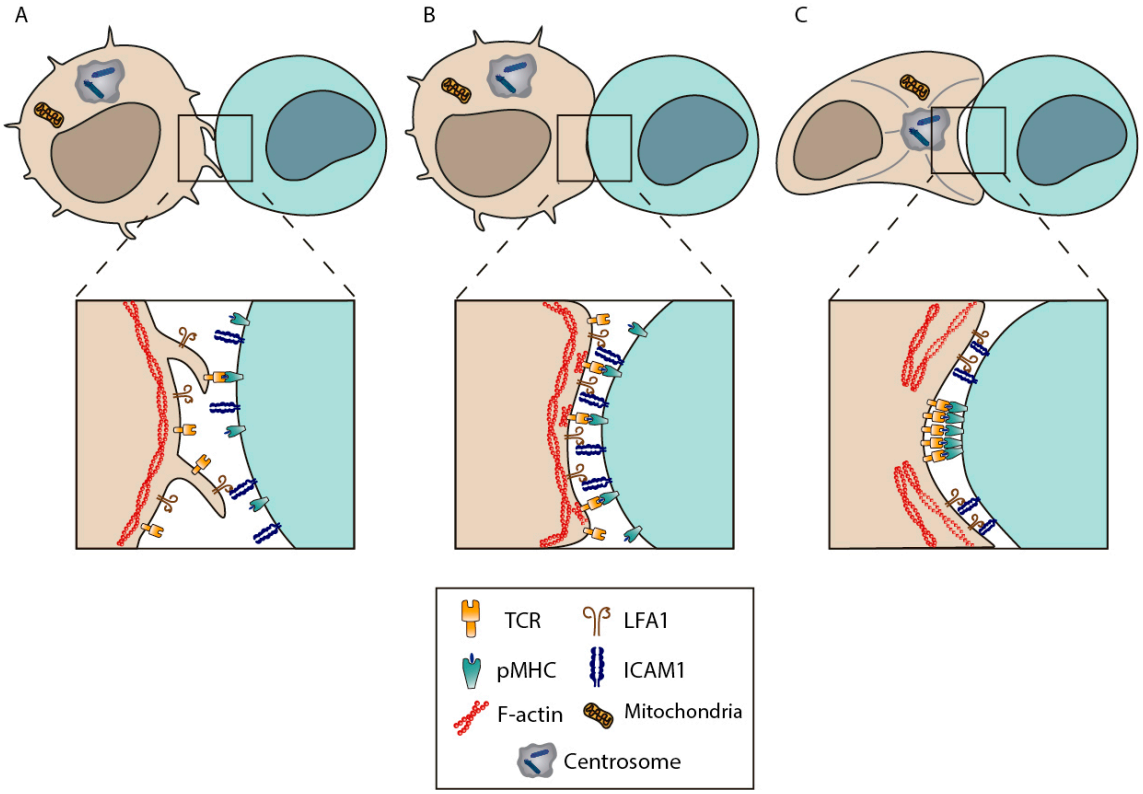

Figure I1. Establishment of an immune synapse. A) The initial interactions between a T cell (left) and an antigen-presenting cell (APC, right) involve the contact of microvilli formed on the surface of the T cell with the APC surface. Integrins such as LFA-1 may contact their ligands (mainly ICAM-1) on the APC. **B)** TCR complexes on the microvilli will engage with antigen-MHC complexes on the APC upon antigen is recognition; the contact expands through the surface of the T-APC. The interaction between LFA-1 and ICAM-1 will be reinforced by TCR signaling, apposing together the T cell and the APC. **C)** Mature immune synapse; receptors will reorganize in different regions directed by the cytoskeleton dynamics, which also shows a polarized distribution.

TCR/CD3 is translocated into specific lipid rafts where it is activated by Lck [12]. TCR in lipid rafts engage with pMHC complexes; if these interactions are productive, TCR microclusters and their associated molecules migrate from the periphery to the center of the IS [13], shaping the so-called central supramolecular activation cluster (cSMAC) where receptors are internalized and recycled [14,15]. This movement is coupled to the retrograde flow of the F-actin [15], the contraction of actomyosin-II arcs [16], and the presence of myosin IIA [17].

On the other hand, classic adhesion molecules maintain the interaction between cells forming the peripheral SMAC (pSMAC), which is highly enriched in integrins such as LFA-1 and ICAM-1 on the T cell and APC respectively **(Figure I1 C)** [3,18]. In this regard, the number of pMHC needed for TCR activation may be as small as one [19]. The formation of clusters of MHC-II and ICAM-1 on the APC helps the localization of TCR and LFA-1 at the T cell side of the IS, respectively, decreasing by 100-fold the threshold of TCR activation and shaping the IS properly [20–22].

The minimal duration of interactions to elicit a proper T cell response is still under debate; however, the establishment of a classical immune synapse does not seem to be essential for a durable interaction, as a dynamic kinapse would be sufficient to activate the T cell [23]. Formation of the SMACs is not specifically needed to observe full T cell activation, but the organized shape of the IS improves signaling by positioning properly the different components at the IS, such as receptors, cytoskeleton and organelles [24,25].

1.1 Organelle polarization in T cell during the Immune Synapse

The reorganization of the cytoskeleton is essential to control the dynamic polarity of organelles and the cell shape at the IS. Actin and Tubulin cytoskeleton act coordinately in order to distribute properly organelles and receptors[25]. Actin cytoskeleton rearranges sequentially underneath the immunological synapse upon TCR activation. It includes the whole cell cytoskeleton and not only the cortical actin beneath the membranes [26]. F-actin plays a role in the distribution of receptors and integrins, and it also controls the proper fusion and secretion of the vesicles at the cSMAC [27]. On the other hand, microtubules relocate the required cellular compartments to the immune synapse, therefore guiding vesicles and organelle movement. Tubulin cytoskeleton rearrangement relies on the polarization of the T cell centrosome, a microtubule-organizing center (MTOC) [28].

The polarization of the MTOC to the immune synapse enables the translocation of specific organelles and the directional secretion towards the antigen-presenting cell [29–31].

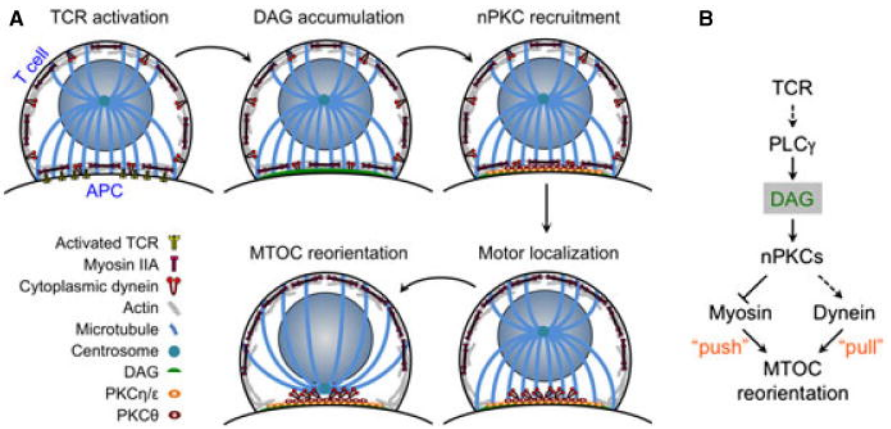

Figure I2. Mechanisms of MTOC reorientation to the IS. A) Upon TCR activation, DAG accumulates at the synaptic surface. DAG recruits nPKC which leads to the polarization of the MTOC through Myosin and Dynein motors. **B)** Schematic diagram of MTOC polarization towards the IS surface, solid arrows denote direct connections, and dotted arrows denote either indirect or multistep connections. Figure from Huse et al. 2015 [32].

CD3 phosphorylation by Lck, activates a downstream cascade[33,34] that ends in the recruitment of PLCγ1 into the cSMAC [25,35]. PLCγ1 hydrolyzes phosphatidylinositol 4,5 bisphosphate (PIP2) into inositol trisphosphate (IP3) and diacylglycerol (DAG). DAG accumulates preferentially at the center of the immune synapse [36]. Centrosomal movement is thus guided by a gradient of diacylglycerol at the IS **(Figure I2)** [37]. MTOC translocation by a DAG gradient is partially explained by the recruitment of different PKC isoforms containing DAG-specific C1 domains. Specifically, PKC-ε and PKC-η, which have redundant recruitment functions, accumulate in a broad area of the membrane. PKC-θ is also required for MTOC reorientation and is synergistically recruited with DAG [38]. Motor proteins are involved in MTOC reorientation. Hence, dynein reorients the MTOC during cognate interaction as it moves along the microtubules from the plus end to the minus end. It accumulates at the immune synapse together with ADAP, therefore connecting the motor to LFA-1 clusters [39]. Impairment of dynein-dynactin complex activity inhibits MTOC translocation after TCR antigen priming [28]. PKC isoenzymes also shape the positioning of non-muscle myosin (NMII) through direct phosphorylation of the regulatory light chain (RLC), which forms clusters behind the MTOC and probably pushes it from behind while dynein would pull from the center of the synaptic region, to move the MTOC [40].

The secretory machinery orientates towards the immune synapse in the T cell. Two main intracellular pathways have been described: the Golgi apparatus-Endoplasmic Reticulum (ER) secretory pathway and the endolysosomal system **(Figure I3)**.

1.2 Polarization of secretory machinery: the Golgi-ER pathway

The Golgi-ER secretory pathway is guided towards the synaptic cleft [28,29,41–44], providing directionality to the secretion of some cytokines and signaling mediators. Specifically, IL4 is preferentially secreted by CD4 T cells towards the site of activation [45] and it accumulates at the site of T-B cell synapse together with IL5, IL2 and Interferon γ (IFNγ) after 24 h **(Figure I3-1)** [31]. In the Golgi-ER secretory pathway, the CD3-TCR complexes are synthetized and retained, which conforms a TCR reservoir ready to be released and engaged to induce activation. These complexes assemble properly and progress through the secretory pathway; the vesicles containing these complexes fuse with the plasma membrane and TCR/CD3 complexes form microclusters and traffic continuously between plasma membrane and endosomes in rapid cycles and can be eventually degraded by lysosomal fusion **(Figure I3-2)** [46] .

As previously mentioned the second secretory pathway polarized towards the immune synapse is the endolysosomal system; specifically, receptors and proteins from the membrane are endocytosed and recycled. TCR signaling and function not only depend on its expression but also on its membrane localization and the dynamics of TCR-CD3 complex, including its recycling into vesicles. The degradation of the TCR is important for synapse termination and its downstream signaling. Upon TCR engagement, endosomal trafficking is redirected towards the immune synapse by microtubules and endosomal traffic regulators such as vesicle transport proteins, docking proteins, and fusion regulatory molecules [47–51]. TCR activation triggers its rapid uptake through a clathrin-dependent pathway, and it is then incorporated into a flotillin-positive endocytic network, which is essential for the correct recycling of the TCR to the membrane again [52]. A complex framework of endosomal vesicles fine-tunes the T cell response beneath the synaptic cleft membrane, by exposing, hiding or degrading receptors and signaling molecules **(Figure I3-3)**.

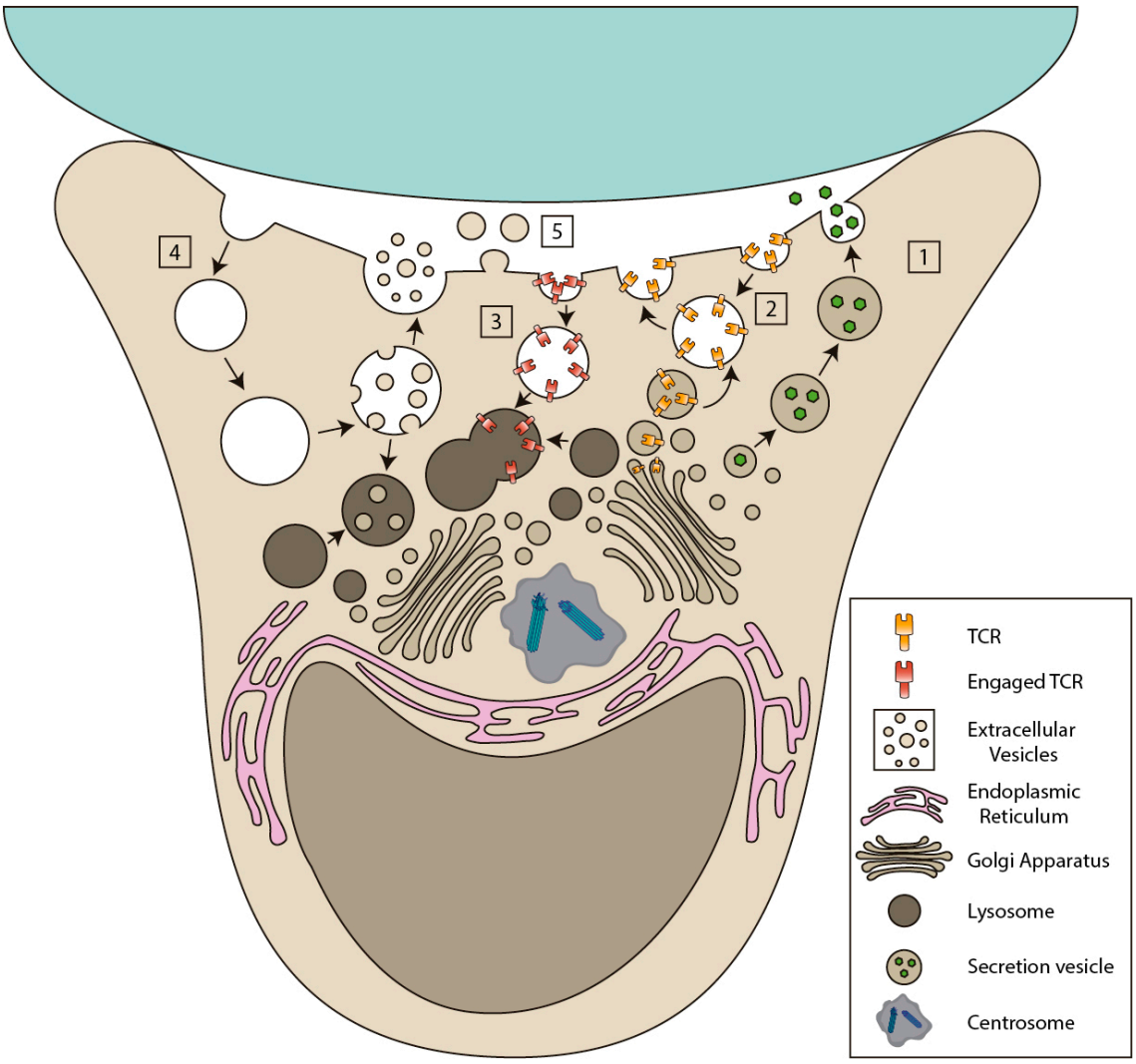

Figure I3. The secretory and recycling pathways at the Immune Synapse. The secretory machinery of the T cell is actively polarized towards the T cell-APC contact by the movement of the centrosome and the coordinated action of molecular motors. (1) The ER-Golgi dependent pathways direct their vesicles towards the immune synapse to deliver newly synthetized adhesion and signaling receptors and soluble mediators such as chemokines and cytokines. (2) TCR-CD3 complexes (orange) cycle between membrane and endosomes in a steadystate loop. Some CD3-TCR complexes are synthetized in excess and retained in the Golgi (3) T Cell Receptor molecules (red) are internalized at the central area of the T cell-APC contact; they can be degraded or recycled through the endolysosomal pathway. (4) Multivesicular bodies (MVB) are formed from the endosomes, through specific sorting of their components. MVB can deliver their content into the immune synapse cleft, as extracellular vesicles (i.e.: exosomes) or soluble components. Viruses can use this pathway to spread into APCs. (5) Ectosomes can be formed, excised and released from the plasma membrane to the IS cleft.

1.3 Polarization of multivesicular bodies and exosomes biogenesis

Another level of complexity includes the role of late endosomes (LE), also called multivesicular bodies (MVB). These organelles are enriched in specific proteins and may form part of the cell recycling system by fusing with lysosomes to degrade their content. On the other hand, they can also serve as secretory organelles, by fusing with the plasma membrane and releasing its content to the extracellular media [53,54]. In T cells, MVB reorient towards the immune synapse and release there their content [55,56].

MVB are part of the endolysosomal system. Upon endocytosis early endosomes (EE) are formed and these vesicles can be recycled back to the plasma membrane either by direct fusion or through the recycling of the endosome compartment. Proteins from EE can also be sorted into vesicles that maturate into MVB/LE [57]. There is a specific selection of proteins that progress through the maturation of the endosomes and protein cargo composition can vary along the maturation process. Cytosolic proteins associate with endosomes and define its function and destiny. Rab5 associates in the first steps of EE formation[58] and it is the main regulator of the conversion to LE. A crucial step for endosome maturation is the Rab5/Rab7 switch; Rab5 recruits Rab7 to the EE and it is replaced by this GTPase which assumes its functions of protein recruitment and fusion with other LE[59]. Absence of Rab7 activity results in loss of lysosomal acidification and functionality, dispersal of endosomes and a block in cargo trafficking to the lysosomes [60]. On the other hand, Rab7 constitutively active mutant (Rab7Q67L) expression leads to the fusion of LE and the formation of larger vesicles that are not restricted to the perinuclear area [61].

Endosomes are motile organelles that change their subcellular localization along its maturation process and function. The number, size and intracellular position of endosomes are not determined randomly but are tightly regulated [62]. The flux of maturation is a centripetal movement; it goes from the cell periphery to the perinuclear area, where the majority of lysosomes are localized **(Figure I4)**. The motor proteins responsible for endosomal trafficking along microtubules are dynein and kinesin [63–67]. Endosomes can directly interact with motor proteins or by its indirect binding mediated by dynactin acting as a scaffold which depends on Rab7 activity[68,69].

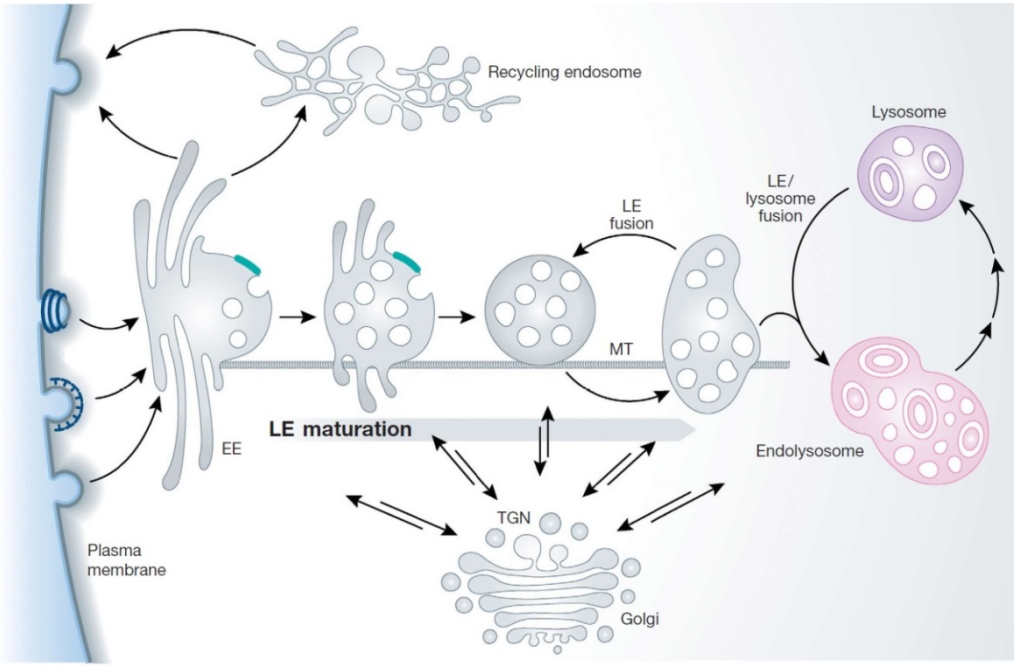

Figure I4. Endolysosomal system. Early endosomes (EE) are formed by the invagination of the plasma membrane. Proteins from EE can cycle back directly to the plasma membrane or through recycling endosomes. Early endosome maturate into late endosomes (LE)/MVB. These vesicles move towards the perinuclear space along microtubules (MT). This compartment combines endocytosed cargo with newly synthetized proteins from the Trans Golgi Network (TGN). They also load proteins from the cytoplasm through the ESCRT complex. Finally LE/MVB can either fuse with lysosomes and degrade their content or fuse back with the plasma membrane and release their content to the extracellular media. Figure from Houtari and Helenius 2011 [57].

During the process of endosome maturation there is bidirectional traffic between the endosomes and the Golgi apparatus, newly synthetized proteins such as hydrolases feeds the system and end up in the lysosomes maintaining their activity, function and localization **(Figure I4)** [60,70]. In addition, cytoplasmic material can be selectively incorporated into endosomes through the invagination of the endosomal membrane, generating intraluminal vesicles (ILV)[71]. ILVs are small vesicles that are confined inside of MVB, that range between 50-100nm of diameter and that are enriched in proteins and genetic material. It has been proposed that ILV can be formed by different mechanisms, therefore coexisting in the same MVB compartment ILV coming from different origins with different protein and lipid composition. There are three models proposed for endosomal membrane invagination and ILV constitution: the Endosomal Sorting Complex for Transport (ESCRT) proteins machinery, the lipid dependent invagination and the tetraspanin mediated mechanism **(Figure I5)** [72].

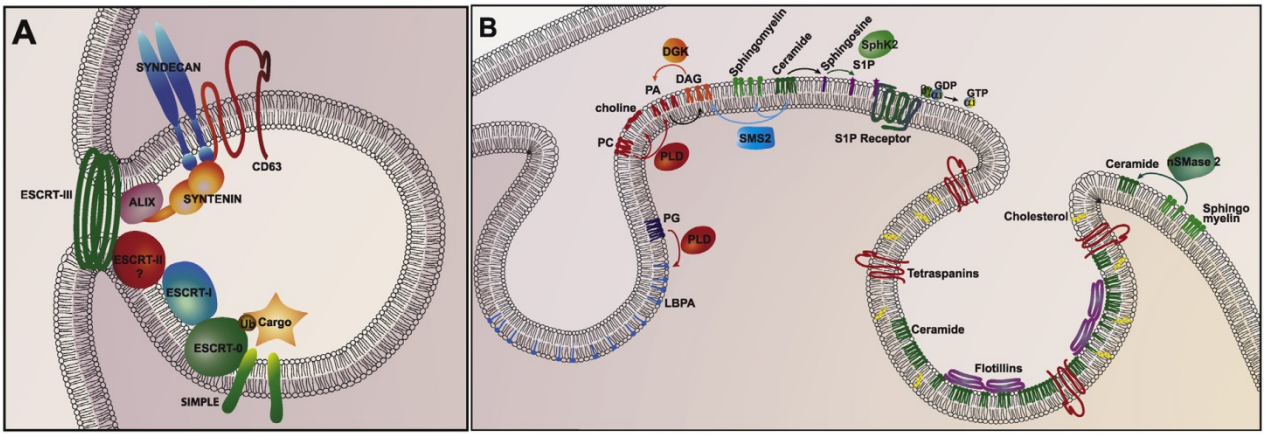

Figure I5. Proposed mechanisms for endosomal membrane invagination. A) ESCRT proteins control the sorting of ubiquitinated proteins into ILV. Syntenin and syndecan are also involved in the ESCRT dependent mechanism [73]. B) Tetraspanin dependent mechanism; CD81, CD9 and CD63 are involved in the formation of ESCRT independent formation of ILV. Lipid-mediated ILV synthesis depends on lipid composition (DAG, S1P, PA, PC, LBPA) and lipid-related enzymes (nSMase2, S1P receptors, SphK2, SMS2, PLD). Modified from Villarroya et al 2014 [72].

The ESCRT recruit other ubiquitinated partner proteins during this process and determine the sorting of different components to ILVs [74]. ESCRT machinery consists in four different protein complexes; ESCRT-0, ESCRT-I, ESCRT-II, ESCRT-III and the Vps4 AAA-ATPase complex [72,75]. Early-endosome-associated proteins such as Hrs (ESCRT-0) recruits ESCRT-I proteins [76] and ubiquitinated proteins [77] to clathrin-coated microdomains of EE which leads to ILV formation. Nevertheless, it is in the late endosome where most of the ILV are formed. Tsg101 is an ESCRT-I protein that has a central role in LE endosome structure, maturation and ILV generation. ESCRT-0/I proteins recruit ESCRT II which in turn recruits and activates ESCRT-III together with the adaptor protein Alix which stabilizes the complex. The energy for bud abscission is provided by the ATPase Vps4 **(Figure I5A)** [78,79].

Membrane-lipid composition is also important for the proper formation of MVB and ILV. Proteolipid (PLP)-containing exosomes are enriched in ceramide and their secretion is not dependent on Hrs, Alix or Tsg101 expression. Ceramide synthesis is mediated by the membrane associated protein neutral sphingomyelinase 2 (nSMase2) which controls exosomes secretion in multiple cell models [55,80–82]. Ceramide-mediated membrane bending and ILV formation is explained by the spontaneous aggregation of lipid microdomains. The coalescence of domains induces a negative curvature in the membrane, probably promoted by the cone-shaped structure of ceramide [80]. Lipid composition can also influence the sorting of ILV cargo and MVB maturation in an ESCRT-independent manner. Gi-coupled sphingosine 1-phosphate

(S1P) receptor is present on endosomal membranes and its sustained activation controls exosomal maturation and cargo sorting through the formation of F-actin networks [83,84]. In addition, sphingosine kinase 2 (SphK2) absence decreases exosomes secretion and cargo loading [83,85] **(Figure I5B)**.

Tetraspanins are highly enriched in ILV membranes, in contrast with other proteins from the MVB such as Lamp1 and Lamp2 [86]. The differential distribution of membrane proteins indicates that it has to be driven by active protein sorting. Tetraspanins form tetraspanin-enriched domains (TEM) and organized membrane dynamics through its association with other transmembrane and cytosolic proteins and lipids[87]. Therefore, tetraspanins are able to influence the cargo sorting; CD9 tetraspanin controls the loading of CD10 metalloproteinase in exososomes by the interaction with its cytoplasmic domain. CD63 tetraspanin controls in melanosomes the loading of PMEL into ILV in an ESCRT independent manner [88,89] **(Figure I5B)**.

Some of these mechanisms described as independent, under physiological conditions, are likely to interact and cooperate producing a mixed population of ILV [72]. For example the deficiency in ESCRT proteins Hrs and Tsg101 decreases the secretion of exosomes containing CD63 and CD81 [90], but still allows MVB to be formed [91]. In addition, the secretion of CD63-positive exosomes from T cells is ceramide-dependent; therefore nSMase2 activity directly affects tetraspanin-containing exosome synthesis [55]. Finally, blockage of an ILV formation pathway usually does not completely abrogate the secretion of exosomes [89]. This piece of evidence points out the existence of heterogeneous populations of MVB and ILV and the complexity of studying these vesicles.

As mentioned above, MVB can either fuse with lysosomes and degrade their content or fuse with the plasma membrane and release its content to the extracellular media; released ILV are better known as exosomes. The mechanisms through which MVB take the degradative pathway or the secretory pathway are still elusive, however there are some molecules described essential for MVB secretion. Rab27 is a small GTPase required for the docking of MVB at the plasma membrane. There are two isoforms, Rab27a and Rab27b, that control different steps of MVB localization, docking and fusion, which are therefore crucial in the exosome secretion pathway [92]. ISGylation, an ubiquitin-like modification, has been proposed as regulatory signal for MVB´s fate. Tsg101 ISGylation promotes MVB fusion with lysosomes and subsequent degradation, impairing exosome secretion [93,94]. Likewise, acetylation also impairs protein sorting into ILV competing for Lysines with the ubiquitination [95]. In B lymphocytes, two pools of MVB can be distinguished and only MVB with high cholesterol levels are able to fuse

with the plasma membrane and release exosomes [96]. In polarized cells, exosomes secreted from the apical and basolateral side contain different cargo and composition implying the existence of distinct MVB pools and secretion mechanisms [97–99]. Transport of MVB to the plasma membrane is dependent on cytoskeleton interactions. Cortactin promotes exosome secretion by stabilizing cortical actin-rich MVB docking sites [100]. In the context of the IS, upon antigen recognition the MTOC relocates close to the interacting area. Dynein/dynactin motor proteins move MVB to the minus-end bringing these organelles near to the plasma membrane, therefore facilitating their fusion and release of its ILV to the synaptic cleft [55].

1.3.1 Exosome cargo

Exosomes contain proteins involved in their biogenesis, vesicle trafficking, lipid membrane organization, as well as proteins and adhesion receptors specific of the producing cell. ESCRT proteins and tetraspanins such as CD63, CD9 and CD81 are found in exosomal fractions [74]. ILV lipids are also different from the limiting membrane of the endosome. ILV contain more cholesterol, sphingolipids and BMP/LBPA, therefore, exosomal lipid content differs from that of the secreting cell [101]. Exosomes are particularly enriched in genetic material, mostly RNA species such as small RNAs and long non-coding RNAs, as well as genomic DNA **(Figure I6)** [102–105]. In addition, it has been reported that some cell lines, such as astrocytes, release exosomes containing mitochondrial DNA [106]. This makes them attractive candidates to mediate cell-to-cell communication. However, the ability of the genetic material contained within exosomes to evoke immune signaling responses in recipient cells is largely unexplored.

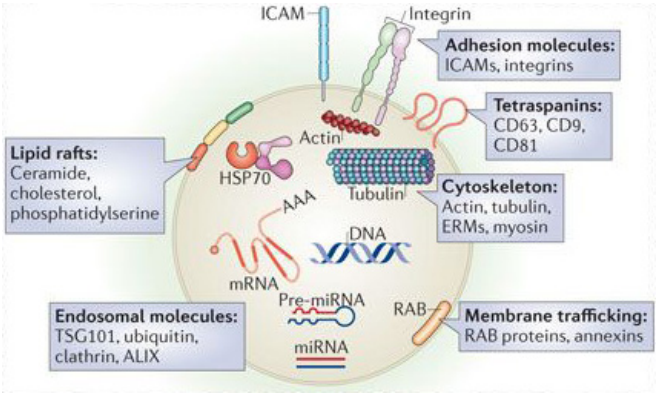

Figure I6. Exosomal components. Lipids present in exosomes include ceramide, cholesterol and phosphatidylserine. Heat shock proteins, actin, tubulin, tetraspanins and proteins from ESCRT complex are usually found in exosomes. Specific repertoires of miRNA and DNA are also loaded in these extracellular vesicles. Figure modified from Mittelbrunn et al 2012 [56]

The specific repertoire of proteins and genetic content in exosomes and its differences in composition with the secreting cell imply the existence of sorting mechanisms that regulate the specific transport of selected RNAs and proteins into the exosomes. Posttranslational modifications are responsible for part of the specificity in cargo sorting [107]. The ESCRT complex is the responsible of sorting ubiquitinated proteins to MVB [108], however, de-ubiquitination is essential for packaging the cargo into the ILV [109]. On the other hand ISGylation tags the proteins for lysosomal degradation and prevents them for being sorted into ILV [94]. Sumoylation also target protein to exosomes [110]. In addition, some miRNA can be sorted into ILV when they are bound to post-translational modified proteins such as sumoylated hnRNPA2B1, which binds specific RNA sequences also called exo-motifs, and transport miRNA to the MVB [111]. Other sequences also target miRNA to MVB. Hence, it has been described an exo-motif that allows the binding of SYNCRIP to the miRNA and sorts it to the MVB in hepatocytes [112]. In addition, miRNA sorting change depending on the cell state proved by exosomal miRNA content variation along cell differentiation and maturation [113]. Another mechanism that could explain miRNA loading is the association of components of miRNA effector complexes and MVB [114], however it is more intriguing the mechanisms of exosomal loading of genomic and mitochondrial DNA since those organelles are separated by several membranes from MVB. It has been proposed that cytosolic DNA could be loaded due to its interaction with DNA binding motifs of connexin43 (Cx43) present in exosomes [115,116]. Although some of the mechanisms for genetic material sorting into exosomes have been reported, this is still an area boasting many outstanding questions to be solved.

Proteins, RNA and DNA contained in exosomes vary depending on cell status and it can provide information about the pathophysiological status of the secreting cell when exosomes were released. In addition, exosomes can be isolated from body fluids such as blood, urine, saliva, etc. Due to the easiness of exosome purification and the great amount of information that researchers can obtain from these extracellular vesicles (EV), exosomes are potentially regarded as non-invasive biomarkers for early diagnostics and prognostic of certain diseases [117–122].

1.3.2 Extracellular vesicle secretion at the Immune Synapse

Almost every cell type secretes a heterogeneous population of vesicles to the extracellular medium in a constitutive manner although cellular stress or activation signals modulate their secretion [72]. The size of those vesicles range from 40-1000 nm, thus the taxonomy and nomenclature of these extracellular vesicles (EV) is still under debate [123].

Nonetheless, they are classically divided into microvesicles, exosomes and apoptotic bodies, depending on their origin, size and molecular composition **(Figure I7)** [124,125].

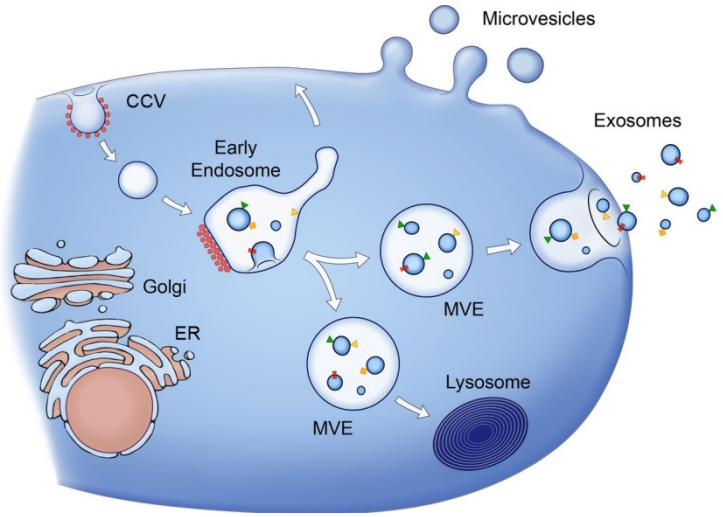

Figure I7. Extracellular vesicle populations. Microvesicles bud directly from the plasma membrane, whereas exosomes have an endocytic origin and are released by fusion of MVBs with the plasma membrane. Figure from Raposo et al 2013 [124]

Immune cells secrete a variety of EVs to the extracellular milieu that can exert diverse immune functions, including antigen presentation, immune activation, induction of tolerance, or suppression of immune responses [126].

At the IS, the MVB external membrane fuses with the plasma membrane to release the ILVs into the synaptic cleft, which are then called exosomes **(Figure I3-4)**. TCR activation can induce the secretion of TCR-TSG101-containing exosomes [127] and lead to proliferation in autologous resting CD8 T cells, acting synergistically with IL2 [128].

These EVs carry proteins and genetic material that are then transferred to recipient cells by using the IS as a focal point for polarized secretion. The uptake of these exosomes facilitates the release of their content into the recipient cells that may modify their behavior. Specifically, the uptake of exosomes loaded with miRNA that are secreted by CD4 T cells in the context of a synapse causes the downregulation of SOX4 in B cells [55]. Viruses (i.e. HIV) are able to hijack the polarized secretory machinery and spread across cells through immune synapses [129,130]. Apart from HIV, other viruses use the exosomal secretory machinery to disseminate [131]. The secretion of larger vesicles that bud directly from plasma membrane, usually called microvesicles or ectosomes has also been described. Upon antigen cognate recognition with the APC, membranes from CD4 T cells start to bud from the cSMAC of the synapse [132] **(Figure I3-5)**. TSG101, located at the cSMAC [133] is the responsible for the sorting of TCR into those EVs, while VPS4, which also belongs to the ESCRT machinery, is the responsible of the scission of the microvesicles from the plasma membrane.

After activation, T cells secrete microvesicles that are loaded with transmembrane-CTLA-4 negative regulator [134]. However, the functional roles of microvesicles containing CTLA-4 needs further investigation.

1.4 Mitochondria reorganization at the Immune Synapse

Mitochondria are dynamic organelles that drive many different functions in cells. They are involved in energy production, constituting a metabolic hub that centralizes the synthesis of many intermediate metabolites [135]. They also play a role in apoptosis, calcium homeostasis and in cell signaling, mediated by ROS production and mtDNA release [136,137]. In T cells, mitochondria are also involved in migration and class differentiation through asymmetric division [138]. Mitochondria also control lysosomal function during inflammatory T cell responses [139]. During IS mitochondria polarize towards the T cell-APC contact and it happens in the T cell [140] and the APC side [141]. In T cells, mitochondria specifically localize around the MTOC at the cSMAC/pSMAC area [41] and once there fuels the IS with local ATP and calcium for proper T cell activation. Mitochondrial enrichment at the IS favors local calcium entry and control the $Ca2^{+}$-dependent activation of transcription factors [140,142,143]. Conceivably, mitochondria move in two phases when polarizing towards the IS: in a first step mitochondria get closer to the IS contact site and in a second one they get distributed and anchored. Although not experimentally proven, mitochondria may follow an initial calcium gradient in a Miro1-dynein dependent manner and accumulate around the polarized MTOC [143–145], which would be a plausible mechanism for mitochondria transport to the IS. TCR engagement is not absolutely required to observe mitochondria accumulation at the T cell-APC area; the initial LFA1-ICAM1 interaction underlies this effect, facilitated by microtubule integrity [146]. Therefore, the increase of calcium flow upon TCR engagement would increase and sustain mitochondria polarization at the IS area, as a second step. This can be achieved through proteins like Miro-1, which links the tubulin and actin cytoskeletons and fine-tunes the mitochondria movement and docking [147]. Miro-1 is a scaffold protein for Myo19, which regulates the subcellular distribution of mitochondria through regulation of long-walks on microtubules and short-walks and anchoring to actin [148]. In this sense, the localization of the centrosome at the IS is prior to mitochondria recruitment, which requires fragmentation by drp1 [41]. The de-localization of the centrosome from the IS through inhibition of dynein/dynactin tubulin-based molecular motor by p50-dynamitin over-expression [28], also prevents mitochondria polarization at the IS [41].

2. Mitochondria horizontal transfer

According to the endosymbiotic theory, mitochondria are derived from eubacteria that engaged in a symbiotic relationship with primitive host cells. They have maintained some of their ancestral bacterial characteristics, such as a double membrane, a proteome similar to the α-proteobacteria, and the ability to generate the majority of ATP from cells in the process of aerobic respiration or oxidative phosphorylation (OXPHOS) [135]. Mitochondria are endowed with their own circular genome, which is 16.6 kb in length in mammalian cells. This mitochondrial DNA (mtDNA) encodes 13 subunits that are essential components of the electron transport chain, and a translational system made of two ribosomal RNAs and 22 tRNAs, required for the translation of these proteins [149]. A typical mammalian cell contains thousands of copies of the mitochondrial genome, which are organized in mtDNA-protein complexes. Tfam protein coats and bends mtDNA in a compact structure known as nucleoid [150]. In mammals, mitochondria and its genome are transmitted to subsequent generations mainly through the maternal lineage. Specific mechanisms regulate the stability and transmission of mitochondria and their genome during germline transmission and somatic cell proliferation [151].

Mitochondria have been recently shown to be horizontally transferred between mammalian cells, challenging current concepts of mitochondria and mtDNA segregation and inheritance. This transfer promotes the incorporation of mitochondria into the endogenous mitochondrial network of recipient cells, contributing to changes in the bioenergetic profile and in other functional properties of recipient cells, not only *in vitro* but also *in vivo*. Moreover, intercellular transfer of mitochondria involves the horizontal transfer of mitochondrial genes, which has important implications in the physiopathology of mitochondrial dysfunction. The intercellular transfer of mitochondria or their components may also result in the initiation of stem cell differentiation, reprogramming of differentiated cells, or activation of inflammatory signaling pathways. The first evidence of functional mitochondrial transfer involved healthy mitochondria from human stem cells rescuing mitochondrial respiration in mitochondria-depleted recipient cells [152]. Cells devoid of intrinsic mitochondrial function by mtDNA depletion through long-term ethidium bromide treatment, do not survive in standard media. However, when these cells were co-cultured with mesenchymal stem cells (MSC) or fibroblasts that donated functional mitochondria, they acquired mitochondria and re-established aerobic respiration. The careful examination of mitochondrial and nuclear DNA polymorphisms in the rescued clones excluded cell fusion as the main mechanism of mitochondrial transfer, also confirming the stem cell origin of the transferred mtDNA [152]. Transfer did not occur through

the passive uptake of mitochondrial fragments or isolated organelles, but rather involved active processes such as the formation of tunneling nanotubes (TNTs) and/or the vesicular transfer of mtDNA or mitochondrial fragments.

Recent evidence strongly supports that mitochondrial transfer does occur in vivo and may be involved in diverse pathophysiological situations, such as tissue injury and cancer progression [153–157]. Mitochondrial transfer from stem cells to lung epithelial cells and endothelial cells is an important mechanism by which MSC exert their protective effects in several animal models of lung diseases. A study demonstrated that transfer of intact mitochondria can contribute to tissue repair in vivo by a mechanism involving connexins and/or extracellular vesicles **(Figure I8).** [155].

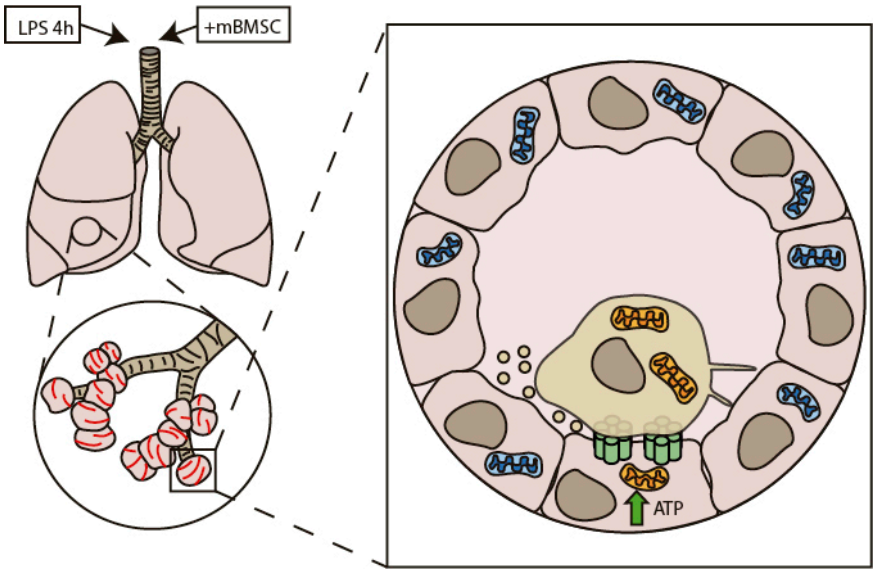

Figure I8. Mitochondrial transfer in a lung disease model. Bone marrow-derived stem cells (BMSC) infused to the trachea of lipopolysaccharides (LPS)-treated mice attached to injured alveolar epithelial cells transfer mitochondria and rescue damaged cells by a mechanism involving connexins and/or extracellular vesicles. Mitochondria acquisition by the alveolar cells triggered the restoration of ATP levels and increased the secretion of pulmonary surfactant. In blue damaged mitochondria, in orange healthy mitochondria.

Cell stress has been proposed as organelle transfer initiator. Mitochondrial transfer is triggered by an almost complete absence of mitochondrial function, such in the case of mtDNA depletion or treatment with mitochondrial inhibitors. Severe damage is necessary to trigger transfer since it is not detected in cells harboring pathogenic mutations that only partially

affect mitochondrial function [158,159]. An intriguing question pertains to the degree of cellular damage required to initiate intercellular transfer of functional mitochondria.

Cells likely possess mechanisms to trigger organelle exchange in response to injury signals emanating from the recipient cell. However, the molecular cues that initiate such crosstalk are still unidentified. Cellular structures that mediate intercellular mitochondrial transfer include TNTs, extracellular vesicles, cell fusion or mitochondrial ejection. Transfer through these diverse structures may result in different functional outcomes for the recipient cells i.e. functional mitochondrial acquisition, immune activation or transmitophagy. The molecular and signaling mechanisms by which cells containing dysfunctional mitochondria acquire mitochondria from other cells and how this process is regulated remain unclear.

Mitochondrial components have been detected in EVs, although the mechanisms by which mitochondrial proteins and mtDNA are loaded in the diverse EVs are still unknown. Exosomes, with a size ranging 40-150 nm, contain genetic material, mostly small RNAs [72], but genomic and mitochondrial DNA have also been detected [103,106,160,161]. Larger EVs can contain entire mitochondrial particles and mtDNA, as observed in mesenchymal stem cells and astrocytes [154,162]. These cells produce EVs with regenerative potential in several tissues under damaging conditions [163–165]. Whether mitochondrial material contained in these vesicles participates in the regenerative potential of stem cells is yet to be shown **(Figure I9)**.

The release of mitochondria or mitochondrial components into the extracellular space has important immune consequences. After an episode of acute injury, release of mitochondrial components into the extracellular medium and bloodstream may trigger potent pro-inflammatory responses. In fact, mitochondrial components can be recognized by cells of the immune system as damage-associated molecular patterns (DAMPs) [166–168]. Different mitochondrial proteins such as TFAM, together with other mitochondrial DAMPs like N-formyl peptides, mtDNA, cardiolipin or extracellular ATP, robustly activate the inflammatory response [169].

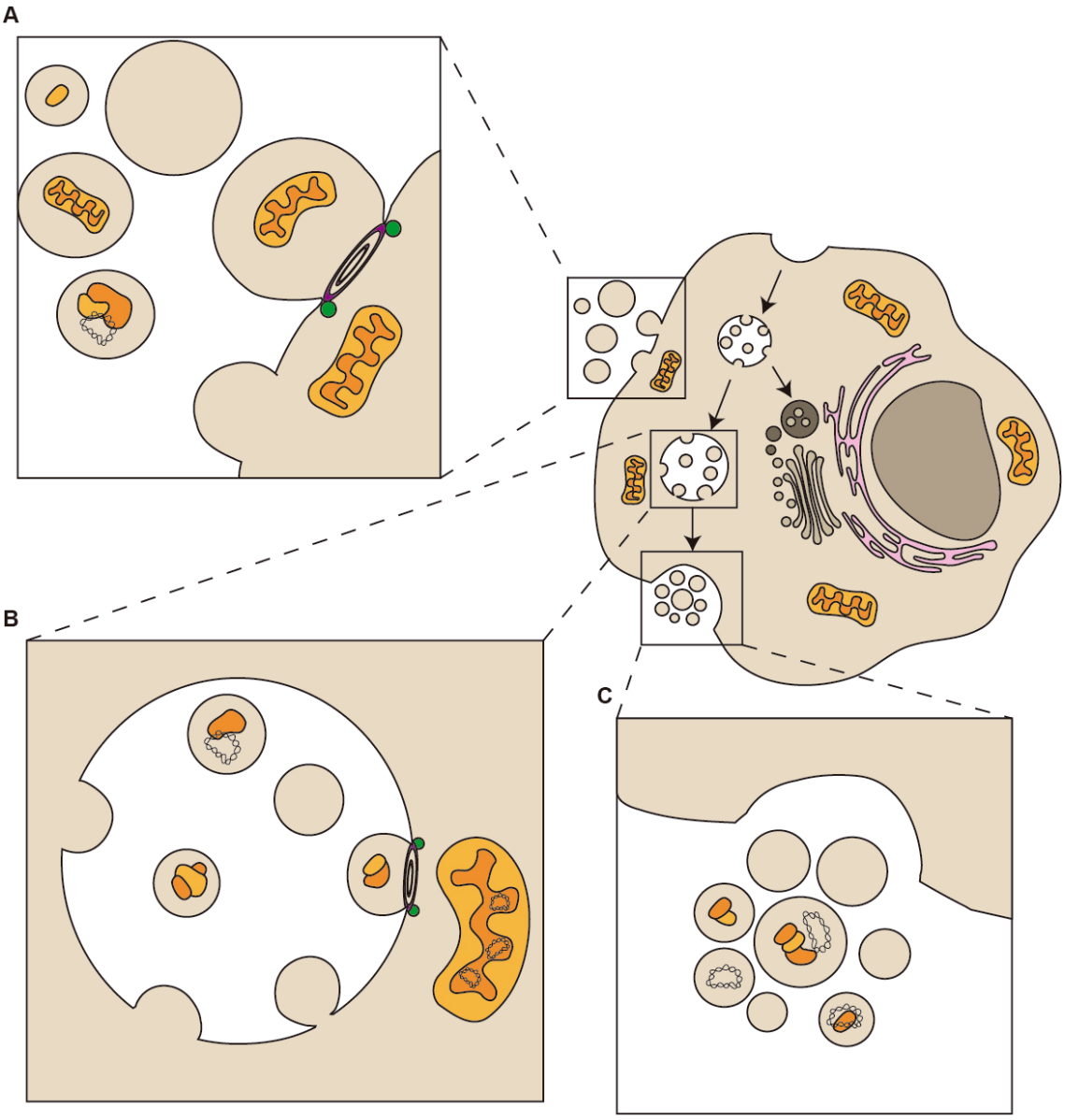

Figure I9. Loading of mitochondrial components in Extracellular Vesicles. A) Microvesicles that shed directly from plasma membrane are very heterogeneous in size and composition. B) The inward budding of MVB forms intraluminal vesicles that are released into the extracellular environment as exosomes, small vesicles from 50-150nm with an endocytic origin. C) Exosome release is achieved through the fusion of the MVB with the plasma membrane. Extracellular vesicles can contain mitochondrial components which include mitochondrial proteins and mtDNA (depicted in yellow and orange). Bigger particles such as microvesicles can be loaded with full functional mitochondria [162].

Mitochondrial DNA induces inflammation when found beyond mitochondrial membrane boundaries [168]. Mitochondrial DNA injected directly into mice joints causes inflammation and arthritis [170]. Moreover, mitochondrial DNA that escapes autophagy leads to Toll-like receptor (TLR) 9-mediated inflammatory responses in a cell-autonomous manner [171]. When abnormally found in the cytosol, mtDNA triggers NRLP3-inflammasome activation and STING-dependent antiviral signaling [167,172], which ultimately leads to cell death. Neutrophils release to the extracellular environment oxidized mitochondrial nucleoids that activate the interferon response in pathological situations such as human systemic lupus erythematosus [173], whereas activated platelets release into the bloodstream entire mitochondria or mitochondria encapsulated in microparticles to boost the inflammatory response [174]. Interestingly, mtDNA released by eosinophils or basophils contribute to inflammatory responses creating DNA net traps to fight against invading pathogens [175,176].

Mitochondria-dependent activation of the inflammatory response is relevant to understand intercellular mitochondrial transfer. In this regard, innate immune cells target cells containing allogenic mtDNA [177]. Such recognition mechanism, displayed by natural killer cells and dendritic cells, is not yet understood, but it is likely to control the extent of intercellular mitochondrial transfer in pathophysiological conditions. As a consequence, careful modulation of immune surveillance mechanisms in recipient cells could be a potential strategy to boost exogenous mitochondrial donation for therapeutic purposes.

Objectives

Objectives

Previous studies have shown that extracellular vesicles, specifically exosomes, are transferred during Immune synapse. T cells secrete exosomes that contain genetic material that can be transferred to the antigen presenting cell. Both the secretory machinery and mitochondria are polarized towards the contact area of the immune synapse upon antigen specific interactions. In addition, whole mitochondria or mitochondrial components can be transferred between contacting cells. Based on this background knowledge we postulate the following hypothesis: *Mitochondrial constituents are transferred through extracellular vesicles during cognate interactions which induces a response in receptor cells*.

In order to challenge our hypothesis, we have addressed 3 main objectives:

1) Dissect the constituents of CD4 T lymphocyte exosomes transferred to dendritic cells during the immune synapse.
    - Analyze the exosomes secreted by CD4 T cells.
    - Study the exosomal proteome of CD4 T lymphocytes.
    - Identification of mitochondrial genome presence in CD4 T cells exosomes.
    - Understand the relation between mitochondrial and endolysosomal compartments.

2) Define the transfer of mitochondrial material during cognate interactions.
    - Analyze the mitochondrial protein constituents transfer from the CD4 T cell to the antigen presenting cell.
    - Elucidation of unidirectional transfer of mtDNA from T lymphocytes to dendritic cells during specific immune interactions.

3) Assess the effect in dendritic cells upon uptake of mitochondrial cargo carried in exosomes from T cells during during immune synapse.
    - Identification of the effects induced by T cell exosomes in dendritic cells
    - Determine the signaling pathway responsible for the antigen presenting cell response
    - Ascertain the effects of exosomal uptake during specific T-Dendritic cell interactions.

Material and Methods

Materials and Methods

Reagents and antibodies

Antibodies used are indicated in the table below:

Antibody	Manufacturer	Catalog number	Application and dilution
anti-human CD63	Calbiochem	OP171	WB (1:1000)
anti-human CD81 5A6	Santa Cruz	sc-23962	WB (1:500)
anti-human TSG101	Abcam	Ab83	WB (1:1000)
anti-GFP	Clontech	632381	WB (1:2000)
anti-TFAM	Abcam	ab47517	WB (1:500)
anti-HRS	Abcam	ab72053	WB (1:500)
anti-COX1	Invitrogen	459600	WB (1:1000)
anti-VDAC1	Abcam	ab14734	WB (1:1000)
anti-Cyt C	Abcam	ab110325	WB (1:1000)
anti-LC3	Cell Signaling	2775S	WB (1:1000)
anti-MnSOD	Enzo Life Sciences	ADI-SOD-110	WB (1:1000)
anti-ATAD3	Abnova	H00055210-D01	WB (1:1000)
anti-Tubulin	Sigma	T6199	WB (1:2000)
anti-nSMase2	RD System	MAB7184	WB (1:1000)
anti-Rab27a	RD System	AF7245	WB (1:1000)

Secondary antibodies used are indicated in the table below:

Antibody	Manufacturer	Catalog number	Application and dilution
anti-mouse peroxidase	Thermo Scientific	31430	WB (1:5000)
anti-rabbit peroxidase	Thermo Scientific	31460	WB (1:5000)

For immunofluorescence and flow cytometry the following antibodies were used:

Antibody	Manufacturer	Catalog number	Application and dilution
anti-CD63 Tea 3/18	Generated in the laboratory		IF (1µg/ml)
anti-HRS	Abcam	ab72053	IF (1:200)
anti-EE1A	Santa Cruz	sc-137130	IF (1:200)
anti-LBPA	Tebu-Bio	ML062915-21	IF (1:200)
anti-Ceramide	Sigma	C8104-50TST	IF (1:200)
anti-8 hydroxyguanosine	Abcam	ab62623	IF & Cyt (1:500)
anti-DNA AC-30-10	Progen	61014	IF & Cyt (1:50)
anti-Tmem173/Sting	Proteintech	19851-1-AP	IF (1:100)
anti-SSBP1	Novus Bio	NBP1-80720	IF (1:200)
anti-CD69	BD Pharmigen	552879	IF & Cyt (1:200)

Secondary antibodies used are indicated in the table below:

Antibody	Manufacturer	Catalog number	Application and dilution
GAM-488/568/647	Invitrogen	# A-11001	IF & Cyt (1:500)
GAR-488/568/647	Invitrogen	# A-11034	IF & Cyt (1:500)
DAG-488/568/647	Invitrogen	# A-11055	IF & Cyt (1:500)

Cells

Human cells

Human T lymphoblasts were isolated from buffy coats obtained from healthy donors by separation on a biocoll gradient (Biochrom). After 30 min of adhesion at 37 °C, non-adherent cells were cultured in RPMI (Gibco) for 2 days in the presence of 5 µg/ml phytohemagglutinin (PHA) to induce lymphocyte proliferation. T lymphoblasts were maintained by addition of IL-2 (50 U/ml) to the medium every 2 days over 8-10 days. For T lymphoblast restimulation, cells were incubated overnight with 50 ng/ml PMA and 750 ng/ml ionomycin.

Human peripheral blood mononuclear cells (PBMC) were isolated from buffy coats obtained from healthy donors by separation on a Lymphoprep gradient (Nycomed, Oslo, Norway) according to standard procedures. Buffy coats of healthy donors were received from the Blood Transfusion Center of Comunidad de Madrid, and all donors signed their consent for the use of samples for research purposes. All the procedures using primary human cells were approved by the Ethics Committee of the Hospital Universitario de la Princesa. Monocytes were purified from PBMC by a 30 min adherence step at 37°C in RPMI supplemented with 10% fetal calf serum. Non-adherent cells were washed off and the adhered monocytes were cultured in RPMI, 10% FCS containing IL-4 (10 ng/ml, R&D Systems Inc, Minneapolis, MN USA) and GM-CSF (200 ng/ml, Schering-Plough, Madrid, Spain). Cells were cultured for 6 days, with cytokine re-addition every other day, to obtain a population of immature hDC.

The human Jurkat-derived T cell line J77 E6.1 (TCR Vαl. 2 Vβ8) (from NIH AIDS reagent program) and the lymphoblastoid B cell line Raji (Burkitt lymphoma) (from ATCC, CCL-86™) were cultured in RPMI (Gibco) containing 10% FBS. Stable cell line clones overexpressing CD63-GFP were generated by transfection and selection with G418 (1 mg/ml, Sigma).

HEK293T cells (from ATCC, CRL-3216™), were cultured in DMEM (Gibco) containing 10% FBS. For colocalization experiments HEK293T cells were treated with 1µM FCCP 4 h (low dose), then washed and immediately fixed with PFA 6%. HEK923T cells were used as a bona-fide cell factory for exogenous protein synthesis and organelle compartmentalization.

Cells were regularly tested for mycoplasma contamination by PCR.

Mouse strains

Mice were housed under specific pathogen-free conditions at the Centro Nacional de Investigaciones Cardiovasculares Carlos III (CNIC), and experiments were approved by the CNIC Ethical Committee for Animal Welfare and by the Spanish Ministry of Agriculture, Food, and the Environment. Animal care and animal procedures license were reviewed and approved by the local Ethics Committee for Basic research at the CNIC Ethical Committee for Animal Welfare and the Organo Encargado del Bienestar Animal (OEBA) del Gabinete Veterinario de la Universidad Autonoma de Madrid (UAM). C57BL/6JOlaHsd (or C57BL/6), C57BL/6 OT-II, C57BL/6JOlaHsd with NZB mtDNA (or C57BL/6 NZB) and C57BL/6NZB OT-II mice were bred under specific pathogen-free conditions at the CNIC (Madrid, Spain) in accordance with European Union recommendations. The C57BL/6JOlaHsd strain does not harbour the nicotinamide nucleotide transhydrogenase (NNT) spontaneous mutation that renders the encoded enzyme undetectable, and which is characteristic of the C57BL/6J strain provided directly by Jackson Laboratories. C57BL/6 NZB OT-II mice were obtained by backcrossing C57BL/6 OT-II transgenic males with C57BL/6 NZB females. *Sting*$^{Gt/Gt}$ (STING-deficient) mice were provided by Dr. Gloria González Aseguinolaza, Gene Therapy and Regulation of Gene Expression Program, Center for Applied Medical Research, Health Research Institute of Navarra (IdisNA), Pamplona, Spain. These mice have a single nucleotide variant (T596A) which is a null mutation resulting in failure to produce STING protein[178]. *Irf3*$^{-/-}$ mice were kindly provided by Prof. Adolfo García Sastre, Icahn School of Medicine at Mount Sinai, New York, USA.

Mouse cell isolation, differentiation and activation

CD4^{+} T cells were obtained from spleen-cell suspensions obtained from C57BL/6 OT-II transgenic mice. Splenic cells were incubated for 30 min at 4ºC with a biotinylated anti-CD4 antibody (BD Pharmingen) followed by extensive washing with PBS, 1% BSA, 5 mM EDTA. Cell suspensions were then incubated for 20 min at 4ºC with streptavidin microbeads (MACS; Miltenyi Biotec) and washed with PBS, 1% BSA, 5 mM EDTA. CD4^{+} T cells were obtained by positive selection using the auto-MACS Pro Separator (Miltenyi Biotec).

Bone marrow-derived dendritic cells (BMDCs) were obtained either from C57BL/6, C57BL/6^{NZB}, Sting$^{Gt/Gt}$ or *Irf3*$^{-/-}$ mice by incubating primary bone marrow cells for 9-10 days in RPMI (Gibco) supplemented with 20 ng/ml recombinant GM-CSF (ImmunoTools) and 1% sodium pyruvate, 50 U/ml penicillin, 50 µg/ml streptomycin, 5×10^{-5} M 2-mercaptoethanol, and 10% FBS (all from Invitrogen).

For T cell blasting, naive $CD4^+$ T cells were isolated from spleen and lymph nodes and cultured for 48 h with 2 ug ml^{-1} concanavalin A (Sigma). Cells were then incubated with 50 U/ml human recombinant IL-2 (Glaxo) every 2 days for at least 7 days to obtain differentiated T lymphoblasts. For antigen-specific restimulation, T lymphoblasts were conjugated with BMDCs and stimulated overnight *in vitro* with 100 ng/ml lipopolysaccharide (LPS) in the presence or absence of 10 µg/ml ovalbumin (OVA) peptide.

Plasmids, interference RNA and cell transfection

The following plasmids were used: mitoDsRed and mitoYFP, (kindly provided by Prof. L. Scorrano, Venetian Institute for Molecular Medicine, Italy), TFAM-GFP and TFAM-DsRED (generated by inserting the human TFAM cDNA into the pEGFP and DsRED plasmids), EGFP-Rab7A Q67L, LC3-GFP and ATG5-GFP (obtained from Addgene: plasmids 28049, 24920 and 22952, respectively), shRNA pLKO control plasmid, shnSMase2 and shRab27a shRNAs (obtained from Open Biosystems), and CD63-GFP [55].

Construct of DNase II with CD63 intraluminal domain: Following Gibson Assembly Protocol (New England Biolabs) hDNaseII (Human DNase II Gene ORF cDNA clone in cloning vector, HG16372-G, Sino Biological inc) was inserted in CD63-GFP plasmid in the intraluminal domain. CD63-GFP plasmid was cut with EcoRI. The following primers were used to amplify insert: Fw_DNaseII-EcoRI: CGAGCTCAAGCTTCGATGATCCCGCTGCTGCT Rv_DNaseII-EcoRI:TACCGTCGACTGCAGGGATCTTATAAGCTCTGCTGG GC

T-cell lines and human T lymphoblasts were transfected with a specific double stranded siRNA targeting human LC3 (GGUGCCUGUAGGUGAUCAA) or negative control siRNA (Eurogentec), using the Gene Pulser II electroporation system (Bio-Rad Laboratories) or the Nucleofector system (Amaxa Biosystems). When indicated, at 24 h post transfection, cells were cultured in exosome-depleted medium for 20 h and exosomes were isolated from supernatants.

For transfection, J77 T cells were transfected with the corresponding plasmids by electroporation; 20×10^6 cells were resuspended in Opti-MEM (Gibco; 5×10^7 cells per ml) with 20 µg of plasmid DNA and electroporated with a Gene Pulser Xcell electroporator (Bio-Rad) at 1200 µFa, 240 mV, 30 ms in 4 mm Bio-Rad cuvettes (Bio-Rad). Fluorescence-positive cells were FACS sorted, cloned, and cultured in RPMI containing 2 mg/ml G418 (Invitrogen). HEK293T cells were transfected using Lipofectamine 2000 (Invitrogen) according to the manufacturer's instructions.

Lentiviral infection

J77 cells with downregulated nSMase2 and Rab27a expression were generated by infection with lentiviral vectors expressing specific shRNAs. HEK293T cells were co-transfected using the Lipofectamine2000 system (Invitrogen) with pCMV-ΔR8.91-(Delta 8.9), pMD2.G-VSV-G, and plasmids encoding shRNAs targeting nSMase2, Rab27a or the corresponding shRNA pLKO control plasmids (Open Biosystems). Supernatants were collected after 48–72 h, filtered (0.45 µm), and added to J77 or HEK293 cell cultures. Cells were centrifuged (2000 x g, 2 h) and incubated for 4 h at 37 °C. Medium was replaced with RPMI containing puromycin (4 µg/ml).

Conjugate formation and assessment of mtDNA transfer

To assess mtDNA transfer during immune cognate interactions we used two mice strains (C57BL/6 and C57BL/6^{NZB}) that differ by 12 missense mutations in their mitochondrial DNA. Differentiated C57BL/6^{NZB} BMDCs were loaded with calcein (37°C, 20 min), extensively washed, and then co-cultured in the presence of ovalbumin (OVA) peptide (10 µg/ml) with C57BL/6 $CD4^+$ OT-II T cells (5:1 T cell/DC ratio; 16 h). To assess mtDNA transfer from $CD4^+$ OT-II cells to BMDCs, C57BL/6 OT-II $CD4^+$ T cells and C57BL/6^{NZB} BMDCs were conjugated (1:5 T cell/DC ratio; 16h). Conjugates were blocked with Fc-block (CD16/CD32, BD Pharmingen), washed in PBS, 1% BSA, and incubated with antibodies against MHCII and CD3 (BD Pharmingen) diluted in PBS, 1% BSA. Viable cells were identified by propidium iodide exclusion. Singlet cells were discerned with a stringent multiparametric gating strategy based on FSC and SSC (pulse width and height). $CD4^+$ T cells and BMDCs were distinguished by calcein staining and MHCII and CD3 fluorescence, and sorted on a FACSAria flow cytometer (BD Biosciences). DNA was extracted, and C57BL/6 and NZB mtDNAs were detected by restriction fragment length polymorphism (RFLP) analysis as follows. DNA (50 ng) was PCR-amplified using the RED Extract-N-Amp PCR Ready Mix Kit (Sigma Aldrich) with the oligonucleotides 5’ AAGCTATCGGGCCCATACCCCG 3’ (Fw) and 5’ GTTGAGTAGAGTGAGGGATGGG 3’ (Rv) at a concentration of 250 nM (Tm: 58º). After PCR amplification, samples were digested with BamH1 (10 units) for 2 h. Digested samples were loaded on a 2% agarose gel. $C57^{C57}$ haplotype includes a BamHI restriction site; enzyme digestion results in two smaller fragments of 414 pb and 250 pb. Digestion of PCR products from C57BL/6^{NZB} haplotype results in a single band of 664 pb corresponding to the full length PCR product.

Conjugate formation of cell lines and mitoDsRed transfer

To distinguish Raji B cells from T cells, Raji cells were loaded with the cell tracer CMAC (7-amino-4-chloromethylcoumarin, Invitrogen). For antigen stimulation and IS formation, Raji cells were pulsed for 30 min with 0.5-1 µg/ml of *Staphylococcus enterotoxin superantigen* (SEE, Toxin Technology) and mixed with Jurkat cells expressing CD63-GFP, TFAM-dsRED, or mitoYFP at a ratio of 1:5 for 18-24 h at 37º C. Cell conjugates were analyzed by FACS in a FACS LSRFortessa Cell Analyzer (BD Biosciences) and data were analyzed with FACSDiva software (BD Biosciences).

To assess gene expression after IS formation, stable J77 CD63-GFP cells and CMAC-stained Raji cells were conjugated as described. After 16 h, cells were sorted according to CMAC staining and CD63 green fluorescence. The Raji population was split into 2 groups according to CD63-GFP uptake: Raji GFP+ Low (cells acquiring low amounts of CD63) and Raji GFP+ High (acquiring high amounts of CD63). After sorting, total RNA was isolated and qPCR performed to analyze antiviral response genes.

Exosome purification and sucrose-gradient purification

Cells were cultured in medium supplemented with 10% exosome-depleted fetal bovine serum (FBS, Invitrogen; FBS was depleted of bovine exosomes by overnight centrifugation at 100 000 x g for at least 16-20 h. Exosomes were obtained by serial centrifugation as described [179]. Briefly, cells were pelleted (300 x g for 10 min) and the supernatant was centrifuged at 2000 x g for 20 min to remove debris and dead cells. The collected supernatant was then ultracentrifuged at 10 000 x g for 40 min at 4 ºC (Beckman Coulter Optima L-100 XP, Beckman Coulter) to remove debris, apoptotic bodies, and shedding vesicles. Exosomes were pelleted by ultracentrifugation at 100 000 x g for 70 min at 4 °C, washed in PBS, and collected by ultracentrifugation at 100 000 x g for 70 min. DNase treatment was performed with RQ1 RNase-Free DNase (Promega) according to the manufacturer's instructions.

Exosomes were isolated by sucrose density gradient . Briefly, exosomes were obtained by serial centrifugation of 200 ml cell culture supernatant. Isolated exosomes were layered on top of a discontinuous sucrose gradient, ranging from 2.5 M sucrose at the bottom to 0.4 M sucrose at the top, in an SW40 centrifuge tube (14 x 95 mm; Beckman Coulter). Tubes were centrifuged overnight (18-20 h) in a SW40 rotor at 192 000 x g at 4 °C. One ml fractions were collected from the top of the gradient and were resuspended in an equal volume of acetone for protein precipitation and Western blot analysis or were treated as indicated for DNA isolation and PCR analysis.

Exosome adsorption to aldehyde-sulfate beads and detection

Exosomes were obtained as described above, resuspended in PBS, and coupled to 4 µm aldehyde-sulfate beads (Invitrogen) 15 min in rotation at room temperature. Then, coupled beads where incubated in overnight rotation in PBS containing 0.1% BSA and 0.01% sodium azide. Beads were washed twice with PBS, 0.1% BSA, 0,01% sodium azide. For surface staining, beads were washed and incubated with the indicated primary antibodies for 30-45 min on ice. For intraluminal staining, beads were fixed and permeabilized in PBS containing 1% Paraformaldehyde and 0.01% Triton X-100 for 20 min on ice, washed, and incubated with primary antibodies for 1 hour on ice. Beads were then washed and incubated with the appropriate secondary antibodies for 30 min on ice. Beads were analyzed with a FACS LSRFortessa Cell Analyzer (BD Biosciences) and data were analyzed with FACSDiva software (BD Biosciences). Negative controls were obtained with permeabilized and non-permeabilized exosome-coupled beads incubated with the indicated secondary antibodies.

Nanoparticle tracking analysis

Exosome numbers and size distribution were measured from the rate of Brownian motion in a NanoSight LM10 system, which is equipped with fast video capture and particle-tracking software (NanoSight, Amesbury, U.K.). Briefly, 0.5 mL of diluted exosome fraction was loaded into the sample chamber of an LM10 unit (Nanosight, Amesbury, UK) and three 30-second videos were recorded of each sample. Data were analyzed with NTA 2.1 software (Nanosight). Samples were analyzed using manual shutter and gain adjustments, which resulted in shutter speeds of 15 or 30 ms, with camera gains between 280 and 560. The detection threshold was kept above 4; blur: auto; minimum expected particle size: 50 nm. Samples were diluted before analysis to concentrations between 2×10^8 and 20×10^8 particles/ml.

Deep sequencing analysis

Total RNA was extracted with the RNeasy kit (Qiagen). Contaminating genomic DNA was removed using the specific column from the kit. RNA integrity and quantity were determined in an Agilent 2100 Bioanalyzer. Equal RNA amounts from 4 individual samples per group were analyzed in the Illumina Genome Analyzer IIx. Sequencing reads were pre-processed by means of a pipeline that used FastQC to assess read quality and Cutadapt to trim sequencing reads, eliminate Illumina adaptor remains, and discard reads shorter than 30 bp. The resulting reads were mapped against the mouse transcriptome (GRCm38, release 76; aug2014 archive) and quantified using RSEM v1.17. Data were then processed with a pipeline that used the EdgeR Bioconductor package for normalization and differential expression analysis in a paired strategy.

The number of reads obtained per sample was in the range of 12 to 17 million. The percentage of reads eliminated in the pre-processing step was below 1%. Genes with at least 1 count per million in at least 4 samples (11 383 genes) were considered for further analysis. Fold change and log(ratio) values were calculated to represent gene expression differences between conditions. Sets of genes differentially expressed across conditions were analyzed for functional associations using the Ingenuity Knowledge Database (IPA, http://www.ingenuity.com).

Exosome proteomic analysis

Exosomes from mouse T lymphoblasts were isolated by serial ultracentrifugation, and protein extracts (200 µg) were digested using the FASP method as previously described[180]. After digestion, the resulting peptides were desalted onto C18 OMIX tips (Agilent Technologies). Peptides were separated into 4 fractions by cation exchange chromatography with MCX cartridges (Waters) using graded concentrations of ammonium formate, pH 3.0 in acetonitrile (ACN), and desalted again before analysis by liquid chromatography–tandem mass spectrometry (LC-MS/MS).

Analyses were performed using a nano-HPLC Easy nLC 1000 chromatograph coupled to a Q-Exactive hybrid quadrupole orbitrap mass spectrometer (Thermo Scientific). Peptides were loaded in an analytical C18 nano-column (EASY-Spray column PepMap RSLC C18, 75 µm internal diameter, 3 µm particle size, and 50 cm length, Thermo Scientific) and separated in a continuous gradient consisting of 8-30% B for 60 min and 30-90% B for 2 min (B = 90% ACN, 0.1% formic acid) at 200 nL/min. The chromatographic run acquired an FT-resolution spectrum of 140 000 ions in the mass range of m/z 390–1600 followed by data-dependent MS/MS spectra of the 15 most intense parent ions. Normalized HCD collision energy was set to 28% and the parent ion mass isolation width was 2-Da.

Peptides were identified from MS/MS spectra using the SEQUEST HT algorithm integrated in Proteome Discoverer 2.1 (Thermo Scientific). MS/MS scans were matched against a mouse protein database (UniProt 2016_07 Release) and the parameters were selected as follows: a maximum of 2 missed trypsin cleavages, a precursor mass tolerance of 800 ppm, and a fragment mass tolerance of 0.02 ppm. Cysteine carbamidomethylation was chosen as the fixed modification and methionine oxidation as the dynamic modification. The same MS/MS spectra collections were searched against inverted databases constructed from the same target databases. SEQUEST results were analyzed by the probability ratio method. False discovery

rate (FDR) was calculated for peptides identified in the inverted database search results using the refined method [181].

Detection of oxidized DNA by chromatin immunoprecipitation

T lymphoblast exosomes were purified by differential ultracentrifugation and lysed in buffer containing 25 mM Tris-HCl, 150 mM NaCl, 2 mM MgCl, 0.5%, NP40, 5 mM DTT. Protein G-coupled magnetic beads (Protein G Dynabeads, Invitrogen) were washed and incubated for 2-3 h with 5 µg anti-8 hydroxyguanosine (8-OHdG) antibody [15A3] (Abcam), 5 µg of anti-DNA AC-30-10 (Progen) or with 5 µg of the isotype control (SantaCruz, sc-2015). Lysates were precleared with Protein G Dynabeads and then incubated overnight at 4ºC with antibody-coupled beads. Samples were washed 5 times with lysis buffer and eluted with 50 mM Tris-HCl pH 8.0, 10 mM EDTA, and 1% SDS for 1 hour at 65ºC. DNA was purified with the ChIP DNA Clean & Concentration kit (D5205-Zymo Research). qPCR was performed on whole samples with technical duplicates.

Mitochondrial enriched fraction was obtained from T lymphoblasts by resuspending them in mitochondrial extraction buffer (1mM EDTA ph8, 1mM DTT, 10mM NaCl, 3mM MgCl2, 5mM Tris-HCl ph8) during 15 min at 4ºC (Osmotic Lysis). Then, lysates were subjected to three freeze/thaw cycles with 5 min liquid nitrogen exposition and 10 min immersion in a water bath at 37ºC. Following lysis the tubes were centrifuged at 500*g* for 10 min at 4ºC. Supernatants were collected and spun down at 12000*g* for 20 min at 4ºC. The final pellets (mitochondria enriched fraction) were resuspended in lysis buffer and treated as exosomal fractions.

Analysis of antiviral response induction by exosomes

BMDCs were cultured and differentiated in vitro. After culture for 9-11 days, BMDCs were plated in p12 plates at 3×10^5 per well. Exosomes from T lymphoblasts were isolated by differential ultracentrifugation and 10-15 µg added to BMDCs for 6 h. BMDCs were then washed and frozen for RNA extraction.

Vaccinia infection

The recombinant vaccinia virus VACV-GFP was a gift from J. Yewdell (National Institutes of Health, Bethesda, MD). For analysis of exosome-mediated viral protection, BMDCs were cultured as previously described. After 9-11 days, cells were plated in p96 plates at 1×10^5 per well. T lymphoblast exosomes were purified by differential ultracentrifugation and 5-10 µg were added to BMDCs for 4-6 h. Vaccinia-GFP was added to cells at the indicated BMDC:virus ratios. After incubation for 4 h, cells were harvested, fixed for 10 min with BD

Cytofix/Cytoperm (BD Biosciences), and analyzed by flow cytometry. Viability was assessed with the LIVE/DEAD® Fixable Aqua Dead Cell Stain Kit (Molecular Probes).

For the analysis of antiviral protection during IS formation, BMDCs were cultured for 9-11 days and then plated in p24 plates at 2×10^5 per well. Receptor BMDCs were primed with 100 ng/ml LPS overnight, extensively washed, and co-cultured in the presence of ovalbumin (OVA) peptide (5 µg/ml) with C57BL/6 $CD4^+$ OT-II T cells (5:1 T cell/DC ratio). After conjugate formation for 4 h, vaccinia-GFP was added at a 1:1 ratio (total number of cells in the well) for 4h. Cells were harvested, blocked with Fc-block (CD16/CD32, BD Pharmingen), and stained with CD4 PE-Cy7 and CD11c PE. Viability was assessed with the LIVE/DEAD® Fixable Aqua Dead Cell Stain Kit (Molecular Probes). Cells were fixed for 10 min with BD Cytofix/Cytoperm (BD Biosciences) and analyzed by flow cytometry.

Cell viability Assay

In order to measure cell viability upon manumycin treatment and activation, $CD4^+$ OTII T lymphoblasts were incubated for 24h with increasing amounts of manumycin (0, 1 and 2,5 µM) and with anti-CD3 (10 µg/ml) and anti-CD28 (2 µg/ml). Cells were harvested and stained with anti-CD4 and DAPI to measure the percentage of DAPI negative (alive) CD4+ cells by flow cytometry.

To ascertain cell viability in the context of immune cognate interactions, CD4+ OTII T lymphoblasts were pre-treated for 2h with increasing amounts of manumycin (0, 1 and 2,5 µM) ,then CD4 T cells were conjugated with OVA-pulsed dendritic cells (5:1T cell/DC ratio; 4h). Cells were harvested and stained with anti-CD4 and DAPI to measure the percentage of DAPI negative (alive) CD4+ cells by flow cytometry.

Flow cytometry

For cytometry, adherent cells were harvested with 0.25% Trypsin-EDTA (Gibco), blocked with Fc-block (CD16/CD32, BD Biosciences), washed in PBS, 1% BSA, and incubated with primary antibodies diluted in PBS, 1% BSA. Viable cells were identified by HOECHST 58 exclusion. Singlet cells were discerned based on FSC and SSC (pulse width and height). For surface labeling, cells were stained with antibodies diluted in PBS, 0.5% BSA on ice.

For intracellular and surface staining, cells were fixed with 1% formaldehyde and permeabilized with 0.01% Triton X-100 (Sigma). After washing, cells were blocked with Fc-block (CD16/CD32, BD Biosciences), washed in PBS, 1% BSA, and incubated sequentially with primary and secondary antibodies (diluted 1:500) in PBS, 1% BSA. Cells were then analyzed by

FACS in a FACS LSRFortessa Cell Analyzer (BD Biosciences). Data were analyzed with FACSDiva software (BD Biosciences).

To detect intracellular ROS, HEK293T cells were incubated with 2',7'–dichlorofluorescin diacetate (DCDFA, Thermofisher), and to detect mitochondrial mass cells were loaded with mitotracker green (Invitrogen). Cells were analyzed in a FACS LSRFortessa Cell Analyzer (BD Biosciences) and data were analyzed with FACSDiva software (BD Biosciences).

Western blot

Cells or exosomes were lysed in RIPA buffer (50 mM Tris-HCl pH 8, 150 mM NaCl, 1% Triton X-100, 0.1% sodium deoxycholate, and 0.1% SDS) supplemented with a protease inhibitor cocktail (Complete, Roche). Proteins were separated on 10-12% acrylamide/bisacrylamide gels and transferred to nitrocellulose or methanol-pretreated PVDF membranes. Membranes were incubated with primary antibodies (1:1000) and peroxidase-conjugated secondary antibodies (1:5000), and proteins were visualized with LAS-3000.

Immunofluorescense

For immunofluorescence assays, cells were plated onto slides coated with fibronectin (50 µg/ml), incubated overnight, and fixed with 2% paraformaldehyde in PBS. Cells were permeabilized with PBS, 0.1% Triton X-100 (Sigma), washed and stained with the corresponding primary antibodies (1:100-1:200) followed by secondary antibodies (1:500) (Life Technologies). When indicated, cells were previously transfected with the indicated plasmids. Cells were fixed and stained with the indicated antibodies at 24 h post transfection. Samples were examined with a Leica SP5 confocal microscope fitted with a × 63 objective, and images were processed and assembled using Leica software. Quantification of images was done with Fiji software (ImageJ) using Manders' coefficient M2 as a marker for colocalization of mitochondrial markers (SSBP1) with endosomal markers (EEA1 and CD63)[182]. More than one hundred cells were quantified for experiment.

TIRFm analysis of isolated exosomal particles

Isolated exosomal particles (8x106 particles per coverslip) generated as described and quantified with Nanosight were spun in a sucrose cushion (10% in HBSS; 10000xg, 15 min, 25ºC. HS-4 rotor, Sorvall) over 13 mm diameter precision coverslips (thickness No. 1.5H; 0.170 mm ± 0.005 mm, 0117530 Marienfield) coated with 250 µg.ml-1 Poly-L-Lys (P6407 Sigma Aldrich) and fixed in 1% paraformaldehyde (HBSS, 5% sucrose; RT15710 Electron Microscopy Sciences) for 5 min, R/T. Coverslips were treated with Glycine 200 mM in Tris-HCL (pH 7.4) for 10 min, R/T and blocked (3% BSA, 20 µg.ml-1 human gamma-globulins in HBSS) for 1 h R/T.

Staining with anti-CD81 (rat anti-mouse clone MT81; 5 µg.ml-1, 4ºC, o/n) was followed by highly-cross-adsorbed Alexa-568-conjugated goat anti-rat Antibody (A-11077 Thermofisher Scientific 1:1000). Samples were then permeabilized with a 0.2% TX-100 solution (HBSS supplemented with 0.5% paraformaldehyde and 1.5% BSA), treated for autofluorescence and stained with anti-DNA (0.001 µg.ml-1) or anti-TSG101 (20 µg.ml-1, ab83 Abcam) mouse monoclonal antibodies for 3 h at 4ºC, followed by highly-Cross-absorbed Alexa-488-conjugated goat anti-mouse Antibody (A-11029 Thermofisher Scientific 1:1000). Samples were mounted on Prolong Gold antifade mountant (P36930 Thermofisher Scientifc). Coverslips were extensively washed with HBSS and a final wash with deionized water. Antibodies were diluted in 1.5% BSA in HBSS. Secondary antibodies were incubated for 1 h at R/T. All the solutions used for coverslip preparation and immunofluorescence were previously ultracentrifuged at 100000xg for 70 min (4ºC) in a swinging bucket rotor (Beckman Coulter) or for 30 min at 13200xg in a fixed-angle rotor (Eppendorf). Samples were imaged under a Leica AM TIRF MC M system mounted on a Leica DMI 6000B microscope fitted with a HCX PL APO 100×1.46 NA oil objective and coupled to an Andor-DU8285 VP-4094 camera. Penetration depth was 90 nm and 2x zoom was used to obtain an optical magnification of the samples. Equal experimental conditions for acquisition were used for the different coverslips. Brightness and Contrast adjustments were equal for all images. Processing of images was performed with Image J 1.51n (Wayne Rasband national Institutes of Health, USA. http://imagej.nih.gov/ij; Java 1.8.0_66; 64 bit).

Electron microscopy

Adherent HEK293 cells stably transfected with control shRNA, shRab27a, or shnMNase2 were washed in PBS and fixed for 1 h in 2.5% glutaraldehyde in 0.1 M phosphate buffer at room temperature. Cells were pelleted in 15ml Falcon tubes. Pellets were washed with phosphate buffer and incubated with 1% OsO_4 for 90 min at 4 °C. Samples were then dehydrated, embedded in Spurr, and sectioned on a Leica ultramicrotome (Leica Microsystems). Ultrathin sections (50–70 nm) were stained with 2% uranyl acetate for 10 min and with a lead-staining solution for 5 min and observed under a JEOL JEM-1010 transmission electron microscope fitted with a Gatan Orius SC1000 (model 832) digital camera.

For immunogold staining, cells were fixed in 4% PFA 0.5% glutaraldehyde in PBS at 4ºC. Samples were dehydrated, embedded and sectioned. Grids were rehydrated in TBS and treated with 0.01 M glycine to deactivate reactive aldehydes. Samples were blocked with goat blocking solution (Aurion) for 1h and incubated with primary antibodies; anti-Tfam (1:50) (Cell Signalling) and anti-DNA (1:15) (Promega) overnight in blocking solution. Grids were washed in

blocking solution and incubated with secondary antibodies conjugated to 12nm colloidal gold (1:75 for TFAM and 1:25 for DNA, Jackson ImmunoResearch) for 2h. Samples were washed in blocking solution and distilled water. Grids were air dried for 2h, stained with lead citrate and uranyl acetated and carbon coated for viewing under transmission electron microscope.

Extracellular Flux Analysis

Oxygen consumption rate was measured in a XF-96 Extracellular Flux Analyzer (Seahorse Bioscience) in equal numbers of shControl, shRab27a and shnSMase2 HEK293 cells incubated with XF medium. Three measurements were obtained under basal conditions and upon addition of oligomycin (1 mM), fluoro-carbonyl cyanide phenylhydrazone (FCCP; 1.5 mM), and rotenone (100 nM) + antimycin A (1 mM).

Quantitative PCR and assessment of mitochondrial DNA by PCR

Total RNA was isolated using the RNeasy kit (Qiagen). Genomic DNA was removed using the specific column from the kit. Reverse transcription was performed using the High Capacity cDNA Reverse Transcriptase kit (Applied Biosystems). Quantitative real-time PCR was performed in a 7900 HT Fast Real-Time PCR system (Life technologies) using SYBR green qPCR Master Mix (Promega). Data were normalized to the expression of beta-actin, beta-2-microglobulin, and/or ywhaz and analyzed with Biogazelle QBasePlus (Biogazelle). Primer sequences are specified below:

	Sequence	gene	Organism
Forward	CACCCAAGAACAGGGTTTGT	tRNA Leu	Human
Reverse	TGGCCATGGGTATGTTGTTA	tRNA Leu	Human
Forward	GCCTTCCCCCGTAAATGATA	16S RNA	Human
Reverse	TTATGCGATTACCGGGCTCT	16S RNA	Human
Forward	TGCTGTCTCCATGTTTGATGTATCT	B2 Microglob	Human
Reverse	TCTCTGCTCCCCACCTCTAAGT	B2 Microglob	Human
Forward	TTCGGCGCATGAGCTGGAGTCC	hCOX	Human
Reverse	TATGCGGGGAAACGCCATATCG	hCOX	Human
Forward	CTCACGGGAGCTCTCCATGC	HVRII	Human
Reverse	CTGTTAAAAGTGCATACCGCCA	HVRII	Human
Forward	ACCCCTTCTCTGTCTACCG	SDH	Mouse
Reverse	AATGCTCGCTTCTCCTTGTAG	SDH	Mouse
Forward	CCCAGATATAGCATTCCCACG	mtCOXI	Mouse
Reverse	ACTGTTCATCCTGTTCCTGC	mtCOXI	Mouse

Forward	TGCACCTACCCTATCACTCA	mtND1	Mouse
Reverse	GGCTCATCCTGATCATAGAATGG	mtND1	Mouse
Forward	TCCCAATCGTTGTAGCCATC	mtATP6	Mouse
Reverse	TGTTGGAAAGAATGGAGTCGG	mtATP6	Mouse

For the analysis of mitochondrial DNA contained in exosomes, DNA from T lymphoblast-derived exosomes was isolated with the Cell Lysis Solution and Protein Precipitation Solution from Qiagen. After DNA isolation, PCR was performed, primer sequences are specified in the table below:

	Sequence	gen	Organism
Forward	CCAGTGCTGCCGTCATTTTC	CXCL10	Mouse
Reverse	GGCTCGCAGGGATGATTTCAA	CXCL10	Mouse
Forward	CTAGAGCTAGAGCCTGCAG	ISG15	Mouse
Reverse	AGTTAGTCACGGACACCAG	ISG15	Mouse
Forward	GAGAGGACCATGAAGAGGA	USP18	Mouse
Reverse	TAAACCAACCAGACCATGAG	USP18	Mouse
Forward	TTCCCAGCAGCACAGAAAC	IFIT3	Mouse
Reverse	AAATTCCAGGTGAAATGGCA	IFIT3	Mouse
Forward	CAAGGCAGGTTTCTGAGGAG	IFIT1	Mouse
Reverse	GACCTGGTCACCATCAGCAT	IFIT1	Mouse
Forward	CGCGCATGCAACTGGCATATAACT	STAT1	Mouse
Reverse	ATGCTTCCGTTCCCACGTAGACTT	STAT1	Mouse
Forward	TAGTCCTTCCTACCCCAATTTCC	IL6	Mouse
Reverse	TTGGTCCTTAGCCACTCCTTC	IL6	Mouse
Forward	AGCAGAGGAACCTCCAGTCT	CXCL10	Human
Reverse	ATGCAGGTACAGCGTACAGT	CXCL10	Human

Statistical analysis

All values were expressed as the mean ± S.E.M. or mean with individual values included for data distribution. For in vitro experiments, statistical differences were evaluated with Student's *t* test and between group differences were evaluated with the Mann-Whitney U test for unpaired data (GraphPad Prism). Differences were considered significant when *$p < 0.05$, **$p < 0.01$, ***$p < 0.001$.

Data Availability

The authors declare that the data supporting the findings of this study are available within the article and its supplementary information files, or are available in a persistent repository or upon reasonable requests to the authors.

Deep sequencing analysis data supporting the findings of this study are deposited in GEO repository with the accession number: GSE110165

[https://www.ncbi.nlm.nih.gov/geo/query/acc.cgi?acc=GSE110165].

DNA seq data are deposited in BioSample repository: SRP148571 [https://www.ncbi.nlm.nih.gov/sra/SRP148571]

Raw data from RNAseq and DNAseq analysis are under a common umbrella project: Bioproject PRJNA472779 [https://www.ncbi.nlm.nih.gov/bioproject/PRJNA472779]:

PRJNA432987: Mouse RNA-seq data in GEO [https://www.ncbi.nlm.nih.gov/bioproject/PRJNA432987]

PRJNA472354: Human DNASeq data in SRA [https://www.ncbi.nlm.nih.gov/bioproject/PRJNA472354]

The mass spectrometry proteomics data are deposited to the ProteomeXchange Consortium via the PRIDE partner repository with the dataset identifier PXD008843 [http://www.ebi.ac.uk/pride/archive/projects/PXD008843]

Results

Results

Exosomes transferred from the T cell to the APC contain many different types of biologically active molecules, including proteins and genetic material [55,132]. To investigate the possible specific function of the different components of the biologic material transferred from the T cell to the DC, the protein and genetic content of EVs isolated from the culture supernatant of primary T lymphoblasts were characterized by differential ultracentrifugation [179] according to the current recommendations of the International Society of Extracellular Vesicles (ISEV) [183] **(Figure R1)**.

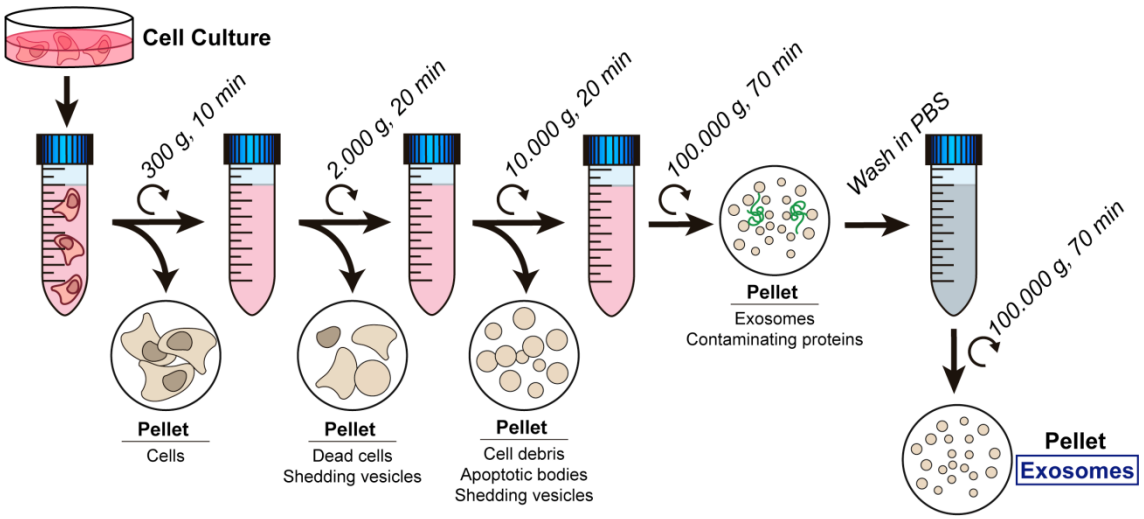

Figure R1. Differential centrifugation protocol for isolating exosomes from cell culture supernatants. Supernatants were centrifuged and pellets were consecutively discarded. After the 100.000g ultracentrifugation the supernatant was discarded and the pellet resuspended in PBS and centrifuged again in order to obtain a purified fraction of exosomes.

Diameters of exosomes obtained in the 100 000 ×g fraction ranged from 50 to 200 nm **(Figure R2a, R2b)**, in agreement with the reported size and shape of exosomes [124].

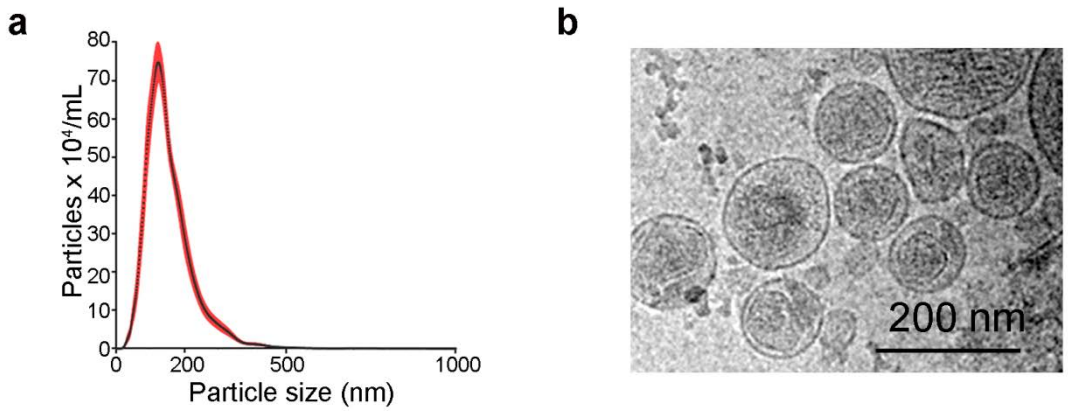

Figure R2. Size and shape of exosomes from T cell supernatants. (a) Size distribution analysis by Nanoparticle Tracking Analysis (NTA) of purified exosomes from primary human T lymphoblasts. **(b)** Electron microscopy of exosomal fraction from primary human T lymphoblasts. Bar 200nm.

1. T cells incorporate mitochondrial proteins in exosomes

Proteomic characterization of T cell Exosomes identified abundant peptides derived from canonical exosome components, including tetraspanins, endosomal proteins, cytoskeletal proteins, Rab-related trafficking proteins, heat-shock proteins and nucleotide-binding proteins. Gene Ontology (GO) term enrichment analysis revealed that a major fraction of the total number of identified peptides (>3000 peptides in 4 biological replicates) were significantly associated with the nuclear and mitochondrial fractions **(Figure R3a**). Mitochondrial peptides constituted 7.5 ± 0.3 % of the total exosome proteome, consistent with proteomic studies on exosomes isolated from other cell types, including immune cells [184,185]. Exosomes isolated from resting T lymphoblasts and cells activated with a polyclonal stimulus barely contained proteins of the mitochondrial matrix and the inner or outer mitochondrial membranes **(Figure R3b)**. Exosomes from activated T lymphoblasts contained significant amounts of mitochondrial transcription factor A (TFAM), a highly abundant mtDNA-binding protein, and the mitochondrial nucleoid-forming protein ATPase family AAA-Domain containing protein 3 (ATAD3) [186] **(Figure R3b)**. The presence of the canonical exosomal proteins CD81 and TSG101 in the purified 100.000 ×g fraction suggested an endosomal origin **(Figure R3b)**.

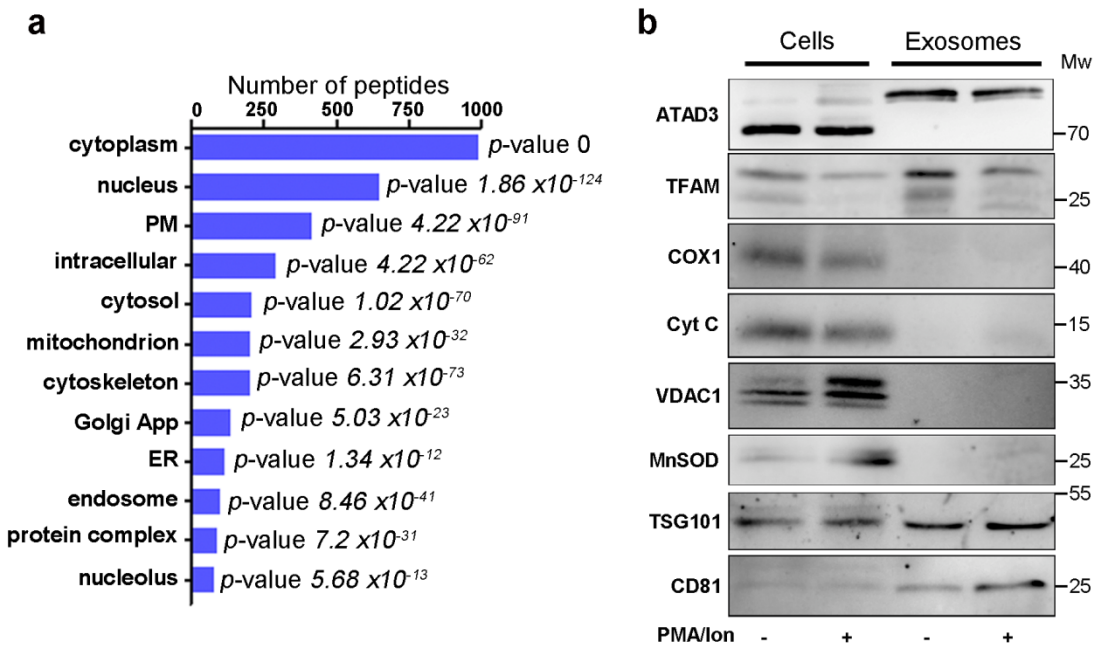

Figure R3. Cellular origin of protein content in T cell exosomes. (a) Gene ontology (GO) cellular component analysis of peptides identified in T cell exosomes. **(b)** Western Blot analysis of mitochondrial proteins in exosomes obtained from the culture supernatant of primary human T lymphoblast upon treatment with phorbol myristate acetate (PMA) together with Ionomycin to induce T cell activation.

TFAM and ATAD3 co-fractionated with the exosomal proteins CD81 and TSG101 in the 100.000×g EV fraction from sucrose-gradient isolation, **(Figure R4b and R4b)**, localizing mtDNA-binding proteins to exosomes.

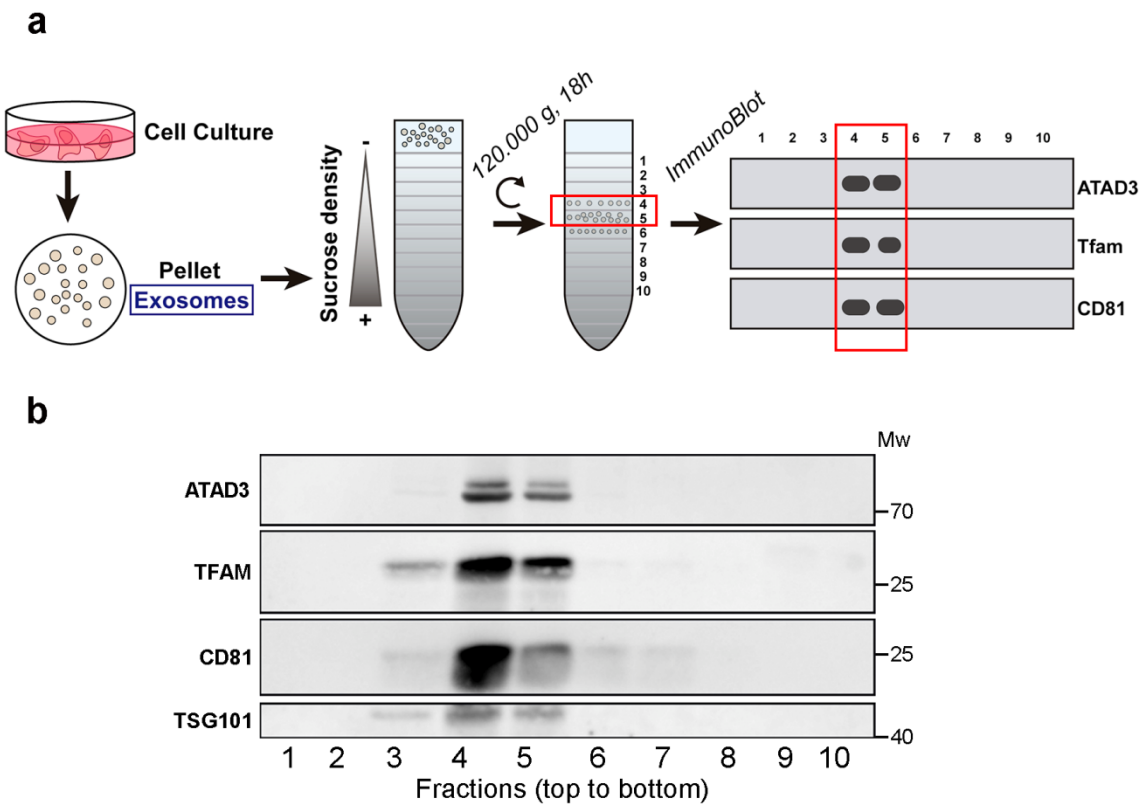

Figure R4. Sucrose gradient analysis of T cell exosomes (a) EVs obtained from the culture supernatant of human T lymphoblasts were laid on a discontinuous sucrose gradient and floated by overnight centrifugation. Gradient fractions were collected and analyzed by immunoblot to reveal the distribution of mtDNA-binding proteins and exosomal proteins in the sucrose fractions from lower to higher sucrose density (left to right). **(b)** Western blot analysis of ATAD3, TFAM, and the exosome markers CD81 and TSG101 in sucrose fractions. Gels shown are representative out of 3 independent experiments.

2. T cells incorporate genomic and mitochondrial DNA in exosomes

Among EVs, exosomes are enriched in genetic material, mostly non-coding RNAs [102,187]. Exosomes from cancer cell lines and patients contain DNA that reflects the mutational status of the parental tumor cells [103,105]. Deep-sequencing analysis of DNA in the EVs secreted by primary T lymphoblasts identified several reads that covered nuclear sequences and the entire mitochondrial genome **(Figure R5a)**. These results were confirmed by polymerase chain reaction (PCR) amplification of indicated regions of the mitochondrial genome and the B2M nuclear gene from the DNA obtained from the 100 000 ×g fraction **(Figure R5b)**.

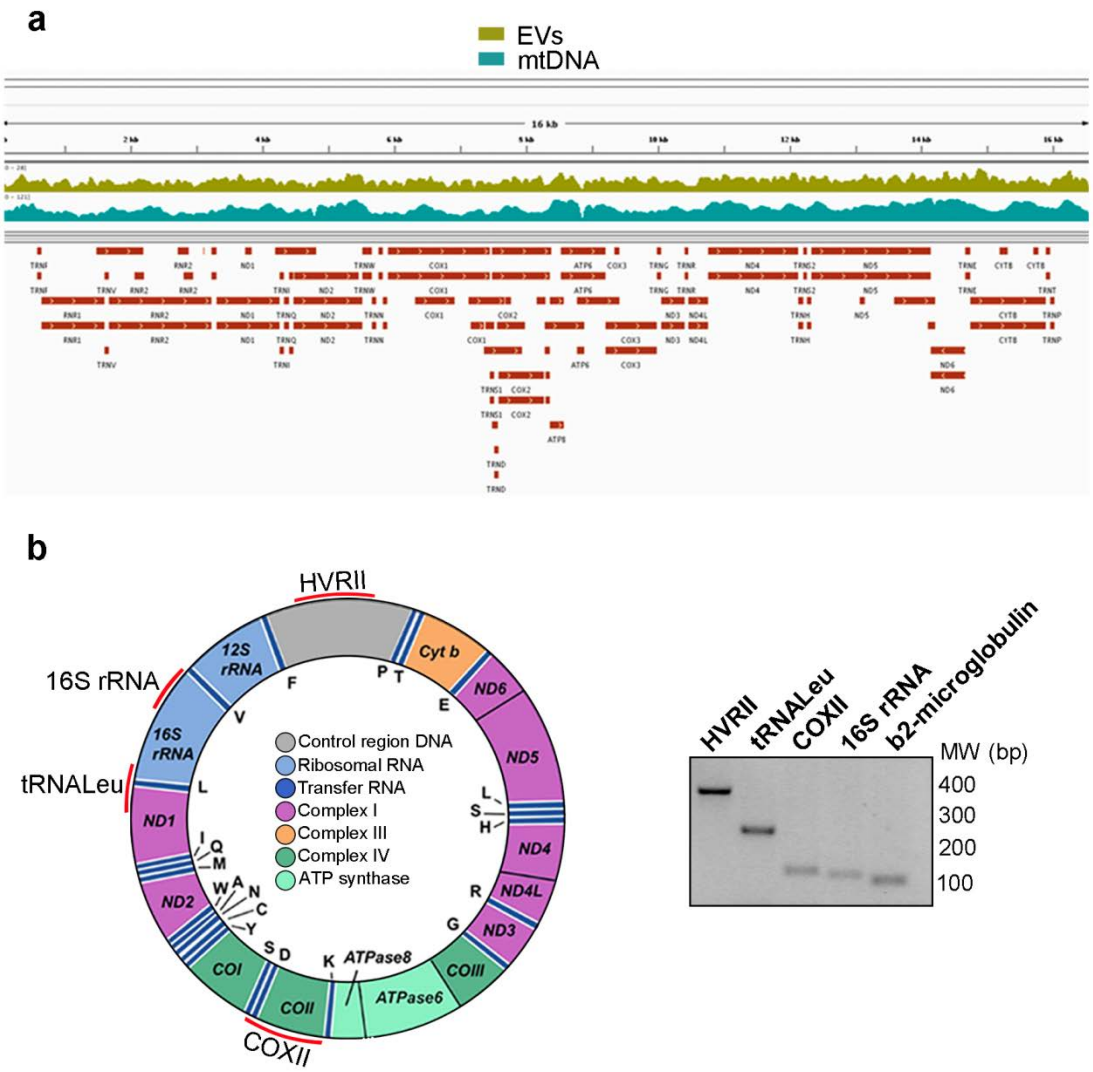

Figure R5. T cell exosomes shuttle mtDNA and genomic DNA. (a) Representation of the number of sequence reads aligned with the mitochondrial genome in EVs (EVs) and mitochondrial extracts (mtDNA) isolated from human primary T cells. **(b)** Left panel, Diagram of the mitochondrial genome, indicating the mtDNA regions analyzed by PCR (marked in red: HVRII, tRNALeu, COXII, and 16S rRNA). Right panel, Agarose gel showing the amplification products of the different mtDNA regions and the genomic DNA (β2-Microglobulin) analyzed in EVs purified from primary human T cells.

The DNA content of the isolated EVs was reduced by DNase treatment whereas a small fraction of the DNA remained protected unless vesicles were treated with DNase and a lipid destabilizing agent **(Figure R6a).** Two pools of DNA were present, one accessible (likely on the surface of the vesicle) and one inaccessible (likely in the lumen of the vesicle). The presence of mtDNA in the 100 000 ×g EV fraction was confirmed by the partial co-fractionation on sucrose gradients with the exosomal proteins CD63 and TSG101 **(Figure R6b)**.

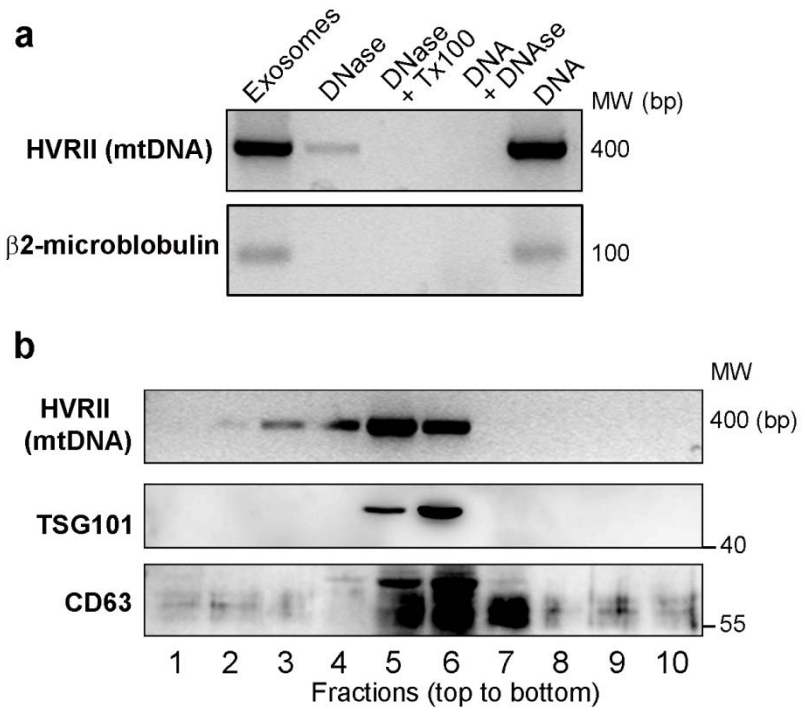

Figure R6. mtDNA is present both inside and outside of exosomes. (a) Agarose gel electrophoresis showing the detection of DNA in purified EVs. EVs obtained from the culture supernatant of J77 T were treated with DNase or DNase and Tx-100. Levels of mtDNA and genomic DNA were assessed by PCR amplification (HVRII and β2-MICROGLOBULIN, respectively). Isolated DNA from J77 T cells treated or not with DNase (DNA, DNA+DNase) is shown as control for DNase activity. **(b)** Distribution of mtDNA and TSG101 and CD63 in sucrose fractions. EVs from human Jurkat T cells were laid on a discontinuous sucrose gradient and floated by overnight centrifugation. DNA from gradient fractions was PCR-amplified for the HVRII mtDNA region. Proteins from gradient fractions were analyzed by immunoblot for TSG101 and CD63. A representative gel is shown (n=3).

3. mtDNA is partially oxidized and present only in a specific exosomal subpopulation

Flow cytometry analysis of EVs coupled to aldehyde sulfate beads reveals that the majority of beads were positive for both CD81 and DNA **(Figure R7a and R7b**). Total Internal Reflection Fluorescence (TIRF) microscopy-based analysis of the co-localization of exosomal marker CD81 with TSG101 or with DNA in isolated EVs showed that CD81 fully co-localized with TSG101, but only partly with DNA **(Figure R7c)**, suggesting the presence of DNA in a subset of $CD81^+$ exosomes in addition to other different populations of EVs.

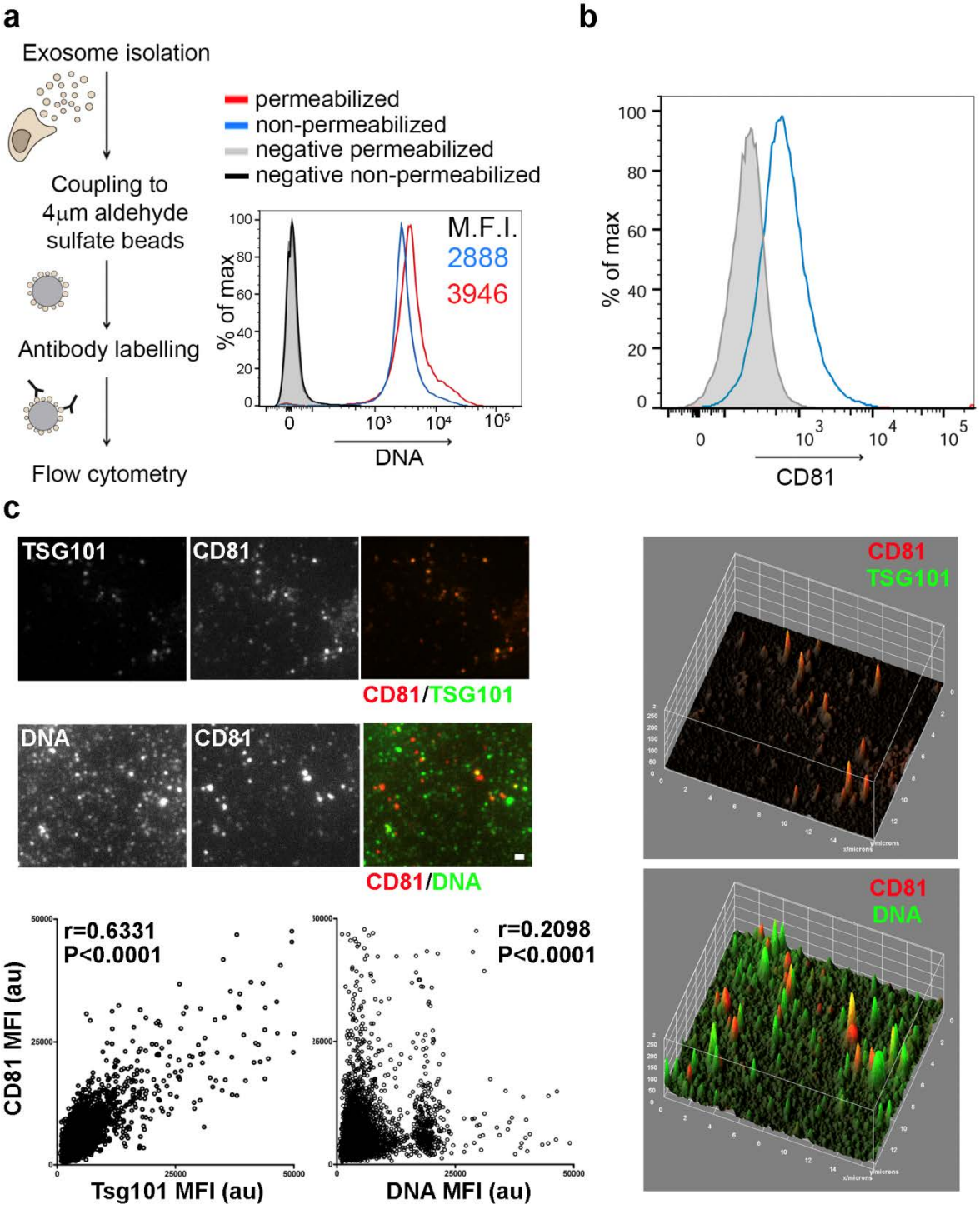

Figure R7. Characterization of the mtDNA containing vesicular subpopulation. Legend on the next page

Figure R7. Characterization of the mtDNA containing vesicular subpopulation.(a) Exosomes from primary mouse T lymphoblasts were purified, coupled to aldehyde sulfate beads, and analyzed by flow cytometry by staining with the anti-DNA Ab under permeabilizing and non-permeabilizing conditions. Histograms show DNA staining in exosomes. Numbers are mean fluorescence intensities of the positive population from a representative experiment (n=3). **(b)** Exosomes from primary mouse T lymphoblasts were purified, coupled to aldehyde sulfate beads and analyzed by flow cytometry by staining with the anti-CD81 Ab under non-permeabilizing conditions. Histograms show CD81 staining in exosomes coupled to aldehyde sulfate beads. **(c)** Images from isolated exosomal preparations stained for CD81 (red in merged images) and TSG101 or DNA (green in merged images). Exosomal preparations were spun on coverslips, fixed, processed for immunofluorescence and imaged in parallel. Permeabilization was performed upon CD81 staining. Imaging was performed with a TIRFm with a laser penetrance of 90 nm. Individual spots were detected. Scale bar, 1 µm. Graphs, Qualitative co-localization of fluorescence (yellow in merged images and graphs). The fluorescence intensity is plotted versus xy localization of the merged images showed. Scatter plots, correlation between mean fluorescence intensity from CD81:Tsg101 or CD81:DNA from TIRF images (r, Spearman coefficient for correlation; $P<0.001$, n=5937). Graphs were obtained with the Interactive 3D Surface Plot Plugging from Image J (https://imagej.nih.gov/ij/plugins/surface-plot-3d.html). Scatter plots correspond to the data from analysis with Image J from 20 different images from two different exosomal preparations from mouse T lymphoblasts. Images were normalized and processed in parallel.

DNA staining in non-permeabilized EVs increased upon permeabilization, confirming that DNA is present both outside and inside EVs. To examine the oxidative status of EV DNA, the 8-hydroxy deoxyguanosine (8-OHdG) DNA modification was evaluated as a hallmark of DNA oxidation. Staining with anti-oxidized-DNA antibody (Ab) is also detected in non-permeabilized EVs **(Figure R8a)**. In agreement with these results, chromatin immunoprecipitation of EV lysates with 8-OHdG Ab followed by DNA isolation and PCR analysis revealed the presence of several oxidized mtDNA and genomic DNA regions in EVs when compared with the control isotype Ab **(Figure R8b)**. To address the preferential localization of oxidized mtDNA, EVs and mitochondrial fractions of the corresponding cells were isolated and chromatin immunoprecipitation (ChIP) was performed with the 8-OHdG and total-DNA Abs. The enrichment in oxidized mtDNA at the EV fraction was demonstrated by qPCR analysis of mitochondrial genes in ChIP and quantification of the ratio between oxidized DNA vs total DNA **(Figure R8c)**. These results indicate that T cells release EVs carrying genomic DNA and mtDNA and associated mtDNA-binding proteins, and that the released DNA is partially oxidized.

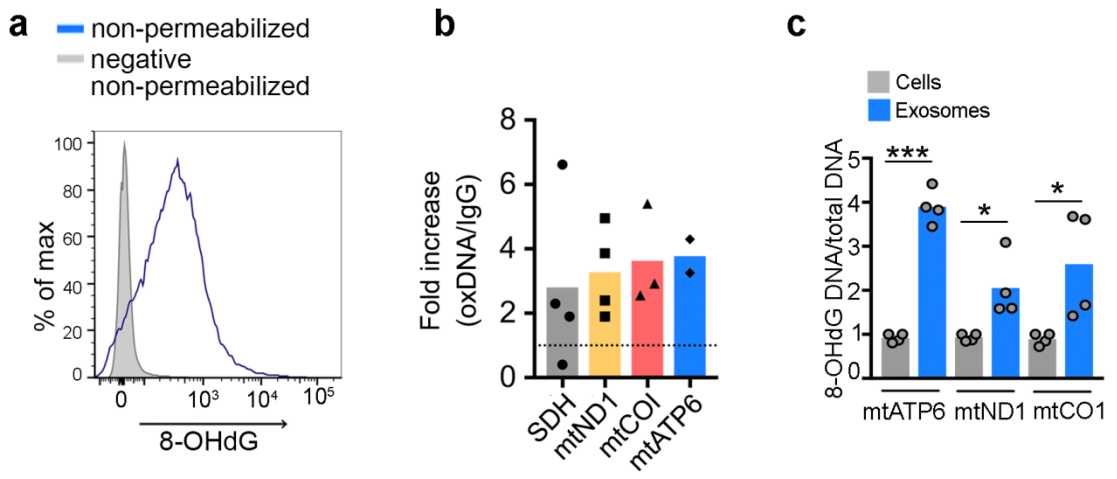

Figure R8. Analysis of oxidized state of mtDNA present in exosomes. (a) Histogram shows oxidized DNA staining in exosomes coupled to aldehyde sulfate beads with anti-8 hydroxydeoxyguanosine (8OHdG)Ab under non-permeabilizing conditions. **(b)** PCR analysis of the enrichment of the indicated mitochondrial (mtCO1, mtND1, mtATP6) or genomic (succinate dehydrogenase, SDH) genes in the DNA obtained from exosomes and immunoprecipitated with 8-OHdG Ab relative to isotype control IgG. Mean from quantification of 4 independent experiments. **(c)** qPCR analysis showing the enrichment of the indicated mitochondrial genes in the DNA obtained from exosomes and mitochondrial fractions from the same exosome-producing cells. DNA from both fractions was immunoprecipitated with 8-OHdG and total DNA Abs. Graph shows the ratio between oxidized DNA and total DNA in exosomes relative to their content in the mitochondrial fractions from the producing cells in duplicates from two independent experiments. t-test:*P-value<0.05, ***P-value<0.0001.

4. mtDNA and related proteins segregate into MVB pathway

The presence of mitochondrial components in EVs prompted us to investigate the molecular mechanisms controlling their extracellular release. We first co-transfected HEK-293 cells with TFAM-GFP and a mitochondria-targeted red fluorescent protein (mitoDsRed), then stained for endosomal markers. Confocal immunofluorescence analysis excluded co-localization of mitochondria and TFAM with the early endosome antigen 1 (EEA1), an early endosomal marker. Mitochondria and TFAM partially co-localized with components of maturing endosomal structures: HRS (hepatocyte growth factor regulated tyrosine kinase substrate), a component of the ESCRT machinery; lysobisphosphatidic acid (LBPA) and ceramide-positive structures, whose are markers of late endosomes and MVBs; and CD63, a highly abundant tetraspanin found in MVBs and exosomes **(Figure R9)**.

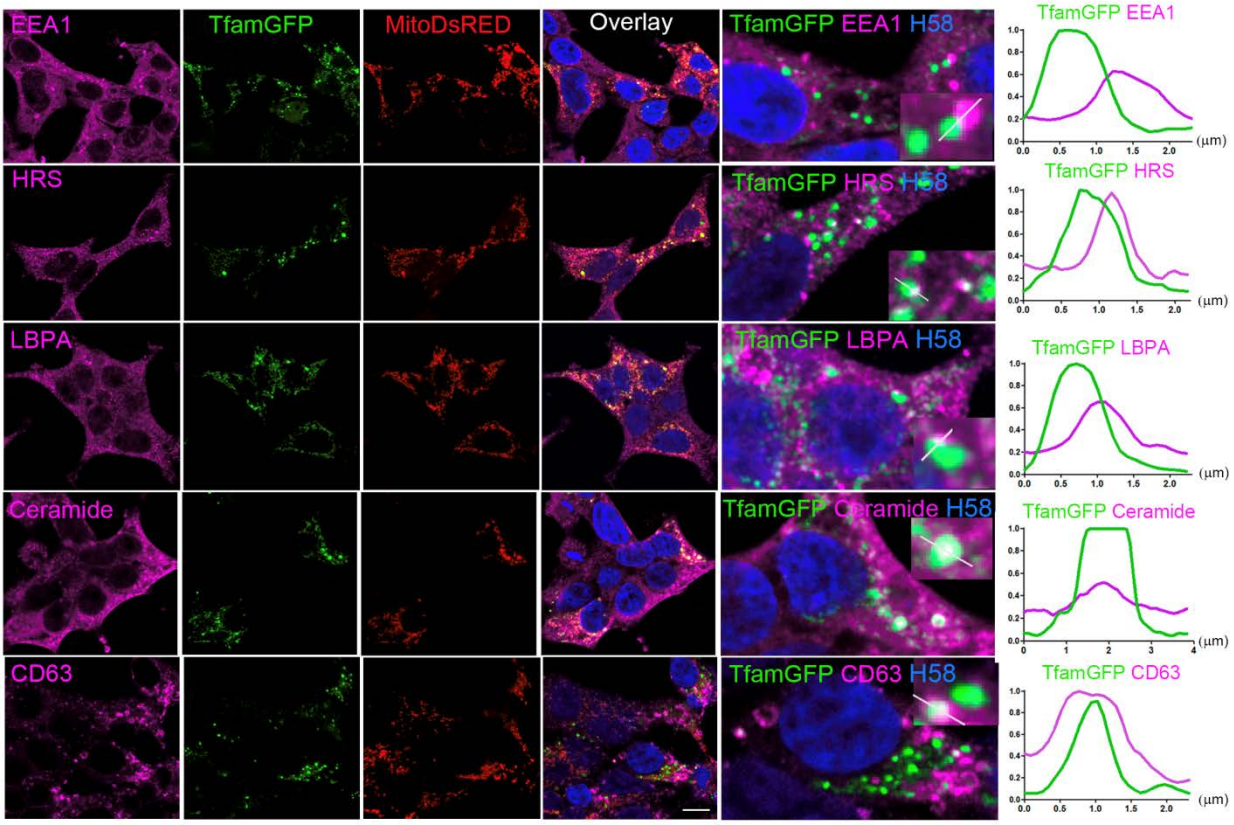

Figure R9. Mitochondrial components colocalize with markers from the endosomal pathway. Confocal co-localization analysis in HEK293 cells co-transfected with TFAM-GFP (green), nuclei with HOECHST 58 (blue) and a mitochondrial targeted fluorescent protein (mitoDsRed, red) and immunostained for endolysosomal compartment markers: the early endosome marker EEA1 and the ESCRT components HRS, LBPA, CD63, and ceramide (purple). Right images show high magnification views of co-localization between TFAM-GFP (green) and the various endolysosomal markers (purple). Charts show the fluorescence profiles along the corresponding white lines in the inset panels. Bar, 10 mm

To rule out potential analysis artifacts produced by the exogenous overexpression of TFAM-GFP, we measured the co-localization of endogenous mtDNA-binding protein single stranded DNA binding protein 1 (SSBP1) with EEA1 and CD63 in HEK-293 cells treated with low doses of FCCP, that promotes these events [188]. Increased co-localization of SSBP1 with CD63 indicates preferential localization in late endosomal structures **(Figure R10a)**.

The segregation of mitochondrial components into maturing endosomal structures was confirmed in HEK-293 cells transfected with constitutively active Rab7 (Q67L), which enhances endosomal trafficking, resulting in the formation of enlarged late endolysosomal structures [189].

Thus, Rab7 (Q67L) triggered the accumulation of endogenous TFAM within Rab7-positive endosomal structures, co-localizing with mitoDsRed **(Figure R10b)**. Also, immunogold labeling of TFAM and DNA revealed their appearance in canonical multivesicular body structures in electron microscopy studies **(Figure R10c)**, overall supporting the involvement of the endosomal pathway in the secretion of mitochondrial components in EVs.

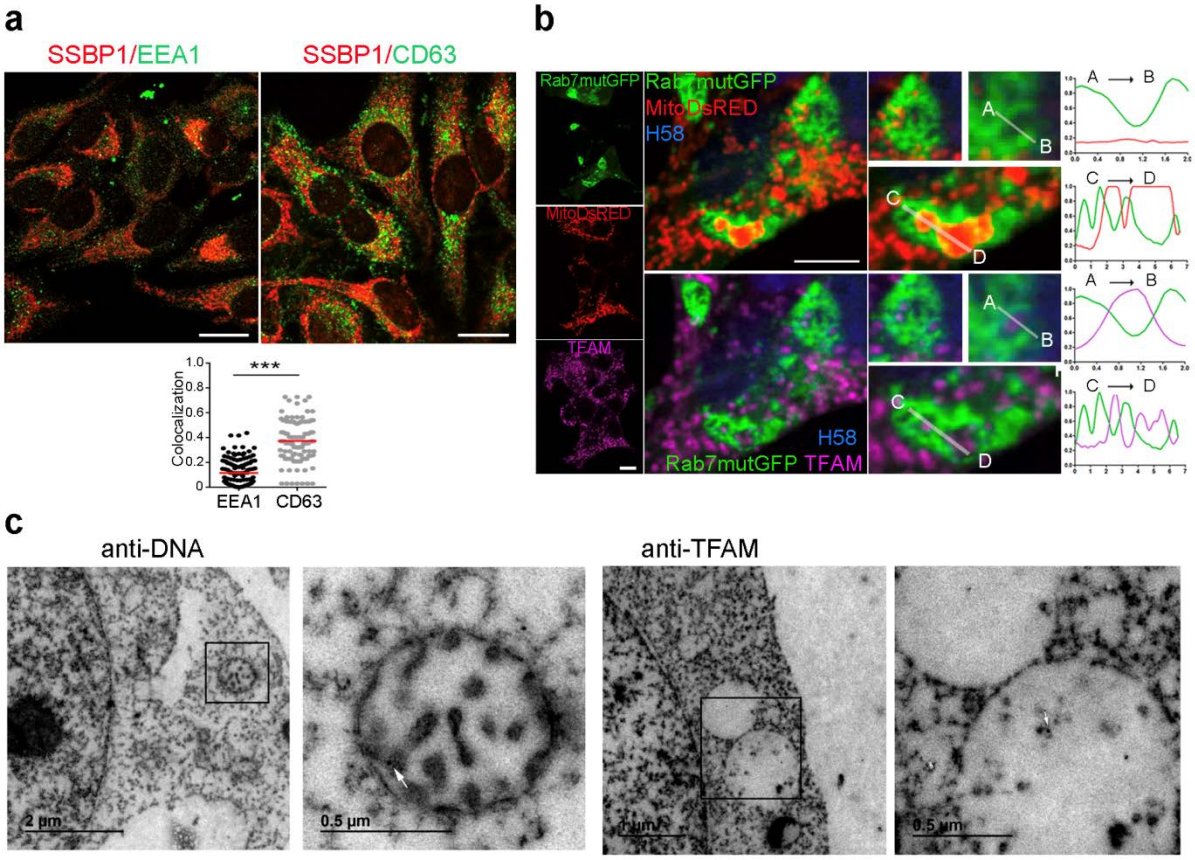

Figure R10. Mitochondrial components segregate into MVBs. (a) Confocal co-localization analysis in HEK293 cells treated with FCCP (4 h) and stained with SSBP1 (red), EEA1 and CD63 (green). Bar, 10 µm. Graph shows means for Mander's colocalization coefficient for SSBP1 and EEA1 or CD63 (n=3). t-test: ***P-value<0.0001. **(b)** Confocal co-localization analysis in HEK293 cells co-transfected with Rab7-Q67L-GFP (Rab7mutGFP, green) and mitoDsRed (red), and immunostained for TFAM (purple) and nuclei (HOECHST 58, blue). Center and right images show high magnification of left images (Rab7-Q67L-GFP and mitoDsRed in upper panels; Rab7-Q67L-GFP and TFAM in lower panels). Charts, Fluorescence profiles along the corresponding white lines. Bar, 10 µm. **(c)** Representative electron microscopy images showing DNA and TFAM immunogold staining in canonical multivesicular bodies from HEK293T cells transfected with the active mutant Rab7-Q67L-GFP.

5. Exosome secretion affects mitochondrial homeostasis

To further elucidate the nature of the vesicles containing mitochondrial components, we inhibited exosome biogenesis in T cells by targeting the neutral sphingomyelinase 2 (nSMase2, SMPD3) **(Figure R11a)**. This enzyme participates in exosome biogenesis by triggering the budding of intraluminal vesicles into MVBs [80]. These conditions reduced the recovery of exosomal proteins as well as mtDNA-binding proteins and mtDNA in the purified 100.000 ×g fraction **(Figure R11b)**, showing that mtDNA and mtDNA-binding proteins are released through canonical exosomal pathway and not in other EVs such as apoptotic bodies. The blocking of exosome biogenesis by silencing nSMase2 or MVB fusion with the plasma membrane by targeting Rab27a with specific shRNAs **(Figure R11a),** increased mitochondrial mass, intracellular TFAM levels, intracellular ROS, and DNA oxidative damage **(Figure R11c)**.

The suppression of nSMase2 or Rab27a altered mitochondrial morphology and cristae organization, with increased mitochondrial cristae width **(Figure R12a)**. Changes in mitochondrial cristae organization relate to changes in mitochondrial electron transport chain complex organization that in turn may result in functional changes in the respiration ability of cells. Specifically, tight cristae provide more efficient mitochondrial OXPHOS [190], whereas loose cristae appear in highly glycolytic cells [191]. Consistent with a loose organization of mitochondrial cristae, Rab27a and nSMase2 silencing significantly decreased mitochondrial respiration **(Figure R12b)**. These findings indicate that mitochondrial function is altered in the absence of proper exosome biogenesis and secretion and suggest that the release of mitochondrial content in exosomes contributes to mitochondrial homeostasis and mtDNA metabolism.

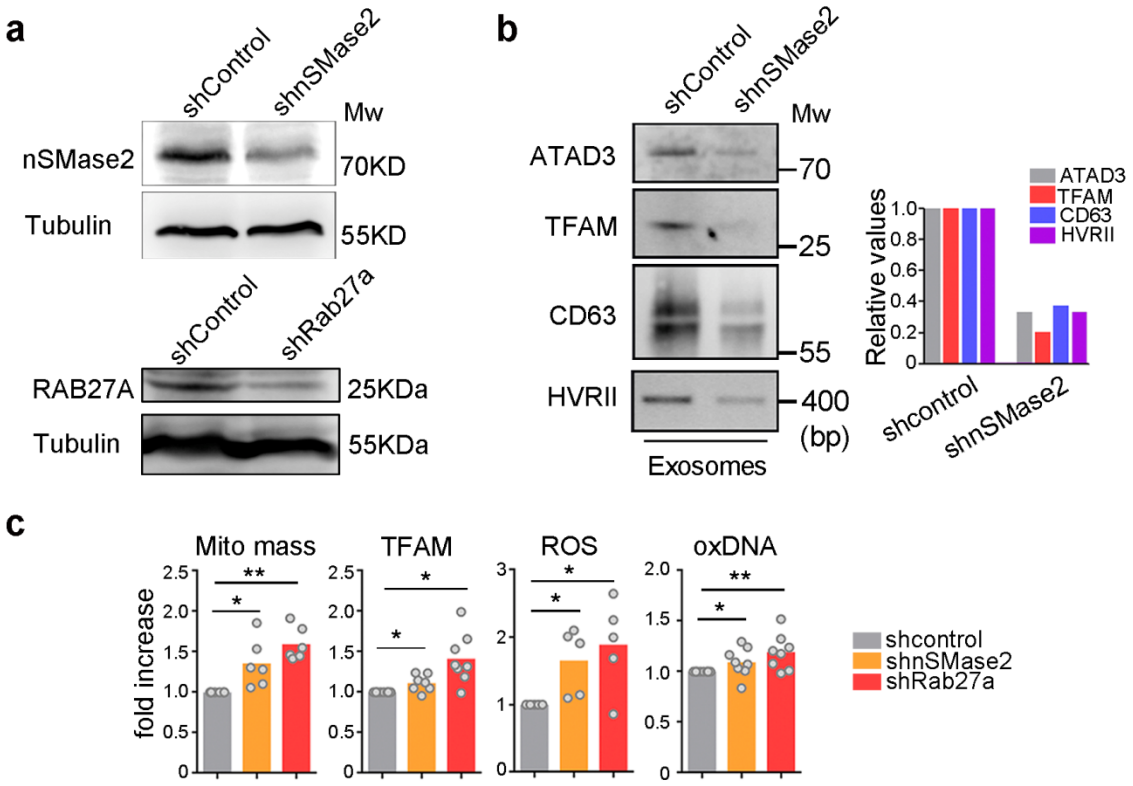

Figure R11. Exosomal secretion impairment affect mitochondrial parameters. (a) Up, Western blot analysis of nSMase 2 knockdown in J77 T cells infected with shControl or shnSMase2 shRNA. Down, Western blot analysis of Rab27a knockdown in HEK293 cells infected with specific shControl or shRab27a RNA. **(b)** Mitochondrial components in the exosome fraction obtained from equal numbers of shControl and shnSMase2 J77 T cells. ATAD3, TFAM, and CD63 were detected by immunoblot; mtDNA was detected by PCR for HVRII. Graph, Quantification of exosomal proteins and mtDNA in a representative experiment (n=3). **(c)** Flow cytometry analysis of mitochondrial mass (Mitotracker green), intracellular ROS levels (DCFDA staining), oxidized DNA (8-OHdG Ab staining), and endogenous TFAM in HEK293 cells knocked down for nSMase2 and Rab27a. Graphs, Quantification from 5-8 independent experiments (Mean). t-test *P-value<0.05; **P-value<0.001.

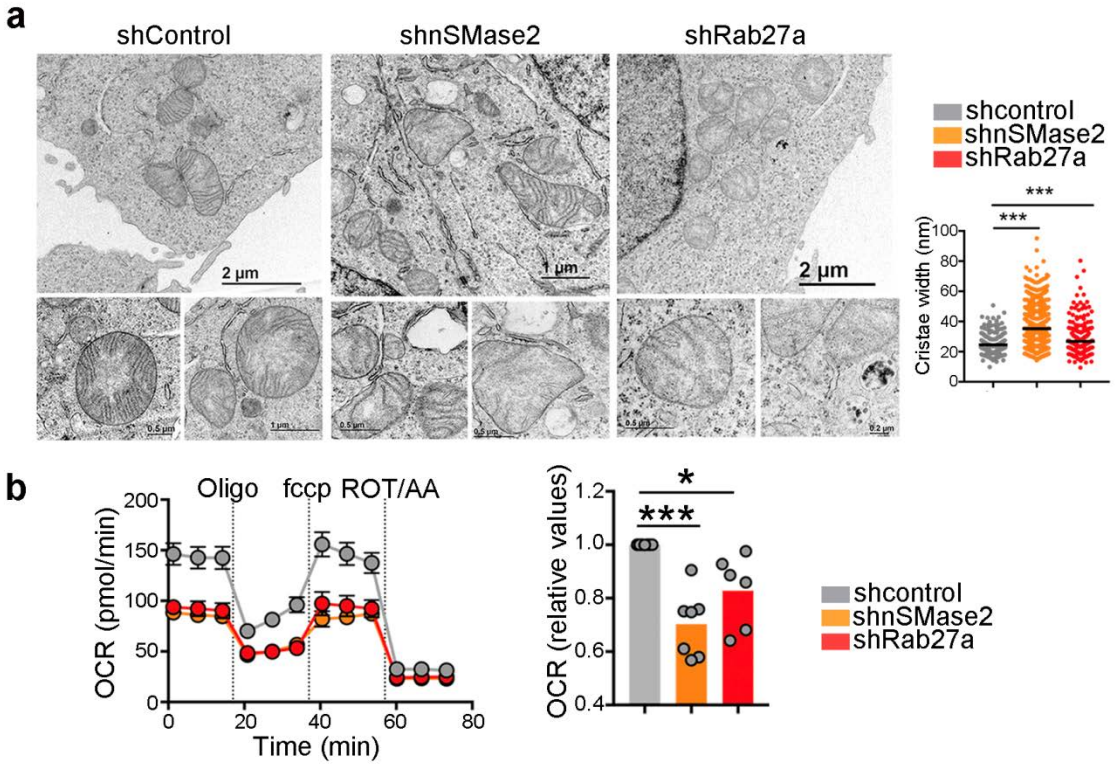

Figure R12. Exosomal secretion impairment affect mitochondrial organization and respiration. (a) Electron microscopy images show defects in mitochondrial ultrastructure and cristae organization in shnSMase2 and shRab27a HEK293 cells. Graph, Quantification of mitochondrial cristae width (Mean). t-test: ***P-value<0.0001 **(b)** Graph, Basal oxygen consumption rate (OCR) of control, shnSMase2 and shRab27a HEK293 cells. Dots represent mean from three independent experiments run in duplicate or triplicate. t-test, *P-value<0.05, ***P-value<0.0001. Chart, OCR from shControl, shnSMase2 and shRab27a HEK293 cells in response to oligomycin (Oligo), fccp, and rotenone plus antimycin A (Rot/AA). (n=2; mean ± S.E.M.)

We next investigated the contribution of mitochondrial turnover and degradation mechanisms to the secretion of mitochondrial components in EVs. Macroautophagy, from here on referred to as autophagy, is a self-degradation process that recycles cellular constituents, including misfolded or aggregated proteins and damaged organelles [192]. Confocal microscopy analysis did not reveal co-localization of autophagy proteins ATG5 and LC3 with MVBs or mitochondria **(Figure R13)**.

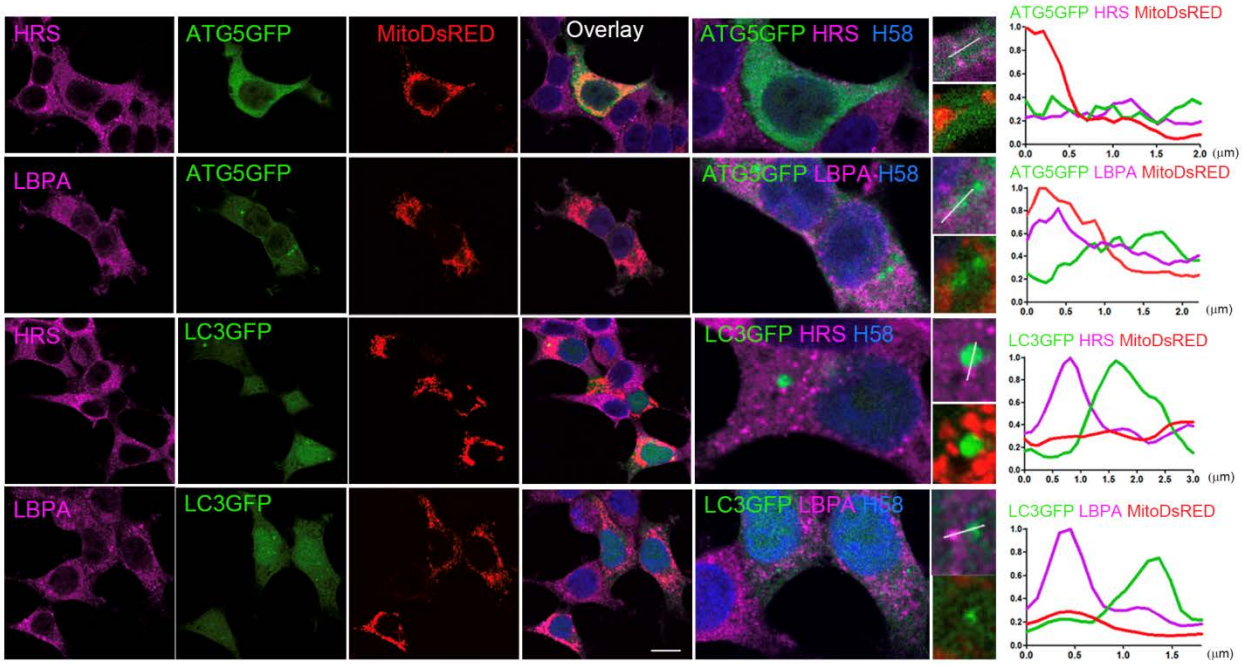

Figure R13. Colocalization of exosomal markers and autophagy proteins. Confocal co-localization analysis in HEK293 cells co-transfected with ATG5-GFP or LC3-GFP (green) and a mitochondria-targeted fluorescent protein (mitoDsRed, red) and stained with the endolysosomal compartment markers HRS and LBPA (purple) and nuclei with HOECHST 58 (blue). Right images show high magnification views of co-localization between ATG5/LC3 (green) and the various endolysosomal markers (purple). Charts show the fluorescence profiles along the corresponding white lines in the adjacent panels. Bar, 10 mm.

Serum deprivation, a reported autophagy stimulus, decreased exosome secretion concomitantly with reduced extracellular release of mitochondrial components **(Figure R14a)**, consistent with the autophagy-promoted specific degradation of MVBs [193]. Moreover, inhibition of autophagosome cargo degradation by bafilomycin-A1-mediated blockade of autophagosome-lysosome fusion did neither alter the detection of TFAM in the exosomal fraction nor the concentration and size of the purified EVs **(Figure R14a and R14b)**.

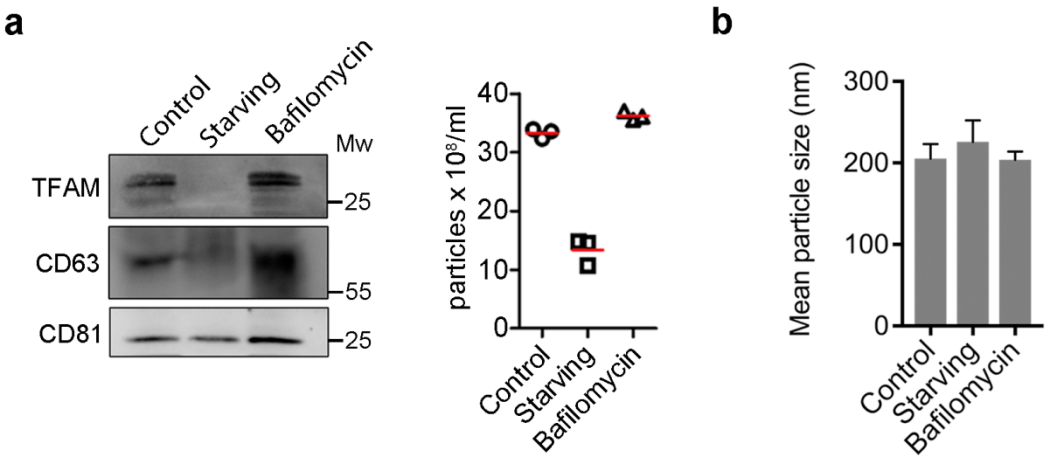

Figure R14. Autophagy is not responsible for the presence of mitochondrial content in exosomes (a) Western blot analysis of exosomes from Jurkat T cells left untreated, serum-starved overnight or treated with bafilomycin A. Membranes were blotted for TFAM, CD81 and CD63. Graph, Nanoparticle concentration in the exosomal fractions (mean, two independent experiments). **(b)** Size distribution analysis by Nanoparticle Tracking Analysis (NTA) of purified exosomes obtained from equal numbers of Jurkat T cells left untreated, serum-starved overnight, or treated with bafilomycin A.

This finding indicated that autophagosome secretion or content release upon bafilomycin-A1 treatment does not account for the presence of mitochondrial components in EVs. Additionally, specific siRNA silencing of the late autophagy mediator LC3 in J77 T cells did not alter exosome concentration and mitochondrial content **(Figure R15a and R15b)**. Together, these findings indicate that the loading and secretion of mitochondrial material in EVs occurs independently of general macroautophagy.

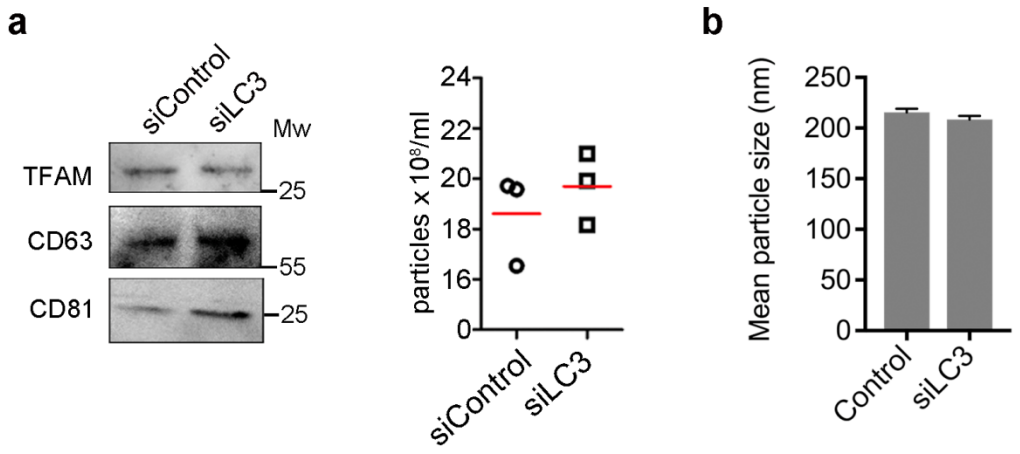

Figure R15. Autophagy is not related with mitochondrial containing exosomes secretion (a) Western blot analysis of exosomes obtained from Jurkat T cells transfected with control or LC3 siRNA. Graph, nanoparticle concentrations in the exosomal fractions (mean, n=2). Western blots are representative out of 3 independent experiments. **(b)** Size distribution analysis by Nanoparticle Tracking Analysis (NTA) of purified exosomes obtained from equal numbers of Jurkat T cells transfected with control siRNA or siRNA targeting LC3 from two independent experiments.

6. DNA and mitochondrial proteins are transferred at cognate immune contacts

The presence of mitochondrial constituents in exosomes led us to hypothesize that mitochondrial material could be transferred from the T cell to the APC during the formation of antigen-dependent contacts. To assess this, we first evaluated whether isolated exosomes shuttle mitochondrial components between cells. Purified exosomes from non-transfected J77 T cells or cells stably transfected with a mitochondria-targeted fluorescent protein, mitoDsRed, were added to Raji B lymphoblastoid cells, used as APCs. After incubation with exosomes from J77mitoDsRed cells, recipient cells exhibited mitoDsRed fluorescence **(Figure R16a)**.

We next assessed whether exosomes can mediate intercellular mtDNA transfer. Donor and acceptor cell mtDNAs were distinguished by the use of conplastic mice with the same nuclear genome (C57BL/6) but different mtDNA haplotypes, from the C57BL/6 mice strain ($C57^{C57}$) or from the NZB strain ($C57^{NZB}$) [194]. These two mtDNA haplotypes differ in 12 missense polymorphisms identifiable by restriction length fragment polymorphism (RFLP) analysis **(Figure R16b)**. Incubation of T cell-derived exosomes from $C57^{C57}$ mice with DCs differentiated

from the C57^{NZB} mice resulted in uptake of C57^{C57} mtDNA by recipient C57^{NZB} DCs, as shown by the acquisition of the C57^{C57} haplotype and the presence of C57^{C57} RFLP fragments in exosome-treated DCs **(Figure R16c)**, supporting the transfer of mitochondrial components and mtDNA between cells through exosomes.

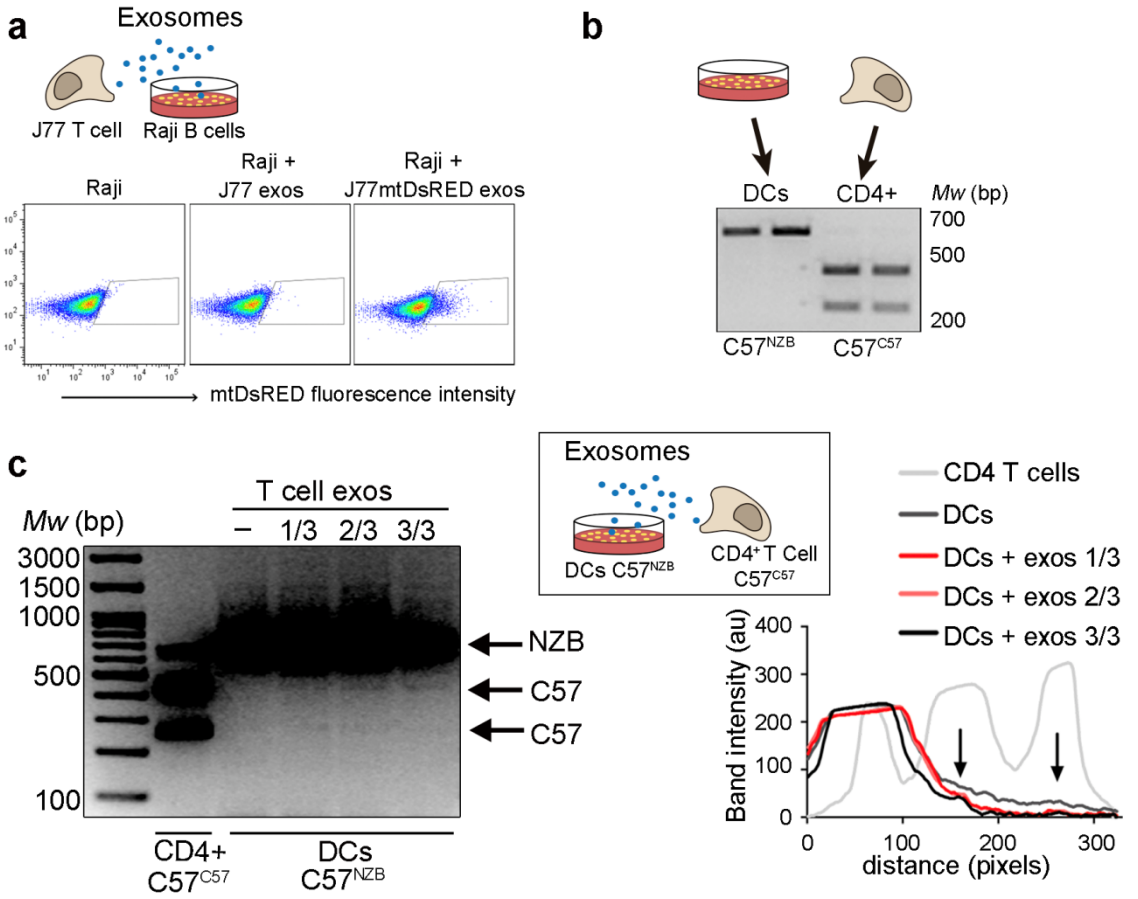

Figure R16. Mitochondrial proteins and DNA are transferred through exosomes to DC. (a) Flow cytometry analysis of Raji B cells incubated overnight with exosomes from J77 T cells control or stably expressing mitoDsRed (Representative experiment, n=3). **(b)** RFLP analysis of the mitochondrial genomes of C57^{C57} and C57^{NZB} mice. Total DNA is from C57^{C57} T lymphocytes and C57^{NZB} BMDCs. C57^{C57} haplotype results in 2 fragments. Digestion of PCR products from C57^{NZB} haplotype results in a single band. **(c)** RFLP detection of exogenous mtDNA in C57^{NZB} DCs incubated overnight with increasing amounts of exosomes from C57^{C57} CD4^{+} T lymphoblasts. 414 pb and 250 pb fragments appear in C57^{NZB} DCs upon addition of exosomes (lanes 1/3, 2/3 and 3/3). Chart, intensity profile of the RFLP analysis; arrows indicate the C57 mtDNA haplotype. C57^{C57} CD4^{+} lane displays a band of 664 pb which corresponds to an uncompleted digestion of the PCR product in the RFLP analysis and a high exposure of the image. Representative experiment (n= 3).

The mostly unidirectional nature of exosome transfer from T cells to DCs [55,132] suggested that the exchange of mitochondrial information between immune cells occurs upon antigen-dependent contacts. TCR Vβ8+ J77 T cells expressing a mitochondria-targeted fluorescent protein (mitoYFP) or a fluorescent version of TFAM (TFAM-DsRed) were co-cultured with Raji B cells preloaded with Staphylococcus enterotoxin superantigen-E (SEE), which mimics antigen recognition when confronted with TCR Vβ8+ T cells. Flow cytometry analysis revealed transfer of mitochondria (mitoYFP) and TFAM (TFAM-DsRED) from T cells to APCs during antigen-dependent interactions **(Figure R17)**.

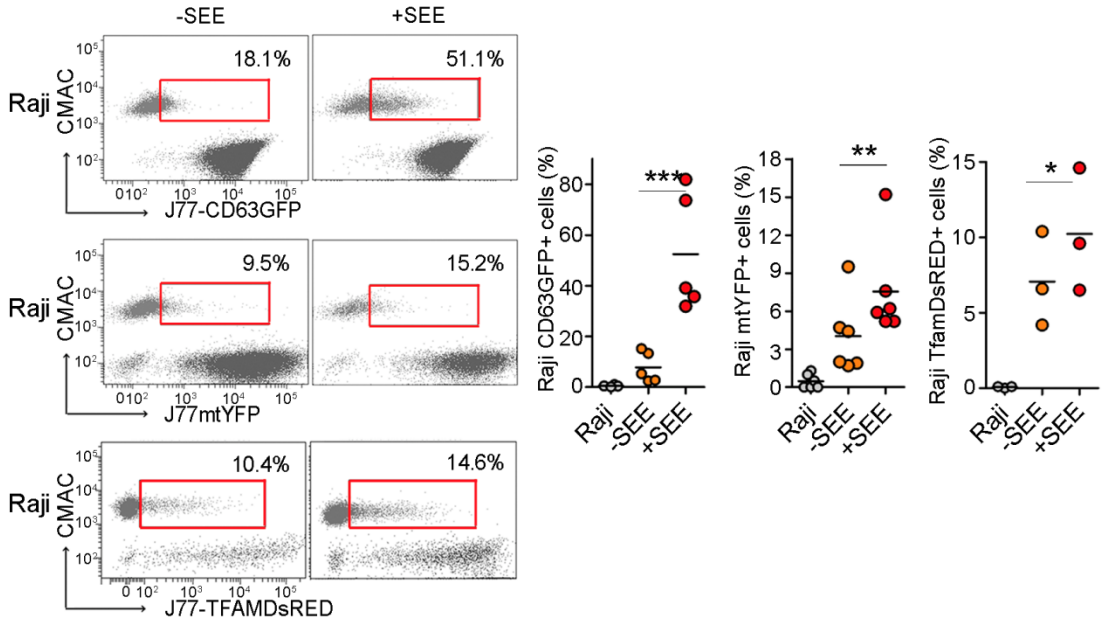

Figure R17. Exosomal and mitochondrial proteins are transferred upon cognate interactions. Exosome and mitochondrial transfer to unpulsed or SEE-pulsed Raji B cells (CMAC) from J77 T cells expressing the exosomal protein CD63GFP, the mitochondria-targeted mitoYFP or the mtDNA-binding protein TFAM-DsRED. Dot plots, cell populations after co-culture. Red boxes enclose Raji B cells that have acquired exosomal or mitochondrial fluorescent markers (percentage from total Raji cells). Graphs, percentage of Raji B cells acquiring fluorescence upon IS formation from 3-5 independent experiments; mean, t-test *P-value<0.05, **P-value<0.001, ***P-value<0.0001.

To address this in primary cells, we set up a model of antigenic presentation in which bone marrow-derived DC (BMDC) from $C57^{NZB}$ mice presented OVA peptide to CD4+ T cells from transgenic OT-II mice ($C57^{C57}$), which are specific for that antigen **(Figure R18a)** [194].

After 16h co-culture in the presence or absence of OVA peptide, we detected CD4+ T cell mtDNA only in recipient APCs from co-cultures including OVA peptide antigen **(Figure R18b)**, indicating that intercellular mtDNA transfer requires antigenic triggering. Using CD4+ T cells from OT-II $C57^{NZB}$ mice and BMDCs from the $C57^{C57}$ mice, we confirmed that mtDNA transfer occurred unidirectionally from T cells to BMDCs **(Figure R18c)**.

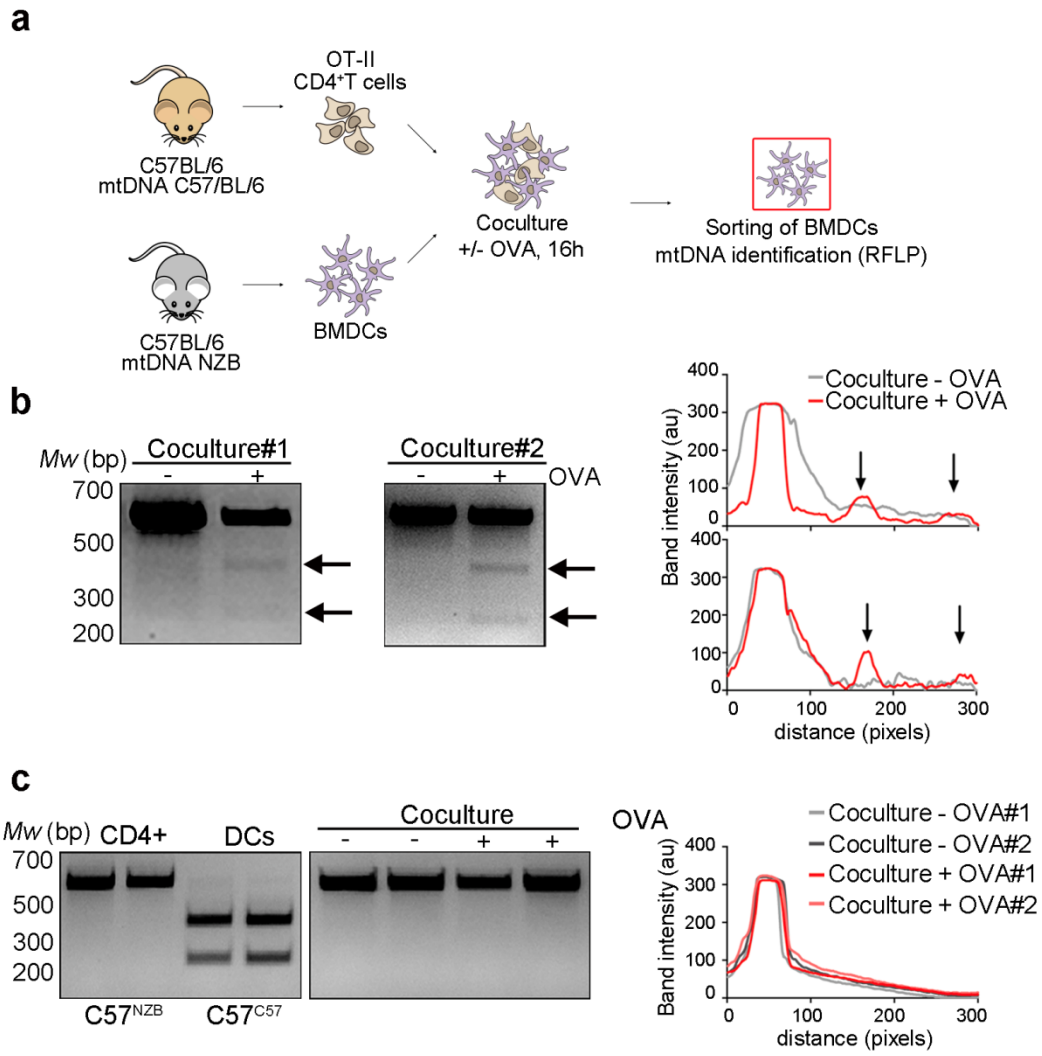

Figure R18. mtDNA is transfer during immune synapses. (a) Workflow for mtDNA transfer detection by RFLP during immune cognate interactions. **(b)** Detection of exogenous $C57^{C57}$ mtDNA from donor OT-II CD4+ T cells in recipient C57NZB DCs upon antigen stimulation (OVA). Gels, RFLP analysis of the mitochondrial genomes (n=2). Chart, intensity profile for RFLP. **(c)** RFLP analysis of the mitochondrial genomes of $C57^{C57}$ and $C57^{NZB}$ mice. Left gel shows RFLP analysis from $C57^{C57}$ T lymphocytes and C57NZB DCs. Right gel, lack of exogenous $C57^{C57}$ mtDNA from donor DCs in recipient $C57^{NZB}$ CD4+ T cells. Chart, intensity profile for RFLP analysis. Representative experiment (n=3).

7. Antiviral cGAS/STING-IRF3 pathway is activated upon exosome uptake

Mitochondrial components are a major source of danger-associated molecular patterns (DAMPs). They can trigger innate immune responses, likely due to their similarities to bacterial ancestors [195]. We hypothesized that the transfer of mitochondrial content and mtDNA during T cell-APC antigen-dependent contacts may represent a mode of cell-to-cell transmission of danger-associated messages. To examine this possibility, we interrogated which signaling pathways were controlled by T cell exosomes in recipient DCs. This was carried out by characterizing the changes to the gene profile of DCs upon incubation with T cell exosomes by RNA deep sequencing analysis **(Figure R19)**.

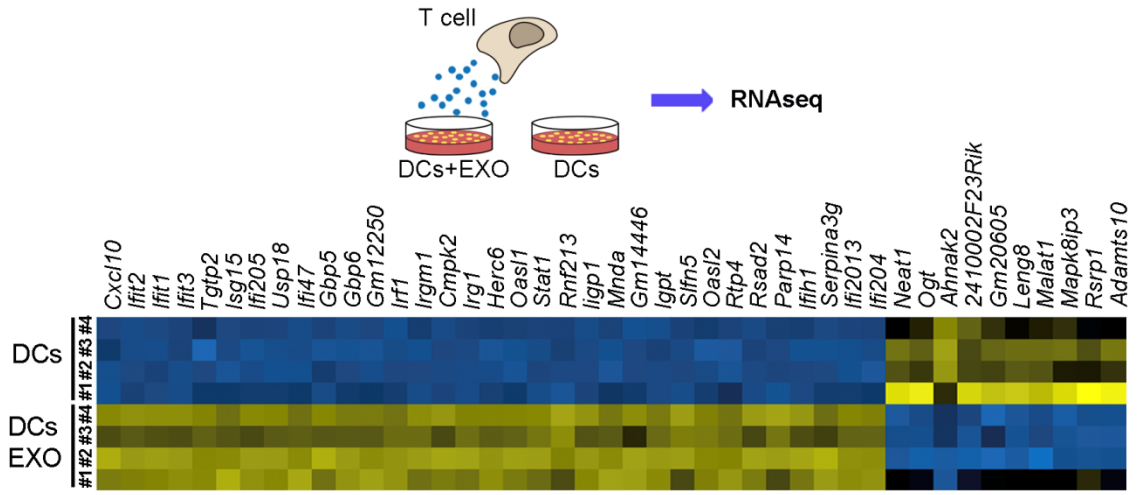

Figure R19. T cell exosomes prime DCs. Scheme explaining workflow for RNAseq analysis of DCs upon T cell exosome acquisition. Lower panel, RNAseq heat maps of 4 DC biological replicates with or without exosome uptake (DCs+EXO vs DCs). The panel shows upregulated (yellow) or downregulated (blue) genes with the highest significant fold changes.

Gene expression profiling identified more than 1600 significantly altered genes in recipient DCs exposed to T cell exosomes **(Figure R20a and R20b)**. Exosomes regulated the expression of a major set of genes involved in interferon (IFN) type I responses and antiviral activity, including IFN-stimulated genes (ISGs) Ifit1, Ifit2, Ifit3, Isg15, Usp18, and Cxcl10, and the antiviral signaling factors Gbp5 and Gbp6 **(Figure R19a)**. We validated the RNA sequencing results by quantitative PCR for the genes Cxcl10, Isg15, Ifit1, Ifit3, Usp18, and Stat1 **(Figure R20c)**.

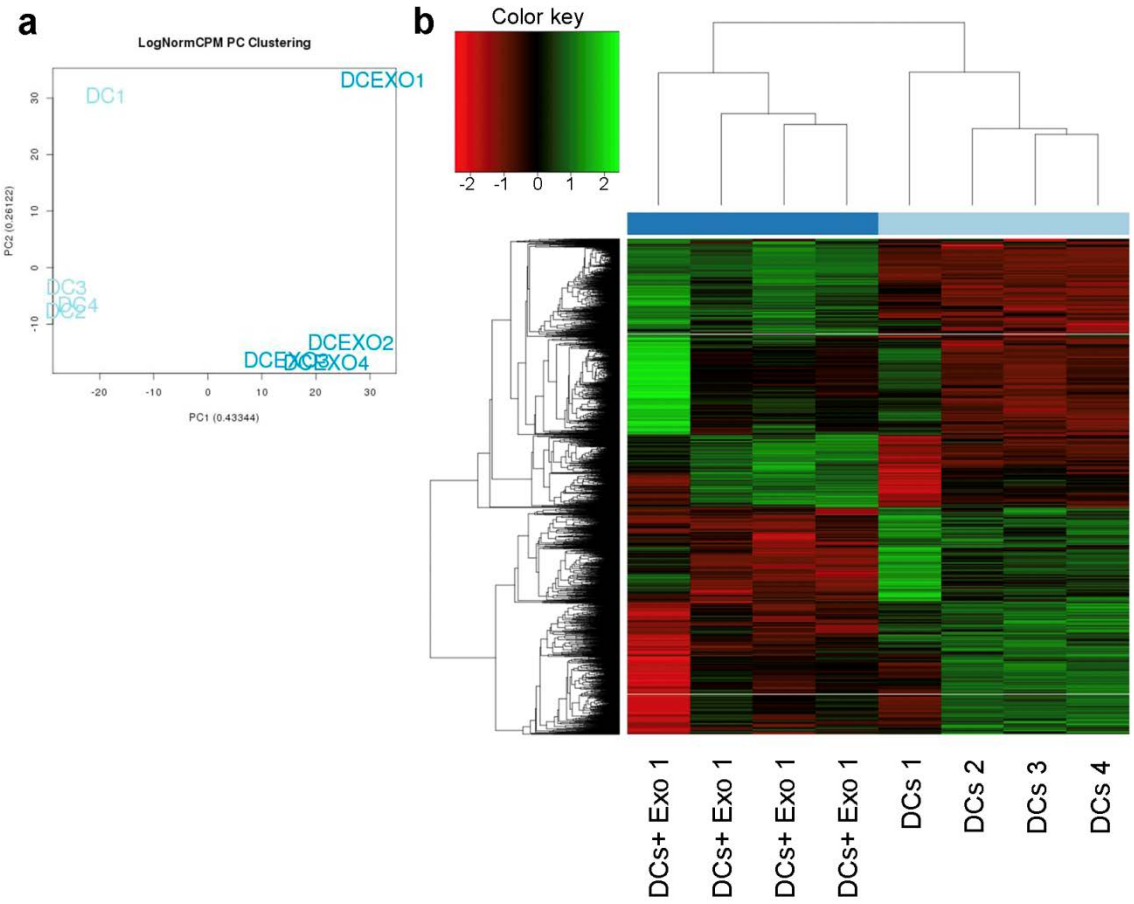

Figure R20. Bioinformatics analysis of the exosome-primed DC. (a) Principal Component Analysis (PCA) of the RNA samples obtained from 4 biological replicates of DCs and DCs incubated with exosomes. **(b)** Heatmap for the differently regulated genes in 4 biological replicates of DCs left untreated or treated with exosomes.

Analysis of the genes that changed their expression profile in response to T cell exosomes by Gene Ontology annotation indicated they were mainly involved in IFN signaling, exogenous DNA and RNA sensing, bacteria and viruses recognition, and crosstalk between innate and adaptive immune cells **(Figure R21a)**. These findings suggested that T cell exosomes prime the antiviral innate immune response in DCs, creating a gene signature that upregulates antiviral and antimicrobial responses to control pathogen infection and replication **(Figure R21b)**.

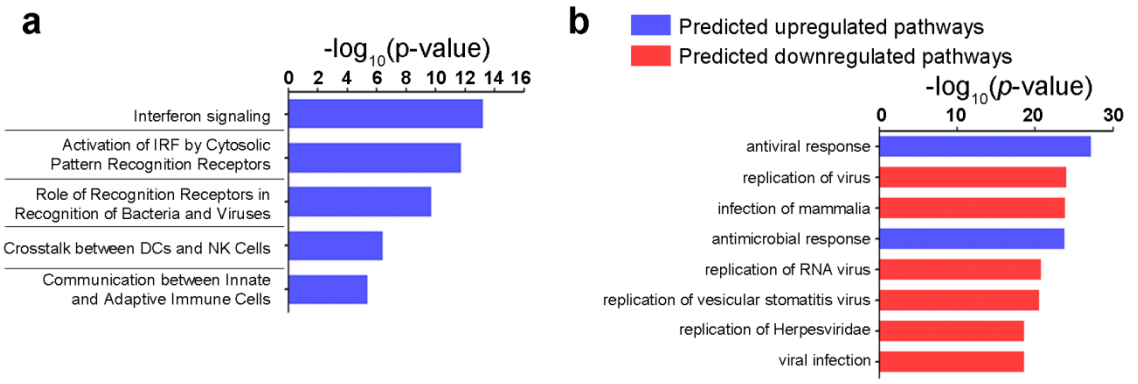

Figure R21. Pathogen defense pathways are upregulated in primed DC. (a) GO annotation of the biological processes differently regulated upon exosome addition; p-values are presented for the top-ranking biological processes. **(b)** Ingenuity analysis predictions of DC pathways upregulated or downregulated upon acquisition of T cell exosomes.

One of the most relevant pathways involved in ISG expression depends on cGAS/STING interaction upon cytoplasmic detection of endogenous or exogenous DNA [196]. cGAS functions as a main sensor of viral and bacterial DNA in the cytoplasm of infected cells. Upon its activation by DNA detection, it generates the second messenger cyclic dinucleotide cGAMP, which binds to and activates STING. STING in turn activates TANK-binding Kinase 1 (TBK1), which phosphorylates interferon regulatory factor 3 (IRF3) to promote its translocation to the nucleus, where it induces the expression of IFNγ and ISGs. Triggering of cytoplasmic DNA sensors is associated with intracellular clustering of STING [197]. Consistent with activation of the cGAS/STING DNA sensing pathway, exosomes induced a significant aggregation of STING in DCs **(Figure R22a)**. The expression of ISGs in response to exosomes was reduced in STING-deficient ($Sting^{Gt/Gt}$) DCs **(Figure R22b)**, and completely abrogated in Irf3-/- DCs **(Figure R22c)**.

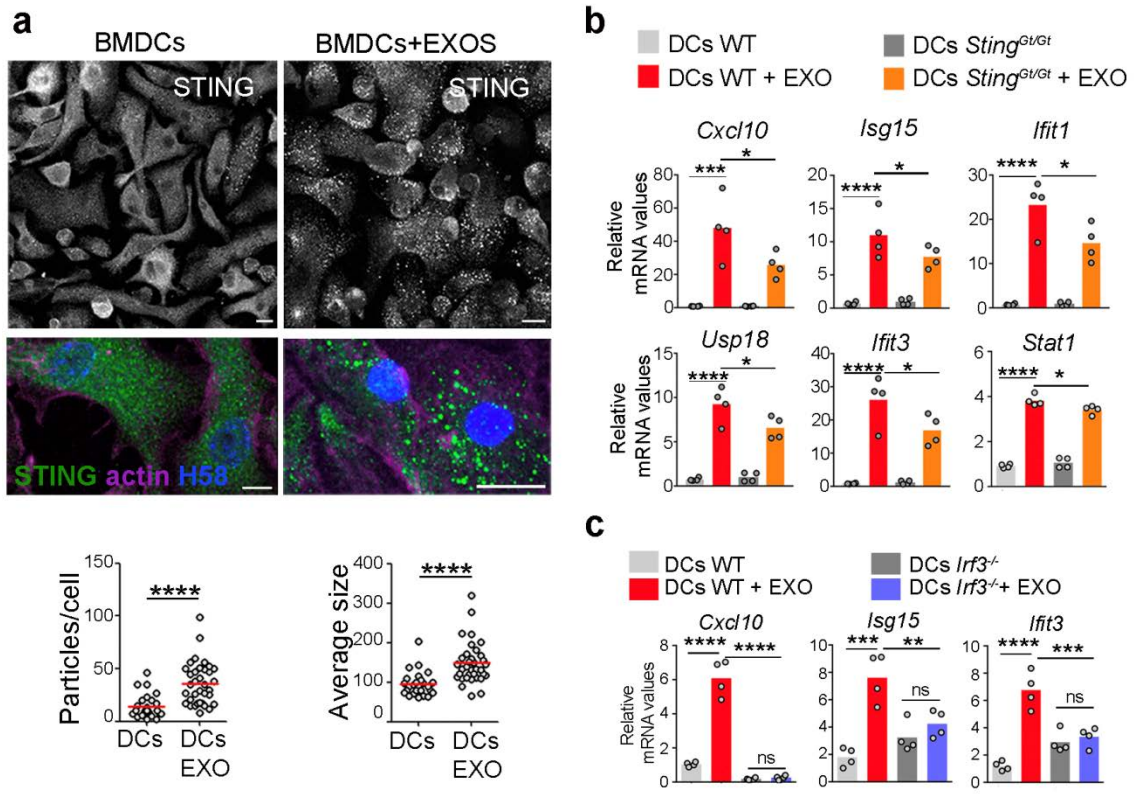

Figure R22. cGAS/STING DNA sensing pathway is partially responsible for the antiviral response signaling. (a) Upper panel, Immunofluorescence microscopy images showing STING aggregation (green) in DCs upon exosome addition. For clarity, DCs were stained for actin with phalloidin (purple) and for nuclei with HOECHST 58 (blue). Bar, 10 µm. Lower panel, Quantification of STING aggregate size and number upon exosome addition. Mean, n=26 (control), n=35 (STING), t-test ***P-value<0.0001 and ****P-value<0.00001 **(b)** Quantitative real-time PCR (qRT-PCR) of antiviral response genes in wild-type DCs and Sting$^{Gt/Gt}$ DCs upon exosome addition. **(c)** qRT-PCR analysis of antiviral response genes in wild-type DCs and Irf3$^{-/-}$ DCs upon exosome addition. Data (d,f) show quantification of mRNA levels of a representative experiment with four mice per genotype: t-test *P-value<0.05, **P-value<0.001, ***P-value<0.0001 and ****P-value<0.00001.

8. Antiviral signaling is triggered at least partially by DNA contained in exosomes

The role of exosomal DNA in triggering these responses was evaluated by treating exosomes with DNase. DNase treatment significantly reduced the ability of exosomes to trigger the activation of interferon-related genes in recipient WT DCs **(Figure R23a)**, suggesting that the DNA located in the outer surface of exosomes is important for full induction of antiviral responses in recipient cells.

To ascertain whether DNA located into the lumen of exosomes may also contribute to antiviral responses in recipient DCs, we genetically engineered a plasmid expressing DNase II fused to the intraluminal domain of the exosome-enriched protein CD63. qPCR analysis of isolated exosomes showed that exosomes from cells stably-expressing CD63-DNase II contain less mitochondrial DNA than exosomes from control cells stably-expressing wild-type CD63 (**Figure R23b)**. Exosomes from cells expressing CD63-DNase II triggered a lower antiviral response in recipient cells compared with exosomes obtained from CD63-expressing control cells **(Figure R23c)**. Overall, these results support that DNA on the surface and the inside of T cell exosomes can act transcellularly, i.e. in recipient DCs, to prime antiviral responses through activation of the STING-IRF3 DNA-sensing pathway.

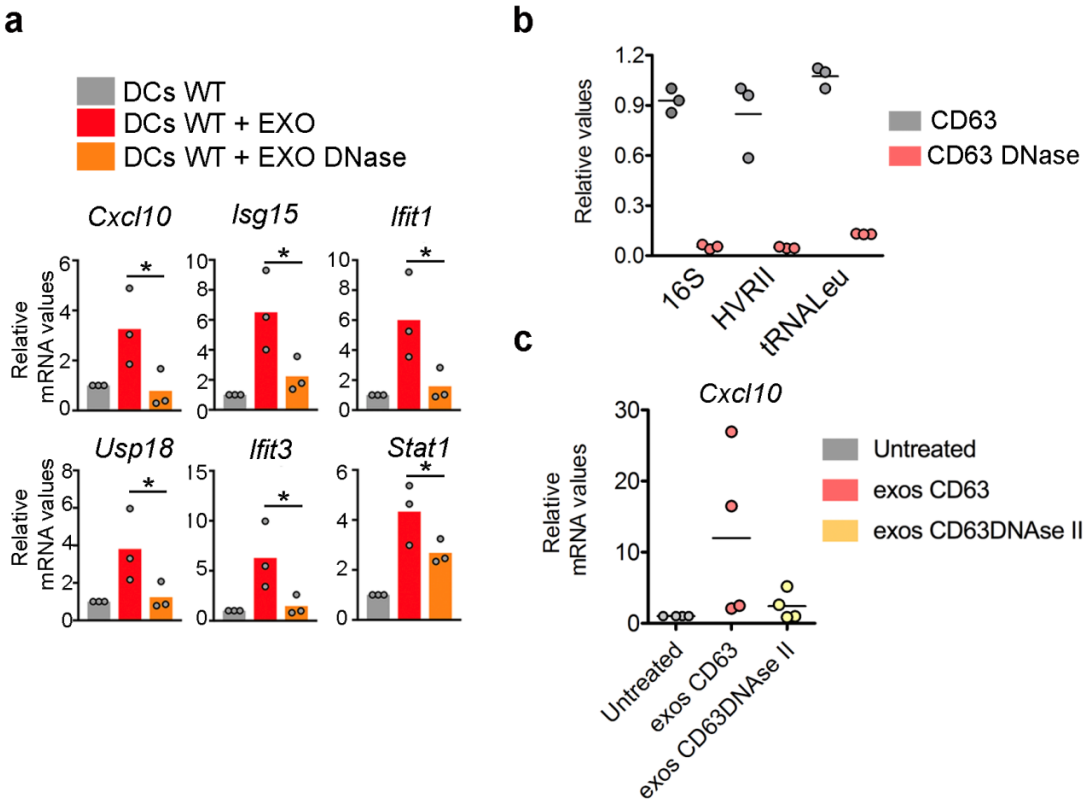

Figure R23. DNA is partially responsible for the antiviral response signaling. (a) qRT-PCR analysis of antiviral response genes in wild-type DCs upon addition of exosomes left untreated or pre-treated with DNase. Data shows mean from three independent experiments. t-test *P-value<0.05. **(b)** The level of mtDNA assessed by PCR amplification in EVs obtained from the culture supernatant of human HEK293 cells overexpressing CD63GFP or CD63 fused to DNase II. Mean. n=3. **(c)** qRT-PCR analysis of Cxcl10 in hDCs upon addition of exosomes from CD63GFP or CD63GFP-DNase II overexpressing HEK293 cells. Data show four independent experiments obtained from the culture supernatant of human HEK293 cells overexpressing CD63GFP or CD63 fused to DNase II. Mean. n=4.

9. DCs are primed by synaptic T-exosomes

We next assessed whether antigen-driven T-APC contacts trigger antiviral responses in recipient cells through the transfer of exosomal components. Gene expression analysis revealed that DCs upregulated ISGs upon immune cognate interactions with OT-II CD4+T cells **(Figure R24a)**. Control or SEE-pulsed Raji B cells were co-cultured with CD63GFP-expressing J77 T cells and then sorted according to the level of GFP-labeled exosome uptake **(Figure R24b)**. Raji B cells with higher acquisition of T cell exosomes showed more potent antiviral responses, as measured by their increased expression of Cxcl10 **(Figure R24c)**, supporting that exosome transfer during antigen-driven immune contacts primes antiviral responses in DCs.

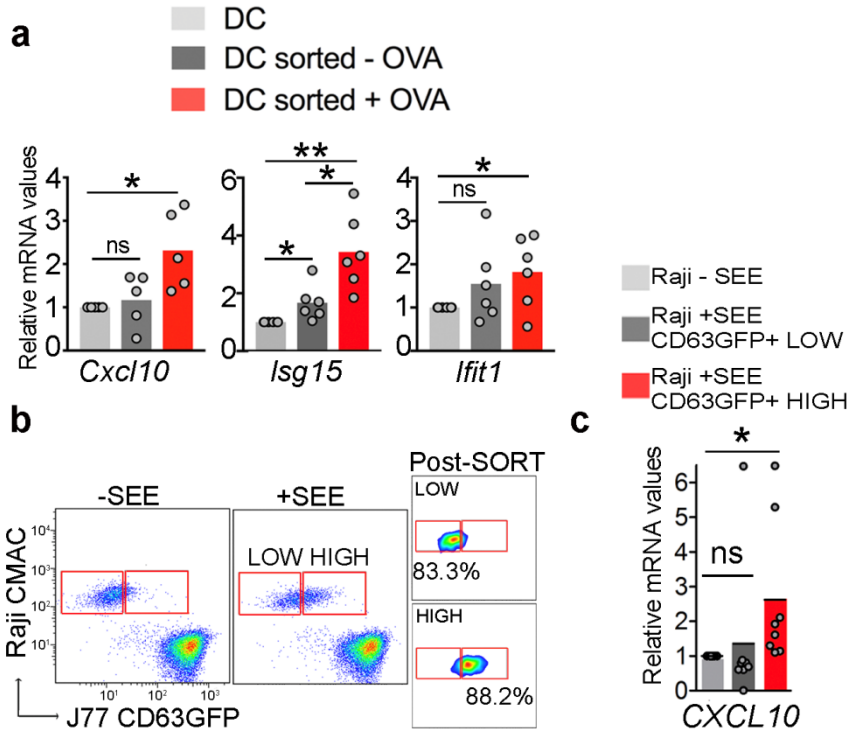

Figure R24. Cognate interations induce antiviral response in DC. (a) qRT-PCR analysis of the DC antiviral response upon antigen-dependent contacts. Gene expression was analyzed in sorted DCs after 16h conjugate formation. Data shows mean from five independent experiments. t-test *P-value<0.05. **(b)** Flow cytometry analysis of exosome uptake after co-culture of J77 T cells stably expressing CD63GFP with unprimed or SEE-primed Raji B cells. After immune interactions, Raji B cells (CMAC) were sorted according to the level of exosome uptake (CD63GFP content). Dot plots show the GFP signal in pre-sort and post-sort Raji populations. **(c)** Chart shows qRT-PCR analysis of Cxcl10 in low and high exosome uptake SEE-primed Raji B cell populations. Mean. n=3. t-test *P-value<0.05.

10. Primed DCs are more resistant to vaccinia infection

To assess the effect of exosome-boosted antiviral responses in recipient cells, we incubated DCs with T cell exosomes, infected them with GFP-expressing recombinant vaccinia virus, and monitored virus spreading and infection. Pre-incubation of DCs with T cell exosomes reduced viral infection, as measured by the number of vaccinia-GFP-positive DCs **(Figure R25)**.

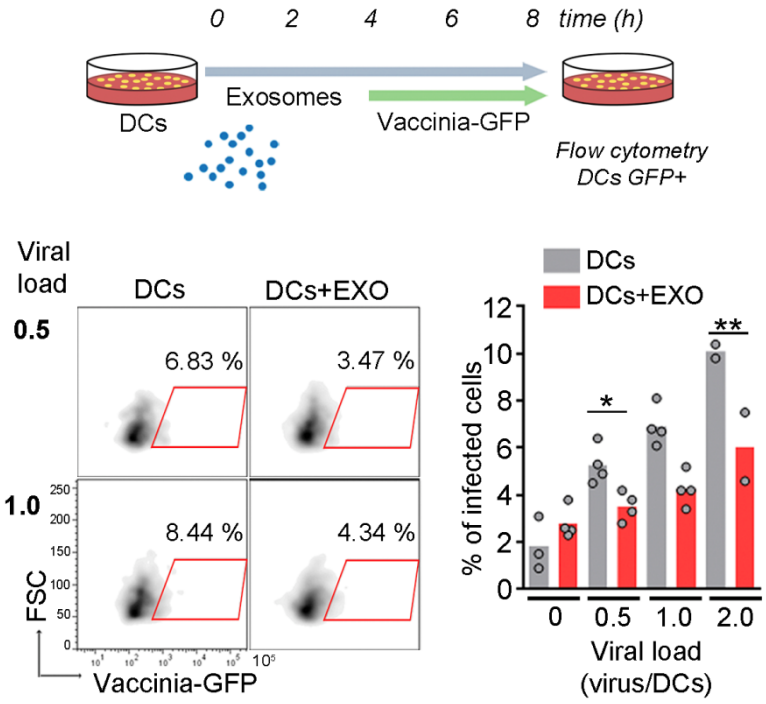

Figure R25. Exosomes protect primed DC against vaccinia. Upper panel, Time flow for the analysis of exosome-mediated antiviral protection. DCs were incubated for 4 h with T cell exosomes, infected with vaccinia-GFP, and analyzed for the level of infection by flow cytometry. Lower Left, Dot plots of DCs infected with vaccinia-GFP with or without exosome pre-treatment. Lower Right, Percentage of infected DCs at different viral loads with or without exosome pre-treatment. Mean; n=4; t-test *P-value<0.05, **P-value<0.01.

Antigen-dependent interactions between DCs and CD4+ T cells increased protection against further vaccinia virus infection of the DCs **(Figure R26a and R26c)**. This effect was dependent on T cell exosomes, since inhibition of their biogenesis by pretreatment of T cells with increasing concentrations of manumycin A, reduced DCs protection against subsequent viral infection **(Figure R26b)**, without interfering significantly with T cell viability and activation **(Figure R26c and R26d)**. Collectively, these results indicate that T cell exosomes delivered during antigen-dependent contacts boost inflammatory responses of DCs, protecting them against subsequent viral infection.

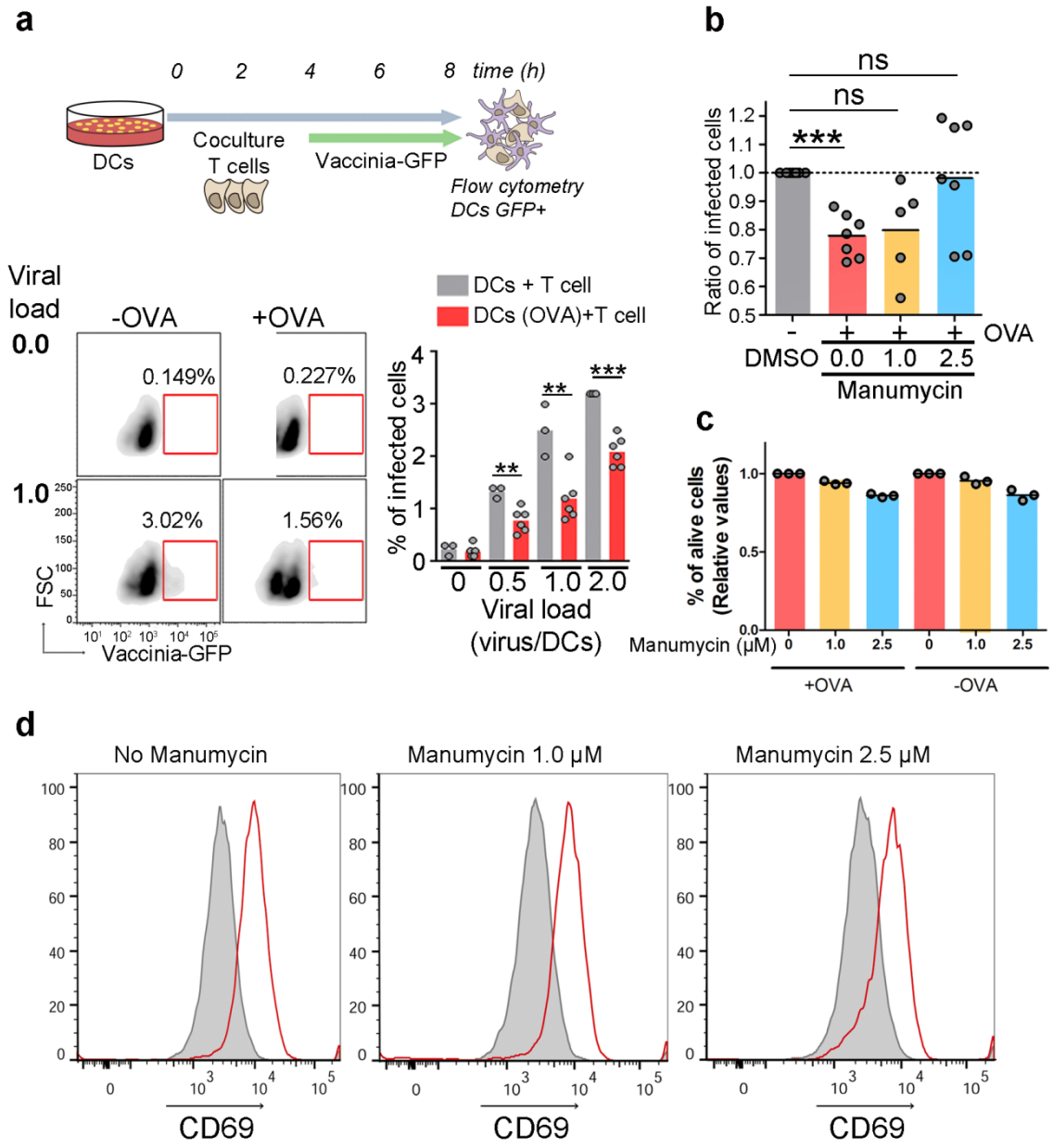

Figure R26. Antigen-driven immune interactions prime DCs to pathogen infection. Figure legend on the next page

Figure R26. Antigen-driven immune interactions prime DCs to pathogen infection. (a) Upper panel, Time flow for the analysis of exosome-mediated antiviral protection after immune cognate interactions. Unloaded or OVA peptide-loaded DCs were incubated for 4 h with $CD4^+$OT-II T cells, infected with vaccinia-GFP, and analyzed for the level of infection by flow cytometry. Lower Left, Dot plots of DCs (gated on CD11c) infected with vaccinia-GFP in the presence or absence of OVA peptide. Lower Right, Percentage of infected DCs at different viral loads in the presence or absence of antigen-dependent immune contacts. Mean; n=3-6; t-test *P-value<0.05, **P-value<0.01, ***P-value<0.0001 **(b)** Unloaded or OVA peptide-loaded DCs were incubated for 4 h with $CD4^+$OT-II T cells pretreated with increasing amounts of manumycin, infected with vaccinia-GFP, and analyzed for the level of infection by flow cytometry. Graph shows the ratio of infected DCs. Right graph, **(c)** Percentage of alive primary T lymphoblasts upon pre-treatment with increasing concentrations of manumycin for 2 h (vehicle = 0, 1 and 2.5 µM) and activation with OVA-pulsed dendritic cells for an additional 4 h period at a 5:1 ratio T cell: DCs. Manumycin was present during activation. Cell survival was measured by FACs, based on exclusion of DAPI staining. All values are relative to survival of non-treated cells. Mean percentage of T cell death was 13.8 % at maximal manumycin concentration. Data represent three independent experiments. **(d)** T lymphoblasts treated with manumycin for 16 h (vehicle = 0, 1 and 2.5 µM) and concomitant activation with anti-CD3 and anti-CD28 monoclonal Abs were stained with anti-CD69 as a measure of T cell activation. Histograms show a representative experiment out of four. No significant changes were observed in CD69 levels.

Discussion

Discussion

Here we present evidence highlighting a new pathway for intercellular communication during immune cognate interactions. Exosomes are crucial mediators for cellular communication; however, the mechanisms underlying the exchange of information are still unclear. In this study, we describe an immune cellular mechanism where mtDNA and mitochondrial components are loaded into exosomes that elicit a response in the antigen-presenting cell. The system for mitochondrial loading into multivesicular bodies is still undefined. We have shed light on how those two compartments influence functionally each other. In addition, our results show that upon non-related cognate encounters with T cells, primed dendritic cells are more resistant to viral infections. Knowledge of basic mechanisms that fine tune immune responses is relevant for future diagnostic and therapeutic applications.

1. Mitochondrial material is loaded into a specific population of extracellular vesicles

T cells secrete a great variety of EV. Depending on its origin they are classified in specific categories, i.e. microvesicles and exosomes. As previously mentioned, ILV are a mixed population of vesicles; when released by fusion of MVB with the plasma membrane the resulting exosomes are most likely a mixed population of vesicles with a common endosomal origin but different lipid and cargo composition [89,198].

Vesicle heterogeneity is evident when exosome synthesis and secretion is induced; for example upon activation of CD4 T cell some vesicle subpopulations increase significantly more than the other subpopulations, which indicates that T cells differentially regulate the release of distinct vesicle subpopulations depending on their activation status [199]. Inhibition of exosome release pathways does not affect all exosomal markers in the same way; for example Rab27 silencing decreases the secretion of classical markers such as CD63 or Tsg101, however it does barely affect CD9 release [198]. Genetic content of exosome subpopulations can vary as well; cancer cells secrete several types of exosomes and they differ on size and miRNA composition [200]. Moreover, vesicles secreted by the same polarized cell can vary depending on the subcellular localization where they are secreted [97–99,201]. For example, vesicles from polarized epithelial cells have different densities and co-fractionate with different exosomal markers depending on basolateral or apical secretion which are independent mechanisms [97]. Together, independent regulation of exosomal subpopulations and subcellular directed exosome secretion strongly suggests the existence of specialized mechanisms that control the selective

sorting of cargo into these vesicles and the transport of specific MVB repertoires to the membrane.

Taking into account that there are at least three mechanisms for ILV formation that act independently or coordinately, it is plausible that other mechanisms for vesicle formation exist and they are not yet described [80,202]. In Figure R4b and R6b we can observe a mild shift in the PCR product amplification and the proteins with mitochondrial origin respect from the classical exosomal markers. This may be due to slight differences in lipid composition between the **mitochondrial-containing extracellular vesicles** (mtExo) and vesicles containing classical markers which would change their density and thus their fractioning properties. In addition, there is only a partial colocalization of DNA and CD81 compared with complete co-localization for Tsg101 and CD81. These results suggest that although those populations share physical properties and their secretion is likely controlled by the MVB secretory pathway, they might differ in composition and probably in biogenesis. mtExo can be a subpopulation released by the fusion of MVB with the plasma membrane, but its origin could be different from the ILV which with they share space. They could even partially share lipid and protein composition and sucrose gradient could be insufficient to distinguish these two different populations.

At any rate, we frequently term exosomes those vesicles that precipitate upon ultracentrifugation at 100.000g. This pellet is enriched in exosomes, but it also may contain other EV and protein aggregates [203]. The greatest problem when studying EV is the difficulty in discriminating singular vesicles and in separating them in specific populations. Even when fractioning within a continuous band in the sucrose gradient, high density and low density subfractions from the "same" population differ in protein and RNA composition. Therefore, cells release distinct exosome subpopulations with unique compositions that elicit differential effects on recipient cells [204]. New technology is required to study in depth the different exosomal populations; only with single vesicle analysis we will be able to dissect the heterogeneous mechanisms of exosome biogenesis and secretion. A proof of concept for single vesicle microscopy is performed with TIRF microscopy techniques which allow us to challenge cells and observe individually fresh obtained vesicles, and then to classify them into subpopulations depending on their protein composition. Combined with single vesicle cytometry [205] and Omic analysis those techniques give us extra information about vesicles, using key markers to sort and analyze these enriched fractions [203].

We hypothesized that the selective secretion of mtExo is induced during T cell activation. This would imply that during cognate interactions an enriched population of exosomes containing mitochondrial components is secreted to the synaptic cleft achieving high concentration of vesicles in this confined space. This process makes possible a targeted delivery of exosomal components and the induction of a response in the antigen-presenting cell.

2. Pathway for mitochondrial content harboring into multivesicular bodies: Mitochondrial derived vesicles

Organelles are integrated into cellular networks regulating many cellular processes including metabolic interaction, intracellular signaling, cellular maintenance, regulation of programmed cell death/cell survival, and pathogen defense [206]. Apart from cytoskeleton, membrane contacts organize the position and motility of organelles. Examples of organelle interaction are mitochondria and endoplasmic reticulum contact sites (MERCs) [207], mitochondria and peroxisomes [208], mitochondria and lysosomes and autophagosomes [209,210]. In addition, the endosomal system directly interacts with mitochondria [211–214]. These contacts are dependent on Drp1, a mitochondrial fission protein present in both organelles [209]. However, there is still much to know about these complex networks.

We have found that mitochondria and multivesicular bodies are tightly linked, since disruption of the endosomal pathway also impairs mitochondrial homeostasis. Specifically, there is an increase in mitochondrial mass and in ROS, and a decrease in mitochondrial OXPHOS. In addition, when a constitutively active isoform of Rab7 was expressed in cells we detect a great accumulation of mitochondrial components inside the enlarged late endosomes. Moreover, we observe a preferential co-localization of mitochondrial proteins with components of the late stages of endosomal pathway. When cells are challenged with the uncoupler FCCP, that causes mitochondrial damage, we detect a higher localization of mitochondrial components within late endosome than within early endosomes. Our observation that mtDNA and mtDNA-binding proteins load into EVs in an autophagy-independent manner indicates the existence of an additional targeting mechanism to the MVB. The role of mitochondrial component release as a danger indicator to surrounding cells is well documented [195].

Our data suggest that the MVB endosomal route can target these components actively into exosomes. Although the signals that mediate the loading and incorporation of mitochondrial components into late endosomes/MVBs remain unidentified, an attractive possibility is that small organelle fragments containing mitochondrial nucleoids might bud toward the cytosol depending on their oxidative status, and would be subsequently loaded and incorporated into the endolysosomal compartment for their degradation or secretion. Cytosolic accumulation of mtDNA has been described following mitochondrial dysfunction and inflammatory stimulation [195,215], and a similar process may operate in the release of mtDNA to the cytoplasm and its subsequent incorporation into ILVs during MVB maturation.

Mitochondria is a highly compartmentalized organelle; release of mitochondrial components into the cytosol usually involves strong signaling in cells in an autologous manner [167]. Loss of mitochondrial permeability leads to Cytochrome c release and Caspase activation that ends in apoptosis; it is likely that mitochondrial loading into ILV is mediated by a highly regulated mechanism that protects the secreting cell from signaling of free mitochondrial content in cytosol [216].

Alternatively, we propose that mitochondrial cargo is delivered into MVB through a relatively new described mechanism. This system does not require mitochondrial depolarization, autophagy signaling or mitochondrial fission [217] and it would be a safe way to deliver dangerous material without damaging the secreting cell. It has been recently shown that small vesicles, called mitochondrial-derived vesicles (MDV), with a size ranging between 60-100nm bud out from mitochondria. MDV connect mitochondria with other organelles and transport mitochondrial components into lysosomes, peroxisomes and MVBs. MDV are essential for the correct homeostasis of mitochondria and help to get rid of unwanted material that can damage the organelle [218,219]. PINK1 and Parkin are some of the described proteins involved in the formation of MDV [220]. We postulate that they might participate in the loading of mitochondrial components into exosomes by fusion with MVB [217,221] and instead of being degraded by lysosomes, MVB could fuse with plasma membrane release a mix of bona fide exosomes together with MDV **(Figure D1)**.

However, we found that the loading of mitochondrial cargo into exosomes is independent of autophagy. In the same manner, MDV transport to lysosomes is ATG5 and LC-3 independent [217], which would support that even silencing autophagy MDV fuse with MVB and mtExo are still secreted.

This model would also explain why we detect separate vesicles containing DNA or exosomal markers such as CD81 by TIRF microscopy. Considering their similarity in size and their endosomal pathway dependence, we can be obtaining two different populations of vesicles in our samples and mixing them due to the lack of resolution of current available techniques.

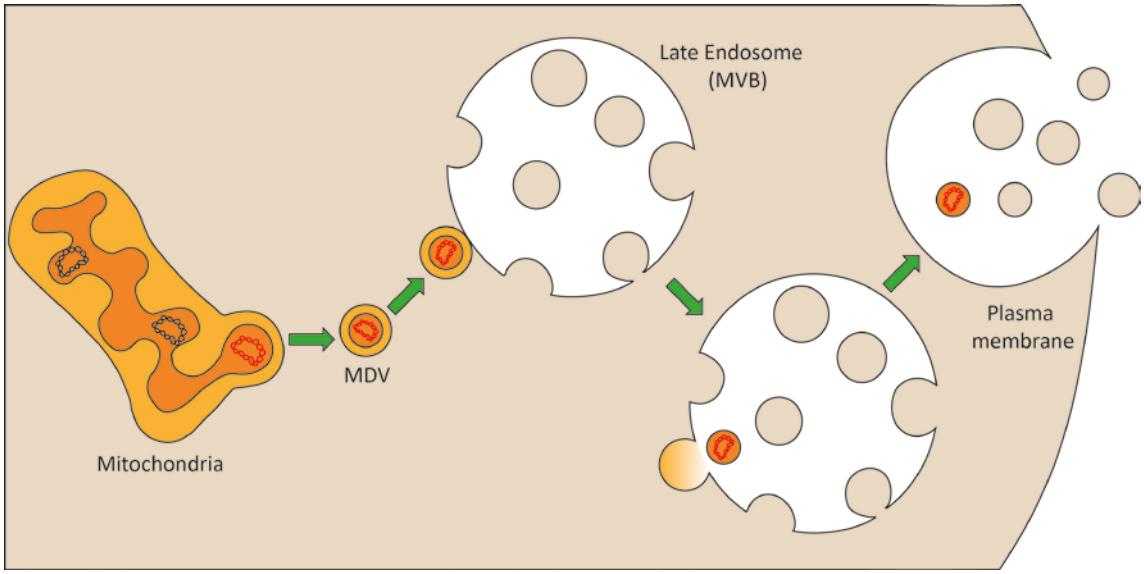

Figure D1. Proposed model for mitochondrial cargo loading into MVB. Mitochondrial-derived vesicles are extruded from mitochondria carrying oxidized cargo (in red) and unfolded proteins. After they fuse with late endosomes MDV release their single membrane cargo into MVB. After maturation MVB fuse with plasma membrane secreting single-membrane MDV and bona fide exosomes to the extracellular media.

3. Physiological cause for mtDNA release in exosomes

Exosomes were first described in reticulocytes[54,222]; initially they were proposed to represent cellular waste [223]. Nowadays, it is clear that apart from being and alternative way of releasing waste product they are essential for maintaining cellular homeostasis and for cell-cell communication [56,104]. We have addressed the role of mitochondrial-containing extracellular vesicles in the T cell-DC interaction; however, there are still several unknown issues in the secretion of mitochondrial content at the T cell side.

In some specific cases, mitochondrial transfer allows the exogenous replacement of damaged mitochondria, thereby rescuing mitochondrial defects [154]. However the effects of mitochondrial release in the secreting cell is not totally understood. The dynamics of mitochondrial networks and their selective degradation or biogenesis maintain a healthy mitochondria repertoire. Constant cycles of fusion and fission promote the intermixing and

homogenization of mitochondrial proteins, lipids and DNA between discrete organelles within the same cell [151]. The selective depletion of mitochondria through mitophagy eliminates deleterious mitochondrial mutations in heteroplasmic cells, restoring ATP levels and mitochondrial function [224–226]. Therefore cells need ways to get rid of damaged mitochondrial material. Mitophagy requires several cell resources and it is an energy consuming process once activated. Even though mtDNA can be degraded by the replication machinery [227] o by autophagy [228], there are other mitophagy/autophagy-independent pathways for degrading the damaged mtDNA that are still elusive. Moretton and colleagues described that there is a rapid loss of mtDNA upon a massive double strand break in mitochondrial genome which is neither dependent of exo/endonucleases nor autophagy [229]. The mode of mtDNA degradation may be determined by the cell type and oxidative stress [230]. Releasing damaged or aged mtDNA through the endosomal secreting pathway can be an appealing system to release stress or mtDNA double strand breaks without the need of starting a mitophagy program. Indeed, genomic DNA damage increases exosome secretion in a p53 and TSAP6-dependent manner [231]. Retention of damaged and oxidized mitochondrial components into the mitochondria is extremely harmful for cell homeostasis. Degradation of mitochondria by autophagy represents an extreme attempt to maintain cell homeostasis, although there are other mechanisms to maintain mitochondrial quality control in steady state or mild damage. Mitochondrial cargo release through MDV can be a way for releasing stress and protect cells from entering in mitophagy [219]. Therefore, exosome secretion could be a pathway for cell stress relieve [232]. As a matter of fact, there are more exosomes in the plasma of virus-infected individuals, where mitochondrial proteins are overrepresented and that contain markers of metabolic and mitochondrial stress [233]. Our results demonstrating the presence of oxidized DNA in exosomes suggest that these EVs may cooperate to manage cellular damage by releasing mitochondrial proteins and oxidized-DNA, acting as an “escape valve” to partially expel mitochondrial damage outside the cell. Recently, a role for exosomes in the secretion of harmful genomic DNA has been documented [104]. Damaged mtDNA is loaded in exosomes of epithelial cells and released to the extracellular media [234]. Supporting this role for exosomes in the preservation of cellular homeostasis[235], we found that inhibition of exosome biogenesis or secretion impair mitochondrial structure and function. A recent study identified that under stress conditions Caenorhabditis elegans secretes large vesicles containing protein aggregates and organelles for maintaining mitochondrial homeostasis and quality control [236]. Upon cell stress, MDV are preferentially loaded with oxidized cargo; the presence of oxidized mtDNA in exosomes also supports that this subpopulation of vesicles comes from a MDV origin and helps mitochondria homeostasis **(Figure D1)** [237].

Our working hypothesis is that mtExo are used as a signal to alert about the status of the donor cell to the surrounding cells by playing a dual role; on one hand, protecting the donor cell from mitochondrial dysfunction and, on the other hand, alerting receptor cells from a potential damage in the local environment. Whereas exosomes facilitate the secretion of harmful or damaged mitochondrial components and sustain mitochondrial function is a possibility that warrants further investigation.

4. Functional mtDNA delivery in antigen presenting cells

The immune synapse only covers the 20% of cell membrane and still it is a platform for cellular communication; clear examples are receptor signaling, cytokine secretion and induced cytolysis. There is no need for high amounts of messenger secretion to mount a response in the receptor cell. The encapsulation of signaling molecules inside the synaptic cleft allows reaching relative high concentrations of molecules that can trigger the signaling. Exosomal secretion inside the synaptic cleft grants high relative levels of EV per surface, which probably makes possible the induction of complete antiviral responses in the APC. However, the functional delivery of exosomal cargo into receptor cells is still not fully studied.

Exosomes allow functional delivery of genetic material to receptor cells. Specifically, miRNAs loaded in exosomes reach acceptor cells and repress target mRNAs [55,113]. In addition, cells can also secrete genomic DNA that is uptaken by recipient cells and translocated to the nucleus where it recruits nuclear factor κB (NF-κB), and is transcribed. In agreement with our data, DNA was shown to be within the exosomes rather than exposed outside [238]. Furthermore, genomic DNA delivery is functional since the exosomal delivery of the mutated gene H-Ras stimulates proliferation in recipient cells [239]. Finally, mitochondrial genes have been reported to be transferred through vesicles [234,240]. Although widely observed in prokaryotes, horizontal gene transfer (HGT) is in general a rare phenomenon in metazoans. However, HGT in eukaryotes might be less rare than previously anticipated [241]. HGT between species of Saccharomyces has been postulated during the evolution of modern yeast species [242]. Likewise, asexual bdelloid rotifers have experienced extensive HGT from non-metazoan genes [243], which might have compensated the lack of genetic heterogeneity due to the absence of sexual recombination [244]. One interesting example is the horizontal transfer of entire genomes via mitochondrial fusion in the angiosperm Amborella. Specifically, Amborella mtDNA includes a diverse collection of foreign sequences corresponding to about six genome equivalents of mtDNA acquired from mosses, angiosperms and green algae [245]. One of the first evidence of in vivo horizontal mitochondrial gene transfer was found in a transmissible canine venereal tumor (CTVT), which is a highly adapted form of cancer that is transmitted as an

allograft during mating of feral dogs. Phylogenetic evidence supports that CTVT cells periodically acquire mitochondria from their hosts to support long-term survival. Gene transfer events might rescue CTVT mitochondrial function, allowing the tumor to overcome the high mutation rate that would promote the accumulation of deleterious mutations in their own mitochondria [246].

Transfer of entire mitochondria between cells or acquisition of mitochondria from the environment in a functional and transmissible way has been demonstrated in culture cells [152,247,248], and in vivo in a cancer context [157,246,249]. Recent reports suggest that the intercellular transmission in vivo of mitochondria and/or mitochondrial components exerts a beneficial effect on the recipient damaged cells [153–155]. The benefits in all cases are attributed to the assumption that entire healthy functional mitochondria travel and colonize the recipient cells. However, the use of interspecies mix for donor cells in some cases and the lack of evidence of long lasting colonization of the recipient cells by the foreign mtDNA question this interpretation. The role of the intercellular transmission of defined mitochondrial components and specifically mtDNA as part of a complex intercellular signaling mechanism, raises the possibility that the observed beneficial effects of transmission of mitochondrial components would be consequences of activation of survival pathways rather than the transmission of fully functional organelles able to colonize the recipient cells. This could, for instance, explain the positive effects of interspecies (human/mice) experiments, since the interspecies incompatibility between nuclear and mtDNA is well described. In this study, we have shown that mtDNA is completely represented in the exosomal fraction, although we have not clarified the integrity of this genetic material. Our results indicate that there is a functional delivery of mtDNA to recipient cells upon cognate interactions. Interestingly, this transfer occurs in an unidirectional manner, from the T cell side to the APC side, as it was previously reported with other exosomal markers [55]. Nonetheless, we do not address whether whole mitochondria are transferred and whether this exchange could restore impaired mitochondrial respiration. Due to the size of exosomes and the minimal dimension of a functional mitochondrion it is not probable that entire functional units are transferred. However, if complete copies of mtDNA integrate in the mitochondria of receptor cells, it could be sufficient to replicate and restore respiration and mitochondrial functions. In fact, horizontal transfer of mtDNA occurrs in cancer cells, associated with increased self-renewal potential of these cells and tumor-initiating efficacy [157]. Cancer-stem like cells secrete extracellular vesicles carrying full mitochondrial genome, which induces exit from metabolic dormancy of other tumor cells [240]. Nevertheless, authors did not characterize properly the EV, which are probably are bigger vesicles than

exosomes, such as microvesicles. In other study, using an ImageStream imaging flow cytometer for single particle analysis, different sized extracellular vesicles from bronchoalveolar lavage contained mitochondrial components that were delivered and internalized into the mitochondrial network from the receptor cells and changed their pro-inflammatory function [234,250]. Islam and colleagues have described that mitochondria are transferred from bone-marrow-derived stromal cells to pulmonary alveoli in a connexin 43-dependent manner [155]. In addition, connexin 43 located in exosomes forming hexameric channels, facilitate the delivery of heterologous DNA and the exosomal uptake by target cells [115]. Together, these results reveal a possible mechanism for functional DNA delivery to the target cell where DNA could change its metabolic pattern or trigger inflammatory signalling. The mechanisms determining whether DNA is degraded, exported to the cytosol or integrated in the corresponding organelle are still elusive.

Finally, we describe a mouse system comprising two different haplotypes that can be differentiated by RFLP which is a suitable model for tracking mitochondrial effective transfer trace back. This model can be used for many exosomal transfer applications; it would be interesting to ascertain whether in a heteroplasmic cell an haplotype is predominantly selected and if the other is secreted via exosomes as a way to releas stress [194,251,252]. Finally, it would be interesting to deep in the transfer of healthy mtDNA to dendritic cells containing damaged DNA and study whether a healthy phenotype is recover or not. Thus, a clear understanding on the mechanisms mediating mitochondrial transmission will shed light on how mitochondrial transfer is regulated and can be exploited for therapeutic purposes.

5. Antiviral response induction upon exosome uptake in dendritic cells

Our results show the specificity of the type of cellular response evoked by the DNA packaged into EVs: type I IFN response and expression of ISGs. Although nuclear DNA is the main endogenous ligand for cGAS, growing evidence indicates a role for mtDNA as a ligand for cGAS in certain conditions. Mitochondrial DNA as well as other mitochondrial constituents such as N-formyl peptides (NFPs), mitochondrial lipids such as cardiolipin, or nuclear-encoded mitochondrial proteins, can elicit a local or systemic innate immune response in conditions of massive episodes of cell damage [195]. Intriguingly, mtDNA can also be released in a rapid, 'catapult-like' manner by neutrophils to create ‘extracellular traps’ that exert antibacterial activity and activate the release of pro-inflammatory cytokines [176,253]. In this regard, secretion of interferogenic mtDNA by neutrophils in systemic lupus erythematosus (SLE) patients contributes to disease by activating the production of potent IFN type I responses [173,254].

Likewise, lymphocytes eject interferogenic mtDNA webs in response to CpG and triggers antiviral signaling in monocytes [255]

The Intracellular accumulation of mtDNA molecules in the cytosol upon mtDNA stress has been also shown to activate type I IFNs response through the cGAS/STING pathway [167], contributing to the acquisition of an antiviral state. Our results demonstrate that in DCs, the DNA present in EVs activate type I IFN responses and expression of ISGs. The contribution of cytoplasmic sensors, e.g. STING, appears to be only partial, and other DNA receptors localized at the endosome or the plasma membrane could also detect the DNA present on the surface or the lumen of EVs and activate interferon-response factors, thus contributing to the induction of a potent antiviral response. Then, understanding which sensors or receptors detect the DNA transported in EVs; and whether the mechanisms (endocytosis, phagocytosis, back-fusion of endosomes) by which vesicular content is acquired by recipient cells affect DNA responses are questions that deserve further investigation. In this study, we have found that the DNA-sensing responses were abrogated in an IRF3-dependent manner. Also, elimination of exosomal DNA, either by DNase treatment or overexpression of DNase II fused to the intraluminal domain of the exosome-enriched protein CD63, significantly reduced the expression of antiviral related genes. However, we cannot rule out the contribution of other EVs constituents in triggering innate immune signaling in DCs. For example, Tfam serves as a danger signal that augments DNA signaling in plasmacitoid dendritic cells [256]. Another possibility is that mtDNA present in vesicles signals through different pathways; specifically, mtDNA associates with Z-binding protein (ZBP1), which recruits the TANK-binding kinase 1 (TBK1) and interferon regulatory factor 3 (IRF3). Those factors migrate to the nucleus and activate an inflammatory response in a STING independent manner [234]. Finally, vesicles containing mtDNA can also activate other pathways such as the inflammasome [257]. Therefore, signaling coming from mtExo are most likely conformed by mixed pathways that overall display a combined inflammatory response

6. Physiological purpose of DC priming

Besides the well-characterized role of IS in instructing T cell activation, it also transmits intracellular signals to the DC side [258]. Upon IS formation, the DC rapidly increases the concentration of MHC class II molecules on the membrane of the synaptic contact to strengthen antigen presentation to cognate T cells [259,260]. DC cytoskeleton undergoes substantial rearrangements during IS formation, allowing the polarization of different compartments such as endosomes and mitochondria [141]. MTOC relocation also grants polarized cytokine secretion [261].

The establishment of immune cognate interactions between T cells and APC is a key element of T cell activation, i.e. the conversion of naive T cells into effector cells, leading to the efficient clearance of pathogens through the adaptive arm of the immune response. This study demonstrates that this signal displays retrograde feedback, in which the T cell imposes additional changes to the activity of the APC, priming those post-synaptic DC (psDC) to respond better in the case of subsequent infections by the same pathogen, or a similar one. We have also identified EVs as the vessels of the information that triggers these changes in DCs, promoting an antiviral response with induction of IFN-related stimulated genes. A key observation is that these effects require antigenic stimulation. This is crucial because it ensures that the acquisition of inflammatory (or antiviral) traits is limited to situations in which a specific stimulus, i.e. the pathogen, is triggering these responses. It also has the potential to drastically alter the fate of the DC. DC supposedly die in lymph nodes after cognate interactions. This is based on evidence of the onset of autoimmune disease when DC apoptosis is inhibited [262]. We postulate that, even if DC are eliminated after activating naive T cells in an antigen specific-dependent manner, T cell exosomes could salvage the psDC by reverting the onset of the apoptotic program. This is consistent with the observation that DCs receive pro-survival signals after IS formation, reducing the percentages of apoptosis in vitro and in vivo [263]. Hence, the reported disappearance of DC from the lymph nodes after the IS [264] could be explained due to their programmed cell death but also due to their migration to other tissues, particularly if they have been fine-tuned by T cell exosomes. In fact, DC can live for 15 days in the lymph node after an immune challenge, and are able to present antigens ex vivo to CD4+ T cells [265]. There is scant evidence of this type of priming, but some indirect evidence points to the potential importance of this mechanism. For example, tissue-resident memory T cells (TRM) have been shown to allow superior protection to homologous infection compared to circulating memory T cells. These TRM can become instructors of innate immune system by initiating a local anti-viral state after reinfection that depends on the secretion of pro-

inflammatory cytokines such as TNF, IL-2 or IFN-γ that rapidly initiate an innate immune response in the infected tissues [266–268]. These experimental observations suggest the existence of cross-priming elements that are transferred by the exposure to one pathogen to improve the response against other pathogens. Hence, it is tempting to speculate a role for exosomes and DNA transfer in this enhanced anti-viral protection exerted by tissue-resident memory T cells.

The mechanism proposed here would function as a mechanism of innate memory, adapting the DC response during antigenic challenge. Obviously, DCs do not bear genetic mechanisms to modulate their ability to recognize antigens similar to the recombination observed in B cells and T cells. However, increasing evidence has demonstrated that DCs and macrophages bear long-lasting modifications to their epigenetic status after infection or vaccination, leading to enhanced responsiveness upon secondary stimulation by microbial pathogens, increased production of inflammatory mediators and enhanced capacity to eliminate infection [269]. We propose that T cell exosomes are powerful DC reprogramming tools that enhance the adaptation of the innate cell against the pathogen. Although this is obviously a short-ranged mechanism, the delivery of T cell exosomes to circulating fluids and their subsequent capture by distant APC could play a significant role in boosting vaccination and the induction of long-distance preparation against infection.

7. Concluding remarks

In summary, this study provides a physiological mechanism for the transfer of mitochondrial components and genome transfer in the context of immune cognate interactions, laying the foundation of a model in which the transfer of DNA between immune cells constitutes a signal-dependent mechanism for alerting responses in innate immune cells. We postulate that mitochondrial components are loaded into MVB of T cells during activation or a stress situation. Those components are released in exosomes-like vesicles to the synaptic cleft when MVB fuse with plasma membrane and they are uptaken by the DC. mtDNA contained in those vesicles triggers a transcriptomic remodeling through the cGas/STING pathway. The main affected genes in primed DC are those from pathogen defense pathways, specifically the antiviral response. Consistently, primed DC are more protected against vaccinia infection *in vitro* **(Figure D2)**.

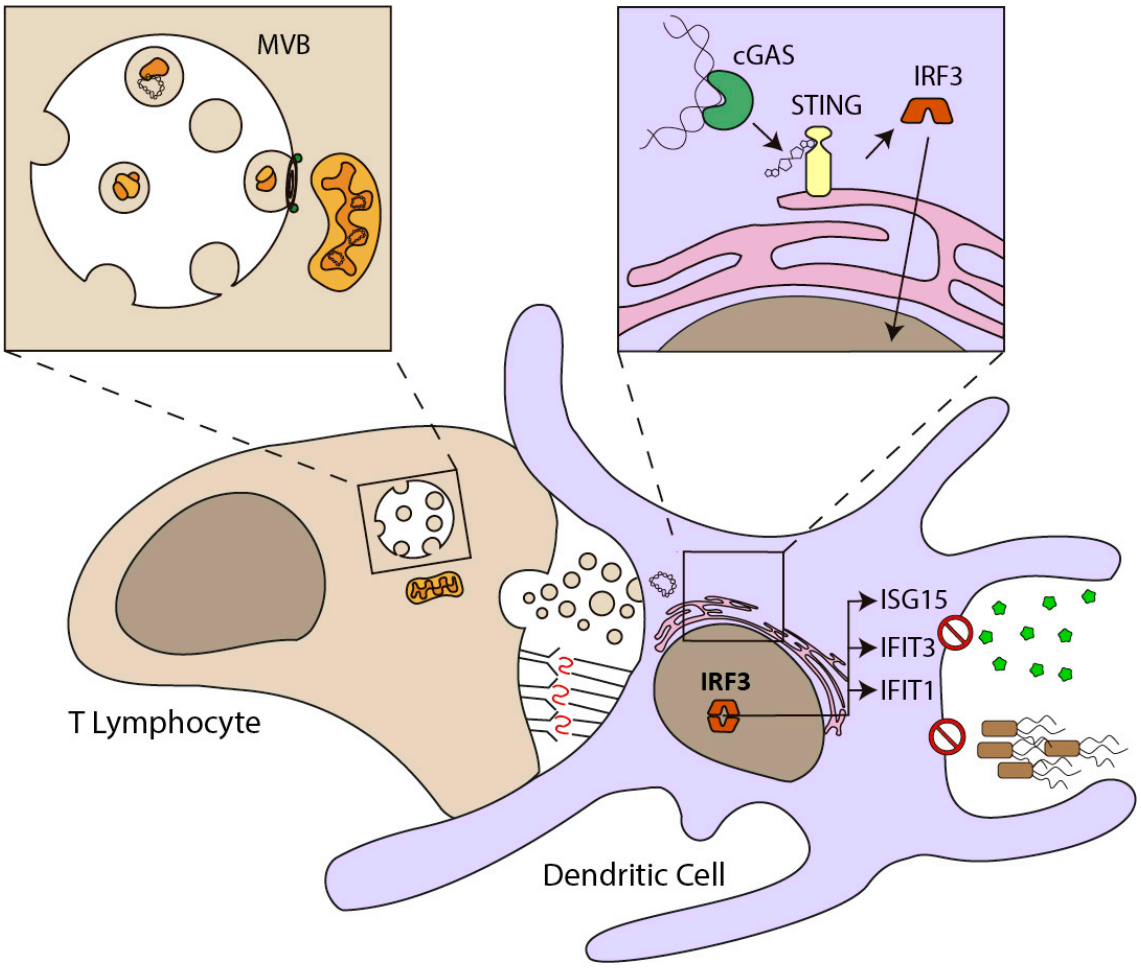

Figure D2. Proposed model for the experimental conclusions. T Lymphocytes load mitochondrial components into ILV of the MVB. Vesicles are released during cognate interactions and mtDNA is incorporated in DC where it triggers antiviral signaling through the cGAS/STING pathway. Due to this interaction primed DC are more protected against further pathogen infections.

Although there are many aspects of our research where more investigation is needed, this study opens a very interesting field. During many years DC were supposed to present antigens and once their mission was accomplished they died [262]. However data show that upon antigen-driven contacts DC induce pro-survival signals, have lower percentages of apoptosis [263] and they can live for more than 15 days after the interaction in the lymph node [264]. In addition, their mitochondria cluster and local autophagy is induced with homeostatic purposes [141]. Finally, our data show that upon cognate interaction psDC acquire an antiviral program and they are more protected. Those data are supported by a study where it is shown that this also happens in DC in vivo [270]. Even if after immune synapse many DC die, some of these post-synaptic Dendritic Cells activate a program that improves their performance [271].

This specific repertoire of cells could have a role in subsequent infections and there is an exciting new field of study that probably can unveil new modes to improve vaccination and fight against infective diseases.

Conclusions

Conclusions

The findings presented herein support the following conclusions:

1. Exosomes isolated from T Lymphocytes are loaded with a repertoire of mitochondrial proteins where mitochondrial DNA binding proteins are enriched.

2. T Lymphocytes shuttle genomic and mitochondrial DNA in exosomes. DNA in exosomes is partially oxidized and it is only present in a specific exosomal subpopulations.

3. Mitochondrial proteins and DNA segregate into multivesicular bodies and the exosomal secretory pathway to reach exosomes.

4. Biogenesis and Release of exosomes regulate mitochondrial function and homeostasis.

5. Mitochondrial proteins and DNA are transferred from T cells to dendritic cells in a unidirectional manner during immune synapsis.

6. DNA contained in exosomes activates the expression of antiviral genes through cGAS/STING-IRF3 pathway in dendritic cells due to exosome uptake.

7. Synaptic exosomes secreted by T cells during cognate interactions prime dendritic cells and protect them against subsequent viral infections.

Conclusiones

Conclusiones

Los resultados presentados en esta tesis apoyan las siguientes conclusiones:

1. Los exosomas provenientes de linfocitos T contienen proteínas mitocondriales entre las que se encuentran especialmente enriquecidas las proteínas de unión a ADN mitocondrial.

2. Los exosomas secretados por los linfocitos T están cargados de ADN genómico y mitocondrial. El ADN de los exosomas está parcialmente oxidado y sólo está presente en una subpoblación específica de exosomas.

3. Las proteínas mitocondriales y el ADN se acumulan en cuerpos multivesiculares y de esta manera llegan a los exosomas.

4. La biogénesis y liberación de exosomas regulan la homeostasis y la función mitocondrial.

5. Las proteínas y El ADN mitocondriales se transfieren de los linfocitos T a las células dendríticas de una manera unidireccional durante la sinapsis inmune.

6. El ADN contenido en los exosomas activa la expresión de los genes antivirales a través de la vía cGAS/STING-IRF3 en las células dendríticas cuando estas captan e incorporan los exosomas de los linfocitos.

7. Los exosomas secretados por las células T durante la sinapsis inmune pre-activan a las células dendríticas y las protegen contra infecciones virales posteriores.

References

References

1. Abbas, A. K., Lichtman, A. H., Pillai, S. & Preceded by: Abbas, A. K. *Cellular and molecular immunology*. (2017).

2. Dustin, M. L. & Choudhuri, K. Signaling and Polarized Communication Across the T Cell Immunological Synapse. *Annu. Rev. Cell Dev. Biol.* **32**, 303–325 (2016).

3. Monks, C. R., Freiberg, B. A., Kupfer, H., Sciaky, N. & Kupfer, A. Three-dimensional segregation of supramolecular activation clusters in T cells. *Nature* **395**, 82–86 (1998).

4. Cai, E. *et al.* Visualizing dynamic microvillar search and stabilization during ligand detection by T cells. *Science (80-.).* (2017).

5. Kim, H. R. *et al.* T cell microvilli constitute immunological synaptosomes that carry messages to antigen-presenting cells. *Nat. Commun.* (2018).

6. Wülfing, C., Sjaastad, M. D. & Davis, M. M. Visualizing the dynamics of T cell activation: intracellular adhesion molecule 1 migrates rapidly to the T cell/B cell interface and acts to sustain calcium levels. *Proc. Natl. Acad. Sci. U. S. A.* **95**, 6302–7 (1998).

7. Robles-Valero, J. *et al.* Integrin and CD3/TCR activation are regulated by the scaffold protein AKAP450. *Blood* **115**, 4174–4184 (2010).

8. Comrie, W. A., Babich, A. & Burkhardt, J. K. F-actin flow drives affinity maturation and spatial organization of LFA-1 at the immunological synapse. *J. Cell Biol.* (2015).

9. Van Der Merwe, P. A. & Dushek, O. Mechanisms for T cell receptor triggering. *Nature Reviews Immunology* (2011).

10. Valitutti, S., Dessing, M., Aktories, K., Gallati, H. & Lanzavecchia, A. Sustained signaling leading to T cell activation results from prolonged T cell receptor occupancy. Role of T cell actin cytoskeleton. *J. Exp. Med.* **181**, 577–84 (1995).

11. Lee, K.-H. *et al.* T Cell Receptor Signaling Precedes Immunological Synapse Formation. *Science (80-.).* **295**, 1539–1542 (2002).

12. He, H.-T. & Marguet, D. T-cell antigen receptor triggering and lipid rafts: a matter of space and time scales. Talking Point on the involvement of lipid rafts in T-cell activation. *EMBO Rep.* **9**, 525–530 (2008).

13. Grakoui, A. *et al.* The immunological synapse: a molecular machine controlling T cell activation. *Science* **285**, 221–7 (1999).

14. Varma, R., Campi, G., Yokosuka, T., Saito, T. & Dustin, M. L. T cell receptor-proximal signals are sustained in peripheral microclusters and terminated in the central supramolecular activation cluster. *Immunity* **25**, 117–127 (2006).

15. DeMond, A. L., Mossman, K. D., Starr, T., Dustin, M. L. & Groves, J. T. T cell receptor microcluster transport through molecular mazes reveals mechanism of translocation. *Biophys J* **94**, 3286–3292 (2008).

16. Yi, J., Wu, X. S., Crites, T. & Hammer 3rd, J. A. Actin retrograde flow and actomyosin II arc contraction drive receptor cluster dynamics at the immunological synapse in Jurkat T cells. *Mol Biol Cell* **23**, 834–852 (2012).

17. Ilani, T., Vasiliver-Shamis, G., Vardhana, S., Bretscher, A. & Dustin, M. L. T cell antigen receptor signaling and immunological synapse stability require myosin IIA. *Nat Immunol* **10**, 531–539 (2009).

18. Freiberg, B. A. *et al.* Staging and resetting T cell activation in SMACs. *Nat Immunol* **3**, 911–917 (2002).

19. Sykulev, Y., Joo, M., Vturina, I., Tsomides, T. J. & Eisen, H. N. Evidence that a single peptide-MHC complex on a target cell can elicit a cytolytic T cell response. *Immunity* **4**, 565–571 (1996).

20. Benvenuti, F. *et al.* Requirement of Rac1 and Rac2 expression by mature dendritic cells for T cell priming. *Science (80-.).* **305**, 1150–1153 (2004).

21. Al-Alwan, M. M. *et al.* Cutting edge: dendritic cell actin cytoskeletal polarization during immunological synapse formation is highly antigen-dependent. *J Immunol* **171**, 4479–4483 (2003).

22. Al-Alwan, M. M., Rowden, G., Lee, T. D. & West, K. A. The dendritic cell cytoskeleton is critical for the formation of the immunological synapse. *J Immunol* **166**, 1452–1456 (2001).

23. Mayya, V. *et al.* Durable Interactions of T Cells with T Cell Receptor Stimuli in the Absence of a Stable Immunological Synapse. *Cell Rep* **22**, 340–349 (2018).

24. Martín-cófreces, N. B., Vicente-manzanares, M. & Sanchez-Madrid, F. Adhesive Interactions Delineate the Topography of the Immune Synapse. **6**, 1–10 (2018).

25. Martin-Cofreces, N. B. & Sanchez-Madrid, F. Sailing to and Docking at the Immune Synapse: Role of Tubulin Dynamics and Molecular Motors. *Front Immunol* **9**, 1174 (2018).

26. Fritzsche, M. *et al.* Cytoskeletal actin dynamics shape a ramifying actin network underpinning immunological synapse formation. *Sci Adv* **3**, e1603032 (2017).

27. Huse, M., Lillemeier, B. F., Kuhns, M. S., Chen, D. S. & Davis, M. M. T cells use two directionally distinct pathways for cytokine secretion. *Nat Immunol* **7**, 247–255 (2006).

28. Martin-Cofreces, N. B. *et al.* MTOC translocation modulates IS formation and controls sustained T cell signaling. *J Cell Biol* **182**, 951–962 (2008).

29. Kupfer, A. & Dennert, G. Reorientation of the microtubule-organizing center and the Golgi apparatus in cloned cytotoxic lymphocytes triggered by binding to lysable target cells. *J Immunol* **133**, 2762–2766 (1984).

30. Kupfer, A., Dennert, G. & Singer, S. J. The reorientation of the Golgi apparatus and the microtubule-organizing center in the cytotoxic effector cell is a prerequisite in the lysis of bound target cells. *J Mol Cell Immunol* **2**, 37–49 (1985).

31. Kupfer, A., Mosmann, T. R. & Kupfer, H. Polarized expression of cytokines in cell conjugates of helper T cells and splenic B cells. *Proc Natl Acad Sci U S A* **88**, 775–779 (1991).

32. Huse, M., Le Floc'h, A. & Liu, X. From lipid second messengers to molecular motors: microtubule-organizing center reorientation in T cells. *Immunol Rev* **256**, 95–106 (2013).

33. Kuhne, M. R. *et al.* Linker for activation of T cells, zeta-associated protein-70, and Src homology 2 domain-containing leukocyte protein-76 are required for TCR-induced microtubule-organizing center polarization. *J Immunol* **171**, 860–866 (2003).

34. Lo, W. L. *et al.* Lck promotes Zap70-dependent LAT phosphorylation by bridging Zap70 to LAT. *Nat Immunol* **19**, 733–741 (2018).

35. Babich, A. *et al.* F-actin polymerization and retrograde flow drive sustained PLCgamma1 signaling during T cell activation. *J Cell Biol* **197**, 775–787 (2012).

36. Spitaler, M., Emslie, E., Wood, C. D. & Cantrell, D. Diacylglycerol and protein kinase D localization during T lymphocyte activation. *Immunity* **24**, 535–546 (2006).

37. Quann, E. J., Merino, E., Furuta, T. & Huse, M. Localized diacylglycerol drives the polarization of the microtubule-organizing center in T cells. *Nat Immunol* **10**, 627–635 (2009).

38. Quann, E. J., Liu, X., Altan-Bonnet, G. & Huse, M. A cascade of protein kinase C isozymes promotes cytoskeletal polarization in T cells. *Nat Immunol* **12**, 647–654 (2011).

39. Combs, J. *et al.* Recruitment of dynein to the Jurkat immunological synapse. *Proc Natl Acad Sci U S A* **103**, 14883–14888 (2006).

40. Liu, X., Kapoor, T. M., Chen, J. K. & Huse, M. Diacylglycerol promotes centrosome polarization in T cells via reciprocal localization of dynein and myosin II. *Proc Natl Acad Sci U S A* **110**, 11976–11981 (2013).

41. Baixauli, F. *et al.* The mitochondrial fission factor dynamin-related protein 1 modulates T-cell receptor signalling at the immune synapse. *EMBO J.* **30**, 1238–50 (2011).

42. Calabia-Linares, C. *et al.* Endosomal clathrin drives actin accumulation at the immunological synapse. *J Cell Sci* **124**, 820–830 (2011).

43. Huse, M., Quann, E. J. & Davis, M. M. Shouts, whispers and the kiss of death: directional secretion in T cells. *Nat. Immunol.* **9**, 1105–1111 (2008).

44. Ueda, H., Morphew, M. K., McIntosh, J. R. & Davis, M. M. CD4+ T-cell synapses involve multiple distinct stages. *Proc Natl Acad Sci U S A* **108**, 17099–17104 (2011).

45. Poo, W. J., Conrad, L. & Janeway Jr., C. A. Receptor-directed focusing of lymphokine release by helper T cells. *Nature* **332**, 378–380 (1988).

46. Alcover, A., Alarcon, B. & Di Bartolo, V. Cell Biology of T Cell Receptor Expression and Regulation. *Annu Rev Immunol* **36**, 103–125 (2018).

47. Finetti, F. *et al.* The small GTPase Rab8 interacts with VAMP-3 to regulate the delivery of recycling T-cell receptors to the immune synapse. *J Cell Sci* **128**, 2541–2552 (2015).

48. Finetti, F. *et al.* Intraflagellar transport is required for polarized recycling of the TCR/CD3 complex to the immune synapse. *Nat Cell Biol* **11**, 1332–1339 (2009).

49. Martin-Cofreces, N. B. *et al.* End-binding protein 1 controls signal propagation from the T cell receptor. *EMBO J* **31**, 4140–4152 (2012).

50. Blas-Rus, N. *et al.* Aurora A drives early signalling and vesicle dynamics during T-cell activation. *Nat Commun* **7**, 11389 (2016).

51. Das, V. *et al.* Activation-induced polarized recycling targets T cell antigen receptors to the immunological synapse; involvement of SNARE complexes. *Immunity* **20**, 577–588 (2004).

52. Compeer, E. B. *et al.* A mobile endocytic network connects clathrin-independent receptor endocytosis to recycling and promotes T cell activation. *Nat Commun* **9**, 1597 (2018).

53. Pan, B. T. & Johnstone, R. M. Fate of the transferrin receptor during maturation of sheep reticulocytes in vitro: selective externalization of the receptor. *Cell* **33**, 967–78 (1983).

54. Harding, C., Heuser, J. & Stahl, P. Receptor-mediated endocytosis of transferrin and recycling of the transferrin receptor in rat reticulocytes. *J. Cell Biol.* **97**, 329–339 (1983).

55. Mittelbrunn, M. *et al.* Unidirectional transfer of microRNA-loaded exosomes from T cells to antigen-presenting cells. *Nat. Commun.* **2**, 282 (2011).

56. Mittelbrunn, M. & Sánchez-Madrid, F. Intercellular communication: diverse structures for exchange of genetic information. *Nat. Rev. Mol. Cell Biol.* **13**, 328–35 (2012).

57. Huotari, J. & Helenius, A. Endosome maturation. *EMBO J.* **30**, 3481–3500 (2011).

58. Nielsen, E., Severin, F., Backer, J. M., Hyman, A. A. & Zerial, M. Rab5 regulates motility of early endosomes on microtubules. *Nat. Cell Biol.* **1**, 376–382 (1999).

59. Rink, J., Ghigo, E., Kalaidzidis, Y. & Zerial, M. Rab Conversion as a Mechanism of Progression from Early to Late Endosomes. *Cell* **122**, 735–749 (2005).

60. Bucci, C., Thomsen, P., Nicoziani, P., McCarthy, J. & van Deurs, B. Rab7: A Key to Lysosome Biogenesis. *Mol. Biol. Cell* **11**, 467–480 (2000).

61. Vitelli, R. *et al.* Role of the Small GTPase RAB7 in the Late Endocytic Pathway. *J. Biol. Chem.* **272**, 4391–4397 (1997).

62. Collinet, C. *et al.* Systems survey of endocytosis by multiparametric image analysis. *Nature* **464**, 243–249 (2010).

63. Driskell, O. J., Mironov, A., Allan, V. J. & Woodman, P. G. Dynein is required for receptor sorting and the morphogenesis of early endosomes. *Nat. Cell Biol.* **9**, 113–120 (2007).

64. Hoepfner, S. *et al.* Modulation of Receptor Recycling and Degradation by the Endosomal Kinesin KIF16B. *Cell* **121**, 437–450 (2005).

65. Bananis, E., Murray, J. W., Stockert, R. J., Satir, P. & Wolkoff, A. W. Microtubule and Motor-Dependent Endocytic Vesicle Sorting in Vitro. *J. Cell Biol.* **151**, 179–186 (2000).

66. Aniento, F., Emans, N., Griffiths, G. & Gruenberg, J. Cytoplasmic dynein-dependent vesicular transport from early to late endosomes [published erratum appears in J Cell Biol 1994 Feb;124(3):397]. *J. Cell Biol.* **123**, 1373–1387 (1993).

67. Brown, C. L. *et al.* Kinesin-2 is a Motor for Late Endosomes and Lysosomes. *Traffic* **6**, 1114–1124 (2005).

68. Jordens, I. *et al.* The Rab7 effector protein RILP controls lysosomal transport by inducing the recruitment of dynein-dynactin motors. *Curr. Biol.* **11**, 1680–5 (2001).

69. Johansson, M. *et al.* Activation of endosomal dynein motors by stepwise assembly of Rab7–RILP–p150Glued, ORP1L, and the receptor βIII spectrin. *J. Cell Biol.* **176**, 459 (2007).

70. Progida, C. & Bakke, O. Bidirectional traffic between the Golgi and the endosomes – machineries and regulation. *J. Cell Sci.* **129**, jcs.185702 (2016).

71. Hessvik, N. P. & Llorente, A. Current knowledge on exosome biogenesis and release. *Cell. Mol. Life Sci.* **75**, 193–208 (2018).

72. Villarroya-Beltri, C., Baixauli, F., Gutierrez-Vazquez, C., Sanchez-Madrid, F. & Mittelbrunn, M. Sorting it out: regulation of exosome loading. *Semin Cancer Biol* **28**, 3–13 (2014).

73. Baietti, M. F. *et al.* Syndecan–syntenin–ALIX regulates the biogenesis of exosomes. *Nat. Cell Biol.* **14**, 677–685 (2012).

74. Colombo, M., Raposo, G. & Théry, C. Biogenesis, Secretion, and Intercellular Interactions of Exosomes and Other Extracellular Vesicles. *Annu. Rev. Cell Dev. Biol.* **30**, 255–289 (2014).

75. Alonso Y Adell, M., Migliano, S. M. & Teis, D. ESCRT-III and Vps4: a dynamic multipurpose tool for membrane budding and scission. *FEBS J.* **283**, 3288–3302 (2016).

76. Bache, K. G., Brech, A., Mehlum, A. & Stenmark, H. Hrs regulates multivesicular body formation via ESCRT recruitment to endosomes. *J. Cell Biol.* **162**, 435–42 (2003).

77. Raiborg, C. *et al.* Hrs sorts ubiquitinated proteins into clathrin-coated microdomains of early endosomes. *Nat. Cell Biol.* **4**, 394–398 (2002).

78. Razi, M. & Futter, C. E. Distinct Roles for Tsg101 and Hrs in Multivesicular Body Formation and Inward Vesiculation. *Mol. Biol. Cell* **17**, 3469–3483 (2006).

79. Bache, K. G. *et al.* The ESCRT-III Subunit hVps24 Is Required for Degradation but Not Silencing of the Epidermal Growth Factor Receptor. *Mol. Biol. Cell* **17**, 2513–2523 (2006).

80. Trajkovic, K. *et al.* Ceramide Triggers Budding of Exosome Vesicles into Multivesicular Endosomes. *Science (80-.).* **319**, 1244–1247 (2008).

81. Yuyama, K., Sun, H., Mitsutake, S. & Igarashi, Y. Sphingolipid-modulated Exosome Secretion Promotes Clearance of Amyloid-β by Microglia. *J. Biol. Chem.* **287**, 10977–10989 (2012).

82. Xu, Y. *et al.* Macrophages transfer antigens to dendritic cells by releasing exosomes containing dead-cell-associated antigens partially through a ceramide-dependent pathway to enhance CD4 $^{+}$ T-cell responses. *Immunology* **149**, 157–171 (2016).

83. Kajimoto, T., Okada, T., Miya, S., Zhang, L. & Nakamura, S. Ongoing activation of sphingosine 1-phosphate receptors mediates maturation of exosomal multivesicular endosomes. *Nat. Commun.* **4**, 2712 (2013).

84. Kajimoto, T. *et al.* Involvement of Gβγ subunits of G $_{i}$ protein coupled with S1P receptor on multivesicular endosomes in F-actin formation and cargo sorting into exosomes. *J. Biol. Chem.* **293**, 245–253 (2018).

85. Mohamed, N. N. I., Okada, T., Kajimoto, T. & Nakamura, S.-I. Essential Role of Sphingosine Kinase 2 in the Regulation of Cargo Contents in the Exosomes from K562 Cells. *Kobe J. Med. Sci.* **63**, E123–E129 (2018).

86. Escola, J.-M. *et al.* Selective Enrichment of Tetraspan Proteins on the Internal Vesicles of Multivesicular Endosomes and on Exosomes Secreted by Human B-lymphocytes. *J. Biol. Chem.* **273**, 20121–20127 (1998).

87. Rocha-Perugini, V., Sánchez-Madrid, F. & Martínez del Hoyo, G. Function and Dynamics of Tetraspanins during Antigen Recognition and Immunological Synapse Formation. *Front. Immunol.* **6**, 653 (2016).

88. van Niel, G. *et al.* The Tetraspanin CD63 Regulates ESCRT-Independent and -Dependent Endosomal Sorting during Melanogenesis. *Dev. Cell* **21**, 708–721 (2011).

89. Edgar, J. R., Eden, E. R. & Futter, C. E. Hrs- and CD63-Dependent Competing Mechanisms Make Different Sized Endosomal Intraluminal Vesicles. *Traffic* **15**, 197–211 (2014).

90. Tamai, K. *et al.* Exosome secretion of dendritic cells is regulated by Hrs, an ESCRT-0 protein. *Biochem. Biophys. Res. Commun.* **399**, 384–390 (2010).

91. Stuffers, S., Sem Wegner, C., Stenmark, H. & Brech, A. Multivesicular Endosome Biogenesis in the Absence of ESCRTs. *Traffic* **10**, 925–937 (2009).

92. Ostrowski, M. *et al.* Rab27a and Rab27b control different steps of the exosome secretion pathway. *Nat. Cell Biol.* **12**, 19–30 (2010).

93. Villarroya-Beltri, C. *et al.* ISGylation controls exosome secretion by promoting lysosomal degradation of MVB proteins. *Nat. Commun.* **7**, (2016).

94. Villarroya-Beltri, C., Guerra, S. & Sanchez-Madrid, F. ISGylation - a key to lock the cell gates for preventing the spread of threats. *J Cell Sci* **130**, 2961–2969 (2017).

95. Li, Z. *et al.* Acetylation modification regulates GRP78 secretion in colon cancer cells. *Sci Rep* **6**, 30406 (2016).

96. Möbius, W. *et al.* Immunoelectron Microscopic Localization of Cholesterol Using Biotinylated and Non-cytolytic Perfringolysin O. *J. Histochem. Cytochem.* **50**, 43–55 (2002).

97. Chen, Q., Takada, R., Noda, C., Kobayashi, S. & Takada, S. Different populations of Wnt-containing vesicles are individually released from polarized epithelial cells. *Sci. Rep.* **6**, 35562 (2016).

98. Tauro, B. J. *et al.* Two Distinct Populations of Exosomes Are Released from LIM1863 Colon Carcinoma Cell-derived Organoids. *Mol. Cell. Proteomics* **12**, 587–598 (2013).

99. van Niel, G. *et al.* Intestinal epithelial cells secrete exosome-like vesicles. *Gastroenterology* **121**, 337–49 (2001).

100. Sinha, S. *et al.* Cortactin promotes exosome secretion by controlling branched actin dynamics. *J. Cell Biol.* **214**, 197–213 (2016).

101. Möbius, W. *et al.* Recycling compartments and the internal vesicles of multivesicular bodies harbor most of the cholesterol found in the endocytic pathway. *Traffic* **4**, 222–31 (2003).

102. Valadi, H. *et al.* Exosome-mediated transfer of mRNAs and microRNAs is a novel mechanism of genetic exchange between cells. *Nat. Cell Biol.* **9**, 654–9 (2007).

103. Thakur, B. K. *et al.* Double-stranded DNA in exosomes: a novel biomarker in cancer detection. *Cell Res* **24**, 766–769 (2014).

104. Takahashi, A., Okada, R., Nagao, K., Kawamata, Y. & Hanyu, A. Exosomes maintain cellular homeostasis by excreting harmful DNA from cells. *Nat. Commun.* **8**, 15287 (2017).

105. Kahlert, C. *et al.* Identification of double-stranded genomic DNA spanning all chromosomes with mutated KRAS and p53 DNA in the serum exosomes of patients with pancreatic cancer. *J Biol Chem* **289**, 3869–3875 (2014).

106. Guescini, M., Genedani, S., Stocchi, V. & Agnati, L. F. Astrocytes and Glioblastoma cells release exosomes carrying mtDNA. *J. Neural Transm.* **117**, 1–4 (2010).

107. Moreno-Gonzalo, O., Fernandez-Delgado, I. & Sanchez-Madrid, F. Post-translational add-ons mark the path in exosomal protein sorting. *Cell Mol Life Sci* **75**, 1–19 (2018).

108. Raiborg, C. & Stenmark, H. The ESCRT machinery in endosomal sorting of ubiquitylated membrane proteins. *Nature* **458**, 445–452 (2009).

109. Nikko, E. & Andre, B. Evidence for a direct role of the Doa4 deubiquitinating enzyme in protein sorting into the MVB pathway. *Traffic* **8**, 566–581 (2007).

110. Kunadt, M. *et al.* Extracellular vesicle sorting of α-Synuclein is regulated by sumoylation. *Acta Neuropathol.* **129**, 695–713 (2015).

111. Villarroya-Beltri, C. *et al.* Sumoylated hnRNPA2B1 controls the sorting of miRNAs into exosomes through binding to specific motifs. *Nat. Commun.* **4**, 2980 (2013).

112. Santangelo, L. *et al.* The RNA-Binding Protein SYNCRIP Is a Component of the Hepatocyte Exosomal Machinery Controlling MicroRNA Sorting. *Cell Rep* **17**, 799–808 (2016).

113. Montecalvo, A. *et al.* Mechanism of transfer of functional microRNAs between mouse dendritic cells via exosomes. *Blood* **119**, 756–766 (2012).

114. Gibbings, D. J., Ciaudo, C., Erhardt, M. & Voinnet, O. Multivesicular bodies associate with components of miRNA effector complexes and modulate miRNA activity. *Nat. Cell Biol.* **11**, 1143–9 (2009).

115. Soares, A. R. *et al.* Gap junctional protein Cx43 is involved in the communication between extracellular vesicles and mammalian cells. *Sci. Rep.* **5**, 13243 (2015).

116. Varela-Eirin, M. *et al.* Recruitment of RNA molecules by connexin RNA-binding motifs: Implication in RNA and DNA transport through microvesicles and exosomes. *Biochim. Biophys. Acta - Mol. Cell Res.* **1864**, 728–736 (2017).

117. Welton, J. L. *et al.* Cerebrospinal fluid extracellular vesicle enrichment for protein biomarker discovery in neurological disease; multiple sclerosis. *J. Extracell. Vesicles* **6**, 1369805 (2017).

118. Cheng, L., Sharples, R. A., Scicluna, B. J. & Hill, A. F. Exosomes provide a protective and enriched source of miRNA for biomarker profiling compared to intracellular and cell-free blood. *J. Extracell. vesicles* **3**, (2014).

119. Thind, A. & Wilson, C. Exosomal miRNAs as cancer biomarkers and therapeutic targets. *J. Extracell. Vesicles* **5**, 31292 (2016).

120. Quinn, J. F. *et al.* Extracellular RNAs: development as biomarkers of human disease. *J. Extracell. Vesicles* **4**, 27495 (2015).

121. Boukouris, S. & Mathivanan, S. Exosomes in bodily fluids are a highly stable resource of disease biomarkers. *Proteomics. Clin. Appl.* **9**, 358–67 (2015).

122. Pitt, J. M., Kroemer, G. & Zitvogel, L. Extracellular vesicles: masters of intercellular communication and potential clinical interventions. *J. Clin. Invest.* **126**, 1139–1143 (2016).

123. van Niel, G., D'Angelo, G. & Raposo, G. Shedding light on the cell biology of extracellular vesicles. *Nat. Rev. Mol. Cell Biol.* **19**, 213–228 (2018).

124. Raposo, G. & Stoorvogel, W. Extracellular vesicles: exosomes, microvesicles, and friends. *J Cell Biol* **200**, 373–383 (2013).

125. Tkach, M. & Thery, C. Communication by Extracellular Vesicles: Where We Are and Where We Need to Go. *Cell* **164**, 1226–1232 (2016).

126. Robbins, P. D. & Morelli, A. E. Regulation of immune responses by extracellular vesicles. *Nat. Rev. Immunol.* **14**, 195–208 (2014).

127. Blanchard, N. *et al.* TCR activation of human T cells induces the production of exosomes bearing the TCR/CD3/zeta complex. *J Immunol* **168**, 3235–3241 (2002).

128. Wahlgren, J., Karlson Tde, L., Glader, P., Telemo, E. & Valadi, H. Activated human T cells secrete exosomes that participate in IL-2 mediated immune response signaling. *PLoS One* **7**, e49723 (2012).

129. Jolly, C., Welsch, S., Michor, S. & Sattentau, Q. J. The regulated secretory pathway in CD4(+) T cells contributes to human immunodeficiency virus type-1 cell-to-cell spread at the virological synapse. *PLoS Pathog* **7**, e1002226 (2011).

130. Soares, H. HIV-1 Intersection with CD4 T Cell Vesicle Exocytosis: Intercellular Communication Goes Viral. *Front Immunol* **5**, 454 (2014).

131. Bukong, T. N., Momen-Heravi, F., Kodys, K., Bala, S. & Szabo, G. Exosomes from hepatitis C infected patients transmit HCV infection and contain replication competent viral RNA in complex with Ago2-miR122-HSP90. *PLoS Pathog* **10**, e1004424 (2014).

132. Choudhuri, K. *et al.* Polarized release of T-cell-receptor-enriched microvesicles at the immunological synapse. *Nature* **507**, 118–23 (2014).

133. Vardhana, S., Choudhuri, K., Varma, R. & Dustin, M. L. Essential role of ubiquitin and TSG101 protein in formation and function of the central supramolecular activation cluster. *Immunity* **32**, 531–540 (2010).

134. Esposito, L. *et al.* Investigation of soluble and transmembrane CTLA-4 isoforms in serum and microvesicles. *J Immunol* **193**, 889–900 (2014).

135. Friedman, J. R. & Nunnari, J. Mitochondrial form and function. *Nature* **505**, 335–343 (2014).

136. Angajala, A. *et al.* Diverse Roles of Mitochondria in Immune Responses: Novel Insights Into Immuno-Metabolism. *Front. Immunol.* **9**, 1605 (2018).

137. Sena, L. a *et al.* Mitochondria are required for antigen-specific T cell activation through reactive oxygen species signaling. *Immunity* **38**, 225–36 (2013).

138. Arsenio, J., Metz, P. J. & Chang, J. T. Asymmetric Cell Division in T Lymphocyte Fate Diversification. *Trends Immunol.* **36**, 670–683 (2015).

139. Baixauli, F. *et al.* Mitochondrial Respiration Controls Lysosomal Function during Inflammatory T Cell Responses. *Cell Metab* **22**, 485–498 (2015).

140. Quintana, A. *et al.* T cell activation requires mitochondrial translocation to the immunological synapse. *Proc. Natl. Acad. Sci.* **104**, 14418–14423 (2007).

141. Gómez-Cabañas, L. *et al.* Immunological Synapse Formation Induces Mitochondrial Clustering and Mitophagy in Dendritic Cells. *J. Immunol.* **202**, 1715–1723 (2019).

142. Lewis, R. S. Calcium signaling mechanisms in T lymphocytes. *Annu. Rev. Immunol.* **19**, 497–521 (2001).

143. Schwindling, C., Quintana, A., Krause, E. & Hoth, M. Mitochondria positioning controls local calcium influx in T cells. *J. Immunol.* **184**, 184–90 (2010).

144. Morlino, G. *et al.* Miro-1 Links Mitochondria and Microtubule Dynein Motors To Control Lymphocyte Migration and Polarity. *Mol. Cell. Biol.* **34**, 1412–1426 (2014).

145. MacAskill, A. F. *et al.* Miro1 Is a Calcium Sensor for Glutamate Receptor-Dependent Localization of Mitochondria at Synapses. *Neuron* **61**, 541–555 (2009).

146. Contento, R. L. *et al.* Adhesion shapes T cells for prompt and sustained T-cell receptor signalling. *EMBO J.* **29**, 4035–4047 (2010).

147. López-Doménech, G. *et al.* Miro proteins coordinate microtubule- and actin-dependent mitochondrial transport and distribution. *EMBO J.* **37**, 321–336 (2018).

148. Quintero, O. A. *et al.* Human Myo19 Is a Novel Myosin that Associates with Mitochondria. *Curr. Biol.* **19**, 2008–2013 (2009).

149. Gustafsson, C. M., Falkenberg, M. & Larsson, N.-G. Maintenance and Expression of Mammalian Mitochondrial DNA. *Annu. Rev. Biochem.* **85**, 133–160 (2016).

150. Kukat, C. *et al.* Cross-strand binding of TFAM to a single mtDNA molecule forms the mitochondrial nucleoid. *Proc. Natl. Acad. Sci.* **112**, 11288–11293 (2015).

151. Mishra, P. & Chan, D. C. Mitochondrial dynamics and inheritance during cell division, development and disease. *Nat. Rev. Mol. Cell Biol.* **15**, 634–46 (2014).

152. Spees, J. L., Olson, S. D., Whitney, M. J. & Prockop, D. J. Mitochondrial transfer between cells can rescue aerobic respiration. *Proc. Natl. Acad. Sci. U. S. A.* **103**, (2006).

153. Ahmad, T. *et al.* Miro 1 regulates intercellular mitochondrial transport & enhances mesenchymal stem cell rescue efficacy. EMBO J. **33**, (2014).

154. Hayakawa, K. *et al.* Transfer of mitochondria from astrocytes to neurons after stroke. *Nature* **535**, 551–555 (2016).

155. Islam, M. N. *et al.* Mitochondrial transfer from bone-marrow-derived stromal cells to pulmonary alveoli protects against acute lung injury. *Nat Med* **18**, 759–765 (2012).

156. Moschoi, R. *et al.* Protective mitochondrial transfer from bone marrow stromal cells to acute myeloid leukemic cells during chemotherapy. *Blood* (2016).

157. Tan, A. S. *et al.* Mitochondrial Genome Acquisition Restores Respiratory Function and Tumorigenic Potential of Cancer Cells without Mitochondrial DNA. *Cell Metab.* **21**, 81–94 (2015).

158. Cho, Y. M. *et al.* Mesenchymal stem cells transfer mitochondria to the cells with virtually no mitochondrial function but not with pathogenic mtDNA mutations. *PLoS One* **7**, 0–7 (2012).

159. Wang, X. & Gerdes, H.-H. Transfer of mitochondria via tunneling nanotubes rescues apoptotic PC12 cells. *Cell Death Differ.* **22**, 1181–91 (2015).

160. Guescini, M. *et al.* C2C12 myoblasts release micro-vesicles containing mtDNA and proteins involved in signal transduction. *Exp. Cell Res.* **316**, 1977–84 (2010).

161. Kahlert, C. *et al.* Identification of double-stranded genomic DNA spanning all chromosomes with mutated KRAS and p53 DNA in the serum exosomes of patients with pancreatic cancer. *J. Biol. Chem.* **289**, 3869–75 (2014).

162. Phinney, D. G. *et al.* Mesenchymal stem cells use extracellular vesicles to outsource mitophagy and shuttle microRNAs. *Nat. Commun.* **6**, 8472 (2015).

163. Ong, S.-G. & Wu, J. C. Exosomes as potential alternatives to stem cell therapy in mediating cardiac regeneration. *Circ. Res.* **117**, 7–9 (2015).

164. Nakamura, Y. *et al.* Mesenchymal-stem-cell-derived exosomes accelerate skeletal muscle regeneration. *FEBS Lett.* **589**, 1257–1265 (2015).

165. Khan, M. *et al.* Embryonic Stem Cell-Derived Exosomes Promote Endogenous Repair Mechanisms and Enhance Cardiac Function Following Myocardial Infarction. *Circ. Res.* **117**, 52–64 (2015).

166. Galluzzi, L., Kepp, O. & Kroemer, G. Mitochondria: master regulators of danger signalling. *Nat. Rev. Mol. Cell Biol.* **13**, 780–788 (2012).

167. West, A. P. *et al.* Mitochondrial DNA stress primes the antiviral innate immune response. *Nature* **520**, 553–557 (2015).

168. Zhang, Q. *et al.* Circulating mitochondrial DAMPs cause inflammatory responses to injury. *Nature* **464**, 104–7 (2010).

169. Weinberg, S. E., Sena, L. A. & Chandel, N. S. Mitochondria in the Regulation of Innate and Adaptive Immunity. *Immunity* **42**, 406–417 (2015).

170. Collins, L. V., Hajizadeh, S., Holme, E., Jonsson, I. & Tarkowski, A. Endogenously oxidized mitochondrial DNA induces in vivo and in vitro inflammatory responses. *J. Leukoc. Biol.* **75**, 995–1000 (2004).

171. Oka, T. *et al.* Mitochondrial DNA that escapes from autophagy causes inflammation and heart failure. *Nature* **485 VN**-, 251–255 (2012).

172. Shimada, K. *et al.* Oxidized Mitochondrial DNA Activates the NLRP3 Inflammasome during Apoptosis. *Immunity* **36**, 401–414 (2012).

173. Caielli, S. *et al.* Oxidized mitochondrial nucleoids released by neutrophils drive type I interferon production in human lupus. *J. Exp. Med.* **213**, 697–713 (2016).

174. Boudreau, L. H. *et al.* Platelets release mitochondria serving as substrate for bactericidal group IIA-secreted phospholipase a to promote inflammation. *Blood* **124**, 2173–2183 (2014).

175. Morshed, M. *et al.* NADPH oxidase-independent formation of extracellular DNA traps by basophils. *J. Immunol.* **192**, 5314–23 (2014).

176. Yousefi, S. *et al.* Catapult-like release of mitochondrial DNA by eosinophils contributes to antibacterial defense. *Nat Med* **14**, 949–953 (2008).

177. Ishikawa, K. *et al.* The innate immune system in host mice targets cells with allogenic mitochondrial DNA. *J. Exp. Med.* **207**, 2297–305 (2010).

178. Sauer, J. D. *et al.* The N-ethyl-N-nitrosourea-induced Goldenticket mouse mutant reveals an essential function of Sting in the in vivo interferon response to Listeria monocytogenes and cyclic dinucleotides. *Infect Immun* **79**, 688–694 (2011).

179. Thery, C., Amigorena, S., Raposo, G. & Clayton, A. Isolation and characterization of exosomes from cell culture supernatants and biological fluids. *Curr Protoc Cell Biol* **Chapter 3**, Unit 3 22 (2006).

180. Wisniewski, J. R., Zougman, A., Nagaraj, N. & Mann, M. Universal sample preparation method for proteome analysis. *Nat Methods* **6**, 359–362 (2009).

181. Bonzon-Kulichenko, E., Garcia-Marques, F., Trevisan-Herraz, M. & Vazquez, J. Revisiting peptide identification by high-accuracy mass spectrometry: problems associated with the use of narrow mass precursor windows. *J Proteome Res* **14**, 700–710 (2015).

182. Manders, E. M., Stap, J., Brakenhoff, G. J., van Driel, R. & Aten, J. A. Dynamics of three-dimensional replication patterns during the S-phase, analysed by double labelling of DNA and confocal microscopy. *J Cell Sci* **103 (Pt 3**, 857–862 (1992).

183. Théry, C. *et al.* Minimal information for studies of extracellular vesicles 2018 (MISEV2018): a position statement of the International Society for Extracellular Vesicles and update of the MISEV2014 guidelines. *J. Extracell. Vesicles* **7**, 1535750 (2018).

184. Zhang, Y. *et al.* Inflammasome-Derived Exosomes Activate NF-kappaB Signaling in Macrophages. *J Proteome Res* (2016).

185. Perez-Hernandez, D. *et al.* The intracellular interactome of tetraspanin-enriched microdomains reveals their function as sorting machineries toward exosomes. *J Biol Chem* **288**, 11649–11661 (2013).

186. Gilkerson, R. *et al.* The mitochondrial nucleoid: integrating mitochondrial DNA into cellular homeostasis. *Cold Spring Harb Perspect Biol* **5**, a011080 (2013).

187. Nolte-'t Hoen, E. N. *et al.* Deep sequencing of RNA from immune cell-derived vesicles uncovers the selective incorporation of small non-coding RNA biotypes with potential regulatory functions. *Nucleic Acids Res* **40**, 9272–9285 (2012).

188. Hammerling, B. C. *et al.* A Rab5 endosomal pathway mediates Parkin-dependent mitochondrial clearance. *Nat Commun* **8**, 14050 (2017).

189. Vanlandingham, P. A. & Ceresa, B. P. Rab7 regulates late endocytic trafficking downstream of multivesicular body biogenesis and cargo sequestration. *J Biol Chem* **284**, 12110–12124 (2009).

190. Cogliati, S. *et al.* Mitochondrial cristae shape determines respiratory chain supercomplexes assembly and respiratory efficiency. *Cell* **155**, 160–171 (2013).

191. Buck, M. D. *et al.* Mitochondrial Dynamics Controls T Cell Fate through Metabolic Programming. *Cell* **166**, 63–76 (2016).

192. Mizushima, N. & Levine, B. Autophagy in mammalian development and differentiation. *Nat Cell Biol* **12**, 823–830 (2010).

193. Fader, C. M., Sanchez, D., Furlan, M. & Colombo, M. I. Induction of autophagy promotes fusion of multivesicular bodies with autophagic vacuoles in k562 cells. *Traffic* **9**, 230–250 (2008).

194. Latorre-Pellicer, A. *et al.* Mitochondrial and nuclear DNA matching shapes metabolism and healthy ageing. *Nature* **535**, 561–565 (2016).

195. West, A. P. & Shadel, G. S. Mitochondrial DNA in innate immune responses and inflammatory pathology. *Nat Rev Immunol* (2017).

196. Chen, Q., Sun, L. & Chen, Z. J. Regulation and function of the cGAS-STING pathway of cytosolic DNA sensing. *Nat Immunol* **17**, 1142–1149 (2016).

197. Ishikawa, H., Ma, Z. & Barber, G. N. STING regulates intracellular DNA-mediated, type I interferon-dependent innate immunity. *Nature* **461**, 788–792 (2009).

198. Bobrie, A., Colombo, M., Krumeich, S., Raposo, G. & Théry, C. Diverse subpopulations of vesicles secreted by different intracellular mechanisms are present in exosome preparations obtained by differential ultracentrifugation. *J. Extracell. Vesicles* **1**, 18397 (2012).

199. van der Vlist, E. J. *et al.* CD4 $^{+}$ T cell activation promotes the differential release of distinct populations of nanosized vesicles. *J. Extracell. Vesicles* **1**, 18364 (2012).

200. Palma, J. *et al.* MicroRNAs are exported from malignant cells in customized particles. *Nucleic Acids Res.* **40**, 9125–9138 (2012).

201. Sreekumar, P. G. *et al.* αB Crystallin Is Apically Secreted within Exosomes by Polarized Human Retinal Pigment Epithelium and Provides Neuroprotection to Adjacent Cells. *PLoS One* **5**, e12578 (2010).

202. White, I. J., Bailey, L. M., Aghakhani, M. R., Moss, S. E. & Futter, C. E. EGF stimulates annexin 1-dependent inward vesiculation in a multivesicular endosome subpopulation. *EMBO J.* **25**, 1–12 (2006).

203. Kowal, J. *et al.* Proteomic comparison defines novel markers to characterize heterogeneous populations of extracellular vesicle subtypes. *Proc. Natl. Acad. Sci. U. S. A.* (2016).

204. Willms, E. *et al.* Cells release subpopulations of exosomes with distinct molecular and biological properties. *Sci. Rep.* **6**, 22519 (2016).

205. Mastoridis, S. *et al.* Multiparametric Analysis of Circulating Exosomes and Other Small Extracellular Vesicles by Advanced Imaging Flow Cytometry. *Front. Immunol.* **9**, 1583 (2018).

206. Schrader, M., Godinho, L. F., Costello, J. L. & Islinger, M. The different facets of organelle interplay-an overview of organelle interactions. *Front. cell Dev. Biol.* **3**, 56 (2015).

207. Martinvalet, D. The role of the mitochondria and the endoplasmic reticulum contact sites in the development of the immune responses. *Cell Death Dis.* **9**, 336 (2018).

208. Sugiura, A., Mattie, S., Prudent, J. & McBride, H. M. Newly born peroxisomes are a hybrid of mitochondrial and ER-derived pre-peroxisomes. *Nature* **542**, 251–254 (2017).

209. Itoh, K. *et al.* A brain-enriched Drp1 isoform associates with lysosomes, late endosomes, and the plasma membrane. *J. Biol. Chem.* **293**, 11809–11822 (2018).

210. Green, D. R., Galluzzi, L. & Kroemer, G. Mitochondria and the Autophagy-Inflammation-Cell Death Axis in Organismal Aging. *Science (80-.).* **333**, 1109–1112 (2011).

211. Sheftel, A. D., Zhang, A.-S., Brown, C., Shirihai, O. S. & Ponka, P. Direct interorganellar transfer of iron from endosome to mitochondrion. *Blood* **110**, 125–132 (2007).

212. Hamdi, A. *et al.* Erythroid cell mitochondria receive endosomal iron by a “kiss-and-run” mechanism. *Biochim. Biophys. Acta - Mol. Cell Res.* **1863**, 2859–2867 (2016).

213. Soto-Heredero, G., Baixauli, F. & Mittelbrunn, M. Interorganelle Communication between Mitochondria and the Endolysosomal System. *Front. Cell Dev. Biol.* **5**, 95 (2017).

214. Cioni, J.-M. *et al.* Late Endosomes Act as mRNA Translation Platforms and Sustain Mitochondria in Axons. *Cell* **176**, 56-72.e15 (2019).

215. Nakahira, K. *et al.* Autophagy proteins regulate innate immune responses by inhibiting the release of mitochondrial DNA mediated by the NALP3 inflammasome. *Nat Immunol* **12**, 222–230 (2011).

216. Wang, C. & Youle, R. J. The role of mitochondria in apoptosis*. *Annu. Rev. Genet.* **43**, 95–118 (2009).

217. Soubannier, V. *et al.* A vesicular transport pathway shuttles cargo from mitochondria to lysosomes. *Curr. Biol.* **22**, 135–41 (2012).

218. Cadete, V. J. J. *et al.* Formation of mitochondrial-derived vesicles is an active and physiologically relevant mitochondrial quality control process in the cardiac system. *J. Physiol.* **594**, 5343–5362 (2016).

219. Sugiura, A., McLelland, G. L., Fon, E. A. & McBride, H. M. A new pathway for mitochondrial quality control: mitochondrial-derived vesicles. *EMBO J* **33**, 2142–2156 (2014).

220. Mclelland, G., Soubannier, V., Chen, C. X., Mcbride, H. M. & Fon, E. A. Parkin and PINK 1 function in a vesicular trafficking pathway regulating mitochondrial quality control. **33**, 282–296 (2014).

221. McLelland, G.-L., Lee, S. A., McBride, H. M. & Fon, E. A. Syntaxin-17 delivers PINK1/parkin-dependent mitochondrial vesicles to the endolysosomal system. *J. Cell Biol.* **214**, 275–291 (2016).

222. Pan, B. T., Teng, K., Wu, C., Adam, M. & Johnstone, R. M. Electron microscopic evidence for externalization of the transferrin receptor in vesicular form in sheep reticulocytes. *J. Cell Biol.* **101**, 942–948 (1985).

223. Johnstone, R. M., Adam, M., Hammond, J. R., Orr, L. & Turbide, C. Vesicle formation during reticulocyte maturation. Association of plasma membrane activities with released vesicles (exosomes). *J. Biol. Chem.* **262**, 9412–20 (1987).

224. Dai, Y. *et al.* Rapamycin drives selection against a pathogenic heteroplasmic mitochondrial DNA mutation. *Hum. Mol. Genet.* **23**, 637–47 (2014).

225. Suen, D.-F., Narendra, D. P., Tanaka, A., Manfredi, G. & Youle, R. J. Parkin overexpression selects against a deleterious mtDNA mutation in heteroplasmic cybrid cells. *Proc. Natl. Acad. Sci.* **107**, 11835–11840 (2010).

226. Valenci, I., Yonai, L., Bar-Yaacov, D., Mishmar, D. & Ben-Zvi, A. Parkin modulates heteroplasmy of truncated mtDNA in Caenorhabditis elegans. *Mitochondrion* **20**, 64–70 (2015).

227. Peeva, V. *et al.* Linear mitochondrial DNA is rapidly degraded by components of the replication machinery. *Nat. Commun.* **9**, 1727 (2018).

228. Medeiros, T. C., Thomas, R. L., Ghillebert, R. & Graef, M. Autophagy balances mtDNA synthesis and degradation by DNA polymerase POLG during starvation. *J. Cell Biol.* **217**, 1601–1611 (2018).

229. Moretton, A. *et al.* Selective mitochondrial DNA degradation following double-strand breaks. *PLoS One* **12**, e0176795 (2017).

230. Shokolenko, I. N., Wilson, G. L. & Alexeyev, M. F. The “fast” and the “slow” modes of mitochondrial DNA degradation. *Mitochondrial DNA* **27**, 490–498 (2016).

231. Lespagnol, A. *et al.* Exosome secretion, including the DNA damage-induced p53-dependent secretory pathway, is severely compromised in TSAP6/Steap3-null mice. *Cell Death Differ.* **15**, 1723–1733 (2008).

232. Hessvik, N. P. *et al.* PIKfyve inhibition increases exosome release and induces secretory autophagy. *Cell. Mol. Life Sci.* **73**, 4717–4737 (2016).

233. Jeannin, P. *et al.* Proteomic analysis of plasma extracellular vesicles reveals mitochondrial stress upon HTLV-1 infection. *Sci. Rep.* **8**, 5170 (2018).

234. Szczesny, B. *et al.* Mitochondrial DNA damage and subsequent activation of Z-DNA binding protein 1 links oxidative stress to inflammation in epithelial cells. *Sci. Rep.* **8**, 914 (2018).

235. Kalluri, R. & LeBleu, V. S. Discovery of Double-Stranded Genomic DNA in Circulating Exosomes. *Cold Spring Harb. Symp. Quant. Biol.* **81**, 275–280 (2016).

236. Melentijevic, I. *et al.* C. elegans neurons jettison protein aggregates and mitochondria under neurotoxic stress. *Nature* **542**, 367–371 (2017).

237. Soubannier, V., Rippstein, P., Kaufman, B. a, Shoubridge, E. a & McBride, H. M. Reconstitution of mitochondria derived vesicle formation demonstrates selective enrichment of oxidized cargo. *PLoS One* **7**, e52830 (2012).

238. Cai, J. *et al.* Extracellular vesicle-mediated transfer of donor genomic DNA to recipient cells is a novel mechanism for genetic influence between cells. *J. Mol. Cell Biol.* **5**, 227–238 (2013).

239. Lee, T. H. *et al.* Oncogenic ras-driven cancer cell vesiculation leads to emission of double-stranded DNA capable of interacting with target cells. *Biochem. Biophys. Res. Commun.* **451**, 295–301 (2014).

240. Sansone, P. *et al.* Packaging and transfer of mitochondrial DNA via exosomes regulate escape from dormancy in hormonal therapy-resistant breast cancer. *Proc. Natl. Acad. Sci.* **114**, E9066–E9075 (2017).

241. Crisp, A., Boschetti, C., Perry, M., Tunnacliffe, A. & Micklem, G. Expression of multiple horizontally acquired genes is a hallmark of both vertebrate and invertebrate genomes. *Genome Biol.* **16**, 50 (2015).

242. Marinoni, G. *et al.* Horizontal transfer of genetic material among Saccharomyces yeasts. *J. Bacteriol.* **181**, 6488–96 (1999).

243. Gladyshev, E. A., Meselson, M. & Arkhipova, I. R. Massive Horizontal Gene Transfer in Bdelloid Rotifers. *Science (80-.).* **320**, 1210–1213 (2008).

244. Eyres, I. *et al.* Horizontal gene transfer in bdelloid rotifers is ancient, ongoing and more frequent in species from desiccating habitats. *BMC Biol.* **13**, 90 (2015).

245. Rice, D. W. *et al.* Horizontal Transfer of Entire Genomes via Mitochondrial Fusion in the Angiosperm Amborella. *Science (80-.).* **342**, 1468–1473 (2013).

246. Rebbeck, C. A., Leroi, A. M. & Burt, A. Mitochondrial capture by a transmissible cancer. *Science (80-.).* **331**, 303 (2011).

247. Clark, M. A. & Shay, J. W. Mitochondrial transformation of mammalian cells. *Nature* **295**, 605–607 (1982).

248. Manfredi, G., Thyagarajan, D., Papadopoulou, L. C., Pallotti, F. & Schon, E. A. The fate of human sperm-derived mtDNA in somatic cells. *Am J Hum Genet* **61**, 953–960 (1997).

249. Dong, L. F. *et al.* Horizontal transfer of whole mitochondria restores tumorigenic potential in mitochondrial DNA-deficient cancer cells. *Elife* **6**, (2017).

250. Hough, K. P. *et al.* Exosomal transfer of mitochondria from airway myeloid-derived regulatory cells to T cells. *Redox Biol.* **18**, 54–64 (2018).

251. Li, M., Schröder, R., Ni, S., Madea, B. & Stoneking, M. Extensive tissue-related and allele-related mtDNA heteroplasmy suggests positive selection for somatic mutations. *Proc. Natl. Acad. Sci. U. S. A.* **112**, 2491–6 (2015).

252. Sharpley, M. S. *et al.* Heteroplasmy of Mouse mtDNA Is Genetically Unstable and Results in Altered Behavior and Cognition. *Cell* **151**, 333–343 (2012).

253. Branzk, N. *et al.* Neutrophils sense microbe size and selectively release neutrophil extracellular traps in response to large pathogens. *Nat Immunol* **15**, 1017–1025 (2014).

254. Lood, C. *et al.* Neutrophil extracellular traps enriched in oxidized mitochondrial DNA are interferogenic and contribute to lupus-like disease. *Nat Med* **22**, 146–153 (2016).

255. Ingelsson, B. *et al.* Lymphocytes eject interferogenic mitochondrial DNA webs in response to CpG and non-CpG oligodeoxynucleotides of class C. *Proc. Natl. Acad. Sci. U. S. A.* **115**, E478–E487 (2018).

256. Julian, M. W. *et al.* Mitochondrial transcription factor A serves as a danger signal by augmenting plasmacytoid dendritic cell responses to DNA. *J. Immunol. (Baltimore, Md. 1950)* **189**, 433–443 (2012).

257. Tsilioni, I. & Theoharides, T. C. Extracellular vesicles are increased in the serum of children with autism spectrum disorder, contain mitochondrial DNA, and stimulate human microglia to secrete IL-1β. *J. Neuroinflammation* **15**, 239 (2018).

258. Verboogen, D. R. J. *et al.* The dendritic cell side of the immunological synapse. *Biomol. Concepts* **7**, 17–28 (2016).

259. Boes, M. *et al.* T-cell engagement of dendritic cells rapidly rearranges MHC class II transport. *Nature* **418**, 983–988 (2002).

260. Boes, M. *et al.* T Cells Induce Extended Class II MHC Compartments in Dendritic Cells in a Toll-Like Receptor-Dependent Manner. *J. Immunol.* **171**, 4081–4088 (2003).

261. Pulecio, J. *et al.* Cdc42-mediated MTOC polarization in dendritic cells controls targeted delivery of cytokines at the immune synapse. *J. Exp. Med.* **207**, 2719–2732 (2010).

262. Chen, M. & Wang, J. Programmed cell death of dendritic cells in immune regulation. *Immunol Rev* **236**, 11–27 (2010).

263. Riol-Blanco, L. *et al.* Immunological synapse formation inhibits, via NF-kappaB and FOXO1, the apoptosis of dendritic cells. *Nat Immunol* **10**, 753–760 (2009).

264. Ingulli, E., Mondino, A., Khoruts, A. & Jenkins, M. K. In vivo detection of dendritic cell antigen presentation to CD4(+) T cells. *J Exp Med* **185**, 2133–2141 (1997).

265. Garg, S. *et al.* Genetic tagging shows increased frequency and longevity of antigen-presenting, skin-derived dendritic cells in vivo. *Nat Immunol* **4**, 907–912 (2003).

266. Ariotti, S. *et al.* T cell memory. Skin-resident memory CD8(+) T cells trigger a state of tissue-wide pathogen alert. *Science (80-.).* **346**, 101–105 (2014).

267. Iijima, N. & Iwasaki, A. T cell memory. A local macrophage chemokine network sustains protective tissue-resident memory CD4 T cells. *Science (80-.).* **346**, 93–98 (2014).

268. Schenkel, J. M. *et al.* T cell memory. Resident memory CD8 T cells trigger protective innate and adaptive immune responses. *Science (80-.).* **346**, 98–101 (2014).

269. Netea, M. G. *et al.* Trained immunity: A program of innate immune memory in health and disease. *Science (80-.).* **352**, aaf1098 (2016).

270. Curato, C. *et al.* DC Respond to Cognate T Cell Interaction in the Antigen-Challenged Lymph Node. *Front. Immunol.* **10**, 863 (2019).

271. Rodriguez-Fernandez, J. L., Riol-Blanco, L. & Delgado-Martin, C. What Is the Function of the Dendritic Cell Side of the Immunological Synapse? *Sci. Signal.* **3**, re2–re2 (2010).

Annexes

Annexes

1. Publications related with this work (included):

I. **Torralba D**, Baixauli F, Villarroya-Beltri C, Fernández-Delgado I, Latorre-Pellicer A, Acín-Pérez R, Martín-Cófreces NB, Jaso-Tamame ÁL, Iborra S, Jorge I, González-Aseguinolaza G, Garaude J, Vicente-Manzanares M, Enríquez JA, Mittelbrunn M, Sánchez-Madrid F. Priming of dendritic cells by DNA-containing extracellular vesicles from activated T cells through antigen-driven contacts. Nat Commun. 2018 Jul 9;9(1):2658. doi: 10.1038/s41467-018-05077-9.

II. Villarroya-Beltri C, Baixauli F, Mittelbrunn M, Fernández-Delgado I, **Torralba D**, Moreno-Gonzalo O, Baldanta S, Enrich C, Guerra S, Sánchez-Madrid F. ISGylation controls exosome secretion by promoting lysosomal degradation of MVB proteins. Nat Commun. 2016 Nov 24;7:13588. doi: 10.1038/ncomms13588.

2. Reviews related with this work (not included):

I. **Torralba D**, Baixauli F, Sánchez-Madrid F. Mitochondria Know No Boundaries: Mechanisms and Functions of Intercellular Mitochondrial Transfer. Front Cell Dev Biol. 2016 Sep 28;4:107. eCollection 2016. Review.

II. **Torralba D**, Martín-Cófreces NB, Sanchez-Madrid F. Mechanisms of polarized cell-cell communication of T lymphocytes. Immunol Lett. 2019 May;209:11-20. doi: 10.1016/j.imlet.2019.03.009. Epub 2019 Apr 5. Review.

3. Other articles not related with this work:

I. Saiz ML, Cibrian D, Ramírez-Huesca M, **Torralba D**, Moreno-Gonzalo O, Sánchez-Madrid F. Tetraspanin CD9 Limits Mucosal Healing in Experimental Colitis. Front Immunol. 2017 Dec 19;8:1854. doi: 10.3389/fimmu.2017.01854. eCollection 2017.

nature COMMUNICATIONS

ARTICLE

DOI: 10.1038/s41467-018-05077-9 OPEN

Priming of dendritic cells by DNA-containing extracellular vesicles from activated T cells through antigen-driven contacts

Daniel Torralba[1,2], Francesc Baixauli[1,3], Carolina Villarroya-Beltri[1,2], Irene Fernández-Delgado[1,2], Ana Latorre-Pellicer[4], Rebeca Acín-Pérez[5], Noa B Martín-Cófreces[1,2,6], Ángel Luis Jaso-Tamame[7], Salvador Iborra[5], Inmaculada Jorge[6,8], Gloria González-Aseguinolaza[9], Johan Garaude[5], Miguel Vicente-Manzanares[10], José Antonio Enríquez[5,11], María Mittelbrunn[12,13] & Francisco Sánchez-Madrid[1,2,6]

Interaction of T cell with antigen-bearing dendritic cells (DC) results in T cell activation, but whether this interaction has physiological consequences on DC function is largely unexplored. Here we show that when antigen-bearing DCs contact T cells, DCs initiate anti-pathogenic programs. Signals of this interaction are transmitted from the T cell to the DC, through extracellular vesicles (EV) that contain genomic and mitochondrial DNA, to induce antiviral responses via the cGAS/STING cytosolic DNA-sensing pathway and expression of IRF3-dependent interferon regulated genes. Moreover, EV-treated DCs are more resistant to subsequent viral infections. In summary, our results show that T cells prime DCs through the transfer of exosomal DNA, supporting a specific role for antigen-dependent contacts in conferring protection to DCs against pathogen infection. The reciprocal communication between innate and adaptive immune cells thus allow efficacious responses to unknown threats.

[1] Vascular Pathophysiology Research Area, Centro Nacional Investigaciones Cardiovasculares (CNIC), 28029 Madrid, Spain. [2] Servicio de Inmunología, Instituto Investigación Sanitaria Princesa, Universidad Autónoma de Madrid, Diego de León 62, 28006 Madrid, Spain. [3] Immunometabolism Department, Max Planck Institute for Immunobiology and Epigenetics, 79108 Freiburg im Breisgau, Germany. [4] Grupo de Medicina Xenómica, CIBERER, Universidad de Santiago de Compostela, 15782 Santiago de Compostela, Spain. [5] Myocardial Pathophysiology Research Area, Centro Nacional Investigaciones Cardiovasculares (CNIC), 28029 Madrid, Spain. [6] Centro de Investigación Biomédica en Red Enfermedades Cardiovasculares (CIBERCV), Melchor Fernández Almagro 3, 28029 Madrid, Spain. [7] MRC Clinical Sciences Centre, Imperial College Faculty of Medicine, London SW7 2AZ, UK. [8] Laboratory of Cardiovascular Proteomics, Centro Nacional Investigaciones Cardiovasculares (CNIC), 28029 Madrid, Spain. [9] Centro de Investigación Médica Aplicada (CIMA), Universidad de Navarra, 31008 Pamplona, Spain. [10] Instituto de Biología Molecular y Celular del Cáncer USAL-CSIC, 37007 Salamanca, Spain. [11] Centro de Investigaciones en RED (CIBERFES), Melchor Fernández Almagro 9, 28029 Madrid, Spain. [12] Instituto de Investigación Sanitaria, Hospital 12 de Octubre (i+12), 28041 Madrid, Spain. [13] Centro de Biología Molecular, UAM-CSIC, Departamento de Biología Celular e Inflamación, 28049 Madrid, Spain. These authors contributed equally: Daniel Torralba, Francesc Baixauli. Correspondence and requests for materials should be addressed to F.S-M. (email: fsmadrid@salud.madrid.org)

The generation of a specific immune response against a pathogen requires the initial interaction of an antigen-specific T cell with antigen-presenting cells (APCs), specifically dendritic cells (DCs). DCs express antigenic peptides associated to the major histocompatibility complex (MHC) class II, and T cell recognition of these complexes leads to the formation of a stable intercellular junction between the cells, the immune synapse (IS)[1]. The IS comprises a highly organized dynamic supramolecular structure that orchestrates the early events of T cell activation, including the spatiotemporal organization of the TCR signaling and its costimulatory molecules. The IS is a cell polarization event involving the redistribution of membrane-associated receptors and the cytoskeleton, and the polarization of intracellular trafficking and secretory organelles[2]. IS formation generates diverse regulatory checkpoints for the control of antigen-specific T cell response by controlling the spatial and temporal rearrangements of the different T cell receptors and organelles.

Besides its prominent role in instructing T cell activation, the IS transmits intracellular signals that direct DC function[3]. On the DC side, IS formation rapidly increases the concentration of MHC class II molecules in the synaptic contact to strengthen antigen presentation to cognate T cells[4]. The actin and microtubule cytoskeletons of DCs undergo substantial rearrangements during IS formation, allowing the polarization of different compartments. The relocation of endosomal compartments in DCs mediates the polarized secretion of cytokines into the synaptic region[5,6], and the trafficking of the major histocompatibility complexes[4]. IS formation increases DCs survival by inhibition of apoptotic signaling, enhancing DC antigen presentation, and T cell clonal expansion[7]. The IS integrates the signaling provided by the APC and the T cell to modulate the function of both cells and ensure T cell priming, activation, and efficient T cell responses against cognate antigens. The underlying mechanisms and functions of the IS in T cells are widely known although the physiological significance of the IS for DCs is still largely unexplored.

The transfer of bioactive molecules from the T cell to the DC through the IS constitutes a main vehicle of intercellular communication. T cells and DCs exchange numerous molecules, including cytokines, membrane receptors, membrane patches, signaling molecules, or genetic material (mainly functional microRNAs) during IS formation[8]. Immune cells readily transfer membrane fragments to other cells, membrane-associated receptors, and co-receptors. Several cellular mechanisms mediate information transfer between the T cell and the DCs, including transendocytosis, trogocytosis, formation of tunneling nanotubes, and polarized secretion of extracellular vesicles (EVs)[8]. These exchanges fine-tune the activation of the T cell, e.g., by cell-extrinsic depletion of costimulatory proteins from APCs; capture of MHC class I and II from target cells; downregulation of TCR peptide-MHC II complexes from APCs; regulation of DCs gene expression, and transcellular signaling through the transfer of microRNA-loaded exosomes and TCR-enriched EVs[9–12]. Pathogens such as bacteria or virus subvert the architecture of the IS to enhance dissemination between immune cells[13–15]. The IS may act as a portal that supports the transfer of an array of different molecules or even entire pathogens between T cells and DCs.

Immune cells secrete a variety of EVs to the extracellular milieu that can exert diverse immune functions, including antigen presentation, immune activation, induction of tolerance, or suppression of immune responses[16]. EVs comprise apoptotic bodies, ectosomes or microvesicles, and exosomes[17,18]. Exosomes are distinguished by their unique endocytic origin. Exosomes form by invagination of the multivesicular body (MVB) membrane and are released to the extracellular medium upon the fusion of the MVB with the plasma membrane. Protein and lipid sorting and packaging into exosomes occur in a regulated manner involving mono-ubiquitination and the endosomal sorting complexes required for transport (ESCRT) machinery, association with lipid rafts or the tetraspanin network[19]. Exosomes contain proteins involved in their biogenesis, vesicle trafficking, lipid membrane organization, as well as proteins and adhesion receptors specific of the producing cell. Exosomes are particularly enriched in genetic material, mostly RNA species such as small RNAs and long non-coding RNAs, as well as DNA[19]. This makes them attractive candidates to mediate cell-to-cell communication. However, the ability of the genetic material contained within exosomes to evoke immune signaling responses in recipient cells is largely unexplored.

In the present manuscript this question is investigated in the context of the immune cognate interactions. Data show that T cell EV contain genomic and mitochondrial DNA (mtDNA) endowed with the ability to trigger immune signaling in recipient cells. By using different proteomic, genomic, and cell biology approaches, it is demonstrated that the unidirectional transfer of DNA within EVs from T cells to DCs triggers antiviral responses in the DC. Such DNA-based priming confers DCs resistance to subsequent viral infections. In conclusion, resulting data illustrate a way by which T cells promote an alert state in DCs that protects them against posterior infection driven by the vesicular transfer of DNA.

Results

T cells shuttle genomic and mitochondrial DNA in exosomes. EVs transferred from T cell to APC contain many different types of biologically active molecules, including proteins and genetic material[9,10]. To investigate the possible specific function of the different components of the biologic material transferred from the T cell to the DC, the protein and genetic content of EVs isolated from the culture supernatant of primary T lymphoblasts were characterized by differential ultracentrifugation[20] (Fig. 1a). Diameters of EVs obtained in the 100,000 × *g* fraction ranged from 50 to 200 nm (Fig. 1b), in agreement with the reported size of exosomes[17]. Proteomic characterization of T cell EVs identified abundant peptides derived from canonical exosome components, including tetraspanins, endosomal proteins, cytoskeletal proteins, Rab-related trafficking proteins, heat-shock proteins, and nucleotide-binding proteins (Supplementary Data 1). Gene Ontology (GO) term enrichment analysis revealed that a major fraction of the total number of identified peptides (>3000 peptides in four biological replicates) were significantly associated with the nuclear and mitochondrial fractions (Fig. 1c and Supplementary Data 2). Mitochondrial peptides constituted 7.5 ± 0.3% of the total exosome proteome, consistent with proteomic studies on exosomes isolated from other cell types, including immune cells[21,22]. EVs isolated from resting T lymphoblasts and cells activated with a polyclonal stimulus barely contained proteins of the mitochondrial matrix and the inner or outer mitochondrial membranes (Fig. 1d). EVs from activated T lymphoblasts contained significant amounts of mitochondrial transcription factor A (TFAM), a highly abundant mtDNA-binding protein, and the mitochondrial nucleoid-forming protein ATPase family AAA-Domain containing protein 3 (ATAD3)[23] (Fig. 1d). The presence of the canonical exosomal proteins CD81 and TSG101 in the purified 100,000 × *g* fraction suggested an endosomal origin (Fig. 1d). TFAM and ATAD3 co-fractionated with the exosomal proteins CD81 and TSG101 in the 100,000 × *g* EV fraction from sucrose-gradient isolation, (Fig. 1e), localizing mtDNA-binding proteins to exosomes.

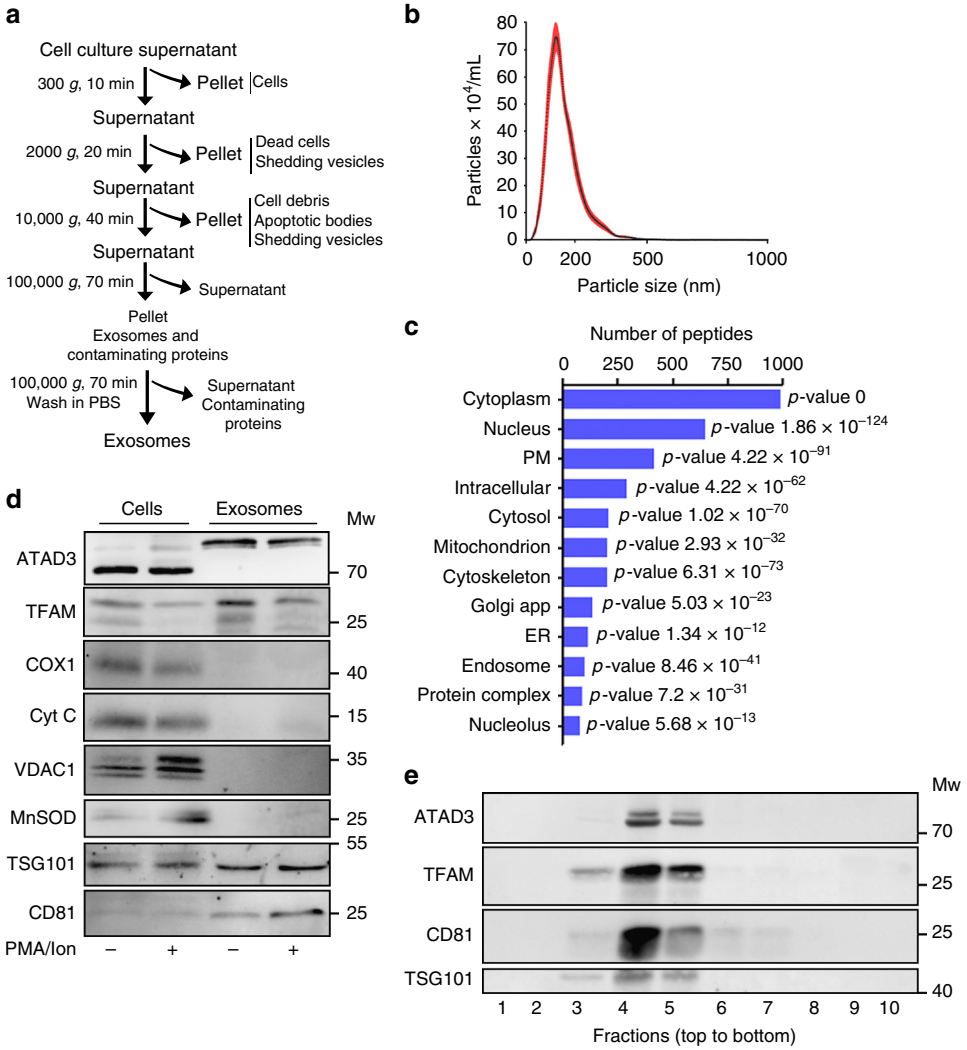

Fig. 1 Exosomes shuttle mitochondrial proteins. **a** Differential ultracentrifugation protocol for isolating and purifying exosomes from cell culture supernatants. **b** Size distribution analysis by Nanoparticle Tracking Analysis (NTA) of purified EVs from primary human T lymphoblasts. **c** Gene ontology (GO) cellular component analysis of peptides identified in T cell EVs. **d** Western blot analysis of mitochondrial proteins in EVs obtained from the culture supernatant of primary human T lymphoblasts with or without treatment with phorbol myristate acetate (PMA) plus ionomycin. Cells and EVs were blotted for proteins associated with mtDNA (TFAM and ATAD3), for proteins located in the inner mitochondrial membrane (COX1 and Cytochrome C), the outer mitochondrial membrane (VDAC1), the mitochondrial matrix (mitochondrial manganese superoxide dismutase, MnSOD), and for the exosome markers TSG101 and CD81. **e** Western blot analysis of ATAD3, TFAM, and the exosome markers CD81 and TSG101 in sucrose fractions. EVs obtained from the culture supernatant of human T lymphoblasts were laid on a discontinuous sucrose gradient and floated by overnight centrifugation. Gradient fractions were collected and analyzed by immunoblot to reveal the distribution of mtDNA-binding proteins and exosomal proteins in the sucrose fractions from lower to higher sucrose density (left to right). Gels shown are representative out of three independent experiments

Among EVs, exosomes are enriched in genetic material, mostly non-coding RNAs[24,25]. Exosomes from cancer cell lines and patients contain DNA that reflects the mutational status of the parental tumor cells[26,27]. Deep-sequencing analysis of DNA in the EVs secreted by primary T lymphoblasts identified several reads that covered nuclear sequences and the entire mitochondrial genome (Fig. 2a). These results were confirmed by polymerase chain reaction (PCR) amplification of indicated regions of the mitochondrial genome and the *B2M* nuclear gene from the DNA obtained from the 100,000 × *g* fraction (Fig. 2b). The DNA content of the isolated EVs was reduced by DNase treatment whereas a small fraction of the DNA remained protected unless vesicles were treated with DNase and a lipid destabilizing agent (Fig. 2c). Two pools of DNA were present, one accessible (likely on the surface of the vesicle) and one inaccessible (likely in the lumen of the vesicle). The presence of mtDNA in the 100,000 × *g* EV fraction was confirmed by the partial co-fractionation on sucrose gradients with the exosomal proteins CD63 and TSG101 (Fig. 2d). Flow cytometry analysis of EVs coupled to aldehyde sulfate beads reveals that the majority of beads were positive for both CD81 and DNA (Fig. 2e, and Supplementary Fig. 1a). Total internal reflection fluorescence (TIRF) microscopy-based analysis of the co-localization of exosomal marker CD81 with TSG101 or with DNA in isolated EVs showed that CD81 fully co-localized with TSG101, but only partly with DNA (Supplementary Fig. 1b), suggesting the presence of DNA in a subset of $CD81^+$ exosomes in addition to other different populations of EVs.

DNA staining in non-permeabilized EVs increased upon permeabilization (Fig. 2e), confirming that DNA is present both outside and inside EVs. To examine the oxidative status of EV DNA, the 8-hydroxydeoxyguanosine (8-OHdG) DNA

modification was evaluated as a hallmark of DNA oxidation. Staining with anti-oxidized DNA antibody (Ab) is also detected in non-permeabilized EVs (Fig. 2f). In agreement with these results, chromatin immunoprecipitation of EV lysates with 8-OHdG Ab followed by DNA isolation and PCR analysis revealed the presence of several oxidized mtDNA and genomic DNA regions in EVs when compared with the control isotype Ab (Supplementary Fig. 1c). To address the preferential localization of oxidized mtDNA, EVs and mitochondrial fractions of the corresponding cells were isolated and chromatin immunoprecipitation (ChIP) was performed with the 8-OHdG and total DNA Abs. The enrichment in oxidized mtDNA at the EV fraction was demonstrated by qPCR analysis of mitochondrial genes in ChIP and quantification of the ratio between oxidized DNA vs total DNA (Fig. 2f). These results indicate that T cells release EVs carrying genomic DNA and mtDNA and associated mtDNA-binding proteins, and that the released DNA is partially oxidized.

Segregation of mtDNA and related proteins into MVB pathway. The presence of mitochondrial components in EVs prompted us to investigate the molecular mechanisms controlling their extracellular release. We first co-transfected HEK293 cells

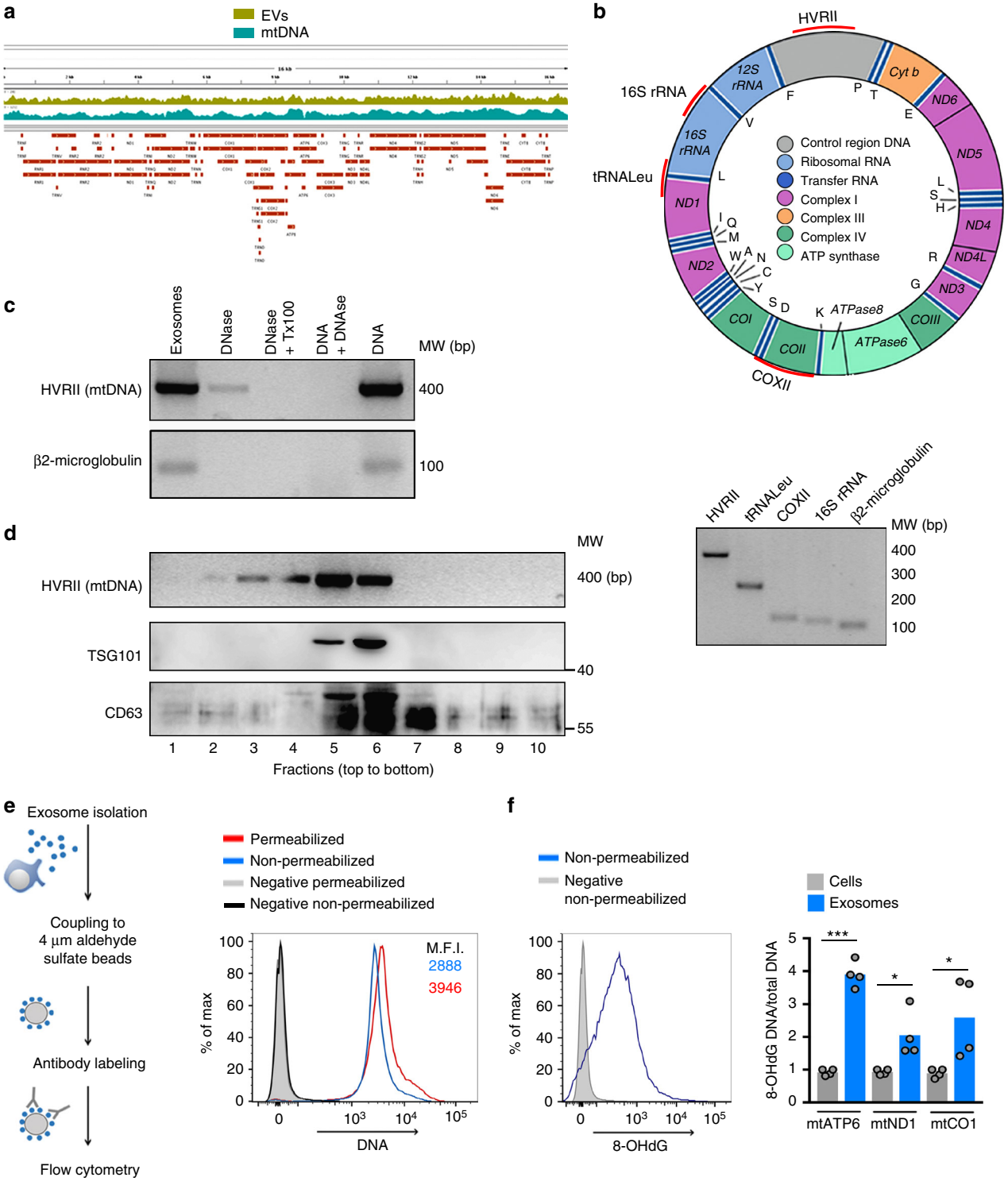

with TFAM-GFP and a mitochondria-targeted red fluorescent protein (mitoDsRed), then stained for endosomal markers. Confocal immunofluorescence analysis excluded co-localization of mitochondria and TFAM with the early endosome antigen 1 (EEA1), an early endosomal marker. Mitochondria and TFAM partially co-localized with components of maturing endosomal structures: HRS (hepatocyte growth factor-regulated tyrosine kinase substrate), a component of the ESCRT machinery; lyso-bisphosphatidic acid (LBPA) and ceramide-positive structures, which are markers of late endosomes and MVBs; and CD63, a highly abundant tetraspanin found in MVBs and exosomes (Supplementary Fig. 2a). To rule out potential analysis artifacts produced by the exogenous overexpression of TFAM-GFP, we measured the co-localization of endogenous mtDNA-binding protein single stranded DNA-binding protein 1 (SSBP1) with EEA1 and CD63 in HEK293 cells treated with low doses of FCCP, that promotes these events[28]. Increased co-localization of SSBP1 with CD63 indicates preferential localization in late endosomal structures (Fig. 3a). The segregation of mitochondrial components into maturing endosomal structures was confirmed in HEK293 cells transfected with constitutively active Rab7 (Q67L), which enhances endosomal trafficking, resulting in the formation of enlarged late endolysosomal structures[29]. Rab7 (Q67L) triggered the accumulation of endogenous TFAM within Rab7-positive endosomal structures, co-localizing with mitoDsRed (Fig. 3b). Also, immunogold labeling of TFAM and DNA revealed their appearance in canonical multivesicular body structures in electron microscopy studies (Supplementary Fig. 2b), overall supporting the involvement of the endosomal pathway in the secretion of mitochondrial components in EVs.

To further elucidate the nature of the vesicles containing mitochondrial components, we inhibited exosome biogenesis in T cells by targeting the neutral sphingomyelinase 2 (nSMase2, SMPD3) (Supplementary Fig. 3a). This enzyme participates in exosome biogenesis by triggering the budding of intraluminal vesicles into MVBs[30]. These conditions reduced the recovery of exosomal proteins as well as mtDNA-binding proteins and mtDNA in the purified 100,000 × *g* fraction (Fig. 3c), showing that mtDNA and mtDNA-binding proteins are released through canonical exosomal pathway and not in other EVs such as apoptotic bodies. The blocking of exosome biogenesis by silencing nSMase2 or MVB fusion with the plasma membrane by targeting Rab27a with specific shRNAs (Supplementary Fig. 3a) increased mitochondrial mass, intracellular TFAM levels, intracellular ROS, and DNA oxidative damage (Fig. 3d). The suppression of nSMase2 or Rab27a altered mitochondrial morphology and cristae organization, with increased mitochondrial cristae width (Fig. 3e). Changes in mitochondrial cristae organization relate to changes in mitochondrial electron transport chain complex organization that in turn may result in functional changes in the respiration ability of cells. Specifically, tight cristae provide more efficient mitochondrial OXPHOS[31], whereas loose cristae appear in highly glycolytic cells[32]. Consistent with a loose organization of mitochondrial cristae, Rab27a and nSMase2 silencing significantly decreased mitochondrial respiration (Fig. 3f). These findings indicate that mitochondrial function is altered in the absence of proper exosome biogenesis and secretion and suggest that the release of mitochondrial content in exosomes contributes to mitochondrial homeostasis and mtDNA metabolism.

We next investigated the contribution of mitochondrial turnover and degradation mechanisms to the secretion of mitochondrial components in EVs. Macroautophagy, from here on referred to as autophagy, is a self-degradation process that recycles cellular constituents, including misfolded or aggregated proteins and damaged organelles[33]. Confocal microscopy analysis did not reveal co-localization of autophagy proteins ATG5 and LC3 with MVBs or mitochondria (Supplementary Fig. 3b). Serum deprivation, a reported autophagy stimulus, decreased exosome secretion concomitantly with reduced extracellular release of mitochondrial components (Fig. 3g), consistent with the autophagy-promoted specific degradation of MVBs[34]. Moreover, inhibition of autophagosome cargo degradation by bafilomycin-A1-mediated blockade of autophagosome–lysosome fusion did neither alter the detection of TFAM in the exosomal fraction nor the concentration and size of the purified EVs (Fig. 3g and Supplementary Fig. 3c). This finding indicated that autophagosome secretion or content release upon bafilomycin-A1 treatment does not account for the presence of mitochondrial components in EVs. Additionally, specific siRNA silencing of the late autophagy mediator LC3 in J77 T cells did not alter exosome concentration and mitochondrial content (Fig. 3h and Supplementary Fig. 3d). Together, these findings indicate that the loading and secretion of mitochondrial material in EVs occurs independently of general macroautophagy.

DNA and mitochondrial components transfer at immune contacts. The presence of mitochondrial constituents in exosomes led us to hypothesize that mitochondrial material could be transferred from the T cell to the APC during the formation of antigen-dependent contacts. To assess this, we first evaluated whether isolated exosomes shuttle mitochondrial components

Fig. 2 T cell exosomes shuttle mtDNA and genomic DNA. **a** Representation of the number of sequence reads aligned with the mitochondrial genome in EVs (EVs) and mitochondrial extracts (mtDNA) isolated from human primary T cells. **b** Upper panel: Diagram of the mitochondrial genome, indicating the mtDNA regions analyzed by PCR (marked in red: HVRII, tRNALeu, COXII, and 16 S rRNA). Lower panel: Agarose gel showing the amplification products of the different mtDNA regions and the genomic DNA (*β2-MICROGLOBULIN*) analyzed in EVs purified from primary human T cells. **c** Agarose gel electrophoresis showing the detection of DNA in purified EVs. EVs obtained from the culture supernatant of J77 T were treated with DNase or DNase and Tx-100. Levels of mtDNA and genomic DNA were assessed by PCR amplification (*HVRII* and *β2-MICROGLOBULIN*, respectively). Isolated DNA from J77 T cells treated or not with DNase (DNA + DNase and DNA, respectively) is shown as control for DNase activity. **d** Distribution of mtDNA and TSG101 and CD63 in sucrose fractions. EVs from human Jurkat T cells were laid on a discontinuous sucrose gradient and floated by overnight centrifugation. DNA from gradient fractions was PCR-amplified for the *HVRII* mtDNA region. Proteins from gradient fractions were analyzed by immunoblot for TSG101 and CD63. A representative gel is shown ($n = 3$). **e** Exosomes from primary mouse T lymphoblasts were purified, coupled to aldehyde sulfate beads, and analyzed by flow cytometry by staining with the anti-DNA Ab under permeabilizing and non-permeabilizing conditions. Histograms show DNA staining in exosomes. Numbers are mean fluorescence intensities of the positive population from a representative experiment ($n = 3$). **f** Left: Histogram shows oxidized DNA staining in exosomes coupled to aldehyde sulfate beads with anti-8-hydroxydeoxyguanosine (8-OHdG)Ab under non-permeabilizing conditions. Right: qPCR analysis showing the enrichment of the indicated mitochondrial genes in the DNA obtained from exosomes and mitochondrial fractions from the same exosome-producing cells. DNA from both fractions was immunoprecipitated with 8-OHdG and total DNA Abs. Graph shows the ratio between oxidized DNA and total DNA in exosomes relative to their content in the mitochondrial fractions from the producing cells in duplicates from two independent experiments. *t*-test: **P*-value < 0.05, ****P*-value < 0.0001

between cells. Purified exosomes from non-transfected J77 T cells or cells stably transfected with a mitochondria-targeted fluorescent protein, mitoDsRed, were added to Raji B lymphoblastoid cells, used as APCs. After incubation with exosomes from J77mitoDsRed cells, recipient cells exhibited mitoDsRed fluorescence (Fig. 4a). We next assessed whether exosomes can mediate intercellular mtDNA transfer. Donor and acceptor cell mtDNAs were distinguished by the use of conplastic mice with the same nuclear genome (C57BL/6) but different mtDNA haplotypes, from the C57BL/6 mice strain ($C57^{C57}$) or from the NZB strain ($C57^{NZB}$)[35]. These two mtDNA haplotypes differ in 12 missense polymorphisms identifiable by restriction length fragment polymorphism (RFLP) analysis (Fig. 4b). Incubation of T cell-derived exosomes from $C57^{C57}$ mice with DCs differentiated from the $C57^{NZB}$ mice resulted in uptake of $C57^{C57}$ mtDNA by recipient $C57^{NZB}$ DCs, as shown by the acquisition of the $C57^{C57}$ haplotype and the presence of $C57^{C57}$ RFLP fragments in exosome-treated DCs (Fig. 4b), supporting the transfer of mitochondrial components and mtDNA between cells through exosomes.

The mostly unidirectional nature of exosome transfer from T cells to DCs[9,10] suggested that the exchange of mitochondrial information between immune cells occurs upon antigen-dependent contacts. TCR Vβ8$^+$ J77 T cells expressing a mitochondria-targeted fluorescent protein (mitoYFP) or a fluorescent version of TFAM (TFAM-DsRed) were co-cultured with Raji B cells preloaded with *Staphylococcus enterotoxin*

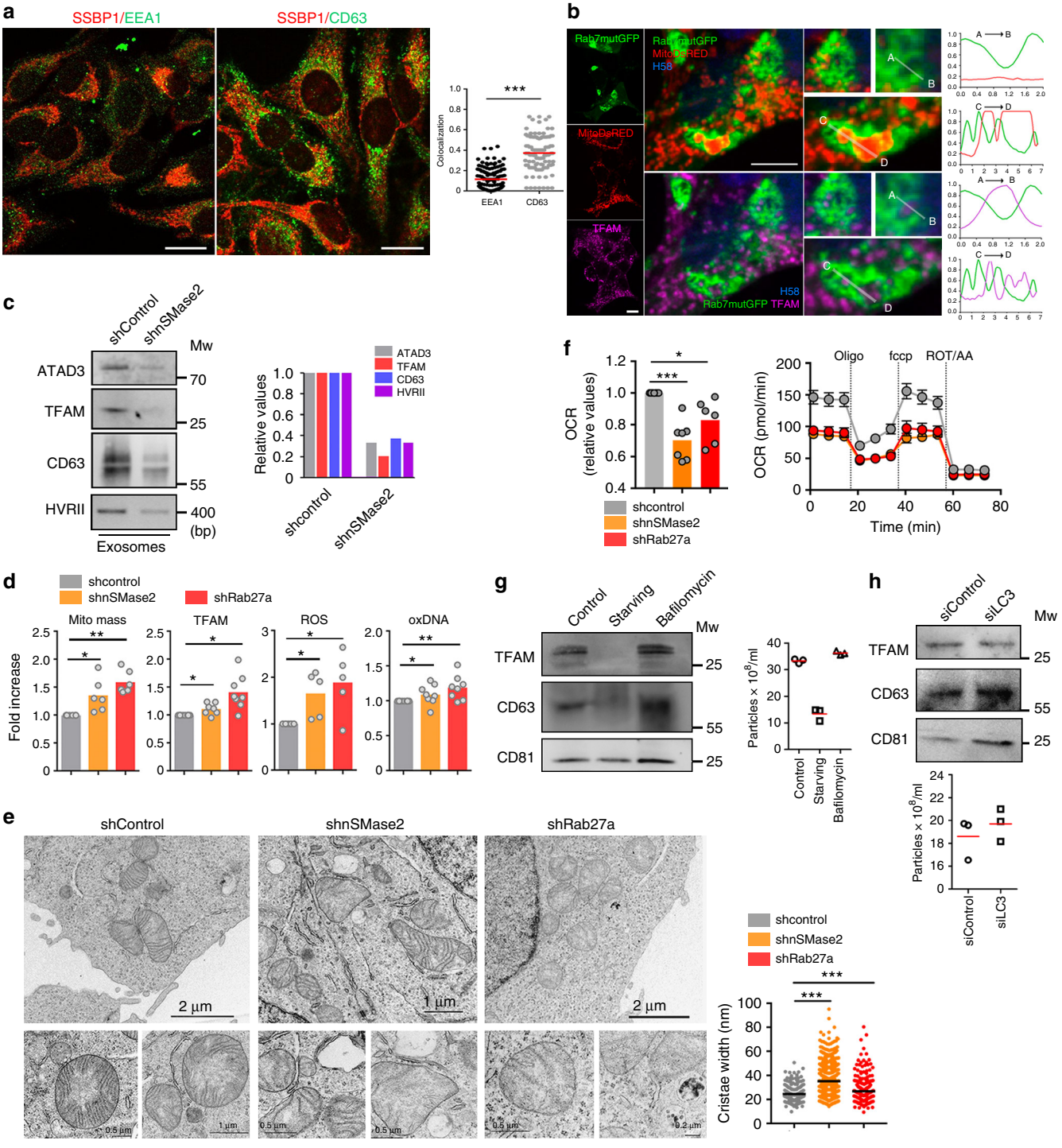

superantigen-E (SEE), which mimics antigen recognition when confronted with TCR Vβ8$^+$ T cells. Flow cytometry analysis revealed transfer of mitochondria (mitoYFP) and TFAM (TFAM-DsRED) from T cells to APCs during antigen-dependent interactions (Fig. 4c). To address this in primary cells, we set up a model of antigenic presentation in which bone marrow-derived DC (BMDC) from C57^{NZB} mice presented OVA peptide to CD4$^+$ T cells from transgenic OT-II mice (C57^{C57}), which are specific for that antigen (Fig. 4d)[35]. After 16 h co-culture in the presence or absence of OVA peptide, we detected CD4$^+$ T cell mtDNA only in recipient APCs from co-cultures including OVA peptide antigen (Fig. 4e), indicating that intercellular mtDNA transfer requires antigenic triggering. Using CD4$^+$ T cells from OT-II C57^{NZB} mice and BMDCs from the C57^{C57} mice, we confirmed that mtDNA transfer occurred unidirectionally from T cells to BMDCs (Fig. 4f).

cGAS/STING-IRF3 pathway senses DNA transfer by exosomes. Mitochondrial components are a major source of danger-associated molecular patterns (DAMPs). They can trigger innate immune responses, likely due to their similarities to bacterial ancestors[36]. We hypothesized that the transfer of mitochondrial content and mtDNA during T cell-APC antigen-dependent contacts may represent a mode of cell-to-cell transmission of danger-associated messages. To examine this possibility, we interrogated which signaling pathways were controlled by T cell exosomes in recipient DCs. This was carried out by characterizing the changes to the gene profile of DCs upon incubation with T cell exosomes by RNA deep-sequencing analysis (Fig. 5a). Gene expression profiling identified more than 1600 significantly altered genes in recipient DCs exposed to T cell exosomes (Supplementary Fig. 4a, b). Exosomes regulated the expression of a major set of genes involved in interferon (IFN) type I responses and antiviral activity, including IFN-stimulated genes (ISGs) *Ifit1, Ifit2, Ifit3, Isg15, Usp18*, and *Cxcl10*, and the antiviral signaling factors *Gbp5* and *Gbp6* (Fig. 5a). Analysis of the genes that changed their expression profile in response to T cell exosomes by Gene Ontology annotation indicated they were mainly involved in IFN signaling, exogenous DNA and RNA sensing, bacteria and viruses recognition, and crosstalk between innate and adaptive immune cells (Fig. 5b). These findings suggested that T cell exosomes prime the antiviral innate immune response in DCs, creating a gene signature that upregulates antiviral and antimicrobial responses to control pathogen infection and replication (Fig. 5c). We validated the RNA sequencing results by PCR for the genes *Cxcl10*, *Isg15*, *Ifit1*, *Ifit3*, *Usp18*, and *Stat1* (Fig. 5d). One of the most relevant pathways involved in ISG expression depends on cGAS/STING interaction upon cytoplasmic detection of endogenous or exogenous DNA[37]. cGAS functions as a main sensor of viral and bacterial DNA in the cytoplasm of infected cells. Upon its activation by DNA detection, it generates the second messenger cyclic dinucleotide cGAMP, which binds to and activates STING. STING in turn activates TANK-binding Kinase 1 (TBK1), which phosphorylates interferon regulatory factor 3 (IRF3) to promote its translocation to the nucleus, where it induces the expression of IFNβ and ISGs. Triggering of cytoplasmic DNA sensors is associated with intracellular clustering of STING[38]. Consistent with activation of the cGAS/STING DNA-sensing pathway, exosomes induced a significant aggregation of STING in DCs (Fig. 5e). The expression of ISGs in response to exosomes was reduced in STING-deficient (*Sting*$^{Gt/Gt}$) DCs (Fig. 5d), and completely abrogated in *Irf3*$^{-/-}$ DCs (Fig. 5f). The role of exosomal DNA in triggering these responses was evaluated by treating exosomes with DNase. DNase treatment significantly reduced the ability of exosomes to trigger the activation of interferon-related genes in recipient WT DCs (Fig. 5g), suggesting that the DNA located in the outer surface of exosomes is important for full induction of antiviral responses in recipient cells. To ascertain whether DNA located into the lumen of exosomes may also contribute to antiviral responses in recipient DCs, we genetically engineered a plasmid expressing DNase II fused to the intraluminal domain of the exosome-enriched protein CD63. qPCR analysis of isolated exosomes showed that exosomes from cells stably expressing CD63-DNase II contain less mitochondrial DNA than exosomes from control cells stably expressing wild-type CD63 (Supplementary Fig. 4c). Exosomes from cells expressing CD63-DNase II triggered a lower antiviral response in recipient cells compared with exosomes obtained from CD63-expressing control cells (Supplementary Fig. 4d). Overall, these results support that DNA on the surface and the inside of T cell exosomes can act transcellularly, i.e., in recipient DCs, to prime antiviral responses through activation of the STING-IRF3 DNA-sensing pathway.

Primed antiviral responses in DCs by synaptic T-exosomes. We next assessed whether antigen-driven T-APC contacts trigger antiviral responses in recipient cells through the transfer of exosomal components. Gene expression analysis revealed that

Fig. 3 Mitochondrial components segregate into MVBs and are secreted in exosomes. **a** Confocal co-localization analysis in HEK293 cells treated with FCCP (4 h) and stained with SSBP1 (red), EEA1 and CD63 (green). Bar, 10 μm. Graph shows means for Mander's co-localization coefficient for SSBP1 and EEA1 or CD63 ($n = 3$). *t*-test: ***P-value < 0.0001. **b** Confocal co-localization analysis in HEK293 cells co-transfected with Rab7-Q67L-GFP (Rab7mutGFP, green) and mitoDsRed (red), and immunostained for TFAM (purple) and nuclei (HOECHST 58, blue). Center and right images show high magnification of left images (Rab7-Q67L-GFP and mitoDsRed in upper panels; Rab7-Q67L-GFP and TFAM in lower panels). Charts: Fluorescence profiles along the corresponding white lines. Bar, 10 μm. **c** Mitochondrial components in the exosome fraction obtained from equal numbers of shControl and shnSMase2 J77 T cells. ATAD3, TFAM, and CD63 were detected by immunoblot; mtDNA was detected by PCR for *HVRII*. Graph: Quantification of exosomal proteins and mtDNA in a representative experiment ($n = 3$). **d** Flow cytometry analysis of mitochondrial mass (Mitotracker green), intracellular ROS levels (DCFDA staining), oxidized DNA (8-OHdG Ab staining), and endogenous TFAM in HEK293 cells knocked down for nSMase2 and Rab27a. Graphs: Quantification from 5–8 independent experiments (Mean). *t*-test *P-value < 0.05; **P-value < 0.001. **e** Electron microscopy images show defects in mitochondrial ultrastructure and cristae organization in shnSMase2 and shRab27a HEK293 cells. Graph: Quantification of mitochondrial cristae width (Mean). *t*-test: ***P-value < 0.0001. **f** Graph: Basal oxygen consumption rate (OCR) of control, shnSMase2 and shRab27a HEK293 cells. Dots represent mean from three independent experiments run in duplicate or triplicate. *t*-test, *P-value < 0.05, ***P-value < 0.0001. Chart: OCR from shControl, shnSMase2 and shRab27a HEK293 cells in response to oligomycin (Oligo), fccp, and rotenone plus antimycin A (Rot/AA). ($n = 2$; mean ± S.E.M.). **g** Western blot analysis of exosomes from Jurkat T cells left untreated, serum-starved overnight or treated with bafilomycin A. Membranes were blotted for TFAM, CD81, and CD63. Graph: Nanoparticle concentration in the exosomal fractions (mean, two independent experiments). **h** Western blot analysis of exosomes obtained from Jurkat T cells transfected with control or LC3 siRNA. Graph: Nanoparticle concentrations in the exosomal fractions (mean, $n = 2$). Western blots are representative out of three independent experiments

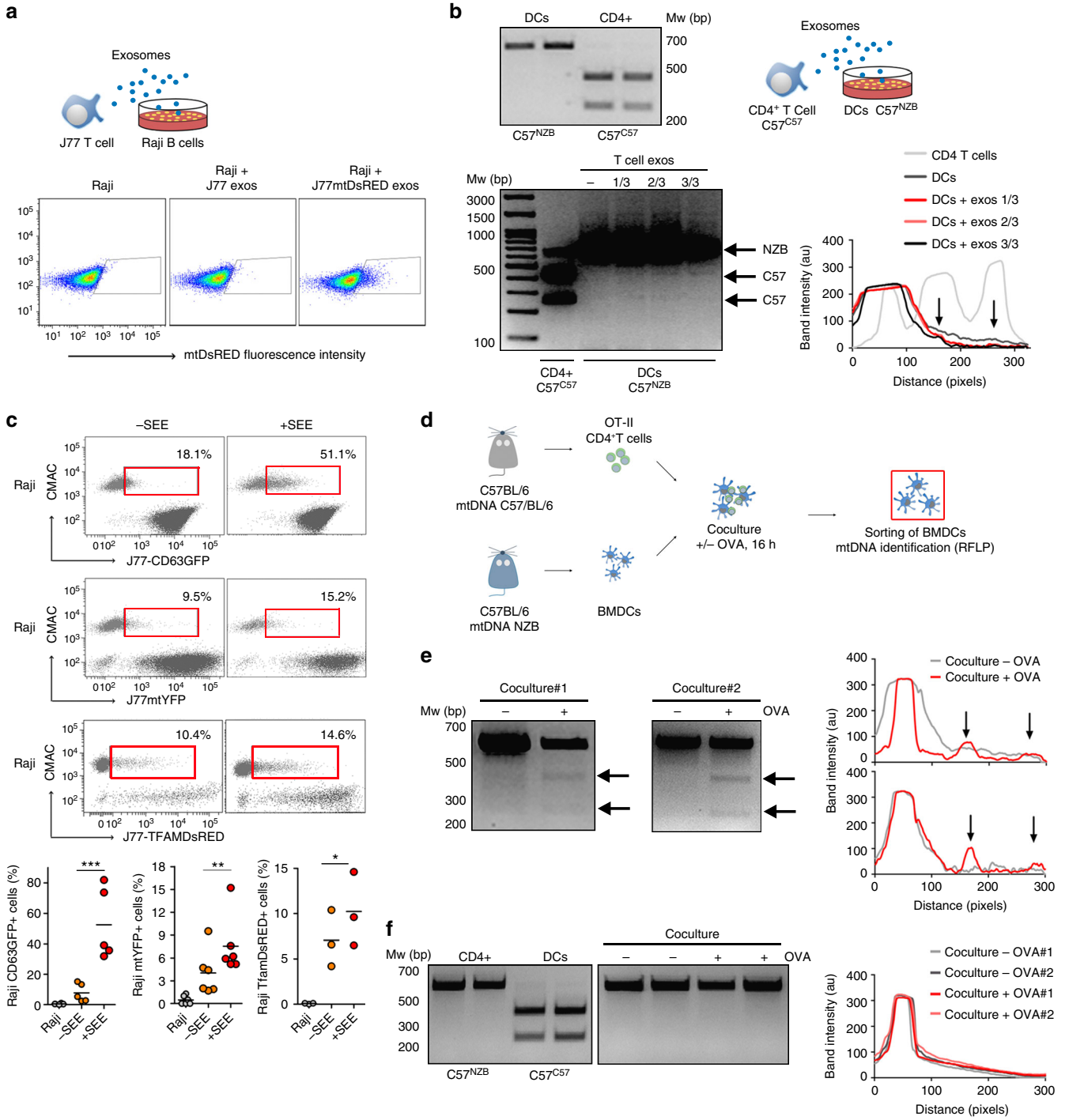

Fig. 4 Transfer of mitochondrial components during immune cognate interactions. **a** Flow cytometry analysis of Raji B cells incubated overnight with exosomes from J77 T cells control or stably expressing mitoDsRed (Representative experiment, $n = 3$). **b** Up: RFLP analysis of the mitochondrial genomes of $C57^{C57}$ and $C57^{NZB}$ mice. Total DNA is from $C57^{C57}$ T lymphocytes and $C57^{NZB}$ BMDCs. $C57^{C57}$ haplotype includes a BamHI restriction site; enzyme digestion results in two smaller fragments of 414 pb and 250 pb. Digestion of PCR products from C57 ^{NZB} haplotype results in a single band of 664 pb (full length). Down, RFLP detection of exogenous mtDNA in $C57^{NZB}$ DCs incubated overnight with increasing amounts of exosomes from $C57^{C57}$ $CD4^+$ T lymphoblasts. 414 pb and 250 pb fragments appear in $C57^{NZB}$ DCs upon addition of exosomes (lanes 1/3, 2/3, and 3/3). Chart: Intensity profile of the RFLP analysis; arrows indicate the C57 mtDNA haplotype. $C57^{C57}CD4^+$ lane displays a band of 664 pb which corresponds to an uncompleted digestion of the PCR product in the RFLP analysis and a high exposure of the image. Representative experiment ($n = 3$). **c** Exosome and mitochondrial transfer to unpulsed or SEE-pulsed Raji B cells (CMAC) from J77 T cells expressing the exosomal protein CD63GFP, the mitochondria-targeted mitoYFP or the mtDNA-binding protein TFAM-DsRED. Dot plots, Cell populations after co-culture. Red boxes enclose Raji B cells that have acquired exosomal or mitochondrial fluorescent markers (percentage from total Raji cells). Graphs: Percentage of Raji B cells acquiring fluorescence upon IS formation from 3 to 5 independent experiments; mean, *t*-test **P*-value < 0.05, ***P*-value < 0.001, ****P*-value < 0.0001. **d** Workflow for mtDNA transfer detection by RFLP during immune cognate interactions. **e** Detection of exogenous $C57^{C57}$ mtDNA from donor OT-II $CD4^+$ T cells in recipient $C57^{NZB}$ DCs upon antigen stimulation (OVA). Gels, RFLP analysis of the mitochondrial genomes ($n = 2$). Chart: Intensity profile for RFLP. **f** RFLP analysis of the mitochondrial genomes of $C57^{C57}$ and $C57^{NZB}$ mice. Left gel shows RFLP analysis from $C57^{C57}$ T lymphocytes and $C57^{NZB}$ DCs. Right gel: lack of exogenous $C57^{C57}$ mtDNA from donor DCs in recipient $C57^{NZB}$ $CD4^+$ T cells. Chart: intensity profile for RFLP analysis. Representative experiment ($n = 3$)

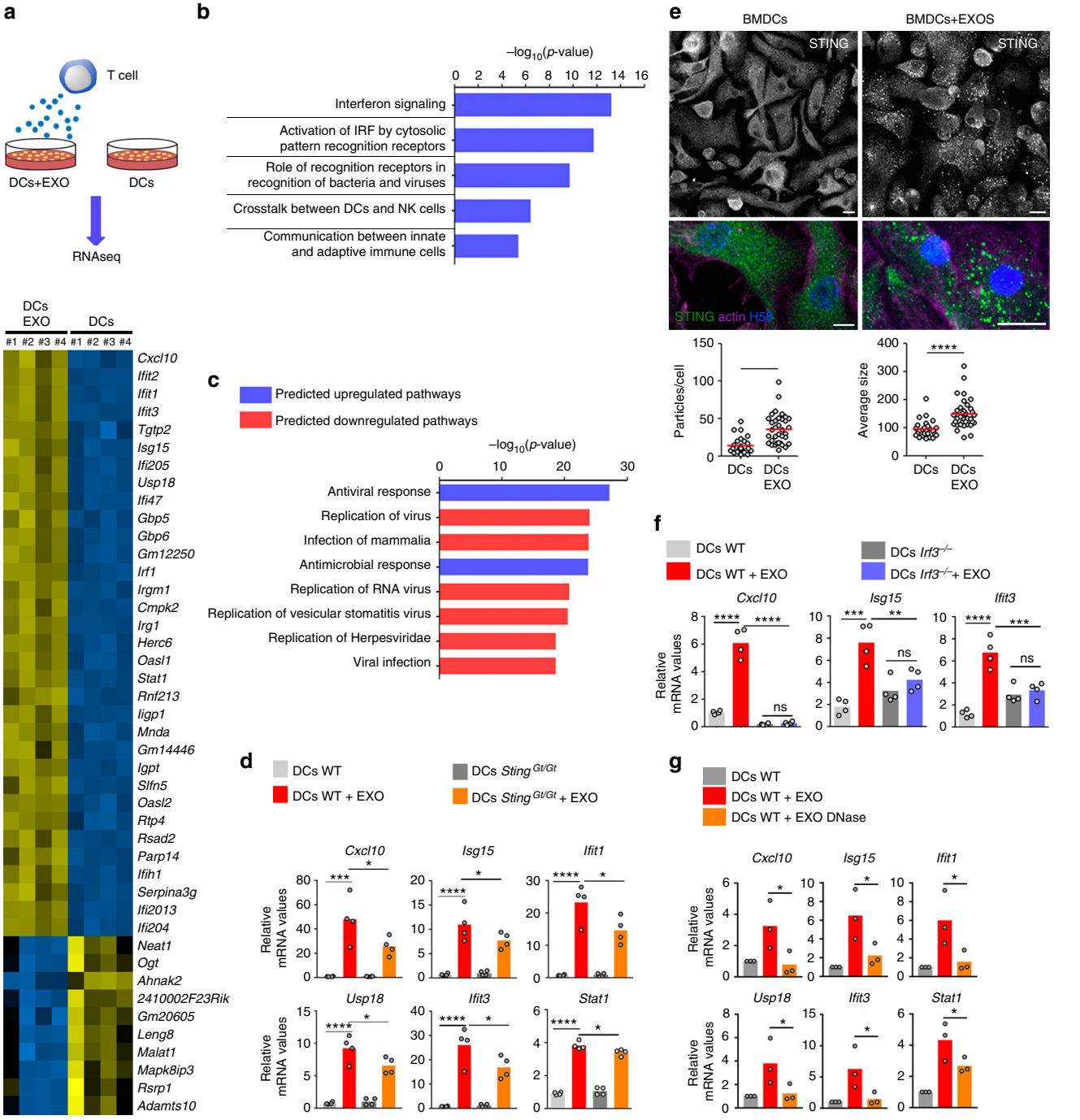

Fig. 5 Exosomes prime antiviral innate immune responses in DCs. **a** Upper panel: Workflow for RNAseq analysis of DCs upon T cell exosome acquisition. Lower panel: RNAseq heat maps of four DC biological replicates with or without exosome uptake (DCs + EXO vs DCs). The panel shows upregulated (yellow) or downregulated (blue) genes with the highest significant fold changes. **b** GO annotation of the biological processes differently regulated upon exosome addition; *p*-values are presented for the top-ranking biological processes. **c** Ingenuity analysis predictions of DC pathways upregulated or downregulated upon acquisition of T cell exosomes. **d** Quantitative real-time PCR (qRT-PCR) of antiviral response genes in wild-type DCs and *Sting*$^{Gt/Gt}$ DCs upon exosome addition. Mean, $n = 4$, *t*-test ***P-value < 0.0001 and ****P-value < 0.00001. **e** Upper panel: Immunofluorescence microscopy images showing STING aggregation (green) in DCs upon exosome addition. For clarity, DCs were stained for actin with phalloidin (purple) and for nuclei with HOECHST 58 (blue). Bar, 10 µm. Lower panel: Quantification of STING aggregate size and number upon exosome addition. Mean, $n = 26$ (control), 35 (STING), *t*-test ***P-value < 0.0001 and ****P-value < 0.00001. **f** qRT-PCR analysis of antiviral response genes in wild-type DCs and *Irf3*$^{-/-}$ DCs upon exosome addition. Data (**d**, **f**) show quantification of mRNA levels of a representative experiment with four mice per genotype: *t*-test *P-value < 0.05, **P-value < 0.001, ***P-value < 0.0001, and ****P-value < 0.00001. **g** qRT-PCR analysis of antiviral response genes in wild-type DCs upon addition of exosomes left untreated or pre-treated with DNase. Data shows mean from three independent experiments. *t*-test *P-value < 0.05

DCs upregulated ISGs upon immune cognate interactions with OT-II $CD4^+$T cells (Fig. 6a). Control or SEE-pulsed Raji B cells were co-cultured with CD63GFP-expressing J77 T cells and then sorted according to the level of GFP-labeled exosome uptake (Fig. 6b). Raji B cells with higher acquisition of T cell exosomes showed more potent antiviral responses, as measured by their increased expression of *Cxcl10* (Fig. 6b), supporting that exosome transfer during antigen-driven immune contacts primes antiviral responses in DCs.

To assess the effect of exosome-boosted antiviral responses in recipient cells, we incubated DCs with T cell exosomes, infected them with GFP-expressing recombinant vaccinia virus, and monitored virus spreading and infection. Pre-incubation of DCs with T cell exosomes reduced viral infection, as measured by the number of vaccinia-GFP-positive DCs (Fig. 6c). Antigen-dependent interactions between DCs and $CD4^+$ T cells increased protection against further vaccinia virus infection of the DCs (Fig. 6d and Supplementary Fig. 5a). This effect was dependent on T cell exosomes, since inhibition of their biogenesis by pre-treatment of T cells with increasing concentrations of manumycin A, reduced DCs protection against subsequent viral infection (Fig. 6e), without interfering significantly with T cell viability and activation (Supplementary Fig. 5b, c). Collectively, these results indicate that T cell exosomes delivered during antigen-dependent contacts boost inflammatory responses of DCs, protecting them against subsequent viral infection.

Discussion

The establishment of immune cognate interactions between T cells and APC is a key element of T cell activation, i.e., the conversion of naive T cells into effector cells, leading to the efficient clearance of pathogens through the adaptive arm of the immune response. This study demonstrates that this signal displays retrograde feedback, in which the T cell imposes additional changes to the activity of the APC, priming it to respond better in the case of subsequent infections by the same pathogen, or a similar one. We have also identified EVs as the vessels of the information that triggers these changes in DCs (the type of APC studied throughout), promoting an antiviral response with induction of IFN-related stimulated genes. A key observation is that these effects require antigenic stimulation. This is crucial because it ensures that the acquisition of inflammatory (or antiviral) traits is limited to situations in which a specific stimulus, i.e., the pathogen, is triggering these responses. It also has the potential to drastically alter the fate of the DC. DCs supposedly die in lymph nodes after cognate interactions. This is based on evidence of the onset of autoimmune disease when DC apoptosis is inhibited[39]. We postulate that, even if DC are eliminated after activating naive T cells in an antigen-specific-dependent manner, T cell exosomes could salvage the DC by reverting the onset of the apoptotic program. This is consistent with the observation that DCs receive pro-survival signals after IS formation, reducing the percentages of apoptosis in vitro and in vivo[7]. Hence, the reported disappearance of DCs from the lymph nodes after the IS[40] could be explained due to their programmed cell death but also due to their migration to other tissues, particularly if they have been fine-tuned by T cell exosomes. In fact, DCs can live for 15 days in the lymph node after an immune challenge, and are able to present antigens ex vivo to $CD4^+$ T cells[41]. There is scant evidence of this type of priming, but some indirect evidence points to the potential importance of this mechanism. For example, tissue-resident memory T cells (T_{RM}) have been shown to allow superior protection to homologous infection compared to circulating memory T cells. These T_{RM} can become instructors of innate immune system by initiating a local antiviral state after reinfection that depends on the secretion of pro-inflammatory cytokines such as TNF, IL-2, or IFN-γ that rapidly initiate an innate immune response in the infected tissues[42–44]. These experimental observations suggest the existence of cross-priming elements that are transferred by the exposure to one pathogen to improve the response against other pathogens. Hence, it is tempting to speculate a role for exosomes and DNA transfer in this enhanced antiviral protection exerted by tissue-resident memory T cells.

The mechanism proposed here would function as a mechanism of innate memory, adapting the DC response during antigenic challenge. Obviously, DCs do not bear genetic mechanisms to modulate their ability to recognize antigens similar to the recombination observed in B cells and T cells. However, increasing evidence has demonstrated that DCs and macrophages bear long-lasting modifications to their epigenetic status after infection or vaccination, leading to enhanced responsiveness upon secondary stimulation by microbial pathogens, increased production of inflammatory mediators, and enhanced capacity to eliminate infection[45]. We propose that T cell EVs are powerful DC reprogramming tools that enhance the adaptation of the innate cell against the pathogen. Although this is obviously a short-ranged mechanism, the delivery of T cell EVs to circulating fluids and their subsequent capture by distant APC could play a significant role in boosting vaccination and the induction of long-distance preparation against infection.

A most striking result is the specificity of the type of cellular response evoked by the DNA packaged into EVs: type I IFN response and expression of ISGs. Although nuclear DNA is the main endogenous ligand for cGAS, growing evidence indicates a role for mtDNA as a ligand for cGAS in certain conditions. Mitochondrial DNA as well as other mitochondrial constituents such as N-formyl peptides (NFPs), mitochondrial lipids such as cardiolipin, or nuclear-encoded mitochondrial proteins, can elicit a local or systemic innate immune response in conditions of massive episodes of cell damage[36]. Intriguingly, mtDNA can also be released in a rapid, “catapult-like” manner by neutrophils to create “extracellular traps” that exert antibacterial activity and activate the release of pro-inflammatory cytokines[46,47]. In this regard, secretion of interferogenic mtDNA by neutrophils in systemic lupus erythematosus (SLE) patients contributes to disease by activating the production of potent IFN type I responses[48,49]. Intracellularly, the accumulation of mtDNA molecules in the cytosol upon mtDNA stress has been also shown to activate type I IFNs response through the cGAS/STING pathway[50], contributing to the acquisition of an antiviral state. Our results demonstrate that in DCs, the DNA present in EVs activate type I IFN responses and expression of ISGs. The contribution of cytoplasmic sensors, e.g., STING, appears to be only partial, and other DNA receptors localized at the endosome or the plasma membrane could also detect the DNA present on the surface or the lumen of EVs and activate interferon response factors, thus contributing to the induction of a potent antiviral response. Then, understanding which sensors or receptors detect the DNA transported in EVs; and whether the mechanisms (endocytosis, phagocytosis, back-fusion of endosomes) by which vesicular content is acquired by recipient cells affect DNA responses are questions that deserve further investigation. In this study we found that the DNA-sensing responses were abrogated in an IRF3-dependent manner. Also, elimination of exosomal DNA, either by DNase treatment or overexpression of DNase II fused to the intraluminal domain of the exosome-enriched protein CD63, significantly reduced the expression of antiviral-related genes. However, we cannot rule out the contribution of other EVs constituents in triggering innate immune signaling in DCs.

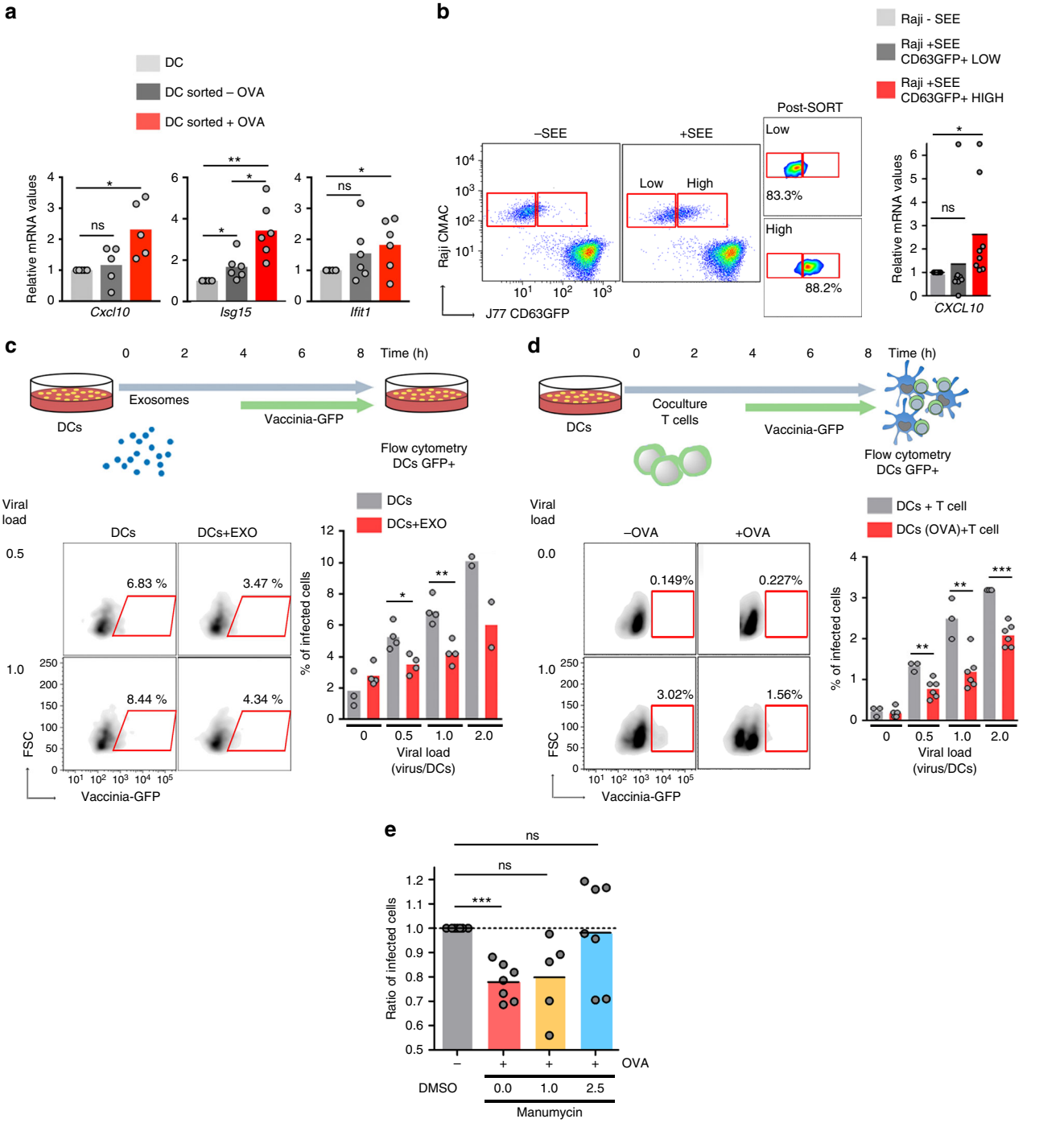

Fig. 6 Antigen-driven immune interactions prime DCs to pathogen infection. **a** qRT-PCR analysis of the DC antiviral response upon antigen-dependent contacts. Gene expression was analyzed in sorted DCs after 16 h conjugate formation. Data shows mean from five independent experiments. *t*-test **P*-value < 0.05. **b** Left: Flow cytometry analysis of exosome uptake after co-culture of J77 T cells stably expressing CD63GFP with unprimed or SEE-primed Raji B cells. After immune interactions, Raji B cells (CMAC) were sorted according to the level of exosome uptake (CD63GFP content). Dot plots show the GFP signal in pre-sort and post-sort Raji populations. Right: Chart shows qRT-PCR analysis of *Cxcl10* in low and high exosome uptake SEE-primed Raji B cell populations. Mean; $n = 3$. *t*-test **P*-value < 0.05. **c** Upper panel: Time flow for the analysis of exosome-mediated antiviral protection. DCs were incubated for 4 h with T cell exosomes, infected with vaccinia-GFP, and analyzed for the level of infection by flow cytometry. Lower left: Dot plots of DCs infected with vaccinia-GFP with or without exosome pre-treatment. Lower right: Percentage of infected DCs at different viral loads with or without exosome pre-treatment. Mean; $n = 4$; *t*-test **P*-value < 0.05, ***P*-value < 0.01. **d** Upper panel: Time flow for the analysis of exosome-mediated antiviral protection after immune cognate interactions. Unloaded or OVA peptide-loaded DCs were incubated for 4 h with CD4^{+}OT-II T cells, infected with vaccinia-GFP, and analyzed for the level of infection by flow cytometry. Lower left: Dot plots of DCs (gated on CD11c) infected with vaccinia-GFP in the presence or absence of OVA peptide. Lower right: Percentage of infected DCs at different viral loads in the presence or absence of antigen-dependent immune contacts. Mean; $n = 3$–6; *t*-test **P*-value < 0.05, ***P*-value < 0.01, ****P*-value < 0.0001. **e** Unloaded or OVA peptide-loaded DCs were incubated for 4 h with CD4^{+}OT-II T cells pre-treated with increasing amounts of manumycin, infected with vaccinia-GFP, and analyzed for the level of infection by flow cytometry. Graph shows the ratio of infected DCs. Data (**b**, **c**, **d**, **e**) are Mean from quantification of five to seven independent experiments: *t*-test **P*-value < 0.05, ***P*-value < 0.001, and ****P*-value < 0.0001

The molecular mechanism of inhibition of exosome production by manumycin A in T cells was initially related to neutral sphingomyelinase inhibition and lack of ceramide production, as reported previously[9]. Our data show that manumycin A prevents exosome production in T cells without interfering with activation at 1.0 and 2.5 μM. In addition, manumycin effect on exosome biogenesis has been recently reported to be dependent on its inhibition of Ras farnesyl transferase[51]. Therefore, the effect of manumycin on T cells maybe mediated by a combination of effects on these systems, leading to a final defect on exosome production. Manumycin has also been described to induce a certain degree of cell death mainly in tumor cells through Ras Farnesyl transferase and IKKbeta inhibition activity[51,52]. Although our data show a decrease of 13% in T cell viability at manumycin 2.5 μM, since the ratio of T cells: DCs in the activation assay is 5:1, the viable, active T cells present would constitute a 4.35:1 effective ratio, enough to promote the antiviral response in DCs. Such a modest degree of cell death would not explain the complete loss of antiviral protection by manumycin.

Our observations of mtDNA and mtDNA-binding proteins loading into EVs in an autophagy-independent manner indicate the existence of an additional targeting mechanism. The role of mitochondrial component release as a danger indicator to surrounding cells is well documented[36], but our data suggest that the MVB endosomal route can target these components actively into exosomes. Although the signals that mediate the loading and incorporation of mitochondrial components into late endosomes/MVBs remain unidentified, an attractive possibility is that small organelle fragments containing mitochondrial nucleoids might bud toward the cytosol depending on their oxidative status, and are subsequently loaded and incorporated into the endolysosomal compartment for their degradation or secretion. Cytosolic accumulation of mtDNA has been described following mitochondrial dysfunction and inflammatory stimulation[36,53], and a similar process may operate in the release of mtDNA to the cytoplasm and its subsequent incorporation into ILVs during MVB maturation. Alternatively, mitochondria-derived vesicles (MDVs) transport mitochondrial components into lysosomes, peroxisomes, and MVBs[54], and they might participate in the loading of mitochondrial components into exosomes. Our results demonstrating the presence of oxidized DNA in exosomes suggest that these EVs may cooperate to manage cellular damage by releasing mitochondrial proteins and oxidized DNA, acting as a "escape valve" to partially expel mitochondrial damage outside the cell. Recently, a role for exosomes in the secretion of harmful genomic DNA has been documented[55]. Supporting this role of exosomes in the preservation of cellular homeostasis, we found that inhibition of exosome biogenesis and secretion impairs mitochondrial structure and function. A recent study identified a role for the secretion of large vesicles containing protein aggregates and organelles in *Caenorhabditis elegans* in maintaining mitochondrial homeostasis[56]. Whereas exosomes facilitate the secretion of harmful or damaged mitochondrial components and sustain mitochondrial function is a possibility that warrants further investigation.

Transfer of entire mitochondria between cells or acquisition of mitochondria from the environment in a functional and transmissible way has been demonstrated in culture cells[57–59], and in vivo in a cancer context[60–62]. Recent reports suggested that the intercellular transmission in vivo of mitochondria and/or mitochondrial components exerts a beneficial effect on the recipient damaged cells[63–66].The benefits in all cases are attributed to the assumption that entire healthy functional mitochondria travel and colonize the recipient cells; however, the use of interspecies mix for donor cells in some cases and the lack of evidence of long-lasting colonization of the recipient cells by the foreign mtDNA question this interpretation. The role of the intercellular transmission of defined mitochondrial components and specifically mtDNA as part of a complex intercellular signaling mechanism, raises the possibility that the observed beneficial effects of transmission of mitochondrial components would be consequences of activation of survival pathways rather than the transmission of fully functional organelles able to colonize the recipient cells. This could, for instance, explain the positive effects of interspecies (human/mice) experiments, since it is well described the interspecies incompatibility between nuclear and mtDNA.

In summary, this study provides a physiological mechanism for the transfer of mitochondrial components and genome transfer in the context of immune cognate interactions, laying the foundation of a model in which the transfer of DNA between immune cells constitutes a signal-dependent mechanism for alerting responses in innate immune cells.

Methods

Antibodies and reagents. The following antibodies were used for Western blotting: mouse anti-human CD63 (Calbiochem, OP171; 1:1000); mouse 5A6 anti-human CD81 (Santa Cruz, sc-23962; 1:500); mouse anti-human TSG101 (Abcam, ab83; 1:1000); mouse anti-GFP (Clontech, 632381; 1:2000); anti-TFAM (Abcam, ab47517; 1:500), anti-HRS (Abcam, ab72053; 1:500), anti-COX1 (Human Complex IV subunit I, Invitrogen, 459600; 1:1000), anti-VDAC1 (Abcam, ab14734; 1:1000), and anti-Cyt C (Abcam, ab110325; 1:1000), anti-LC3 (Cell Signaling, 2775 s; 1:1000); anti-MnSOD (Enzo Life Sciences, ADI-SOD-110; 1:1000), anti-ATAD3 (Abnova, H00055210-D01), anti-Tubulin (Sigma, T6199: 1:2000), anti-nSMase2 (RD System, MAB7184;1:1000) and anti-Rab27a (RD System, AF7245; 1:1000). Peroxidase secondary antibodies were from Thermo Scientific: Goat anti-mouse peroxidase (31430; 1:5000) and goat anti-rabbit peroxidase (31460; 1:5000).

For immunofluorescence and flow cytometry the following antibodies were used: anti-CD63 (clone Tea 3/18, generated in the laboratory; 1 μg/ml), anti-HRS (Abcam, ab72053; 1:200), anti-EE1A (Santa Cruz, sc-137130; 1:200), anti-LBPA (Tebu-Bio; ML062915-21), anti-ceramide (Sigma, C8104-50TST: 1:200), anti-8 hydroxyguanosine (Abcam, ab62623; 1:500), anti-DNA AC-30-10 (Progen, 61014; 1:50), anti-Tmem173/Sting antibody (Proteintech, 19851-1-AP; 1:100) and anti-SSBP1 (Novus Bio, NBP1-80720: 1:200), and anti-CD69 (BD Pharmigen, 552879; 1:200)

Human cells. Human T lymphoblasts were isolated from buffy coats obtained from healthy donors by separation on a Biocoll gradient (Biochrom). After 30 min of adhesion at 37 °C, non-adherent cells were cultured in RPMI (Gibco) for 2 days in the presence of 5 μg/ml phytohemagglutinin (PHA) to induce lymphocyte proliferation. T lymphoblasts were maintained by addition of IL-2 (50 U/ml) to the medium every 2 days over 8–10 days. For T lymphoblast restimulation, cells were incubated overnight with 50 ng/ml PMA and 750 ng/ml ionomycin.

Human peripheral blood mononuclear cells (PBMC) were isolated from buffy coats obtained from healthy donors by separation on a Lymphoprep gradient (Nycomed, Oslo, Norway) according to standard procedures. Buffy coats of healthy donors were received from the Blood Transfusion Center of Comunidad de Madrid, and all donors signed their consent for the use of samples for research purposes. All the procedures using primary human cells were approved by the Ethics Committee of the Hospital Universitario de la Princesa. Monocytes were purified from PBMC by a 30 min adherence step at 37 °C in RPMI supplemented with 10% fetal calf serum. Non-adherent cells were washed off and the adhered monocytes were cultured in RPMI, 10% FCS containing IL-4 (10 ng/ml, R&D Systems Inc, Minneapolis, MN USA) and GM-CSF (200 ng/ml, Schering-Plough, Madrid, Spain). Cells were cultured for 6 days, with cytokine re-addition every other day, to obtain a population of immature hDC.

The human Jurkat-derived T cell line J77 E61 (TCR Vαl. 2 Vβ8) (from NIH AIDS reagent program) and the lymphoblastoid B cell line Raji (Burkitt lymphoma) (from ATCC, CCL-86™) were cultured in RPMI (Gibco) containing 10% FBS. Stable cell line clones overexpressing CD63-GFP were generated by transfection and selection with G418 (1 mg/ml, Sigma).

HEK293T cells (from ATCC, CRL-3216™), were cultured in DMEM (Gibco) containing 10% FBS. For co-localization experiments HEK293T cells were treated with 1 μM FCCP 4 h (low dose), then washed and immediately fixed with PFA 6%. HEK923T cells were used as a bona-fide cell factory for exogenous protein synthesis and organelle compartmentalization.

Cells were regularly tested for mycoplasma contamination by PCR.

Mice and cell differentiation and activation. Mice were housed under specific pathogen-free conditions at the Centro Nacional de Investigaciones Cardiovasculares Carlos III (CNIC), and experiments were approved by the CNIC Ethical

Committee for Animal Welfare and by the Spanish Ministry of Agriculture, Food, and the Environment. Animal care and animal procedures license were reviewed and approved by the local Ethics Committee for Basic research at the CNIC Ethical Committee for Animal Welfare and the Organo Encargado del Bienestar Animal (OEBA) del Gabinete Veterinario de la Universidad Autonoma de Madrid (UAM). C57BL/6 JOlaHsd (or C57BL/6), C57BL/6 OT-II, C57BL/6JOlaHsd with NZB mtDNA (or C57BL/6NZB) and C57BL/6NZB OT-II mice were bred under specific pathogen-free conditions at the CNIC (Madrid, Spain) in accordance with European Union recommendations. The C57BL/6JOlaHsd strain does not harbor the nicotinamide nucleotide transhydrogenase (NNT) spontaneous mutation that renders the encoded enzyme undetectable, and which is characteristic of the C57BL/6J strain provided directly by Jackson Laboratories. C57BL/6NZB OT-II mice were obtained by backcrossing C57BL/6 OT-II transgenic males with C57BL/6NZB females. *Sting*$^{Gt/Gt}$ (STING-deficient) mice were provided by Dr. Gloria González-Aseguinolaza, Gene Therapy and Regulation of Gene Expression Program, Center for Applied Medical Research, Health Research Institute of Navarra (IdisNA), Pamplona, Spain. These mice have a single nucleotide variant (T596A) which is a null mutation resulting in failure to produce STING protein[67]. *Irf3*$^{-/-}$ mice were kindly provided by Prof. Adolfo García Sastre, Icahn School of Medicine at Mount Sinai, New York, USA.

CD4^{+} T cells were obtained from spleen-cell suspensions obtained from C57BL/6 OT-II transgenic mice. Splenic cells were incubated for 30 min at 4 °C with a biotinylated anti-CD4 antibody (BD Pharmingen) followed by extensive washing with PBS, 1% BSA, 5 mM EDTA. Cell suspensions were then incubated for 20 min at 4 °C with streptavidin microbeads (MACS; Miltenyi Biotec) and washed with PBS, 1% BSA, 5 mM EDTA. CD4^{+} T cells were obtained by positive selection using the auto-MACS Pro Separator (Miltenyi Biotec).

Bone marrow-derived dendritic cells (BMDCs) were obtained either from C57BL/6, C57BL/6^{NZB}, Sting$^{Gt/Gt}$, or *Irf3*$^{-/-}$ mice by incubating primary bone marrow cells for 9–10 days in RPMI (Gibco) supplemented with 1% sodium pyruvate, 50 U/ml penicillin, 50 µg/ml streptomycin, 5×10^{-5} M 2-mercaptoethanol, and 10% FBS (all from Invitrogen) supplemented with 20 ng/ml recombinant GM-CSF (ImmunoTools).

For T cell blasting, naive CD4^{+} T cells were isolated from spleen and lymph nodes and cultured for 48 h with 2 µg/ml concanavalin A (Sigma). Cells were then incubated with 50 U/ml human recombinant IL-2 (Glaxo) every 2 days for at least 7 days to obtain differentiated T lymphoblasts. For antigen-specific restimulation, T lymphoblasts were conjugated with BMDCs and stimulated overnight in vitro with 100 ng/ml lipopolysaccharide (LPS) in the presence or absence of 10 µg/ml ovalbumin (OVA) peptide.

Cell transfection and plasmids and interference RNA. J77 cells were transfected with the corresponding plasmids by electroporation; 20×10^{6} cells were resuspended in Opti-MEM (Gibco; 5×10^{7} cells per ml) with 20 µg of plasmid DNA and electroporated with a Gene Pulser Xcell electroporator (Bio-Rad) at 1200 µFa, 240 mV, 30 ms in 4 mm Bio-Rad cuvettes (Bio-Rad). Fluorescence-positive cells were FACS sorted, cloned, and cultured in RPMI containing 2 mg/ml G418 (Invitrogen). HEK293T cells were transfected using Lipofectamine 2000 (Invitrogen) according to the manufacturer's instructions.

The following plasmids were used: mitoDsRed and mitoYFP, (kindly provided by Prof. L. Scorrano, Venetian Institute for Molecular Medicine, Italy), TFAM-GFP and TFAM-DsRED (generated by inserting the human TFAM cDNA into the pEGFP and DsRED plasmids), EGFP-Rab7A Q67L, LC3-GFP and ATG5-GFP (obtained from Addgene: plasmids 28049, 24920 and 22952, respectively), shRNA pLKO control plasmid, shnSMase2 and shRab27a shRNAs (obtained from Open Biosystems), and CD63-GFP[9].

Construct of DNase II with CD63 intraluminal domain: Following Gibson Assembly Protocol (New England Biolabs) hDNaseII (Human DNase II Gene ORF cDNA clone in cloning vector, HG16372-G, Sino Biological Inc) was inserted in CD63-GFP plasmid in the intraluminal domain. CD63-GFP plasmid was cut with EcoRI. The following primers were used to amplify insert: Fw_DNaseII-EcoRI: CGAGCTCAAGCTTCGATGATCCCGCTGCTGCT Rv_DNaseII-EcoRI: TACCGTCGACTGCAGGGATCTTATAAGCTCTGCTGG GC

T cell lines and human T lymphoblasts were transfected with a specific double-stranded siRNA targeting human LC3 (GGUGCCUGUAGGUGAUCAA) or negative control siRNA (Eurogentec), using the Gene Pulser II electroporation system (Bio-Rad Laboratories) or the Nucleofector system (Amaxa Biosystems). When indicated, at 24 h post transfection, cells were cultured in exosome-depleted medium for 20 h and exosomes were isolated from supernatants.

Lentiviral infection. J77 cells with downregulated nSMase2 and Rab27a expression were generated by infection with lentiviral vectors expressing specific shRNAs. HEK293T cells were co-transfected using the Lipofectamine 2000 system (Invitrogen) with pCMV-ΔR8.91-(Delta 8.9), pMD2.G-VSV-G, and plasmids encoding shRNAs targeting nSMase2, Rab27a, or the corresponding shRNA pLKO control plasmids (Open Biosystems). Supernatants were collected after 48–72 h, filtered (0.45 µm), and added to J77 or HEK293 cell cultures. Cells were centrifuged ($2000 \times g$, 2 h) and incubated for 4 h at 37 °C. Medium was replaced with RPMI containing puromycin (4 µg/ml).

Conjugate formation and assessment of mtDNA transfer. To assess mtDNA transfer during immune cognate interactions, differentiated C57BL/6^{NZB} receptor BMDCs were loaded with calcein (37 °C, 20 min), extensively washed, and then co-cultured in the presence of ovalbumin (OVA) peptide (10 µg/ml) with C57BL/6 CD4^{+} OT-II T cells (5:1 T cell/DC ratio; 16 h). To assess mtDNA transfer from BMDCs to CD4^{+} OT-II cells, C57BL/6 BMDCs and C57BL/6^{NZB} OT-II CD4^{+} T cells were conjugated (1:5 T cell/DC ratio; 16 h). Conjugates were blocked with Fc-block (CD16/CD32, BD Pharmingen), washed in PBS, 1% BSA, and incubated with antibodies against MHCII and CD3 (BD Pharmingen) diluted in PBS, 1% BSA. Viable cells were identified by propidium iodide exclusion. Singlet cells were discerned with a stringent multiparametric gating strategy based on FSC and SSC (pulse width and height). CD4^{+} T cells and BMDCs were distinguished by calcein staining and MHCII and CD3 fluorescence, and sorted on a FACSAria flow cytometer (BD Biosciences). DNA was extracted, and C57BL/6 and NZB mtDNAs were detected by restriction fragment length polymorphism (RFLP) analysis as follows. DNA (50 ng) was PCR-amplified using the RED Extract-N-Amp PCR Ready Mix Kit (Sigma Aldrich) with the oligonucleotides 5' AAGCTATCGGG CCCATACCCCG 3' (Fw) and 5' GTTGAGTAGAGTGAGGGATGGG 3' (Rv) at a concentration of 250 nM (Tm: 58°). After PCR amplification, samples were digested with BamH1 (10 units) for 2 h. Digested samples were loaded on a 2% agarose gel. C57^{NZB} haplotype includes a BamHI restriction site; enzyme digestion results in two smaller fragments of 414 and 250 pb. Digestion of PCR products from C57^{C57} haplotype results in a single band of 664 pb corresponding to the full length PCR product.

Conjugate formation of cell lines and mitoDsRed transfer. To distinguish Raji B cells from T cells, Raji cells were loaded with the cell tracer CMAC (7-amino-4-chloromethylcoumarin, Invitrogen). For antigen stimulation and IS formation, Raji cells were pulsed for 30 min with 0.5–1 µg/ml of *Staphylococcus enterotoxin superantigen* (SEE, Toxin Technology) and mixed with Jurkat cells expressing CD63-GFP, TFAM-dsRED, or mitoYFP at a ratio of 1:5 for 18–24 h at 37 °C. Cell conjugates were analyzed by FACS in a FACS LSRFortessa Cell Analyzer (BD Biosciences) and data were analyzed with FACSDiva software (BD Biosciences).

To assess gene expression after IS formation, stable J77 CD63-GFP cells and CMAC-stained Raji cells were conjugated as described. After 16 h, cells were sorted according to CMAC staining and CD63 green fluorescence. The Raji population was split into two groups according to CD63-GFP uptake: Raji GFP + Low (cells acquiring low amounts of CD63) and Raji GFP + High (acquiring high amounts of CD63). After sorting, total RNA was isolated and qPCR performed to analyze antiviral response genes.

Exosome purification and sucrose-gradient purification. Cells were cultured in medium supplemented with 10% exosome-depleted fetal bovine serum (FBS, Invitrogen; FBS was depleted of bovine exosomes by overnight centrifugation at $100{,}000 \times g$ for at least 16–20 h. Exosomes were obtained by serial centrifugation as described[20]. Briefly, cells were pelleted ($300 \times g$ for 10 min) and the supernatant was centrifuged at $2000 \times g$ for 20 min to remove debris and dead cells. The collected supernatant was then ultracentrifuged at $10{,}000 \times g$ for 40 min at 4 °C (Beckman Coulter Optima L-100 XP, Beckman Coulter) to remove debris, apoptotic bodies, and shedding vesicles. Exosomes were pelleted by ultracentrifugation at $100{,}000 \times g$ for 70 min at 4 °C, washed in PBS, and collected by ultracentrifugation at $100{,}000 \times g$ for 70 min. DNase treatment was performed with RQ1 RNase-Free DNase (Promega) according to the manufacturer's instructions.

Exosomes were isolated by sucrose density gradient. Briefly, exosomes were obtained by serial centrifugation of 200 ml cell culture supernatant. Isolated exosomes were layered on top of a discontinuous sucrose gradient, ranging from 2.5 M sucrose at the bottom to 0.4 M sucrose at the top, in an SW40 centrifuge tube (14×95 mm; Beckman Coulter). Tubes were centrifuged overnight (18–20 h) in a SW40 rotor at $192{,}000 \times g$ at 4 °C. One ml fractions were collected from the top of the gradient and were resuspended in an equal volume of acetone for protein precipitation and Western blot analysis or were treated as indicated for DNA isolation and PCR analysis.

Exosome adsorption to aldehyde sulfate beads and detection. Exosomes were obtained as described above, resuspended in PBS, and coupled to 4 µm aldehyde sulfate beads (Invitrogen) 15 min in rotation at room temperature. Then, coupled beads where incubated in overnight rotation in PBS containing 0.1% BSA and 0.01% sodium azide. Beads were washed twice with PBS, 0.1% BSA, 0,01% sodium azide. For surface staining, beads were washed and incubated with the indicated primary antibodies for 30–45 min on ice. For intraluminal staining, beads were fixed and permeabilized in PBS containing 1% Paraformaldehyde and 0.01% Triton X-100 for 20 min on ice, washed, and incubated with primary antibodies for 1 h on ice. Beads were then washed and incubated with the appropriate secondary antibodies for 30 min on ice. Beads were analyzed with a FACS LSRFortessa Cell Analyzer (BD Biosciences) and data were analyzed with FACSDiva software (BD Biosciences). Negative controls were obtained with permeabilized and non-permeabilized exosome-coupled beads incubated with the indicated secondary antibodies.

Nanoparticle tracking analysis. Exosome numbers and size distribution were measured from the rate of Brownian motion in a NanoSight LM10 system, which is equipped with fast video capture and particle-tracking software (NanoSight, Amesbury, UK). Briefly, 0.5 ml of diluted exosome fraction was loaded into the sample chamber of an LM10 unit (Nanosight, Amesbury, UK) and three 30-s videos were recorded of each sample. Data were analyzed with NTA 2.1 software (Nanosight). Samples were analyzed using manual shutter and gain adjustments, which resulted in shutter speeds of 15 or 30 ms, with camera gains between 280 and 560. The detection threshold was kept above 4; blur: auto; minimum expected particle size: 50 nm. Samples were diluted before analysis to concentrations between 2×10^8 and 20×10^8 particles/ml.

Deep-sequencing analysis. Total RNA was extracted with the RNeasy kit (Qiagen). Contaminating genomic DNA was removed using the specific column from the kit. RNA integrity and quantity were determined in an Agilent 2100 Bioanalyzer. Equal RNA amounts from four individual samples per group were analyzed in the Illumina Genome Analyzer IIx. Sequencing reads were pre-processed by means of a pipeline that used FastQC to assess read quality and Cutadapt to trim sequencing reads, eliminate Illumina adapter remains, and discard reads shorter than 30 bp. The resulting reads were mapped against the mouse transcriptome (GRCm38, release 76; aug2014 archive) and quantified using RSEM v1.17. Data were then processed with a pipeline that used the EdgeR Bioconductor package for normalization and differential expression analysis in a paired strategy.

The number of reads obtained per sample was in the range of 12 to 17 million. The percentage of reads eliminated in the pre-processing step was below 1%. Genes with at least 1 count per million in at least four samples (11,383 genes) were considered for further analysis. Fold change and log(ratio) values were calculated to represent gene expression differences between conditions. Sets of genes differentially expressed across conditions were analyzed for functional associations using the Ingenuity Knowledge Database (IPA, http://www.ingenuity.com).

Exosome proteomic analysis. Exosomes from mouse T lymphoblasts were isolated by serial ultracentrifugation, and protein extracts (200 µg) were digested using the FASP method as previously described[68]. After digestion, the resulting peptides were desalted onto C18 OMIX tips (Agilent Technologies). Peptides were separated into four fractions by cation exchange chromatography with MCX cartridges (Waters) using graded concentrations of ammonium formate, pH 3.0 in acetonitrile (ACN), and desalted again before analysis by liquid chromatography–tandem mass spectrometry (LC-MS/MS).

Analyses were performed using a nano-HPLC Easy nLC 1000 chromatograph coupled to a Q-Exactive hybrid quadrupole orbitrap mass spectrometer (Thermo Scientific). Peptides were loaded in an analytical C18 nano-column (EASY-Spray column PepMap RSLC C18, 75 µm internal diameter, 3 µm particle size, and 50 cm length, Thermo Scientific) and separated in a continuous gradient consisting of 8–30% B for 60 min and 30–90% B for 2 min (B = 90% ACN, 0.1% formic acid) at 200 nl/min. The chromatographic run acquired an FT-resolution spectrum of 140,000 ions in the mass range of *m/z* 390–1600 followed by data-dependent MS/MS spectra of the 15 most intense parent ions. Normalized HCD collision energy was set to 28% and the parent ion mass isolation width was 2-Da.

Peptides were identified from MS/MS spectra using the SEQUEST HT algorithm integrated in Proteome Discoverer 2.1 (Thermo Scientific). MS/MS scans were matched against a mouse protein database (UniProt 2016_07 Release) and the parameters were selected as follows: a maximum of two missed trypsin cleavages, a precursor mass tolerance of 800 ppm, and a fragment mass tolerance of 0.02 ppm. Cysteine carbamidomethylation was chosen as the fixed modification and methionine oxidation as the dynamic modification. The same MS/MS spectra collections were searched against inverted databases constructed from the same target databases. SEQUEST results were analyzed by the probability ratio method. False discovery rate (FDR) was calculated for peptides identified in the inverted database search results using the refined method[69].

Detection of oxidized DNA by chromatin immunoprecipitation. T lymphoblast exosomes were purified by differential ultracentrifugation and lysed in buffer containing 25 mM Tris-HCl, 150 mM NaCl, 2 mM MgCl, 0.5%, NP40, 5 mM DTT. Protein G-coupled magnetic beads (Protein G Dynabeads, Invitrogen) were washed and incubated for 2–3 h with 5 µg anti-8 hydroxyguanosine (8-OHdG) antibody [15A3] (Abcam), 5 µg of anti-DNA AC-30-10 (Progen), or with 5 µg of the isotype control (Santa Cruz, sc-2015). Lysates were precleared with Protein G Dynabeads and then incubated overnight at 4 °C with antibody-coupled beads. Samples were washed five times with lysis buffer and eluted with 50 mM Tris-HCl pH 8.0, 10 mM EDTA, and 1% SDS for 1 h at 65 °C. DNA was purified with the ChIP DNA Clean & Concentration kit (D5205-Zymo Research). qPCR was performed on whole samples with technical duplicates.

Mitochondrial enriched fraction was obtained from T lymphoblasts by resuspending them in mitochondrial extraction buffer (1 mM EDTA pH 8.0, 1 mM DTT, 10 mM NaCl, 3 mM MgCl2, 5 mM Tris-HCl pH 8.0) during 15 min at 4 °C (Osmotic Lysis). Then, lysates were subjected to three freeze/thaw cycles with 5 min liquid nitrogen exposition and 10 min immersion in a water bath at 37 °C. Following lysis the tubes were centrifuged at 500× *g* for 10 min at 4 °C. Supernatants were collected and spun down at 12,000 × *g* for 20 min at 4 °C. The final pellets (mitochondria enriched fraction) were resuspended in lysis buffer and treated as exosomal fractions.

Analysis of antiviral response induction by exosomes. BMDCs were cultured and differentiated in vitro. After culture for 9–11 days, BMDCs were plated in p12 plates at 3×10^5 per well. Exosomes from T lymphoblasts were isolated by differential ultracentrifugation and 10–15 µg added to BMDCs for 6 h. BMDCs were then washed and frozen for RNA extraction.

Vaccinia infection. The recombinant vaccinia virus VACV-GFP was a gift from J. Yewdell (National Institutes of Health, Bethesda, MD). For analysis of exosome-mediated viral protection, BMDCs were cultured as previously described. After 9–11 days, cells were plated in p96 plates at 1×10^5 per well. T lymphoblast exosomes were purified by differential ultracentrifugation and 5–10 µg were added to BMDCs for 4–6 h. Vaccinia-GFP was added to cells at the indicated BMDC:virus ratios. After incubation for 4 h, cells were harvested, fixed for 10 min with BD Cytofix/Cytoperm (BD Biosciences), and analyzed by flow cytometry. Viability was assessed with the LIVE/DEAD® Fixable Aqua Dead Cell Stain Kit (Molecular Probes).

For the analysis of antiviral protection during IS formation, BMDCs were cultured for 9–11 days and then plated in p24 plates at 2×10^5 per well. Receptor BMDCs were primed with 100 ng/ml LPS overnight, extensively washed, and co-cultured in the presence of ovalbumin (OVA) peptide (5 µg/ml) with C57BL/6 $CD4^+$ OT-II T cells (5:1 T cell/DC ratio). After conjugate formation for 4 h, vaccinia-GFP was added at a 1:1 ratio (total number of cells in the well) for 4 h. Cells were harvested, blocked with Fc-block (CD16/CD32, BD Pharmingen), and stained with CD4 PE-Cy7 and CD11c PE. Viability was assessed with the LIVE/DEAD® Fixable Aqua Dead Cell Stain Kit (Molecular Probes). Cells were fixed for 10 min with BD Cytofix/Cytoperm (BD Biosciences) and analyzed by flow cytometry.

Cell viability assay. In order to measure cell viability upon manumycin treatment and activation, $CD4^+$ OT-II T lymphoblasts were incubated for 24 h with increasing amounts of manumycin (0, 1, and 2.5 µM) and with anti-CD3 (10 µg/ml) and anti-CD28 (2 µg/ml). Cells were harvested and stained with anti-CD4 and DAPI to measure the percentage of DAPI negative (alive) CD4+ cells by flow cytometry.

To ascertain cell viability in the context of immune cognate interactions, CD4 + OT-II T lymphoblasts were pre-treated for 2 h with increasing amounts of manumycin (0, 1, and 2.5 µM),then CD4 T cells were conjugated with OVA-pulsed dendritic cells (5:1 T cell/DC ratio; 4 h). Cells were harvested and stained with anti-CD4 and DAPI to measure the percentage of DAPI negative (alive) CD4 + cells by flow cytometry.

Flow cytometry. For cytometry, adherent cells were harvested with 0.25% Trypsin-EDTA (Gibco), blocked with Fc-block (CD16/CD32, BD Biosciences), washed in PBS, 1% BSA, and incubated with primary antibodies diluted in PBS, 1% BSA. Viable cells were identified by HOECHST 58 exclusion. Singlet cells were discerned based on FSC and SSC (pulse width and height). For surface labeling, cells were stained with antibodies diluted in PBS, 0.5% BSA on ice.

For intracellular and surface staining, cells were fixed with 1% formaldehyde and permeabilized with 0.01% Triton X-100 (Sigma). After washing, cells were blocked with Fc-block (CD16/CD32, BD Biosciences), washed in PBS, 1% BSA, and incubated sequentially with primary and secondary antibodies (diluted 1:500) in PBS, 1% BSA. Cells were then analyzed by FACS in a FACS LSRFortessa Cell Analyzer (BD Biosciences). Data were analyzed with FACSDiva software (BD Biosciences).

To detect intracellular ROS, HEK293T cells were incubated with 2',7'–dichlorofluorescin diacetate (DCDFA, Thermofisher), and to detect mitochondrial mass cells were loaded with mitotracker green (Invitrogen). Cells were analyzed in a FACS LSRFortessa Cell Analyzer (BD Biosciences) and data were analyzed with FACSDiva software (BD Biosciences).

Western blot. Cells or exosomes were lysed in RIPA buffer (50 mM Tris-HCl pH 8.0, 150 mM NaCl, 1% Triton X-100, 0.1% sodium deoxycholate, and 0.1% SDS) supplemented with a protease inhibitor cocktail (Complete, Roche). Proteins were separated on 10–12% acrylamide/bisacrylamide gels and transferred to nitrocellulose or methanol-pre-treated PVDF membranes. Membranes were incubated with primary antibodies (1:1000) and peroxidase-conjugated secondary antibodies (1:5000), and proteins were visualized with LAS-3000.

Immunofluorescense. For immunofluorescence assays, cells were plated onto slides coated with fibronectin (50 µg/ml), incubated overnight, and fixed with 2% paraformaldehyde in PBS. Cells were permeabilized with PBS, 0.1% Triton X-100 (Sigma), washed and stained with the corresponding primary antibodies (1:100–1:200) followed by secondary antibodies (1:500) (Life Technologies). When indicated, cells were previously transfected with the indicated plasmids. Cells were

fixed and stained with the indicated antibodies at 24 h post transfection. Samples were examined with a Leica SP5 confocal microscope fitted with a ×63 objective, and images were processed and assembled using Leica software. Quantification of images was done with Fiji software (ImageJ) using Manders' coefficient M2 as a marker for co-localization of mitochondrial markers (SSBP1) with endosomal markers (EEA1 and CD63)[70]. More than one hundred cells were quantified for experiment.

TIRFm analysis of isolated exosomal particles. Isolated exosomal particles (8×10^6 particles per coverslip) generated as described and quantified with Nanosight were spun in a sucrose cushion (10% in HBSS; 10,000 × *g*, 15 min, 25 °C. HS-4 rotor, Sorvall) over 13 mm diameter precision coverslips (thickness No. 1.5 H; 0.170 mm ± 0.005 mm, 0117530 Marienfield) coated with 250 µg/ml Poly-L-Lys (P6407 Sigma Aldrich) and fixed in 1% paraformaldehyde (HBSS, 5% sucrose; RT15710 Electron Microscopy Sciences) for 5 min, R/T. Coverslips were treated with Glycine 200 mM in Tris-HCL (pH 7.4) for 10 min, R/T and blocked (3% BSA, 20 µg/ml human gamma-globulins in HBSS) for 1 h R/T. Staining with anti-CD81 (rat anti-mouse clone MT81; 5 µg/ml, 4 °C, o/n) was followed by highly cross-adsorbed Alexa-568-conjugated goat anti-rat Antibody (A-11077 Thermofisher Scientific 1:1000). Samples were then permeabilized with a 0.2% TX-100 solution (HBSS supplemented with 0.5% paraformaldehyde and 1.5% BSA), treated for autofluorescence and stained with anti-DNA (0.001 µg/ml) or anti-TSG101 (20 µg/ml, ab83 Abcam) mouse monoclonal antibodies for 3 h at 4 °C, followed by highly Cross-absorbed Alexa-488-conjugated goat anti-mouse Antibody (A-11029 Thermofisher Scientific 1:1000). Samples were mounted on Prolong Gold antifade mountant (P36930 Thermofisher Scientific). Coverslips were extensively washed with HBSS and a final wash with deionized water. Antibodies were diluted in 1.5% BSA in HBSS. Secondary antibodies were incubated for 1 h at R/T. All the solutions used for coverslip preparation and immunofluorescence were previously ultra-centrifuged at 100,000 × *g* for 70 min (4 °C) in a swinging bucket rotor (Beckman Coulter) or for 30 min at 13,200 × *g* in a fixed-angle rotor (Eppendorf). Samples were imaged under a Leica AM TIRF MC M system mounted on a Leica DMI 6000B microscope fitted with a HCX PL APO 100 × 1.46 NA oil objective and coupled to an Andor-DU8285 VP-4094 camera. Penetration depth was 90 nm and ×2 zoom was used to obtain an optical magnification of the samples. Equal experimental conditions for acquisition were used for the different coverslips. Brightness and Contrast adjustments were equal for all images. Processing of images was performed with Image J 1.51n (Wayne Rasband national Institutes of Health, USA. http://imagej.nih.gov/ij; Java 1.8.0_66; 64 bit).

Electron microscopy. Adherent HEK293 cells stably transfected with control shRNA, shRab27a, or shnMNase2 were washed in PBS and fixed for 1 h in 2.5% glutaraldehyde in 0.1 M phosphate buffer at room temperature. Cells were pelleted in 15 ml Falcon tubes. Pellets were washed with phosphate buffer and incubated with 1% OsO_4 for 90 min at 4 °C. Samples were then dehydrated, embedded in Spurr, and sectioned on a Leica ultramicrotome (Leica Microsystems). Ultrathin sections (50–70 nm) were stained with 2% uranyl acetate for 10 min and with a lead-staining solution for 5 min and observed under a JEOL JEM-1010 transmission electron microscope fitted with a Gatan Orius SC1000 (model 832) digital camera.

For immunogold staining, cells were fixed in 4% PFA 0.5% glutaraldehyde in PBS at 4 °C. Samples were dehydrated, embedded, and sectioned. Grids were rehydrated in TBS and treated with 0.01 M glycine to deactivate reactive aldehydes. Samples were blocked with goat blocking solution (Aurion) for 1 h and incubated with primary antibodies; anti-Tfam (1:50) (Cell Signalling) and anti-DNA (1:15) (Promega) overnight in blocking solution. Grids were washed in blocking solution and incubated with secondary antibodies conjugated to 12 nm colloidal gold (1:75 for TFAM and 1:25 for DNA, Jackson ImmunoResearch) for 2 h. Samples were washed in blocking solution and distilled water. Grids were air dried for 2 h, stained with lead citrate and uranyl acetated and carbon coated for viewing under transmission electron microscope.

Extracellular flux analysis. Oxygen consumption rate was measured in a XF-96 Extracellular Flux Analyzer (Seahorse Bioscience) in equal numbers of shControl, shRab27a and shnSMase2 HEK293 cells incubated with XF medium. Three measurements were obtained under basal conditions and upon addition of oligomycin (1 mM), fluoro-carbonyl cyanide phenylhydrazone (FCCP; 1.5 mM), and rotenone (100 nM) + antimycin A (1 mM).

Quantitative PCR and assessment of mitochondrial DNA by PCR. Total RNA was isolated using the RNeasy kit (Qiagen). Genomic DNA was removed using the specific column from the kit. Reverse transcription was performed using the High Capacity cDNA Reverse Transcriptase kit (Applied Biosystems). Quantitative real-time PCR was performed in a 7900 HT Fast Real-Time PCR system (Life technologies) using SYBR green qPCR Master Mix (Promega). Data were normalized to the expression of beta-actin, beta-2-microglobulin, and/or ywhaz and analyzed with Biogazelle QBasePlus (Biogazelle). Primer sequences are specified in Supplementary Table 1.

For the analysis of mitochondrial DNA contained in exosomes, DNA from T lymphoblast-derived exosomes was isolated with the Cell Lysis Solution and Protein Precipitation Solution from Qiagen. After DNA isolation, PCR was performed, primer sequences are specified in Supplementary Table 2.

Statistical analysis. All values were expressed as the mean ± S.E.M. or mean with individual values included for data distribution. For in vitro experiments, statistical differences were evaluated with Student's *t*-test and between group differences were evaluated with the Mann–Whitney *U* test for unpaired data (GraphPad Prism). Differences were considered significant when $^{*}p < 0.05$, $^{**}p < 0.01$, $^{***}p < 0.001$.

Data availability. The authors declare that the data supporting the findings of this study are available within the article and its Supplementary Information files, or are available in a persistent repository or upon reasonable requests to the authors.

Deep-sequencing analysis data supporting the findings of this study are deposited in GEO repository with the accession number: GSE110165

DNAseq data are deposited in BioSample repository: SRP148571

Raw data from RNAseq and DNAseq analysis are under a common umbrella project: Bioproject PRJNA472779:

PRJNA432987: Mouse RNAseq data in GEO

PRJNA472354: Human DNASeq data in SRA

The mass spectrometry proteomics data are deposited to the ProteomeXchange Consortium via the PRIDE partner repository with the data set identifier PXD008843.

Received: 22 June 2017 Accepted: 14 June 2018
Published online: 09 July 2018

References

1. Monks, C. R., Freiberg, B. A., Kupfer, H., Sciaky, N. & Kupfer, A. Three-dimensional segregation of supramolecular activation clusters in T cells. *Nature* **395**, 82–86 (1998).
2. Martin-Cofreces, N. B., Baixauli, F. & Sanchez-Madrid, F. Immune synapse: conductor of orchestrated organelle movement. *Trends Cell Biol.* **24**, 61–72 (2014).
3. Benvenuti, F. The dendritic cell synapse: a life dedicated to T cell activation. *Front. Immunol.* **7**, 70 (2016).
4. Boes, M. et al. T-cell engagement of dendritic cells rapidly rearranges MHC class II transport. *Nature* **418**, 983–988 (2002).
5. Borg, C. et al. NK cell activation by dendritic cells (DCs) requires the formation of a synapse leading to IL-12 polarization in DCs. *Blood* **104**, 3267–3275 (2004).
6. Semino, C., Angelini, G., Poggi, A. & Rubartelli, A. NK/iDC interaction results in IL-18 secretion by DCs at the synaptic cleft followed by NK cell activation and release of the DC maturation factor HMGB1. *Blood* **106**, 609–616 (2005).
7. Riol-Blanco, L. et al. Immunological synapse formation inhibits, via NF-kappaB and FOXO1, the apoptosis of dendritic cells. *Nat. Immunol.* **10**, 753–760 (2009).
8. Mittelbrunn, M. & Sanchez-Madrid, F. Intercellular communication: diverse structures for exchange of genetic information. *Nat. Rev. Mol. Cell Biol.* **13**, 328–335 (2012).
9. Mittelbrunn, M. et al. Unidirectional transfer of microRNA-loaded exosomes from T cells to antigen-presenting cells. *Nat. Commun.* **2**, 282 (2011).
10. Choudhuri, K. et al. Polarized release of T-cell-receptor-enriched microvesicles at the immunological synapse. *Nature* **507**, 118–123 (2014).
11. Martinez-Martin, N. et al. T cell receptor internalization from the immunological synapse is mediated by TC21 and RhoG GTPase-dependent phagocytosis. *Immunity* **35**, 208–222 (2011).
12. Qureshi, O. S. et al. Trans-endocytosis of CD80 and CD86: a molecular basis for the cell-extrinsic function of CTLA-4. *Science* **332**, 600–603 (2011).
13. Hubner, W. et al. Quantitative 3D video microscopy of HIV transfer across T cell virological synapses. *Science* **323**, 1743–1747 (2009).
14. Sowinski, S. et al. Membrane nanotubes physically connect T cells over long distances presenting a novel route for HIV-1 transmission. *Nat. Cell Biol.* **10**, 211–219 (2008).
15. Thoulouze, M. I. et al. Human immunodeficiency virus type-1 infection impairs the formation of the immunological synapse. *Immunity* **24**, 547–561 (2006).
16. Robbins, P. D. & Morelli, A. E. Regulation of immune responses by extracellular vesicles. *Nat. Rev. Immunol.* **14**, 195–208 (2014).
17. Raposo, G. & Stoorvogel, W. Extracellular vesicles: exosomes, microvesicles, and friends. *J. Cell. Biol.* **200**, 373–383 (2013).

18. Tkach, M. & Thery, C. Communication by extracellular vesicles: where we are and where we need to go. *Cell* **164**, 1226–1232 (2016).
19. Villarroya-Beltri, C., Baixauli, F., Gutierrez-Vazquez, C., Sanchez-Madrid, F. & Mittelbrunn, M. Sorting it out: regulation of exosome loading. *Semin. Cancer Biol.* **28**, 3–13 (2014).
20. Thery, C., Amigorena, S., Raposo, G. & Clayton, A. Isolation and characterization of exosomes from cell culture supernatants and biological fluids. *Curr. Protoc. Cell. Biol.* https://doi.org/10.1002/0471143030.cb0322s30 (2006).
21. Zhang, Y. et al. Inflammasome-derived exosomes activate NF-kappaB signaling in macrophages. *J. Proteome Res.* **16**, 170–178 (2016).
22. Perez-Hernandez, D. et al. The intracellular interactome of tetraspanin-enriched microdomains reveals their function as sorting machineries toward exosomes. *J. Biol. Chem.* **288**, 11649–11661 (2013).
23. Gilkerson, R. et al. The mitochondrial nucleoid: integrating mitochondrial DNA into cellular homeostasis. *Cold Spring Harb. Perspect. Biol.* **5**, a011080 (2013).
24. Nolte-'t Hoen, E. N. et al. Deep sequencing of RNA from immune cell-derived vesicles uncovers the selective incorporation of small non-coding RNA biotypes with potential regulatory functions. *Nucleic Acids Res.* **40**, 9272–9285 (2012).
25. Valadi, H. et al. Exosome-mediated transfer of mRNAs and microRNAs is a novel mechanism of genetic exchange between cells. *Nat. Cell Biol.* **9**, 654–659 (2007).
26. Kahlert, C. et al. Identification of double-stranded genomic DNA spanning all chromosomes with mutated KRAS and p53 DNA in the serum exosomes of patients with pancreatic cancer. *J. Biol. Chem.* **289**, 3869–3875 (2014).
27. Thakur, B. K. et al. Double-stranded DNA in exosomes: a novel biomarker in cancer detection. *Cell Res.* **24**, 766–769 (2014).
28. Hammerling, B. C. et al. A Rab5 endosomal pathway mediates Parkin-dependent mitochondrial clearance. *Nat. Commun.* **8**, 14050 (2017).
29. Vanlandingham, P. A. & Ceresa, B. P. Rab7 regulates late endocytic trafficking downstream of multivesicular body biogenesis and cargo sequestration. *J. Biol. Chem.* **284**, 12110–12124 (2009).
30. Trajkovic, K. et al. Ceramide triggers budding of exosome vesicles into multivesicular endosomes. *Science* **319**, 1244–1247 (2008).
31. Cogliati, S. et al. Mitochondrial cristae shape determines respiratory chain supercomplexes assembly and respiratory efficiency. *Cell* **155**, 160–171 (2013).
32. Buck, M. D. et al. Mitochondrial dynamics controls T cell fate through metabolic programming. *Cell* **166**, 63–76 (2016).
33. Mizushima, N. & Levine, B. Autophagy in mammalian development and differentiation. *Nat. Cell Biol.* **12**, 823–830 (2010).
34. Fader, C. M., Sanchez, D., Furlan, M. & Colombo, M. I. Induction of autophagy promotes fusion of multivesicular bodies with autophagic vacuoles in k562 cells. *Traffic* **9**, 230–250 (2008).
35. Latorre-Pellicer, A. et al. Mitochondrial and nuclear DNA matching shapes metabolism and healthy ageing. *Nature* **535**, 561–565 (2016).
36. West, A. P. & Shadel, G. S. Mitochondrial DNA in innate immune responses and inflammatory pathology. *Nat. Rev. Immunol.* **17**, 363–375 (2017).
37. Chen, Q., Sun, L. & Chen, Z. J. Regulation and function of the cGAS-STING pathway of cytosolic DNA sensing. *Nat. Immunol.* **17**, 1142–1149 (2016).
38. Ishikawa, H., Ma, Z. & Barber, G. N. STING regulates intracellular DNA-mediated, type I interferon-dependent innate immunity. *Nature* **461**, 788–792 (2009).
39. Chen, M. & Wang, J. Programmed cell death of dendritic cells in immune regulation. *Immunol. Rev.* **236**, 11–27 (2010).
40. Ingulli, E., Mondino, A., Khoruts, A. & Jenkins, M. K. In vivo detection of dendritic cell antigen presentation to CD4(+) T cells. *J. Exp. Med.* **185**, 2133–2141 (1997).
41. Garg, S. et al. Genetic tagging shows increased frequency and longevity of antigen-presenting, skin-derived dendritic cells in vivo. *Nat. Immunol.* **4**, 907–912 (2003).
42. Ariotti, S. et al. T cell memory. Skin-resident memory $CD8^+$ T cells trigger a state of tissue-wide pathogen alert. *Science* **346**, 101–105 (2014).
43. Iijima, N. & Iwasaki, A. T cell memory. A local macrophage chemokine network sustains protective tissue-resident memory CD4 T cells. *Science* **346**, 93–98 (2014).
44. Schenkel, J. M. et al. T cell memory. Resident memory CD8 T cells trigger protective innate and adaptive immune responses. *Science* **346**, 98–101 (2014).
45. Netea, M. G. et al. Trained immunity: a program of innate immune memory in health and disease. *Science* **352**, aaf1098 (2016).
46. Yousefi, S. et al. Catapult-like release of mitochondrial DNA by eosinophils contributes to antibacterial defense. *Nat. Med.* **14**, 949–953 (2008).
47. Branzk, N. et al. Neutrophils sense microbe size and selectively release neutrophil extracellular traps in response to large pathogens. *Nat. Immunol.* **15**, 1017–1025 (2014).
48. Caielli, S. et al. Oxidized mitochondrial nucleoids released by neutrophils drive type I interferon production in human lupus. *J. Exp. Med.* **213**, 697–713 (2016).
49. Lood, C. et al. Neutrophil extracellular traps enriched in oxidized mitochondrial DNA are interferogenic and contribute to lupus-like disease. *Nat. Med.* **22**, 146–153 (2016).
50. West, A. P. et al. Mitochondrial DNA stress primes the antiviral innate immune response. *Nature* **520**, 553–557 (2015).
51. Datta, A. et al. Manumycin A suppresses exosome biogenesis and secretion via targeted inhibition of Ras/Raf/ERK1/2 signaling and hnRNP H1 in castration-resistant prostate cancer cells. *Cancer Lett.* **408**, 73–81 (2017).
52. Bernier, M. et al. Binding of manumycin A inhibits IkappaB kinase beta activity. *J. Biol. Chem.* **281**, 2551–2561 (2006).
53. Nakahira, K. et al. Autophagy proteins regulate innate immune responses by inhibiting the release of mitochondrial DNA mediated by the NALP3 inflammasome. *Nat. Immunol.* **12**, 222–230 (2011).
54. Sugiura, A., McLelland, G. L., Fon, E. A. & McBride, H. M. A new pathway for mitochondrial quality control: mitochondrial-derived vesicles. *EMBO J.* **33**, 2142–2156 (2014).
55. Takahashi, A. et al. Exosomes maintain cellular homeostasis by excreting harmful DNA from cells. *Nat. Commun.* **8**, 15287 (2017).
56. Melentijevic, I. et al. C. elegans neurons jettison protein aggregates and mitochondria under neurotoxic stress. *Nature* **542**, 367–371 (2017).
57. Clark, M. A. & Shay, J. W. Mitochondrial transformation of mammalian cells. *Nature* **295**, 605–607 (1982).
58. Manfredi, G., Thyagarajan, D., Papadopoulou, L. C., Pallotti, F. & Schon, E. A. The fate of human sperm-derived mtDNA in somatic cells. *Am. J. Hum. Genet.* **61**, 953–960 (1997).
59. Spees, J. L., Olson, S. D., Whitney, M. J. & Prockop, D. J. Mitochondrial transfer between cells can rescue aerobic respiration. *Proc. Natl Acad. Sci. USA* **103**, 1283–1288 (2006).
60. Dong, L. F. et al. Horizontal transfer of whole mitochondria restores tumorigenic potential in mitochondrial DNA-deficient cancer cells. *eLife* **6**, e22187 (2017).
61. Rebbeck, C. A., Leroi, A. M. & Burt, A. Mitochondrial capture by a transmissible cancer. *Science* **331**, 303 (2011).
62. Tan, A. S. et al. Mitochondrial genome acquisition restores respiratory function and tumorigenic potential of cancer cells without mitochondrial DNA. *Cell. Metab.* **21**, 81–94 (2015).
63. Ahmad, T. et al. Miro1 regulates intercellular mitochondrial transport & enhances mesenchymal stem cell rescue efficacy. *EMBO J.* **33**, 994–1010 (2014).
64. Hayakawa, K. et al. Transfer of mitochondria from astrocytes to neurons after stroke. *Nature* **535**, 551–555 (2016).
65. Islam, M. N. et al. Mitochondrial transfer from bone-marrow-derived stromal cells to pulmonary alveoli protects against acute lung injury. *Nat. Med.* **18**, 759–765 (2012).
66. Torralba, D., Baixauli, F. & Sanchez-Madrid, F. Mitochondria know no boundaries: mechanisms and functions of intercellular mitochondrial transfer. *Front. Cell. Dev. Biol.* **4**, 107 (2016).
67. Sauer, J. D. et al. The N-ethyl-N-nitrosourea-induced Goldenticket mouse mutant reveals an essential function of Sting in the in vivo interferon response to *Listeria* monocytogenes and cyclic dinucleotides. *Infect. Immun.* **79**, 688–694 (2011).
68. Wisniewski, J. R., Zougman, A., Nagaraj, N. & Mann, M. Universal sample preparation method for proteome analysis. *Nat. Methods* **6**, 359–362 (2009).
69. Bonzon-Kulichenko, E., Garcia-Marques, F., Trevisan-Herraz, M. & Vazquez, J. Revisiting peptide identification by high-accuracy mass spectrometry: problems associated with the use of narrow mass precursor windows. *J. Proteome Res.* **14**, 700–710 (2015).
70. Manders, E. M., Stap, J., Brakenhoff, G. J., van Driel, R. & Aten, J. A. Dynamics of three-dimensional replication patterns during the S-phase, analysed by double labelling of DNA and confocal microscopy. *J. Cell. Sci.* **103**, 857–862 (1992).

Acknowledgements

We thank Dr. S. Bartlett for assistance with English editing and Dr A. García-Sastre for providing reagents. This study was supported by grants SAF2017/82886-R from the Spanish Ministry of Economy and Competitiveness, CAM S2017/BMD-3671 from the Comunidad de Madrid, CIBER Cardiovascular (Fondo de Investigación Sanitaria del Instituto de Salud Carlos III and co-funding by Fondo Europeo de Desarrollo Regional FEDER), ERC-2011-AdG 294340-GENTRIS and COST-Action BM1202 to F.S.-M.; grant SAF2015-65633-R from the Spanish Ministry of Economy and Competitiveness to J.A.E. M.M. is supported by MS14/00219 from Instituto de Salud Carlos III. Centro Nacional de

Investigaciones Cardiovasculares (CNIC) is supported by the Spanish Ministry of Economy and Competitiveness (MINECO) and the Pro-CNIC Foundation, and is a Severo Ochoa Center of Excellence (MINECO award SEV-2015-0505).

Author contributions

D.T., F.B., C.V.-B., I.F.-D., A.L.-P., R.A.-P., N.B.M.-C., A.L.J., S.I., I.J.-C. performed experimental work. G.G.-A. and S.I. provided materials. F.B., D.T., J.G., M.V.-M., J.A.E., M.M. and F.S.-M. designed research. F.B., D.T., M.V.-M. and F.S.-M. analyzed data and wrote the manuscript.

Additional information

Supplementary Information accompanies this paper at https://doi.org/10.1038/s41467-018-05077-9.

Competing interests: The authors declare no competing interests.

Reprints and permission information is available online at http://npg.nature.com/reprintsandpermissions/

Publisher's note: Springer Nature remains neutral with regard to jurisdictional claims in published maps and institutional affiliations.

nature COMMUNICATIONS

ARTICLE

Received 24 Nov 2015 | Accepted 18 Oct 2016 | Published 24 Nov 2016

DOI: 10.1038/ncomms13588 OPEN

ISGylation controls exosome secretion by promoting lysosomal degradation of MVB proteins

Carolina Villarroya-Beltri[1,2], Francesc Baixauli[1,2], María Mittelbrunn[1], Irene Fernández-Delgado[1,2], Daniel Torralba[1,2], Olga Moreno-Gonzalo[1,2], Sara Baldanta[3], Carlos Enrich[4], Susana Guerra[3,*] & Francisco Sánchez-Madrid[1,2,*]

Exosomes are vesicles secreted to the extracellular environment through fusion with the plasma membrane of specific endosomes called multivesicular bodies (MVB) and mediate cell-to-cell communication in many biological processes. Posttranslational modifications are involved in the sorting of specific proteins into exosomes. Here we identify ISGylation as a ubiquitin-like modification that controls exosome release. ISGylation induction decreases MVB numbers and impairs exosome secretion. Using ISG15-knockout mice and mice expressing the enzymatically inactive form of the de-ISGylase USP18, we demonstrate *in vitro* and *in vivo* that ISG15 conjugation regulates exosome secretion. ISG15 conjugation triggers MVB co-localization with lysosomes and promotes the aggregation and degradation of MVB proteins. Accordingly, inhibition of lysosomal function or autophagy restores exosome secretion. Specifically, ISGylation of the MVB protein TSG101 induces its aggregation and degradation, being sufficient to impair exosome secretion. These results identify ISGylation as a novel ubiquitin-like modifier in the control of exosome production.

[1] Centro Nacional de Investigaciones Cardiovasculares (CNIC), 28029 Madrid, Spain. [2] Immunology Service, Hospital de la Princesa, Instituto Investigación Sanitaria Princesa, Universidad Autónoma de Madrid, 28006 Madrid, Spain. [3] Department of Preventive Medicine, Public Health and Microbiology, Universidad Autónoma de Madrid, 28029 Madrid, Spain. [4] Departament de Biomedicina, Unitat de Biologia Cel·lular, Centre de Recerca Biomèdica CELLEX, Institut d'Investigacions Biomèdiques August Pi i Sunyer (IDIBAPS), Facultat de Medicina, Universitat de Barcelona, 08036 Barcelona, Spain. * These authors contributed equally to this work. Correspondence and requests for materials should be addressed to F.S.-M. (email: fsmadrid@salud.madrid.org).

Exosomes are vesicles secreted to the extracellular environment by most cell types. They are key mediators of cell-to-cell communication in many different contexts, including the immune response[1,2] and tumour progression[3,4]. Exosomes originate in endosomal compartments called multivesicular bodies (MVBs), which are late endosomes containing multiple intraluminal vesicles (ILVs) formed by the invagination of the endosomal membrane. When MVBs fuse with the plasma membrane, ILVs are released as exosomes[5]. Alternatively, MVBs can fuse with the lysosomal compartment, resulting in degradation of their content.

Exosome composition is not a mere copy of cytosolic content; rather, specific proteins and nucleic acids are selectively sorted into exosomes. The amount and content of exosomes can moreover change in response to different stimuli[6,7]. Such changes in exosome composition determine the final outcome of exosome-mediated communication[8,9].

The mechanisms that control exosome composition and content are still not well understood[10]. Posttranslational modifications such as ubiquitination may play an important role in the sorting of proteins into exosomes[11–13]. The endosomal sorting complex required for transport (ESCRT) recognizes ubiquitinated proteins and sorts them into ILVs[14]. The ESCRT complex is essential for the sorting of proteins such as epidermal growth factor receptor into MVBs that are degraded through fusion with lysosomes[15], but is also involved in the regulation of exosome composition and secretion[16,17]. Another ubiquitin-like protein (UBL) that can modify exosomal proteins is SUMO, whose conjugation to hnRNPA2B1 is essential for the sorting of microRNAs into exosomes[18], and enhances the secretion of α-synuclein into extracellular vesicles (EVs) in an ESCRT-dependent manner[19].

ISG15 is an interferon (IFN)-α/β-induced UBL[20], which exerts its functions in two distinct states: as a free molecule (intracellular and extracellular)[21] or conjugated to target proteins (ISGylation)[22,23]. Analogous to ubiquitin, ISG15 conjugation is mediated by the consecutive action of an E1-activating enzyme (Ube1L), an E2-conjugating enzyme (UbCH8) and E3 ligases (mHERC6/hHERC5)[24–26], and counteracted by the specific isopeptidase USP18 (ref. 27). ISGylation was shown to occur in a co-translational process favouring modification of viral proteins in infected cells, which, in turn, interferes with virus assembly or function[28–30]. Furthermore, cellular proteins involved in antiviral defense or export of viral particles have been shown to be ISGylated, supporting the antiviral function of ISG15 (ref. 28). Studies in mice have demonstrated a role for ISG15 in antiviral immunity. Hence, mice lacking ISG15 exhibit a higher susceptibility to several pathogens including virus[31] and bacteria[32], and this is reverted in USP18-mutant mice, in which high levels of ISG15 conjugation are observed[33]. However, human ISG15 seems to have critical immune functions but not in antiviral immunity; unlike mice, ISG15 deficiency increased viral resistance in humans[34]. Specifically, free extracellular human ISG15 is important in IFN-γ-dependent anti-mycobacterial immunity[21], whereas free intracellular ISG15 is involved in USP18-mediated downregulation of IFN-α/β signalling[35].

ISG15 expression blocks the process of virus-budding by different mechanisms such as the blockage of ESCRT machinery in HIV-infected cells[36], or in the case of Ebola and other enveloped virus infections, inhibiting the Nedd4 E3 ubiquitin ligase[37]. Interestingly, exosomes and viruses share many features, and some viruses have been shown to exploit exosome and microvesicle secretion pathways[38,39]. In addition, exosomes are enriched in ISGylation targets, such as TSG101 (ref. 40) and heat-shock proteins[41].

Here we show that IFN-I inhibits exosome secretion by inducing protein ISGylation. We demonstrate that the ISGylation of the MVB protein TSG101 induces its aggregation and degradation, and this is sufficient for impairing exosome secretion. Moreover, the ISGylation-induced defect in exosome secretion is rescued on inhibition of lysosomal function or autophagy.

Results

ISGylation inhibits exosome secretion. To analyse the role of ISGylation on exosome production, we first treated Jurkat T cells with IFN-I, to induce ISG15 expression and conjugation (Supplementary Fig. 1A), and purified the secreted EVs from their culture supernatants by a serial ultracentrifugation protocol. IFN-I treatment inhibited the secretion of the classical exosome markers CD63, TSG101 and CD81 in the purified EVs (Fig. 1a). A concomitant decrease in the exosomal markers on IFN-I treatment was also observed after an additional purification step by ultracentrifugation in a sucrose gradient (Supplementary Fig. 1B). Interestingly, the few EVs secreted by IFN-treated cells were recovered in different fractions than the EVs from non-treated cells, suggesting that they might be of different nature. To further investigate the function of ISGylation in controlling EVs secretion, we next overexpressed ISG15 and the machinery responsible for ISGylation (E1, E2 and E3) in HEK293 cells, which mimics the activation of the ISG15 pathway (Supplementary Fig. 1A)[24,28] without activating other pathways induced by IFN-I treatment. ISGylation induction inhibited the secretion of EVs containing CD63, TSG101 and CD81 (Fig. 1b). To dissect whether the inhibition in exosomal markers secretion was due to ISG15 overexpression itself or to increased ISG15 conjugation to proteins, we overexpressed the ISGylation machinery together with an ISG15 mutated at the carboxy-terminal (ISG15MUT), thus disabling protein conjugation. Cells overexpressing ISG15MUT showed higher levels of exosomal markers in comparison with ISG15WT (Fig. 1c), demonstrating that ISG15 conjugation to proteins, but not free ISG15, is required for the inhibition of exosomal markers secretion. Nanoparticle tracking analysis (NTA) showed a decrease in the number of particles secreted on ISG15WT overexpression in comparison with ISG15MUT-expressing cells (Supplementary Fig. 1C), indicating that ISGylation is not causing a mere decrease in the sorting of exosomal markers in EVs, but an actual decrease in exosome secretion. However, NTA did not reveal any significant decrease in the secretion of nanoparticles on IFN-I treatment (Supplementary Fig. 1D).

To study the role of ISG15 in exosome secretion in a more physiological context, we analysed the secretion of exosomes by primary cells from wild-type (*WT*), ISG15 knockout (*ISG15KO*)[42] and *USP18C61A* mice, which have the ISG15 de-conjugating enzyme USP18 enzymatically inactive and thus show higher levels of protein ISGylation[33]. Consistent with the inhibition of exosome secretion induced by ISGylation, IFN-I treatment decreased exosome secretion in primary bone marrow-derived macrophages (BMDMs) from *WT* mice but not in ISG15-deficient macrophages (Fig. 1d). Furthermore, BMDMs from *USP18C61A* mice secrete less exosomes than either *WT* or *ISG15KO* mice on ISGylation induction by IFN-I, supporting the role of ISG15 protein conjugation in the regulation of exosome secretion. Similar results were also obtained with primary T lymphoblasts (Supplementary Fig. 1E). To assess the role of ISGylation *in vivo,* poly (I:C) was injected intraperitoneally into *WT*, *ISG15KO* and *USP18C61A* mice, to induce ISG15 expression[43], and exosomes from blood serum analysed. Interestingly, there were less exosomes in serum from poly (I:C)-injected *WT* than *ISG15KO* mice, and even less exosomes in

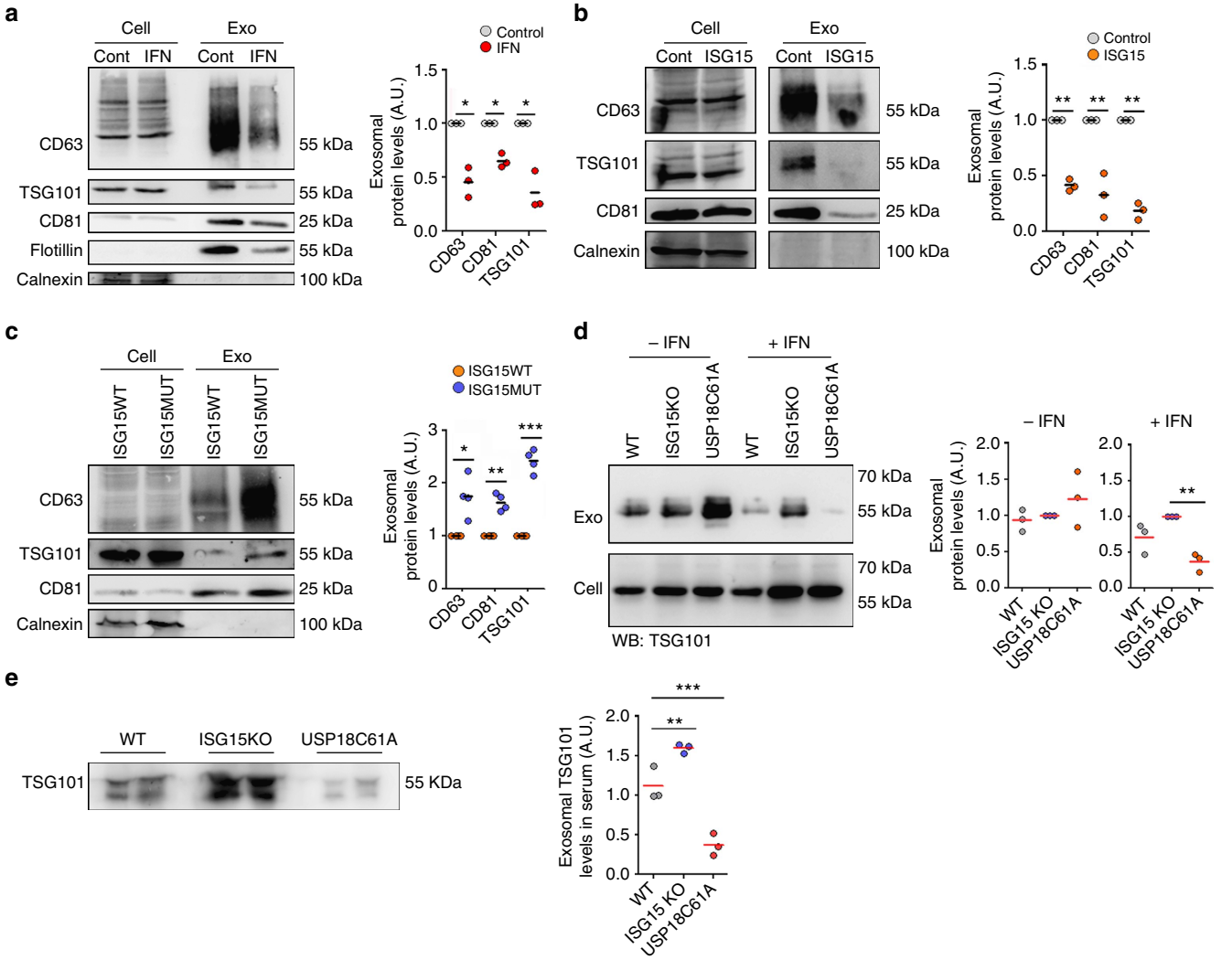

Figure 1 | ISGylation inhibits exosome secretion. (**a**) Western blot analysis of EVs purified by serial ultracentrifugation from cell culture supernatants from equal numbers of Jurkat T cells untreated (Cont) or treated with 1,000 U ml^{-1} IFN-I for 16 h. Cells and EVs (Exo) were blotted for the exosomal markers CD63, TSG101, Flotillin and CD81, and for the endoplasmic reticulum marker Calnexin. Right graph: quantification of exosomal protein levels in the EVs obtained from IFN-I-treated and untreated cells in three independent experiments. (**b**) Western blot analysis of the EVs obtained from equal numbers of untransfected HEK293 cells (Cont) or co-transfected with ISG15 and the ISGylation machinery; E1, E2, E3 ligases (ISG15). Cells and EVs (Exo) were blotted for CD63, TSG101, CD81 and Calnexin. Right graph: quantification of exosomal protein levels in the EVs obtained from untransfected HEK293 cells or co-transfected with ISG15 and the ISGylation machinery in three independent experiments. (**c**) Western blot analysis of the EVs obtained from equal numbers of HEK293 cells co-transfected with plasmids encoding the ISGylation machinery and the functional (ISG15WT) or mutated ISG15 (ISG15MUT). Cells and EVs (Exo) were blotted for CD63, CD81 and Calnexin. Right graph: quantification of exosomal protein levels in four independent experiments. (**d**) Western blot analysis of the EVs obtained from equal numbers of *WT*, *ISG15KO* and *USP18C61A* BMDMs treated 16 h with IFN-I or left untreated. Cells and EVs were blotted for TSG101 and quantification of exosomal protein levels of IFN-I-treated and -untreated cells is shown for three independent experiments. (**e**) Western blot analysis of the EVs obtained in blood serum from poly(I:C)-injected *WT*, *ISG15KO* and *USP18C61A* mice. EVs were isolated from 250 µl of serum and blotted for TSG101. Right graphs: quantification of exosomal TSG101 protein levels of three mice per genotype; *t*-test **P*-value < 0.05, ***P*-value < 0.001 and ****P*-value < 0.0001.

serum from injected *USP18C61A* mice (Fig. 1e), demonstrating the role of ISGylation in the inhibition of exosome secretion *in vivo*. Overall, our gain- and loss-of-function experiments strongly support the role of ISGylation in the regulation of exosome secretion *in vitro* and *in vivo*.

ISGylation decreases MVB numbers. To investigate the mechanisms by which ISGylation controls exosome secretion, MVBs were studied. Hepatocyte growth factor-regulated tyrosine kinase substrate (HRS) is involved in MVB formation and exosome secretion[17,44], and it has been previously used as a marker of MVBs, being present in intermediates between early and late MVBs positive for TSG101 and LBPA[44,45]. ISGylation induction resulted in a more perinuclear and clustered localization of HRS, as shown by the increase in the size of HRS$^+$ structures (Fig. 2a), and decreased the number of HRS$^+$ spots per cell (Supplementary Fig. 2A). Similar results were obtained with the MVB marker CD63 (Fig. 2a and Supplementary Fig. 2A), whereas the early endosome (EE) marker EEA1 did not show any apparent alteration (Supplementary Fig. 2B). Electron microscopy analyses revealed significant reduced MVBs numbers and density on ISGylation induction (Fig. 2b). In accordance, IFN-I treatment reduced HRS$^+$ spots in WT macrophages but not in *ISG15KO*

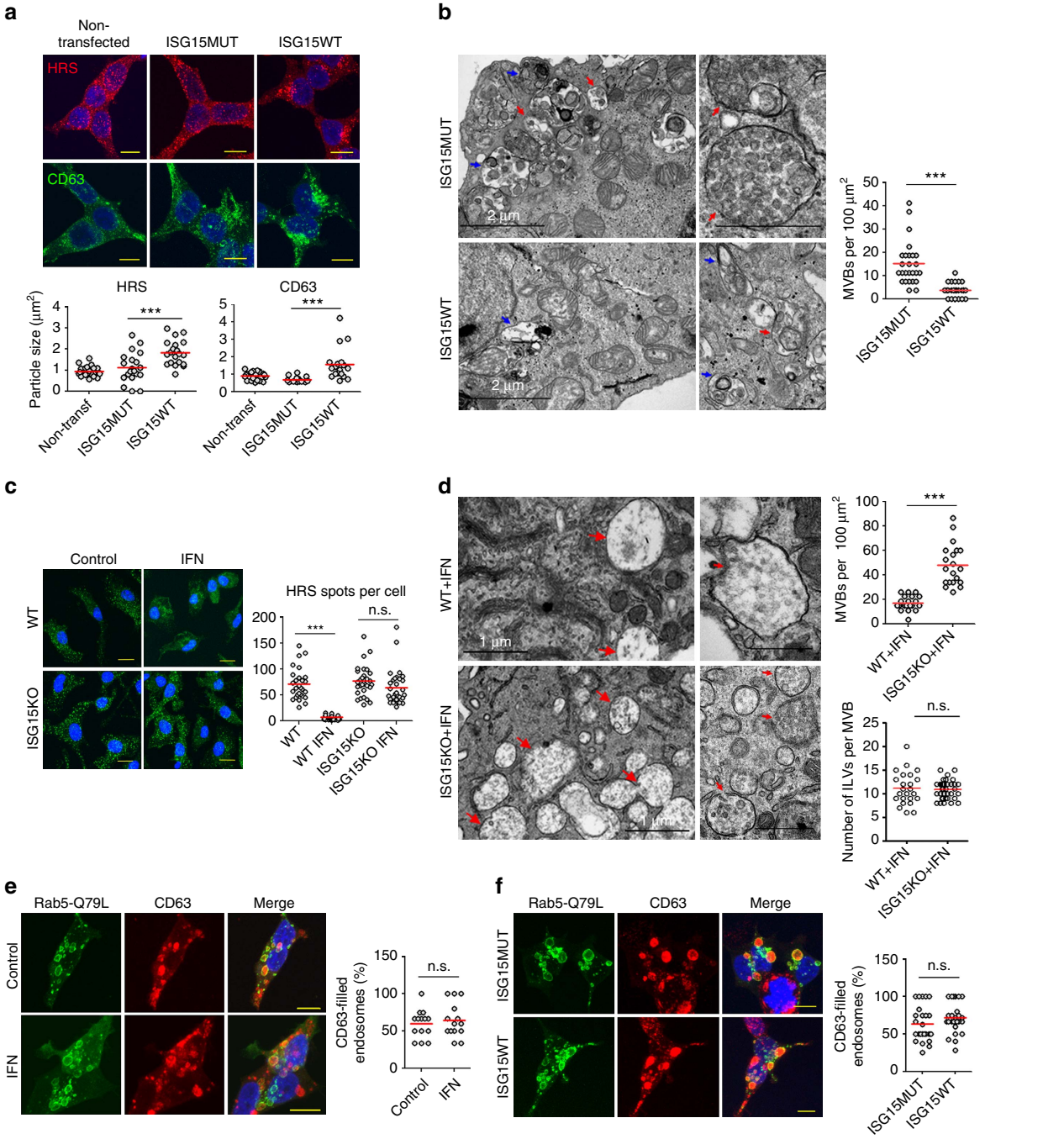

Figure 2 | ISGylation decreases MVB numbers. (**a**) Confocal microscopy analysis of the endosome markers HRS (red) and CD63 (green) in non-transfected HEK293 cells or HEK293 cells co-transfected with plasmids encoding the ISGylation machinery and the functional (ISG15WT) or mutated ISG15 (ISG15MUT). Scale bar, 10 μm. Right graph: quantification of HRS^+ and $CD63^+$ average particle size per cell ($n=20$). Each dot represents the average particle size from individual cells and mean is indicated in red lines. (**b**) Electron microscopy images showing representative fields with MVBs (red arrows) and lysosomes/autophagosomes (blue arrows) in HEK293 transfected as in **a**. Right graph: quantification of MVB numbers in more than 25 fields per condition. Each dot represents the number of MVBs per section and mean is indicated in red lines. Scale bar (insets), 500 nm. (**c**) Confocal microscopy analysis of HRS in *WT* or *ISG15KO* BMDMs left untreated or treated with 1,000 U ml^{-1} IFN for 16 h. Scale bar, 10 μm. Right graph: quantification of the number of HRS^+ particles per cell. Each dot represents the number of HRS^+ particles from individual cells and mean is indicated in red lines ($n=28$). (**d**) Electron microscopy images showing MVBs (red arrows) in *WT* or *ISG15KO* BMDMs treated with 1,000 U ml^{-1} IFN for 16 h. Upper graph, quantification of MVB numbers in 20 fields per condition. Each dot represents the number of MVBs per section and mean is indicated in red lines. Lower graph, quantification of ILV numbers per MVB. Each dot represents the number of ILVs per MVB and mean is indicated in red lines ($n\geq 24$). Scale bar (insets), 500 nm. (**e**) Confocal microscopy analysis of CD63 (red) in Rab5-Q79L-GFP^+ endosomes (green). HEK293 cells were transfected with Rab5-Q79L-GFP and treated 16 h with 1,000 U ml^{-1} IFN or left untreated. (**f**) Confocal microscopy analysis of CD63 (red) in Rab5-Q79L-GFP^+ endosomes (green). HEK293 cells were co-transfected with Rab5-Q79L-GFP mutant, the ISGylation machinery and ISG15WT or ISG15MUT. Images from **e**,**f**: Scale bar, 10 μm. Right graphs: each dot represents the percentage of CD63-filled endosomes per individual cell and mean is indicated in red lines; *t*-test; NS: *P*-value > 0.05 and ***P*-value < 0.0001.

macrophages (Fig. 2c), and MVBs were more abundant in *ISG15KO* macrophages than in their WT counterparts on IFN-I treatment (Fig. 2d), overall suggesting a role for ISG15 in regulating MVB numbers.

To ascertain whether ISGylation decreases MVB numbers by affecting MVB formation, we transfected HEK293 cells with the constitutively active Rab5-Q79L-GFP mutant, which forms large endosomes with a mixed morphology between EE and MVBs, which facilitates the study of the first steps in MVB biogenesis[46,47]. ISGylation induction by either IFN-I or ISG15 overexpression did not affect the sorting of the exosomal protein CD63 into Rab5-Q79L-GFP endosomes (Fig. 2e,f). Furthermore, quantitative electron microscopy analyses did not show any significant differences in the number of ILVs per MVB on ISGylation induction (Supplementary Fig. 2C,D). To rule out any possible side effect derived from the uneven distribution of small ILVs within enlarged MVBs[48], ILV numbers were also quantified in the absence of Rab5-Q79L-GFP overexpression. Accordingly, macrophages from *WT* and *ISG15KO* mice also showed similar levels of ILVs per MVB on ISGylation induction by IFN (Fig. 2d). Altogether, these data support that ISGylation does not impair the formation of ILVs, suggesting that it is mainly affecting later stages on the MVB pathway.

ISGylation induces protein aggregation and degradation. We then sought to understand how ISGylation regulates MVB numbers and exosome secretion. For this, we used ISG15 fusion proteins as models of protein ISGylation, as previously described for other posttranslational modifications such as ubiquitin or other UBLs[49–51]. Although fusion proteins are not exactly the same than endogenous ISGylation in lysines, in our ISG15 fusion proteins the C-terminal glycine of ISG15 is fused to the NH_2 group of the target protein in the N-terminal amino acid through a peptidic bond, which is chemically analogue to the isopeptidic bond formed between the endogenous ISG15 and the NH_2 group of a target protein lysine.

Confocal analysis showed partial co-localization of ISG15-GFP fusion protein with the MVB marker HRS and with the aggresome marker p62 (ref. 52 and Fig. 3a,b), whereas no co-localization was detected with the EE marker EEA1 (Supplementary Fig. 3A). Notably, ISGylation increased the co-localization of HRS with the lysosome marker LAMP1 (Fig. 3c), although neither LAMP1 content nor localization were affected (Supplementary Fig. 3B).

Despite its co-localization with MVB markers, green fluorescent protein (GFP) was not found in exosomes when fused to ISG15 (Fig. 3d) but rather promoted its accumulation in detergent-insoluble cell fractions (Fig. 3e), indicating that ISGylation promotes protein aggregation. Western blot analysis of cycloheximide-treated cells showed that when fused to ISG15, GFP is degraded faster than GFP alone or when fused to the ubiquitin-like modifier SUMO2, and that this degradation is delayed by the lysosome inhibitor Bafilomycin A1 but not by the proteasome inhibitor MG132 (Fig. 3f and Supplementary Fig. 3C–E), thus indicating that ISGylation of proteins promotes their degradation through the lysosome.

Inhibition of MVB–lysosome fusion rescues exosome secretion. To assess whether ISGylation inhibits exosome secretion by inducing MVB lysosomal degradation, we studied whether inhibition of MVB fusion with lysosomes could recover exosome secretion. Bafilomycin A1 is a proton pump inhibitor that increases the pH of lysosomes and inhibits trafficking between MVB and lysosomes[53,54]. Bafilomycin A1 treatment recovered exosome secretion in HEK293 cells in which ISGylation was induced by ISG15 overexpression (Fig. 4a), whereas it did not increase exosome secretion in control cells (Supplementary Fig. 4A), suggesting that ISGylation inhibits exosome secretion by re-routing MVB to lysosomes but is not impairing MVB biogenesis. This is also supported by the detection of ISGylated proteins in exosomes on secretion recovery (Supplementary Fig. 4B). Exosome secretion was also recovered despite ISGylation induction by IFN-I in Jurkat T cells when treated with Bafilomycin A1 (Supplementary Fig. 4C).

To avoid unspecific effects derived from the use of the inhibitor, we also studied exosome recovery on Rab7T22N dominant-negative mutant expression, which inhibits both endosome–lysosome and autophagosome–lysosome fusion[55–58]. Rab7T22N expression rescued exosome secretion in HEK293 cells despite ISGylation induction by ISG15 overexpression (Fig. 4b), whereas it did not increase exosome secretion in control cells (Supplementary Fig. 4D), supporting that the ISGylation-induced inhibition of exosome secretion is mediated by MVB fusion and degradation by the lysosome.

Fusion of MVBs with autophagosomes on induction of autophagy by rapamycin has been reported[56]. Interestingly, the secretion of exosomes on ISGylation induction was also recovered on silencing of the autophagy mediator ATG5 (Fig. 4c), indicating that autophagy probably contributes to the decreased exosome release induced by ISGylation. Accordingly, IFN-I treatment promoted the localization of the autophagy mediator LC3 in more acidic compartments, presumably lysosomes, supported by the loss of GFP fluorescent signal in mRFP-GFP-LC3 tandem reporter (Fig. 4d). Notably, ISGylation induction by IFN-I treatment or ISG15 overexpression did not induce general autophagy, as evidenced by unaltered levels of p62 and other autophagy markers (Supplementary Fig. 4E,F), indicating that ISGylation promotes selective autophagy and degradation of MVB without inducing a global autophagy response.

ISG15 impairs exosome secretion by modifying TSG101. To elucidate the molecular mechanism by which ISGylation regulates exosome secretion, we focused on TSG101, a component of the ESCRT machinery involved in exosome biogenesis that has been shown to be ISGylated and to regulate the secretion of virus[40]. To confirm TSG101 ISGylation, we overexpressed the ISGylation machinery together with *WT* or mutated ISG15 fused to the V5 tag and performed V5 immunoprecipitation. Western blot analysis of TSG101 in V5-ISG15 but not in control or V5-ISG15MUT immunoprecipitates confirmed endogenous TSG101 ISGylation (Fig. 5a). Moreover, ISGylation induction by ISG15 overexpression induced endogenous TSG101 aggregation and accumulation in insoluble fractions (Fig. 5b). To address whether ISGylation of TSG101 is sufficient to inhibit exosome secretion, we generated a TSG101-GFP plasmid that mimics TSG101 ISGylation (referred as ISG15-TSG101-GG), in which ISG15 terminal glycine is conjugated to TSG101 N-terminal through a peptide bound that can be cleaved by the USP18 de-ISGylase (Supplementary Fig. 5A). Consequently, both ISGylated and de-ISGylated TSG101-GFP are detected in cells transfected with this plasmid (Fig. 5c). Interestingly, ISGylated TSG101-GFP accumulated in insoluble fractions and was degraded faster than de-ISGylated TSG101-GFP (Fig. 5d,e), consistent with ISGylation promoting TSG101 protein aggregation and degradation. The expression of the ISG15-TSG101-GG plasmid rescued exosome secretion in cells targeted for endogenous TSG101 (Fig. 5f and Supplementary Fig. 5B), probably due to the presence of a functional de-ISGylated form of TSG101. To circumvent this, we

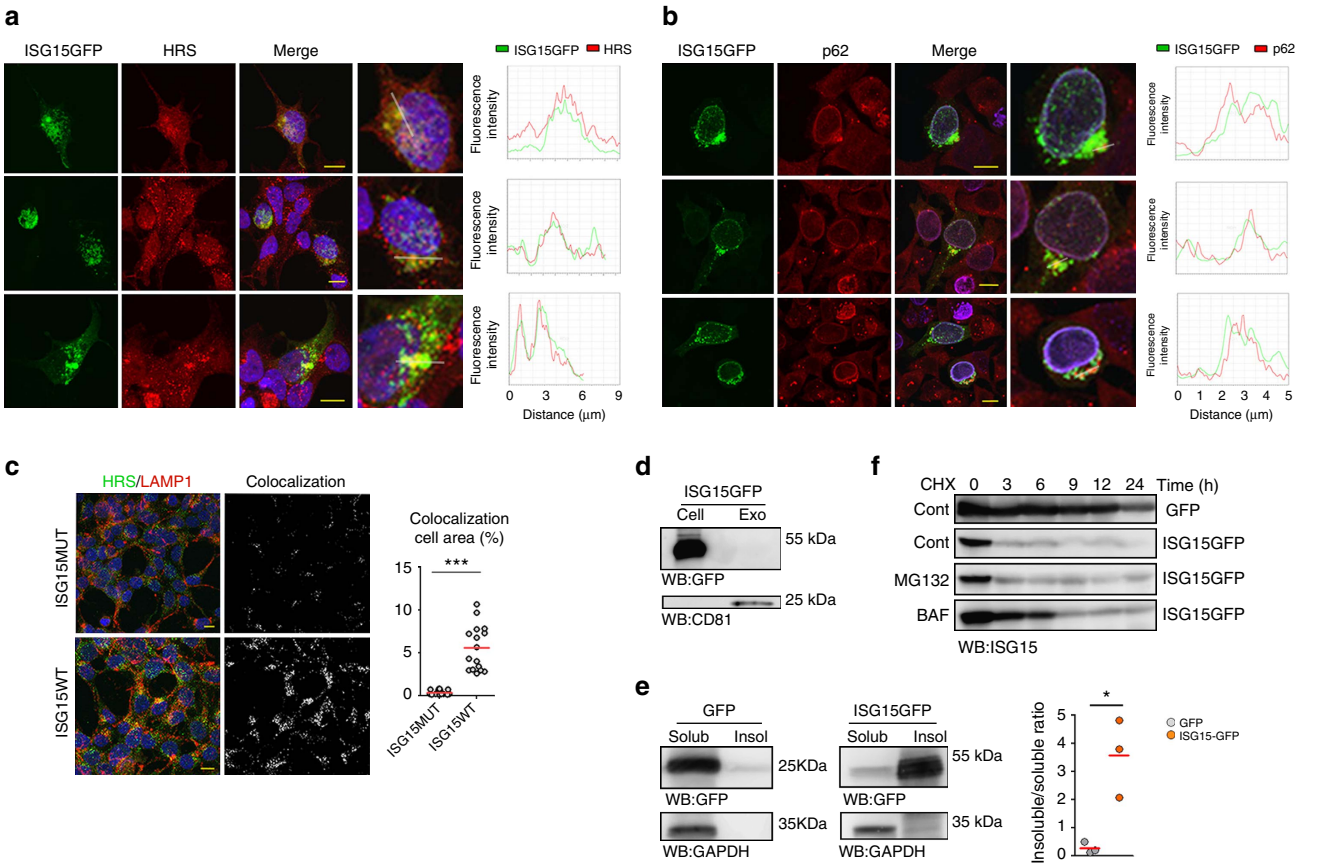

Figure 3 | ISG15 conjugation induces protein aggregation and degradation by lysosomes. (**a**) Confocal co-localization analysis of ISG15-GFP (green) and the MVB marker HRS (red). Right graphs: fluorescence intensity profiles of ISG15-GFP (green) and HRS (red) in the regions delineated by a white line. Nuclei were stained with DAPI. Scale bar, 10 μm. (**b**) Confocal co-localization analysis of ISG15-GFP (green) and p62 (red). Right graphs represent fluorescence intensity profiles of ISG15-GFP (green) and p62 (red) of the regions delineated by a white line. Nuclei were stained with DAPI. Scale bar, 10 μm. (**c**) Confocal microscopy analysis of HRS (green) and LAMP1 (red) co-localization in HEK293 cells co-transfected with ISGylation machinery and functional (ISG15WT) or mutated ISG15 (ISG15MUT). Nuclei were stained with DAPI. Scale bar, 10 μm. Co-localization area per cell was quantified by ImageJ ($n=16$). Each dot represents the percentage of co-localization area per cell surface and mean is indicated in red lines. (**d**) Western blot analysis of exogenous ISG15 in HEK293 cells transfected with ISG15-GFP. Cells and EVs (EXO) were blotted for GFP and CD81. (**e**) Western blot analysis of ISG15-GFP and GFP in 0.5% NP-40 soluble and insoluble cell fractions in HEK293 transfected with GFP or ISG15-GFP. Right graph: quantification of GFP and ISG15-GFP in the insoluble fraction respect to the soluble fraction in three independent experiments. (**f**) Western blot analysis of GFP and ISG15-GFP degradation kinetics in HEK293 cells transfected with GFP or ISG15-GFP and treated with cycloheximide to inhibit protein synthesis during the indicated times. Where specified, the medium was supplemented with the lysosome inhibitor Bafilomycin A1 (BAF) or the proteasome inhibitor MG132. A representative blot from two independent experiments is shown. Data from **c**,**e**: *t*-test $^{*}P$-value <0.05 and $^{***}P$-value <0.0001.

generated a non-de-ISGylable TSG101 mutant by changing ISG15 terminal glycines into alanines (ISG15-TSG101-AA), thus preventing TSG101 de-ISGylation (Fig. 5c). In cells devoid of endogenous TSG101, overexpression of the non-de-ISGylable TSG101 mutant did not restore the secretion of exosomes (Fig. 5g and Supplementary Fig. 5C), supporting that ISG15 conjugation to the ESCRT component TSG101 is sufficient to inhibit the secretion of exosomes.

Discussion

Cells secrete a variety of EVs including shedding vesicles, coming from the direct evagination of the plasma membrane, and exosomes, coming from endosomal compartments called MVBs. The membrane of MVB invaginates to form ILVs, which are secreted to the extracellular environment on MVB fusion with the plasma membrane[5]. MVBs can also fuse with the lysosomal compartment for the degradation of their content. There is evidence that different types of MVB co-exist in cells[59], although the differences in their composition and the mechanisms that control their biogenesis and final fusion with the lysosome or plasma membrane are not well understood[10]. In addition, on specific stimuli such as starvation or rapamycin treatment, MVBs can be re-routed to promote their fusion with the lysosomal compartment and thus avoid their fusion with the plasma membrane and the concomitant secretion of exosomes[56] demonstrating that the final fate of MVBs is not immutable but can change under specific conditions[60].

The role of the ESCRT complex in the sorting of ubiquitinated proteins into ILVs for their degradation in the lysosome is well known[61] and some of the ESCRT complex components are also involved in the secretion of exosomes and other EVs[12,17], although their precise role in the biogenesis of the different types of EVs is not known. Other ubiquitin-like modifiers have been shown to control the composition of EVs, for example, SUMOylation of hnRNPA2B1 promotes the sorting of specific microRNAs into exosomes[18], and also controls the sorting of α-synuclein into EVs[19]. Here we identify the ubiquitin-like modifier ISG15 as a novel regulator of the exosome pathway. We show that ISGylation induction by ISG15 machinery

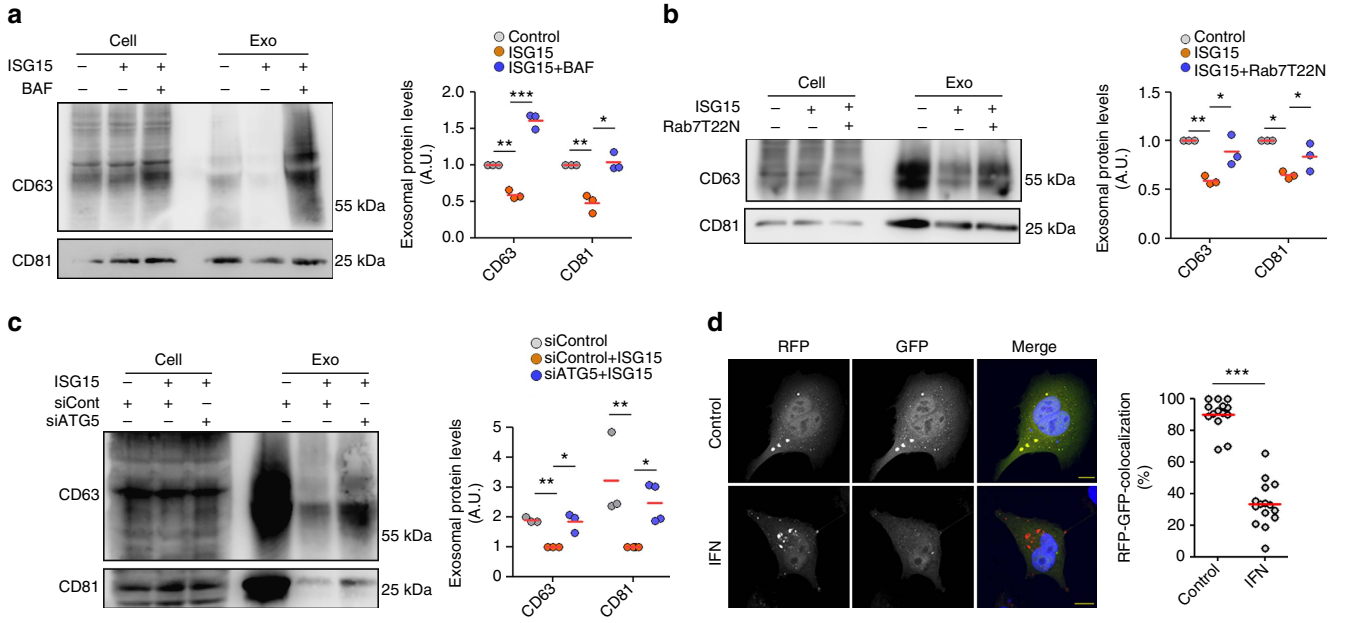

Figure 4 | Inhibition of lysosome function upon ISGylation induction rescues exosome secretion. (**a**) Western blot analysis of exosome secretion in untransfected HEK293 cells and HEK293 cells co-transfected with plasmids encoding the ISGylation machinery and ISG15, and treated with Bafilomycin A1 (BAF), when indicated. Cells and EVs (Exo) were blotted for CD63 and CD81. Right graph: quantification of exosomal protein levels in three independent experiments. (**b**) Western blot analysis of exosome secretion in HEK293 cells transfected with GFP or co-transfected with plasmids encoding ISG15 and the ISGylation machinery, and when indicated, with the Rab7T22N dominant-negative mutant. Cells and EVs were blotted for CD63 and CD81. Right graph: quantification of exosomal protein levels in three independent experiments. (**c**) Western blot analysis of exosome secretion in HEK293 cells transfected with control small interfering RNAs (siRNAs) or siRNAs targeting ATG5. After 48 h, cells were re-transfected with siRNAs together with plasmids encoding ISG15 and ISGylation machinery. Cells and EVs (Exo) were blotted for CD63 and CD81. Right: quantification of exosomal protein levels in three or four independent experiments. (**d**) Confocal analysis of LC3 localization into acidic compartments in HEK293 cells transfected with LC3-RFP-GFP tandem plasmid and treated 16 h with IFN-I where indicated. Nuclei were stained with DAPI. Scale bar, 10 μm. Images were processed by ImageJ and the number of RFP^+ and RFP^+GFP^+ dots quantified. Each dot represents the percentage of RFP^+GFP^+ dots per individual cell and mean is indicated in red lines; *t*-test; ***P-value < 0.001. Data **a**,**b**,**c**: analysis of variance; *P-value < 0.05, **P-value < 0.001 and ***P-value < 0.0001.

overexpression or IFN-I decreases the secretion of exosomal markers. Importantly, experiments with the non-conjugable ISG15MUT and with primary cells from mice with defective function of the specific ISG15 de-ISGylase USP18 demonstrated that this effect is mediated by ISG15 conjugation to proteins and not by free ISG15. ISGylation induction by ISG15 overexpression induces a decrease in microparticle secretion, indicating that ISGylation is not merely decreasing the sorting of certain exosomal markers into ILVs but is actually decreasing exosome secretion. However, ISGylation induction by IFN-I does not induce a significant decrease in the number of secreted microparticles. This could be due to the induction of the secretion of other types of EVs by IFN-I and this is in agreement with previous reports showing that IFN-I can promote the secretion of EVs loaded with antiviral components that are transferred to other cells[62]. In fact, on ultracentrifugation in sucrose gradients, the few EVs secreted by IFN-treated cells are recovered in different fractions than the EVs from non-treated cells, suggesting that they might have a different nature. Alternatively, the absence of effect of IFN on global particle secretion may indicate that only the EVs derived from MVBs are affected.

We also show that ISGylation decreases the numbers of MVBs, but does not prevent the formation of ILVs. The secretion of exosomes is recovered when the fusion of MVB with lysosomes or autophagosomes is inhibited, indicating that the observed inhibition of exosome secretion is mainly mediated by the induction of MVB degradation by the lysosome. In accordance, we show that ISGylation promotes the aggregation and degradation of proteins by the lysosome, and this is in agreement with previous reports in which ISG15-linked proteins associated with the proteins p62 and HDAC-6 involved in the autophagic process[52]. We have observed that ISGylation decreases the number of HRS^+ structures without preventing the formation of ILVs, possibly reflecting an accelerated degradation of endosomes. In addition, ISGylation increases the co-localization of the lysosome marker LAMP-1 with HRS, which is usually absent from LAMP-1-positive structures[44]. Whether ISGylation of MVB proteins induces the rapid fusion of MVB with lysosomes in an earlier stage of maturation, or whether it directly impairs HRS dissociation from endosomal membranes is not known.

A number of ISG15 target proteins are typically present in exosomes and MVBs[41], including several components of the ESCRT complex such as TSG101, CHMP2A, CHMP4B and CHMP6 (refs 40,63,64). It is therefore conceivable that ISG15 is recruited to MVB by conjugating endosomal proteins. There, it may promote protein aggregation and enhance MVB degradation by the autophagosome–lysosome compartment, thus preventing their fusion with the plasma membrane and the secretion of exosomes (Fig. 6). We have validated the ISGylation of TSG101, which has been previously shown to control the secretion of viral particles[40], and we show that TSG101 ISGylation is sufficient to impair exosome secretion. However, we cannot rule out the possibility that other endosomal proteins are being ISGylated and also contribute to the inhibition of exosome secretion induced by ISG15. TSG101 depletion has been previously shown to inhibit MVB formation[65] or to modify the size of MVBs and/or the number of ILVs[48]. However, there are significant differences

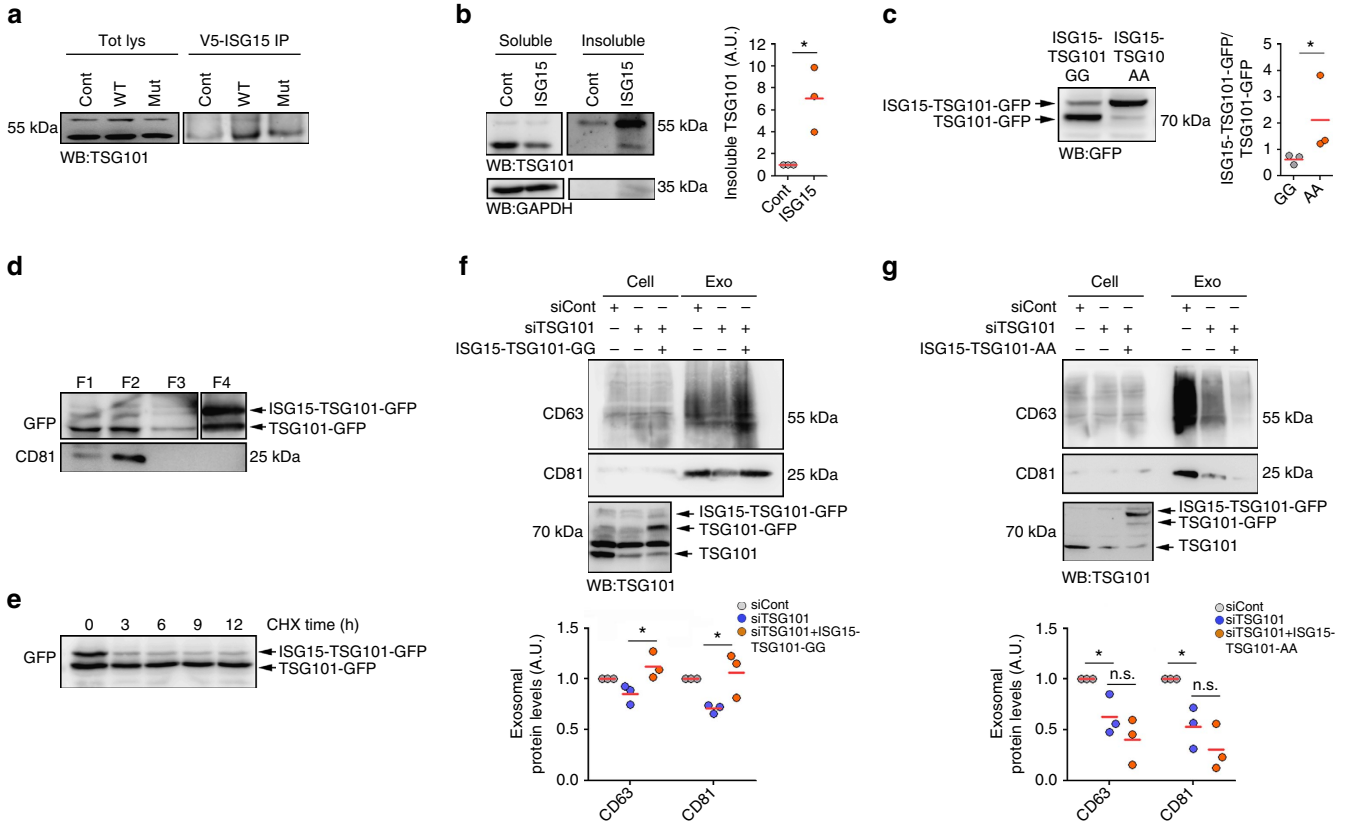

Figure 5 | ISG15 impairs exosome secretion by modifying TSG101. (**a**) Western blot analysis of TSG101 immunoprecipitation in HEK293 cells non-transfected or HEK293 cells co-transfected with plasmids encoding the ISGylation machinery and functional (ISG15WT) or mutated ISG15 (ISG15MUT). Total lysates and V5 immunoprecipitates were blotted for TSG101. (**b**) Western blot analysis of 0.5% NP-40 soluble and insoluble fractions from non-transfected HEK293 cells (Cont) or cells transfected with ISG15 and ISGylation machinery (ISG15). Soluble and insoluble fractions were blotted for TSG101 and GAPDH. Right graph: quantification of TSG101 protein levels in insoluble fractions in three independent experiments. (**c**) Western blot analysis of TSG101-GFP ISGylation in HEK293 cells transfected with ISG15-TSG101-GFP-GG or with the non-de-ISGylable mutant ISG15-TSG101-GFP-AA. Cell lysates were blotted for GFP. Right graph: quantification of ISG15-TSG101-GFP/TSG101-GFP ratio in three independent experiments. (**d**) Western blot analysis of ISG15-TSG101-GFP and TSG101-GFP subcellular distribution in HEK293 cells transfected with ISG15-TSG101-GFP-GG. Fractions corresponding to cytosol (F1), membranes (F2), nucleus (F3) and insoluble aggregates (F4) were extracted and blotted for GFP and CD81. A lower exposition of the same blot is shown for F4. (**e**) Western blot analysis of ISG15-TSG101-GFP and TSG101-GFP degradation kinetics in HEK293 cells transfected with ISG15-TSG101-GFP-GG and treated with cycloheximide during the indicated times. Cell lysates are blotted for GFP. (**f**) Western blot analysis of HEK293 cells transfected with control small interfering RNAs (siRNAs) or siRNAs targeting TSG101. When indicated, cells were co-transfected with ISG15-TSG101-GFP-GG. Cells and EVs (EXO) were blotted for CD63 and CD81. Lower gel shows cell lysates blotted for TSG101 to check TSG101 silencing and exogenous overexpression. Lower graph: quantification of exosomal protein levels in three independent experiments. (**g**) Western blot analysis of HEK293 cells transfected with control siRNAs or siRNAs targeting TSG101. When indicated, cells were co-transfected with the non-de-ISGylable mutant ISG15-TSG101-GFP-AA. Cells and EVs (EXO) were blotted for CD63 and CD81. Lower gel shows cell lysates blotted for TSG101 to check TSG101 silencing and exogenous overexpression. Lower graph: quantification of exosomal protein levels in three independent experiments. Data **b**,**c**: *t*-test; NS: *P*-value > 0.05 and **P*-value < 0.05. Data **f**,**g**: analysis of variance; NS: *P*-value > 0.05 and **P*-value < 0.05.

between depletion and ISGylation of TSG101. ISG15 may be directed to endosomes in a later stage of their maturation and here modify MVB proteins such as TSG101, and promote their aggregation and subsequent degradation by the lysosome without impairing ILV biogenesis. However, we could not completely rule out any effect of ISGylation on MVB biogenesis.

ISGylation has been previously shown to exert an antiviral activity by blocking the exit of viral particles[36,40,64,66]. The ISGylation of multiple MVB proteins and the consequent inhibition of exosome secretion induced by IFN-I would prevent the spreading of viruses that exploit the MVB pathway for their way out the cell. In addition, exosomes play important roles in cell-to-cell communication during the immune response, tumour progression, neuron survival and many other contexts[1,3,4,67]. Therefore, ISGylation induction by different stimuli such as viral infection, IFN, ischaemia[68] or ageing[69] can be an important mechanism to regulate exosome-mediated communication in many different situations.

Methods

Cell culture. The human Jurkat-derived T-cell line J77cl20 (TCR Vαl. 2 Vβ8) was cultured in RPMI (Sigma) containing 10% fetal bovine serum (FBS; Invitrogen). The HEK293T cell line was cultured in DMEM medium (Sigma) containing 10% FBS (Invitrogen).

Mouse primary macrophages (BMDMs) were obtained from the bone marrow of C57BL/6 *WT*, ISG15 knockout[42] and *USP18C61A* mice[33] (kindly provided by K. Knobeloch, Freiburg University, Germany). Cells were cultured RPMI-1640 supplemented with macrophage colony-stimulating factor (30% mycoplasma-free L929 cell supernatant, NCBI Biosample accession number SAMN00155972) for 6 days, to induce cell differentiation.

Mouse primary T lymphocytes were obtained from cell suspensions prepared from spleens and peripheral lymph nodes of C57BL/6 *WT*, *ISG15KO USP18C61A* mice. Cells were cultured for 36–48 h in RPMI with 2 μg ml^{-1} concanavalin A (Sigma) and subsequently 50 U ml^{-1} human recombinant IL-2 (Glaxo) was added

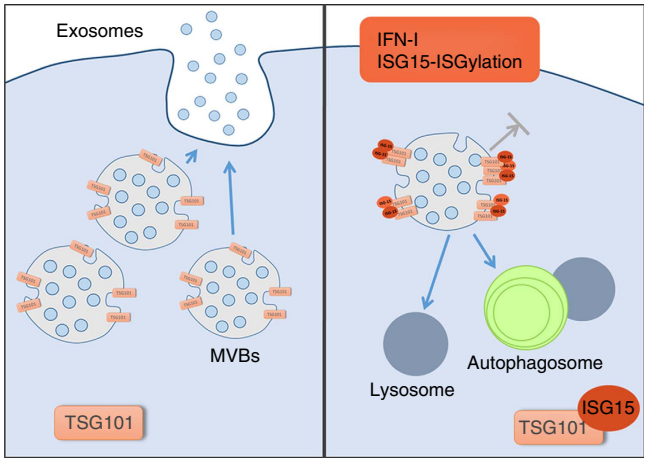

Figure 6 | Proposed model for the role of ISGylation in the regulation of exosome secretion. IFN-I induces ISG15 expression and conjugation to MVB proteins such as TSG101. ISGylation of MVB proteins promotes MVB fusion with lysosomes and degradation, thus inhibiting exosome secretion.

to the medium every 2 days for at least 4–6 days, to obtain differentiated T lymphoblasts.

Exosome purification. Cells were cultured in medium supplemented with 10% exosome-depleted FBS (bovine exosomes were removed by overnight centrifugation at 100,000 *g*). Supernatant fractions were collected from 16 to 20 h cell culture supernatants and exosomes were obtained by serial centrifugation as follows. Cells were pelleted (320 × *g* for 10 min) and the supernatant was centrifuged at 2,000 *g* for 15 min, to discard debris and dead cells. The supernatant was collected and ultracentrifuged at 10,000 *g* for 30 min at 4 °C (Beckman Coulter Optima L-100 XP, Beckman Coulter) and exosomes were pelleted by ultracentrifugation at 100,000 *g* for 70 min at 4 °C. The exosome pellet was washed in PBS and collected by ultracentrifugation at 100,000 *g* for 70 min (Beckman Coulter Optima L-100 XP, Beckman Coulter).

Nanoparticle tracking analysis. Exosome numbers and size distribution were determined by measuring the rate of Brownian motion using a NanoSight LM10 system, which is equipped with fast video capture and particle-tracking software (NanoSight, Amesbury, UK). Samples were diluted before analysis to between 2×10^8 and 20×10^8 particles per ml, and the relative concentration was calculated according to the dilution factor. Data analysis was performed with *NTA 2.1* software (Nanosight). Samples were analysed using manual shutter and gain adjustments, which resulted in shutter speeds of 15 or 30 ms, with camera gains between 280 and 560. The detection threshold was kept above 2; blur: auto; minimum expected particle size: 50 nm.

ISGylation induction by overexpression. HEK293 cells were co-transfected with plasmids encoding human E1, E2 and E3 ligases (kindly provided by A. García-Sastre, Mount Sinai Hospital, NYC) together with plasmids encoding WT or C-terminal mutated human ISG15 fused to the V5 tag. When indicated, cells were co-transfected with the appropriate small interfering RNAs or with the EGFP-Rab7A T22N plasmid (gift from Qing Zhong, Addgene plasmid 28048). Cells were transfected using Lipofectamine 2000 (Invitrogen). Twenty-four hours after transfection, cells were cultured in exosome-depleted medium for 20 h and exosomes were isolated from supernatants as described above. When indicated, cells were incubated overnight in exosome-depleted medium containing 20 nM Bafilomycin A1 (Merck).

Exosome extraction from blood serum. WT, *ISG15KO* and *USP18C61A* mice were treated with 5 μg g^{-1} body weight poly (I:C) (InvivoGen) intraperitoneally. Blood samples were extracted from the heart 24 h after poly (I:C) injection and allowed to clot 3 h at room temperature. Blood samples were kept 2 h at 4 °C and serum was obtained by centrifugation at 400 *g*, 10 min at 4 °C. Cell debris were removed by centrifugation at 3,000 *g*, 15 min at 4 °C and serum samples were stored at − 20 °C. Exosomes were extracted from serum as previously described[70]; briefly, 125 μl of Exoquick reagent were added to 250 μl of serum and incubated overnight at 4 °C. Samples were centrifuged at 1,500 *g*, 30 min and exosome pellets resuspended in RIPA buffer.

Gene silencing. HEK293 cells were transfected using Lipofectamine 2000 (Invitrogen) with the following small interfering RNAs: control (scrambled), ATG5 and TSG101 (SIGMA). Twenty-four hours after transfection, cells were cultured in exosome-depleted medium for 20 h and exosomes were isolated from supernatants as described above.

Western blotting. Cells or exosomes were lysed in RIPA buffer (50 mM Tris-HCl pH 8, 150 mM NaCl, 1% Triton X-100, 0.1% sodium deoxycholate and 0.1% SDS) containing a protease inhibitor cocktail (Complete, Roche). Proteins were separated on 10% acrylamide/bisacrylamide gels and transferred to a nitrocellulose membrane. Membranes were incubated with primary antibodies (1:1,000) and peroxidase-conjugated secondary antibodies (1:5,000), and proteins were visualized with LAS-3000. The following antibodies were used: rabbit anti-human ISG15 (Proteintech, 15981-1-AP), mouse anti-human CD63 (Calbiochem, OP171), mouse 5A6 anti-human CD81 (Santa Cruz, sc-23962), mouse anti-human TSG101 (Abcam, GTX70255), mouse anti-GFP (Living colors, 632381), rabbit anti-p62 (Sigma, P0067), mouse DM1A anti-tubulin (Sigma, F2168), rabbit anti-Calnexin (Abcam, ab10286), goat anti-mouse peroxidase (Thermo Scientific), goat anti-rabbit peroxidase (Thermo Scientific) and donkey anti-goat peroxidase (Thermo Scientific). Full immunoblots are provided in Supplementary Fig. 6.

Fluorescence confocal microscopy. For immunofluorescence assays, cells were plated onto slides coated with fibronectin (20 μg ml^{-1}), incubated for 16 h min, fixed with 2% paraformaldehyde and stained with the indicated primary antibodies (1:100) followed by secondary antibodies (1:500). When indicated, cells were previously transfected with GFP-Rab5CA (Q79L) plasmid (gift from Sergio Grinstein, Addgene plasmid 35140) or LC3-GFP-RFP tandem construct (gift from Tamotsu Yoshimori, Addgene plasmid 21074). Samples were examined with a Leica SP5 confocal microscope (Leica) fitted with a × 63 objective and images were processed and assembled using Leica software. The following antibodies were used: anti-CD63 (clone Tea 3/18, generated in the laboratory), anti-HRS (Abcam, ab72053), anti-EE1A (Santa Cruz, sc-6415), anti-LAMP1-647 (BioLegend, 328612), anti-p62 (Sigma, P0067), goat anti-mouse-488 and goat anti-rabbit-RX (Life Technologies). Images were processed and quantified using LAS-AF and ImageJ.

Cloning. ISG15-GFP plasmids were generated by excision of ISG15 from the pCAGG plasmid with XhoI and EcoICRI restriction enzymes, followed by insertion between the XhoI and AfeI sites of pAcGFP-N1. ISG15 stop codons were mutated using the QuickChange Site-Directed Mutagenesis kit (Agilent). ISG15-TSG101-GFP was obtained by inserting TSG101 into ISG15-GFP plasmid with XhoI and BamHI restriction enzymes. Non-de-ISGylable mutant ISG15-TSG101-GFP-AA was obtained by mutated terminal glycines into alanines using the QuickChange Site-Directed Mutagenesis kit (Agilent). Ubiquitin-GFP expressing plasmid was obtained from Addgene (gift from Nico Dantuma, Addgene plasmid 11928).

Protein aggregation. HEK293 cells were transfected with GFP or ISG15-GFP plasmids using Lipofectamine 2000 (Invitrogen) and 48 h later lysed in lysis buffer (10 mM Tris-HCl pH 8, 100 mM NaCl, 1 mM EDTA, 0.5% NP40 and 50 mM iodoacetamide) supplemented with protease inhibitor cocktail (Complete, Roche). Cells were centrifuged for 5 min a 13,000 *g*, and the supernatant (S1) and pellet (P1) were saved. P1 was resuspended in lysis buffer containing 2% SDS, sonicated and centrifuged at 16,000 *g* for 10 min. The pellet (P2) was resuspended in lysis buffer containing 2% SDS and sonicated. S1 and P2 were loaded on a poly-acrylamide gel and blotted for GFP. Subcellular fractionation was performed with ProteoExctarct Subcellular Proteome Extraction kit (Calbiochem).

Protein degradation. HEK293 cells were cultured in six-well-plates and transfected with GFP or ISG15-GFP using Lipofectamine 2000 (Invitrogen). Cells were treated with 40 μg ml^{-1} cycloheximide (Sigma) to inhibit protein synthesis and were lysed at the indicated time points. When indicated, the medium contained 20 nM Bafilomycin A1 (Merk) or 40 μM MG132 (Sigma).

Immunoprecipitation. 1×10^7 HEK293 cells per condition were lysed (25 mM Tris pH 8, 150 mM NaCl, 2 mM $MgCl_2$, 0.5% NP-40 and protease inhibitors) and incubated for pre-clearing with pre-washed Protein G Dynabeads (Invitrogen; 50 μl per condition; 1 h, 4 °C). Fifty microlitres of Dynabeads per condition were washed twice in 0.01% Tween PBS and resuspended in 200 μl of 0.01% Tween PBS containing 5 μg mouse anti-V5 antibody (Life Technologies) per condition and incubated 1 h at 4 °C. Pre-cleared lysates were incubated with antibody-conjugated Dynabeads (1.5 h, 4 °C). Antibody-conjugated Dynabeads were washed six times with lysis buffer and transferred to clean tubes. Protein loading buffer was added, samples were boiled at 95 °C for 5 min and processed for immunoblotting.

Electron microscopy and MVB quantification. Cells cultured on dishes were washed in PBS and fixed for 1 h in 2.5% glutaraldehyde in 0.1 M phosphate buffer at room temperature. Then, cells were slowly and gently scrapped and pelleted in eppendorf tubes. Pellets were washed in phosphate buffer and incubated with 1%

OsO_4 for 90 min at 4 °C. Then, samples were dehydrated, embedded in Spurr and sectioned using Leica ultramicrotome (Leica Microsystems). Ultrathin sections (50–70 nm) were stained with 2% uranyl acetate for 10 min and with a lead-staining solution for 5 min and observed using a transmission electron microscope, JEOL JEM-1010 fitted with a Gatan Orius SC1000 (model 832) digital camera.

For the calibration of images, quantification and analysis ImageJ was used. MVBs were identified and counted by morphology, having only discrete ILVs. Lysosomes contain multilamellar profiles. At least 20 MVBs were analysed per experiment from separate cells. Data were analysed from duplicate or triplicate separate experiments and two to four grids were used for each condition. The minimum number of cells scored for each condition was 20. Box scatter plots were generated using Prism GraphPad software and statistical tests were performed in Microsoft Excel. Data are means ± s.d. and ***P-value < 0.0001.

Data availability. The data that support the conclusions of this study are available from the corresponding author upon request.

References

1. Andreola, G. *et al.* Induction of lymphocyte apoptosis by tumor cell secretion of FasL-bearing microvesicles. *J. Exp. Med.* **195,** 1303–1316 (2002).
2. Thery, C. *et al.* Indirect activation of naive $CD4^+$ T cells by dendritic cell-derived exosomes. *Nat. Immunol.* **3,** 1156–1162 (2002).
3. Chalmin, F. *et al.* Membrane-associated Hsp72 from tumor-derived exosomes mediates STAT3-dependent immunosuppressive function of mouse and human myeloid-derived suppressor cells. *J. Clin. Invest.* **120,** 457–471 (2010).
4. Peinado, H. *et al.* Melanoma exosomes educate bone marrow progenitor cells toward a pro-metastatic phenotype through MET. *Nat. Med.* **18,** 883–891 (2012).
5. Kowal, J., Tkach, M. & Thery, C. Biogenesis and secretion of exosomes. *Curr. Opin. Cell Biol.* **29,** 116–125 (2014).
6. Blanchard, N. *et al.* TCR activation of human T cells induces the production of exosomes bearing the TCR/CD3/zeta complex. *J. Immunol.* **168,** 3235–3241 (2002).
7. van der Vlist, E. J. *et al.* CD4(+) T cell activation promotes the differential release of distinct populations of nanosized vesicles. *J. Extracell. Vesicles* **1,** 18364 (2012).
8. Hergenreider, E. *et al.* Atheroprotective communication between endothelial cells and smooth muscle cells through miRNAs. *Nat. Cell Biol.* **14,** 249–256 (2012).
9. Kucharzewska, P. *et al.* Exosomes reflect the hypoxic status of glioma cells and mediate hypoxia-dependent activation of vascular cells during tumor development. *Proc. Natl Acad. Sci. USA* **110,** 7312–7317 (2013).
10. Villarroya-Beltri, C., Baixauli, F., Gutierrez-Vazquez, C., Sanchez-Madrid, F. & Mittelbrunn, M. Sorting it out: regulation of exosome loading. *Semin. Cancer Biol.* **28,** 3–13 (2014).
11. Moreno-Gonzalo, O., Villarroya-Beltri, C. & Sanchez-Madrid, F. Post-translational modifications of exosomal proteins. *Front. Immunol.* **5,** 383 (2014).
12. Nabhan, J. F., Hu, R., Oh, R. S., Cohen, S. N. & Lu, Q. Formation and release of arrestin domain-containing protein 1-mediated microvesicles (ARMMs) at plasma membrane by recruitment of TSG101 protein. *Proc. Natl Acad. Sci. USA* **109,** 4146–4151 (2012).
13. Putz, U. *et al.* Nedd4 family-interacting protein 1 (Ndfip1) is required for the exosomal secretion of Nedd4 family proteins. *J. Biol. Chem.* **283,** 32621–32627 (2008).
14. Henne, W. M., Buchkovich, N. J. & Emr, S. D. The ESCRT pathway. *Dev. Cell* **21,** 77–91 (2011).
15. Levkowitz, G. *et al.* Ubiquitin ligase activity and tyrosine phosphorylation underlie suppression of growth factor signaling by c-Cbl/Sli-1. *Mol. Cell* **4,** 1029–1040 (1999).
16. Baietti, M. F. *et al.* Syndecan-syntenin-ALIX regulates the biogenesis of exosomes. *Nat. Cell Biol.* **14,** 677–685 (2012).
17. Colombo, M. *et al.* Analysis of ESCRT functions in exosome biogenesis, composition and secretion highlights the heterogeneity of extracellular vesicles. *J. Cell Sci.* **126,** 5553–5565 (2013).
18. Villarroya-Beltri, C. *et al.* Sumoylated hnRNPA2B1 controls the sorting of miRNAs into exosomes through binding to specific motifs. *Nat. Commun.* **4,** 2980 (2013).
19. Kunadt, M. *et al.* Extracellular vesicle sorting of alpha-Synuclein is regulated by sumoylation. *Acta Neuropathol.* **129,** 695–713 (2015).
20. Farrell, P. J., Broeze, R. J. & Lengyel, P. Accumulation of an mRNA and protein in interferon-treated Ehrlich ascites tumour cells. *Nature* **279,** 523–525 (1979).
21. Bogunovic, D. *et al.* Mycobacterial disease and impaired IFN-gamma immunity in humans with inherited ISG15 deficiency. *Science* **337,** 1684–1688 (2012).
22. Giannakopoulos, N. V. *et al.* ISG15 Arg151 and the ISG15-conjugating enzyme UbE1L are important for innate immune control of Sindbis virus. *J. Virol.* **83,** 1602–1610 (2009).
23. Lai, C. *et al.* Mice lacking the ISG15 E1 enzyme UbE1L demonstrate increased susceptibility to both mouse-adapted and non-mouse-adapted influenza B virus infection. *J. Virol.* **83,** 1147–1151 (2009).
24. Dastur, A., Beaudenon, S., Kelley, M., Krug, R. M. & Huibregtse, J. M. Herc5, an interferon-induced HECT E3 enzyme, is required for conjugation of ISG15 in human cells. *J. Biol. Chem.* **281,** 4334–4338 (2006).
25. Kim, K. I., Giannakopoulos, N. V., Virgin, H. W. & Zhang, D. E. Interferon-inducible ubiquitin E2, Ubc8, is a conjugating enzyme for protein ISGylation. *Mol. Cell Biol.* **24,** 9592–9600 (2004).
26. Yuan, W. & Krug, R. M. Influenza B virus NS1 protein inhibits conjugation of the interferon (IFN)-induced ubiquitin-like ISG15 protein. *EMBO J.* **20,** 362–371 (2001).
27. Ketscher, L. & Knobeloch, K. P. ISG15 uncut: dissecting enzymatic and non-enzymatic functions of USP18 *in vivo*. *Cytokine* **76,** 569–571 (2015).
28. Durfee, L. A., Lyon, N., Seo, K. & Huibregtse, J. M. The ISG15 conjugation system broadly targets newly synthesized proteins: implications for the antiviral function of ISG15. *Mol. Cell* **38,** 722–732 (2010).
29. Rahnefeld, A. *et al.* Ubiquitin-like protein ISG15 (interferon-stimulated gene of 15 kDa) in host defense against heart failure in a mouse model of virus-induced cardiomyopathy. *Circulation* **130,** 1589–1600 (2014).
30. Zhao, C., Hsiang, T. Y., Kuo, R. L. & Krug, R. M. ISG15 conjugation system targets the viral NS1 protein in influenza A virus-infected cells. *Proc. Natl Acad. Sci. USA* **107,** 2253–2258 (2010).
31. Lenschow, D. J. Antiviral Properties of ISG15. *Viruses* **2,** 2154–2168 (2010).
32. Radoshevich, L. *et al.* ISG15 counteracts *Listeria monocytogenes* infection. *eLife* **4,** e06848 (2015).
33. Ketscher, L. *et al.* Selective inactivation of USP18 isopeptidase activity *in vivo* enhances ISG15 conjugation and viral resistance. *Proc. Natl Acad. Sci. USA* **112,** 1577–1582 (2015).
34. Speer, S. D. *et al.* ISG15 deficiency and increased viral resistance in humans but not mice. *Nat. Commun.* **7,** 11496 (2016).
35. Zhang, X. *et al.* Human intracellular ISG15 prevents interferon-alpha/beta over-amplification and auto-inflammation. *Nature* **517,** 89–93 (2015).
36. Okumura, A., Lu, G., Pitha-Rowe, I. & Pitha, P. M. Innate antiviral response targets HIV-1 release by the induction of ubiquitin-like protein ISG15. *Proc. Natl Acad. Sci. USA* **103,** 1440–1445 (2006).
37. Malakhova, O. A. & Zhang, D. E. ISG15 inhibits Nedd4 ubiquitin E3 activity and enhances the innate antiviral response. *J. Biol. Chem.* **283,** 8783–8787 (2008).
38. Booth, A. M. *et al.* Exosomes and HIV Gag bud from endosome-like domains of the T cell plasma membrane. *J. Cell Biol.* **172,** 923–935 (2006).
39. Izquierdo-Useros, N. *et al.* Capture and transfer of HIV-1 particles by mature dendritic cells converges with the exosome-dissemination pathway. *Blood* **113,** 2732–2741 (2009).
40. Sanyal, S. *et al.* Type I interferon imposes a TSG101/ISG15 checkpoint at the Golgi for glycoprotein trafficking during influenza virus infection. *Cell Host Microbe* **14,** 510–521 (2013).
41. Giannakopoulos, N. V. *et al.* Proteomic identification of proteins conjugated to ISG15 in mouse and human cells. *Biochem. Biophys. Res. Commun.* **336,** 496–506 (2005).
42. Osiak, A., Utermohlen, O., Niendorf, S., Horak, I. & Knobeloch, K. P. ISG15, an interferon-stimulated ubiquitin-like protein, is not essential for STAT1 signaling and responses against vesicular stomatitis and lymphocytic choriomeningitis virus. *Mol. Cell Biol.* **25,** 6338–6345 (2005).
43. Doyle, S. *et al.* IRF3 mediates a TLR3/TLR4-specific antiviral gene program. *Immunity* **17,** 251–263 (2002).
44. Bache, K. G., Brech, A., Mehlum, A. & Stenmark, H. Hrs regulates multivesicular body formation via ESCRT recruitment to endosomes. *J. Cell Biol.* **162,** 435–442 (2003).
45. Gibbings, D. J., Ciaudo, C., Erhardt, M. & Voinnet, O. Multivesicular bodies associate with components of miRNA effector complexes and modulate miRNA activity. *Nat. Cell Biol.* **11,** 1143–1149 (2009).
46. Stenmark, H. *et al.* Inhibition of rab5 GTPase activity stimulates membrane fusion in endocytosis. *EMBO J.* **13,** 1287–1296 (1994).
47. Wegner, C. S. *et al.* Ultrastructural characterization of giant endosomes induced by GTPase-deficient Rab5. *Histochem. Cell Biol.* **133,** 41–55 (2010).
48. Edgar, J. R., Eden, E. R. & Futter, C. E. Hrs- and CD63-dependent competing mechanisms make different sized endosomal intraluminal vesicles. *Traffic* **15,** 197–211 (2014).
49. Carter, S. & Vousden, K. H. p53-Ubl fusions as models of ubiquitination, sumoylation and neddylation of p53. *Cell Cycle* **7,** 2519–2528 (2008).
50. Haglund, K. *et al.* Multiple monoubiquitination of RTKs is sufficient for their endocytosis and degradation. *Nat. Cell Biol.* **5,** 461–466 (2003).

51. Li, M. *et al.* Mono- versus polyubiquitination: differential control of p53 fate by Mdm2. *Science* **302,** 1972–1975 (2003).
52. Nakashima, H., Nguyen, T., Goins, W. F. & Chiocca, E. A. Interferon-stimulated Gene 15 (ISG15) and ISG15-linked proteins can associate with members of the selective autophagic process, histone deacetylase 6 (HDAC6) and SQSTM1/p62. *J. Biol. Chem.* **290,** 1485–1495 (2015).
53. van Deurs, B., Holm, P. K. & Sandvig, K. Inhibition of the vacuolar H(+)-ATPase with bafilomycin reduces delivery of internalized molecules from mature multivesicular endosomes to lysosomes in HEp-2 cells. *Eur. J. Cell Biol.* **69,** 343–350 (1996).
54. van Weert, A. W., Dunn, K. W., Geuze, H. J., Maxfield, F. R. & Stoorvogel, W. Transport from late endosomes to lysosomes, but not sorting of integral membrane proteins in endosomes, depends on the vacuolar proton pump. *J. Cell Biol.* **130,** 821–834 (1995).
55. Bucci, C., Thomsen, P., Nicoziani, P., McCarthy, J. & van Deurs, B. Rab7: a key to lysosome biogenesis. *Mol. Biol. Cell* **11,** 467–480 (2000).
56. Fader, C. M., Sanchez, D., Furlan, M. & Colombo, M. I. Induction of autophagy promotes fusion of multivesicular bodies with autophagic vacuoles in k562 cells. *Traffic* **9,** 230–250 (2008).
57. Gutierrez, M. G., Munafo, D. B., Beron, W. & Colombo, M. I. Rab7 is required for the normal progression of the autophagic pathway in mammalian cells. *J. Cell Sci.* **117,** 2687–2697 (2004).
58. Jager, S. *et al.* Role for Rab7 in maturation of late autophagic vacuoles. *J. Cell Sci.* **117,** 4837–4848 (2004).
59. Trajkovic, K. *et al.* Ceramide triggers budding of exosome vesicles into multivesicular endosomes. *Science* **319,** 1244–1247 (2008).
60. Baixauli, F., Lopez-Otin, C. & Mittelbrunn, M. Exosomes and autophagy: coordinated mechanisms for the maintenance of cellular fitness. *Front. Immunol.* **5,** 403 (2014).
61. Raiborg, C. & Stenmark, H. The ESCRT machinery in endosomal sorting of ubiquitylated membrane proteins. *Nature* **458,** 445–452 (2009).
62. Li, J. *et al.* Exosomes mediate the cell-to-cell transmission of IFN-alpha-induced antiviral activity. *Nat. Immunol.* **14,** 793–803 (2013).
63. Kuang, Z., Seo, E. J. & Leis, J. Mechanism of inhibition of retrovirus release from cells by interferon-induced gene ISG15. *J. Virol.* **85,** 7153–7161 (2011).
64. Pincetic, A., Kuang, Z., Seo, E. J. & Leis, J. The interferon-induced gene ISG15 blocks retrovirus release from cells late in the budding process. *J. Virol.* **84,** 4725–4736 (2010).
65. Razi, M. & Futter, C. E. Distinct roles for Tsg101 and Hrs in multivesicular body formation and inward vesiculation. *Mol. Biol. Cell* **17,** 3469–3483 (2006).
66. Okumura, A., Pitha, P. M. & Harty, R. N. ISG15 inhibits Ebola VP40 VLP budding in an L-domain-dependent manner by blocking Nedd4 ligase activity. *Proc. Natl Acad. Sci. USA* **105,** 3974–3979 (2008).
67. Fruhbeis, C. *et al.* Neurotransmitter-triggered transfer of exosomes mediates oligodendrocyte-neuron communication. *PLoS Biol.* **11,** e1001604 (2013).
68. Nakka, V. P. *et al.* Increased cerebral protein ISGylation after focal ischemia is neuroprotective. *J. Cereb. Blood Flow Metab.* **31,** 2375–2384 (2011).
69. Lou, Z. *et al.* Telomere length regulates ISG15 expression in human cells. *Aging (Albany NY)* **1,** 608–621 (2009).
70. Andreu, Z. *et al.* Comparative analysis of EV isolation procedures for miRNAs detection in serum samples. *J. Extracell Vesicles* **5,** 31655 (2016).

Acknowledgements

We thank Dr K. Knobeloch, Dr A. García-Sastre and Dr M.A. Alonso for providing reagents, and Dr S. Bartlett for assistance with English editing. C.E. is thankful to electron microscopy facility (campus Casanova), CCiT-University of Barcelona. This study was supported by grants SAF2014-55579-R from the Spanish Ministry of Economy and Competitiveness, INDISNET-S2011/BMD-2332 from the Comunidad de Madrid, Cardiovascular Network RD12-0042-0056 and PIE13/00041 from Instituto de Salud Carlos III (Fondo de Investigación Sanitaria del Instituto de Salud Carlos III and co-funding by Fondo Europeo de Desarrollo Regional FEDER), ERC-2011-AdG 294340-GENTRIS and COST-Action BM1202 to F.S.-M.; grant SAF2014-54623-R, FIS grant PI11/00127 (Fondo de Investigación Sanitaria del Instituto de Salud Carlos III and Ministry of Health of Spain, State secretary of R+D and FEDER/FSE) and Bayer Group Grants4Grants (ID 2013-08-0982) to S.G.; and grant BFU2015-66785-P from the Spanish Ministry of Economy and Competitiveness to C.E.; Centro Nacional de Investigaciones Cardiovasculares (CNIC) is supported by the Spanish Ministry of Economy and Competitiveness (MINECO) and the Pro-CNIC Foundation, and is a Severo Ochoa Center of Excellence (MINECO award SEV-2015-0505). C.V.-B. was supported by FPU programme (Spanish Ministry of Education). M.M. is supported by MS14/00219 from Instituto de Salud Carlos III.

Author contributions

C.V.-B., F.B., I.F.-D., D.T., O.M.-G., S.B. and C.E. performed experimental work. C.V.-B., F.B., M.M., S.G. and F.S.-M. designed research. C.V.-B., F.B. and F.S.-M. analysed data and wrote the manuscript.

Additional information

Supplementary Information accompanies this paper at http://www.nature.com/naturecommunications

Competing financial interests: The authors declare no competing financial interests.

Reprints and permission information is available online at http://npg.nature.com/reprintsandpermissions/

How to cite this article: Villarroya-Beltri, C. *et al.* ISGylation controls exosome secretion by promoting lysosomal degradation of MVB proteins. *Nat. Commun.* **7,** 13588 doi: 10.1038/ncomms13588 (2016).

Publisher's note: Springer Nature remains neutral with regard to jurisdictional claims in published maps and institutional affiliations.